Observational Cosmology

The Cosmic Microwave Background
Part II

Kaustuv Basu

Course website:
http://www.astro.uni-bonn.de/~kbasu/ObsCosmo

Make your own CMB experiment!

- Design experiment to measure $\frac{\Delta T}{T}(\theta, \phi)$

- Find component amplitudes $a_{\ell m} = \int_\Omega \frac{\Delta T}{T}(\theta, \phi) Y^*_{\ell m}(\theta, \phi) d\Omega$

- Plot $c_\ell = \langle |a_{\ell m}| \rangle^2$ against l (where l is inverse of angular scale, l ~ π / θ)

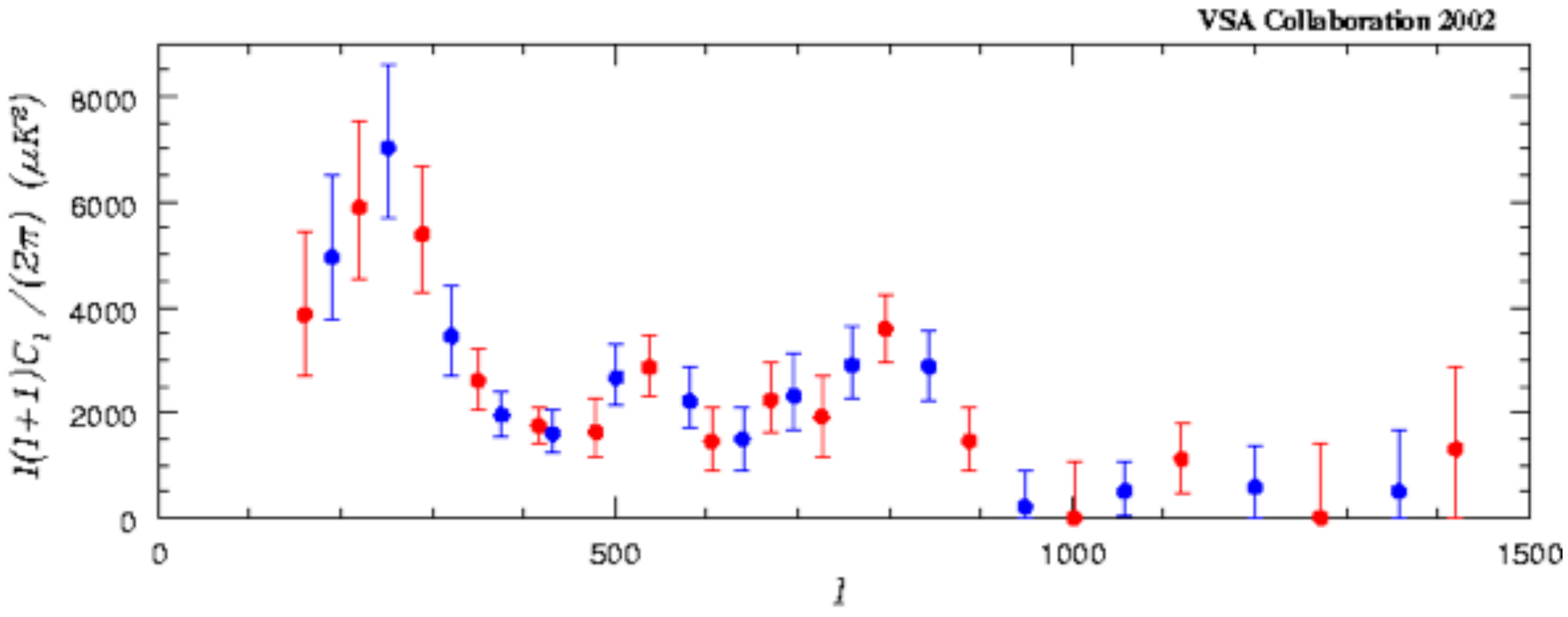

Generating theoretical C_l

INPUT

Favorite cosmological model:
Ω_m, Ω_Λ, σ_8, H_0, ..

Boltzmann solvers

powerful cosmological codes (CMBFAST, CAMB)

OUTPUT

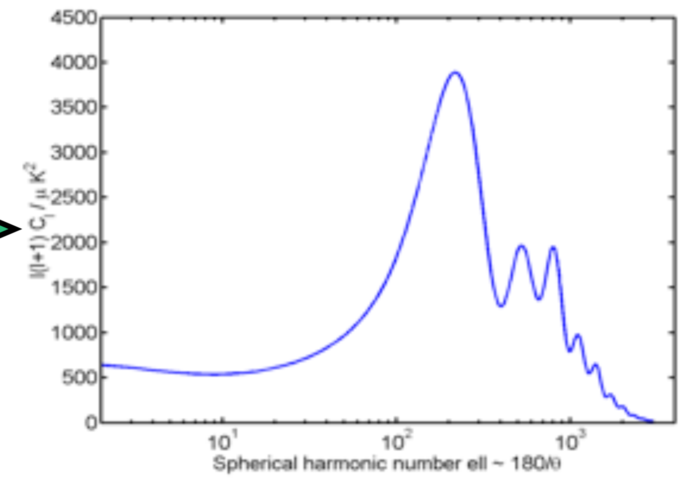

Fit to data

Codes like CMBFAST or CAMB evolve the perturbations in different species (CDM, baryons, photons, neutrinos) independently and then add them up. The perturbations are small so linear theory suffices.

Calculation of the C$_l$-s (e.g. CMBFast)

Boltzmann transport equation describes the evolution of the photon distribution function

$$\delta f_T(\hat{\mathbf{n}}, \mathbf{x}, \eta) = \left(T \frac{\partial f}{\partial T} \right)_{\rm CMB} \frac{\Delta T}{T}$$

$$\frac{\partial}{\partial \eta} \frac{\Delta T}{T}(\hat{\mathbf{n}}, \mathbf{x}, \eta) = \text{Coll.} + \text{Grav.}$$

Collisional part describes the scattering of the photons with electrons

Gravitational part describes the motion of the photons in the perturbed background

Differential form in Fourier space

Scalar perturbations

$$\begin{aligned} &\dot{\Delta}_T + ik\mu\Delta_T = \dot{\Phi} - ik\mu\Psi \\ &+\dot{\tau}\left[-\Delta_T + \Delta_{T_0} + i\mu v_B + \frac{1}{2}P_2(\mu)\Pi\right] \\ &\dot{\Delta}_P + ik\mu\Delta_P = \dot{\tau}\left[-\Delta_P + \frac{1}{2}\{1 - P_2(\mu)\}\,\Pi\right] \end{aligned}$$

$$C_\ell = (4\pi)^2 \int k^2 dk P(k) |\Delta_{T\ell}(k, \eta_0)|^2$$

Reference: Seljak & Zaldarriaga (1996)

Calculation of the C_l–s (e.g. CMBFast)

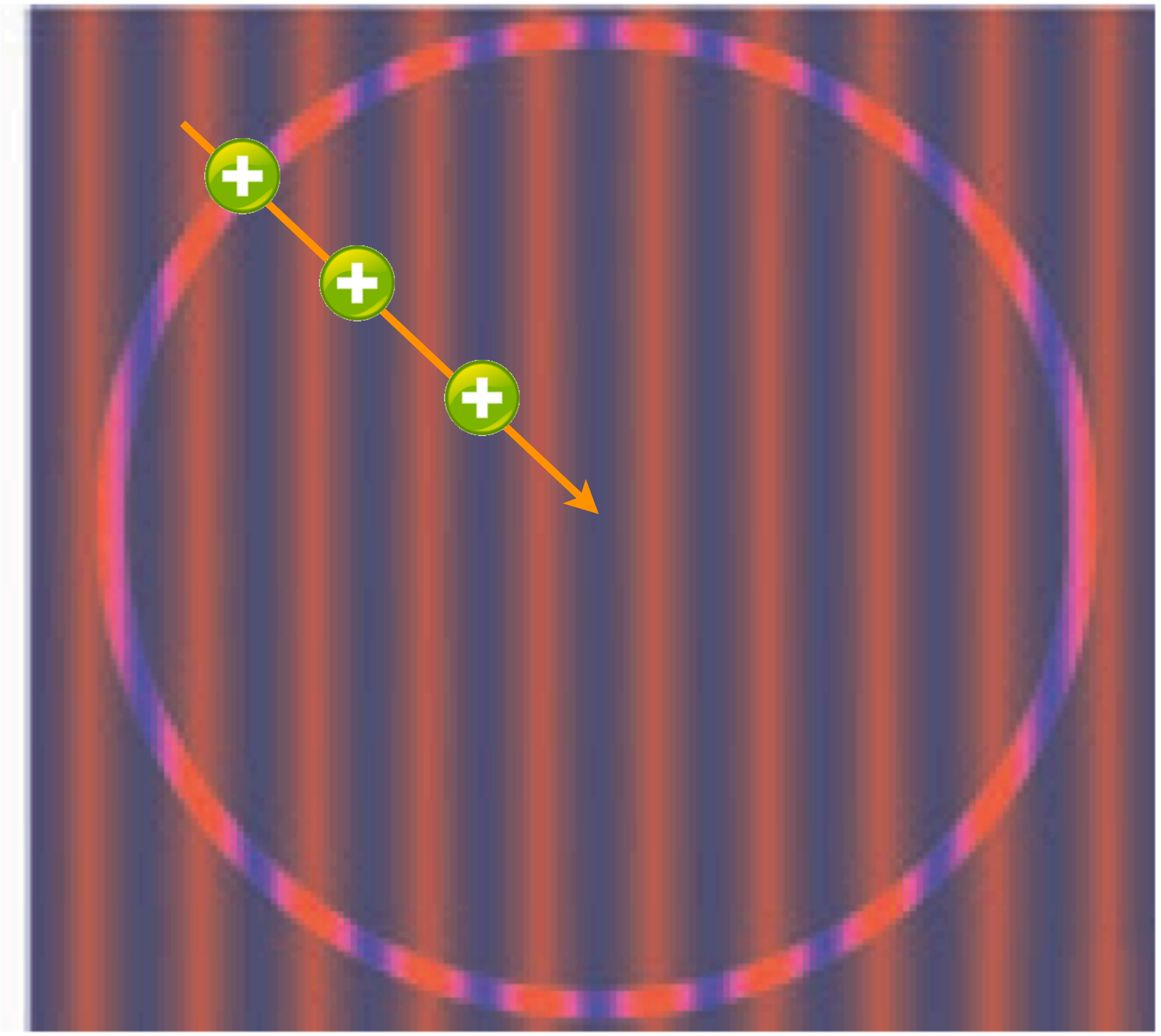

- *We know how the intensity distribution for a single k-mode looks like!*

- Choose one single k–mode and evolve that from before the recombination until today (coupled & linearized Boltzmann and Einstein equations)

- Compute the contribution of that k–mode to the power spectrum (C_l–s) by line of sight integration

- Average over all possible phases, and sum up the contributions from all the k–modes!

Online C_l calculators

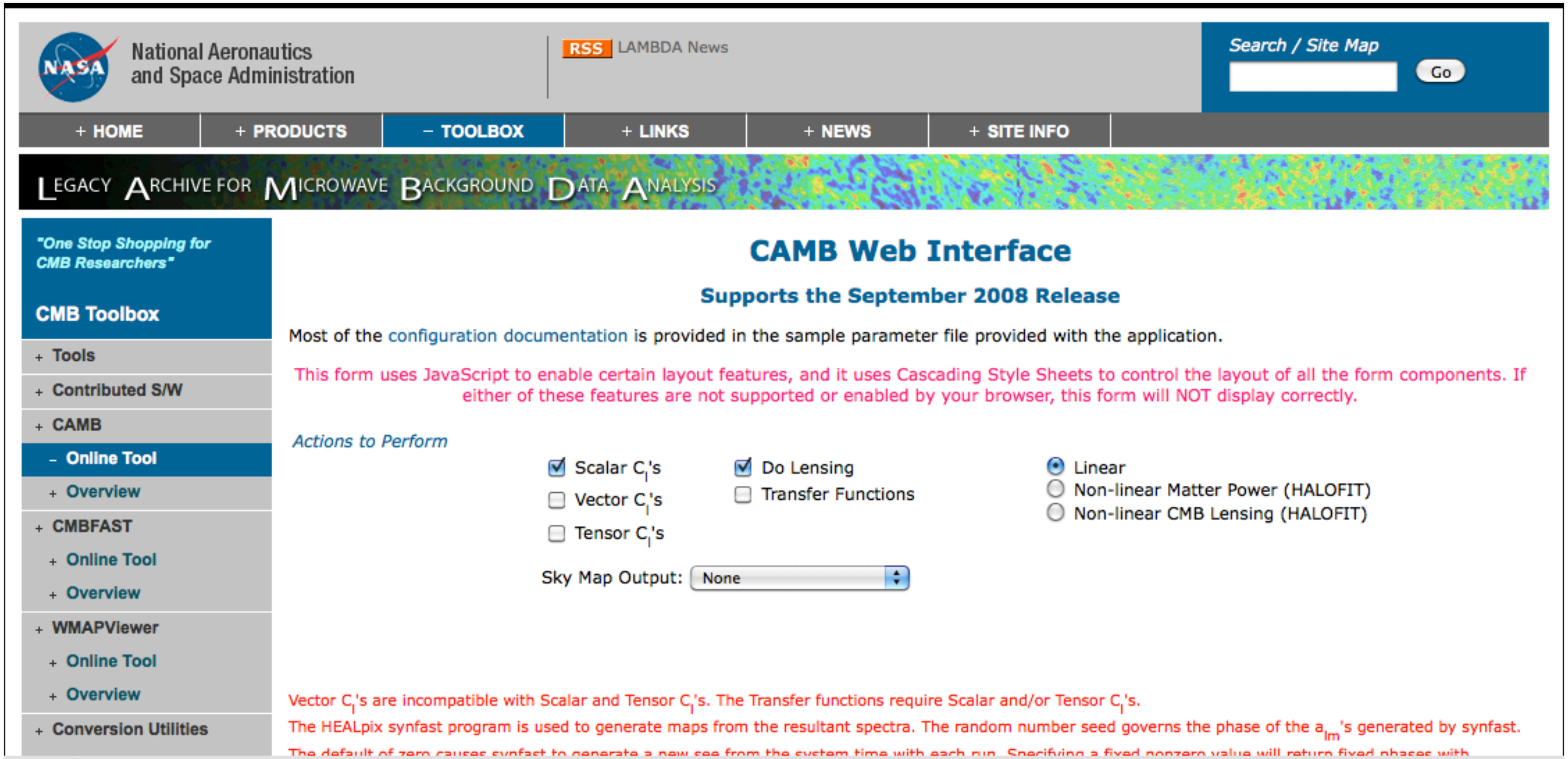

CMB Toolbox: http://lambda.gsfc.nasa.gov/toolbox/

CAMB website: http://camb.info/

CMBFast website: http://www.cmbfast.org/

Parameter estimation (Exercise)

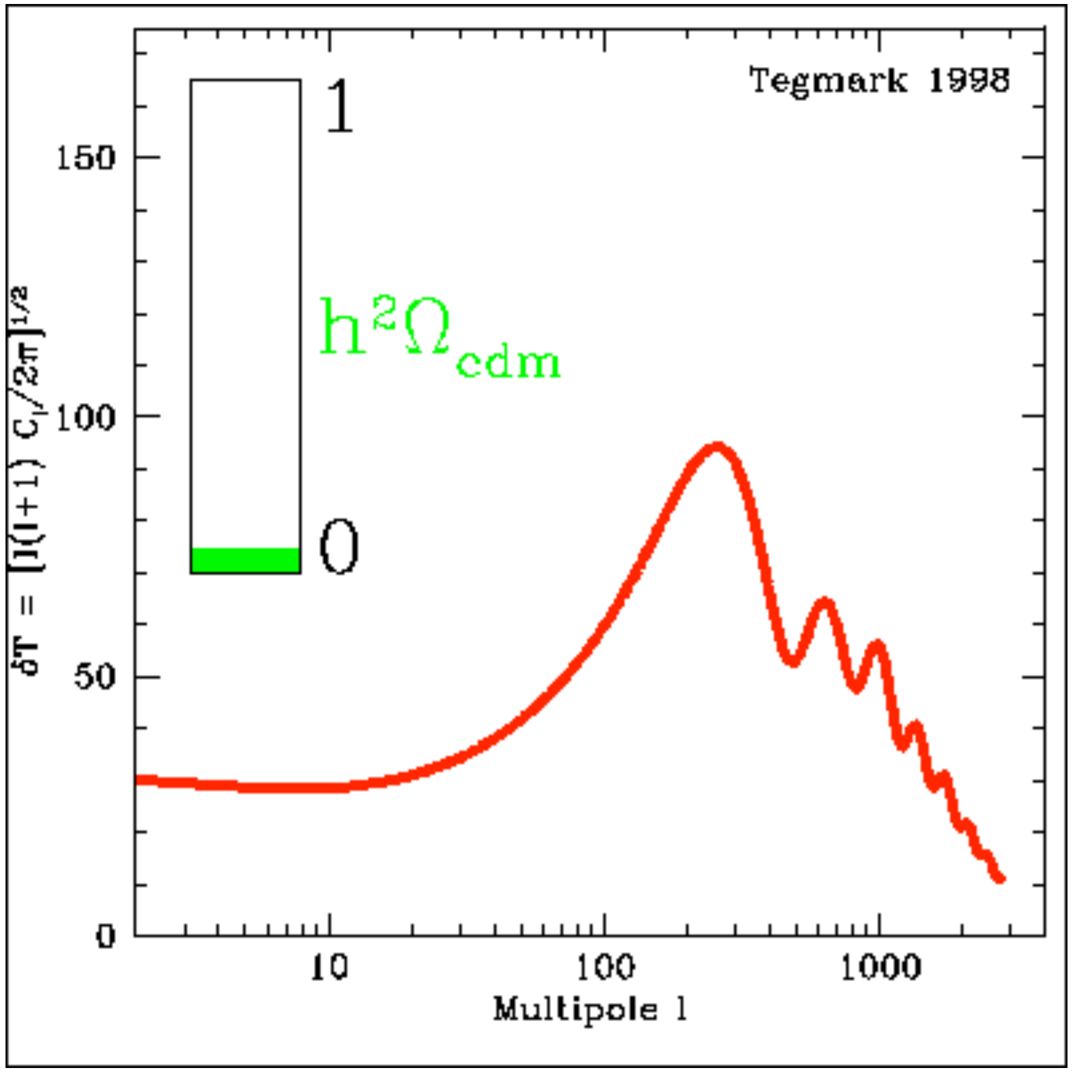

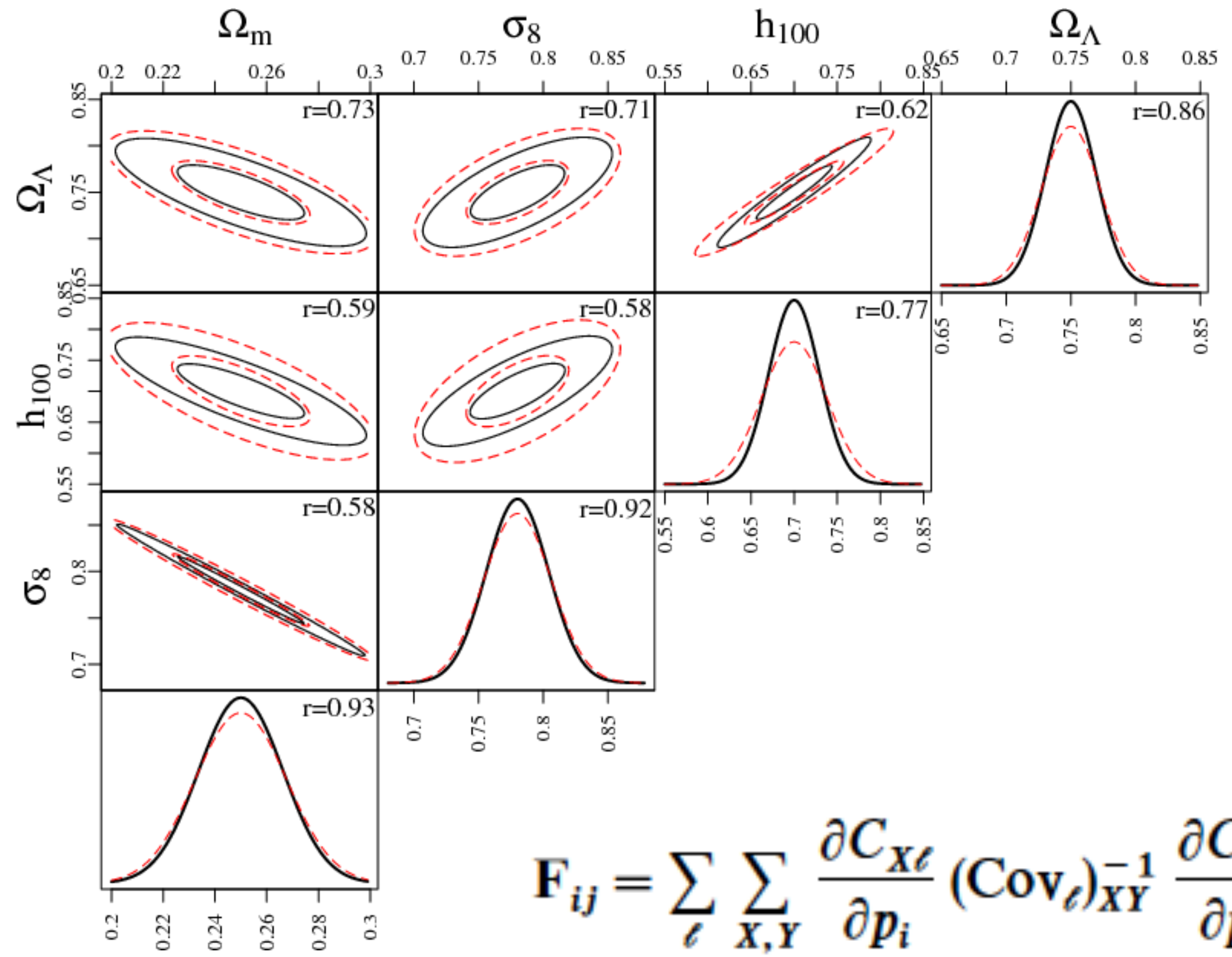

$$\mathbf{F}_{ij} = \sum_{\ell} \sum_{X,Y} \frac{\partial C_{X\ell}}{\partial p_i} (\mathrm{Cov}_\ell)^{-1}_{XY} \frac{\partial C_{X\ell}}{\partial p_j}$$

$$(\mathrm{Cov}_\ell)_{TT} = \frac{2}{(2\ell+1) f_{\mathrm{sky}}} (C_{T\ell} + w_T^{-1} B_\ell^{-2})^2$$

We will use online CMB tools, e.g.
https://lambda.gsfc.nasa.gov/toolbox/tb_camb_form.cfm

parameter constraints

$$\sigma_{\alpha_i} \geq \sqrt{\frac{1}{F_{ii}}}$$

Parameter estimation (Exercise)

$$F_{ij} = \sum_{\ell=2}^{\ell_{max}} \frac{(2\ell+1)f_{sky}}{2} \left[C_\ell + \frac{4\pi}{N}\sigma_N^2 e^{\ell(\ell+1)\sigma_b^2} \right]^{-2} \frac{\partial C_\ell}{\partial s_i}\frac{\partial C_\ell}{\partial s_j}$$

Cosmic variance

Noise per beam

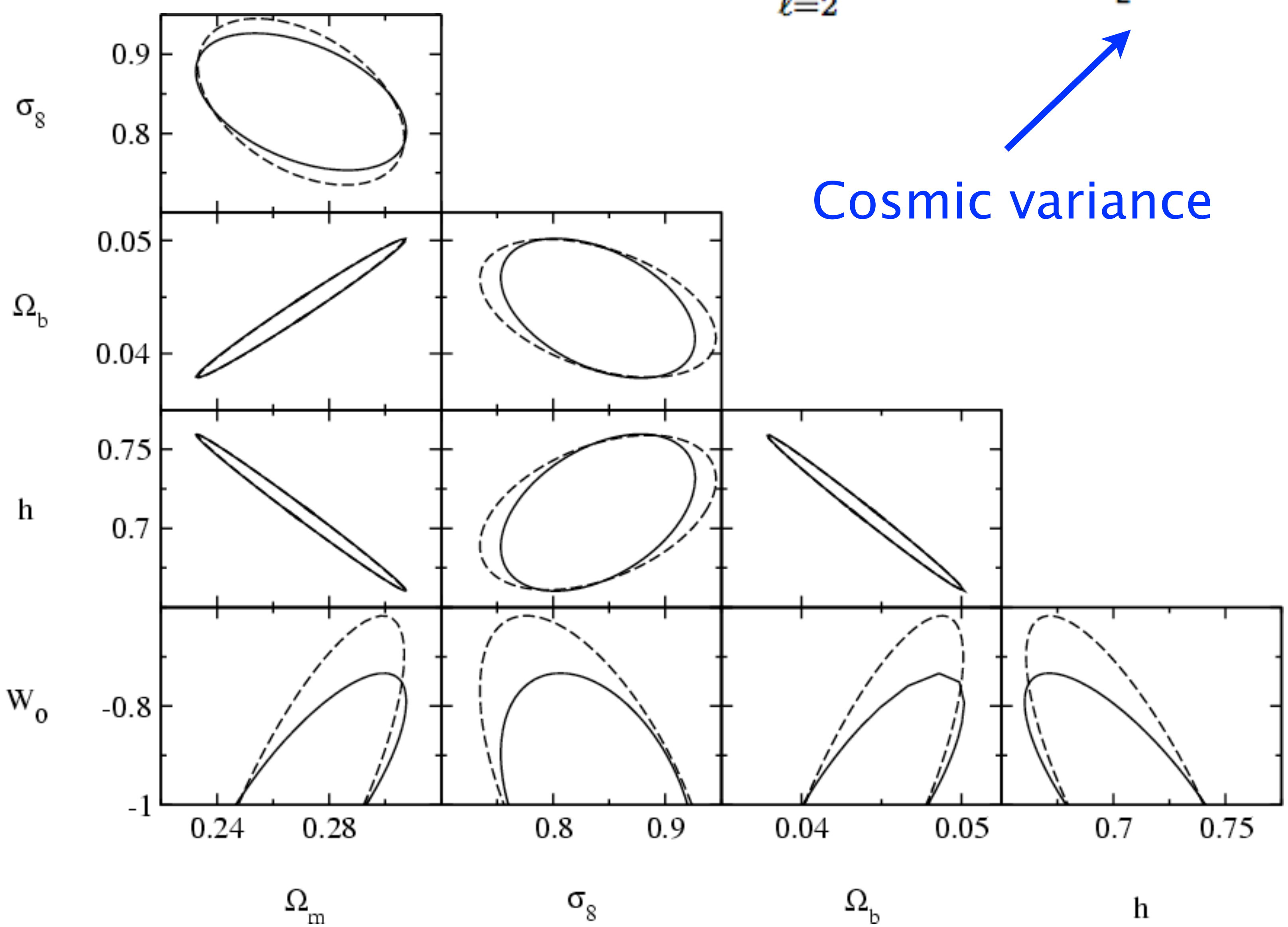

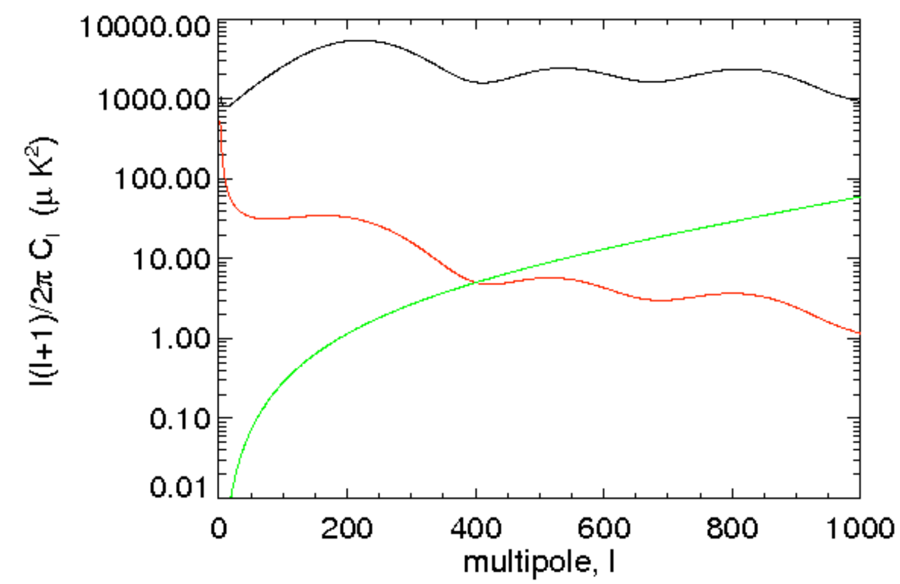

Plot your own power spectra (two for each parameter and the fiducial). Then add-in the noise term and sum up!

Check the LAMBDA website

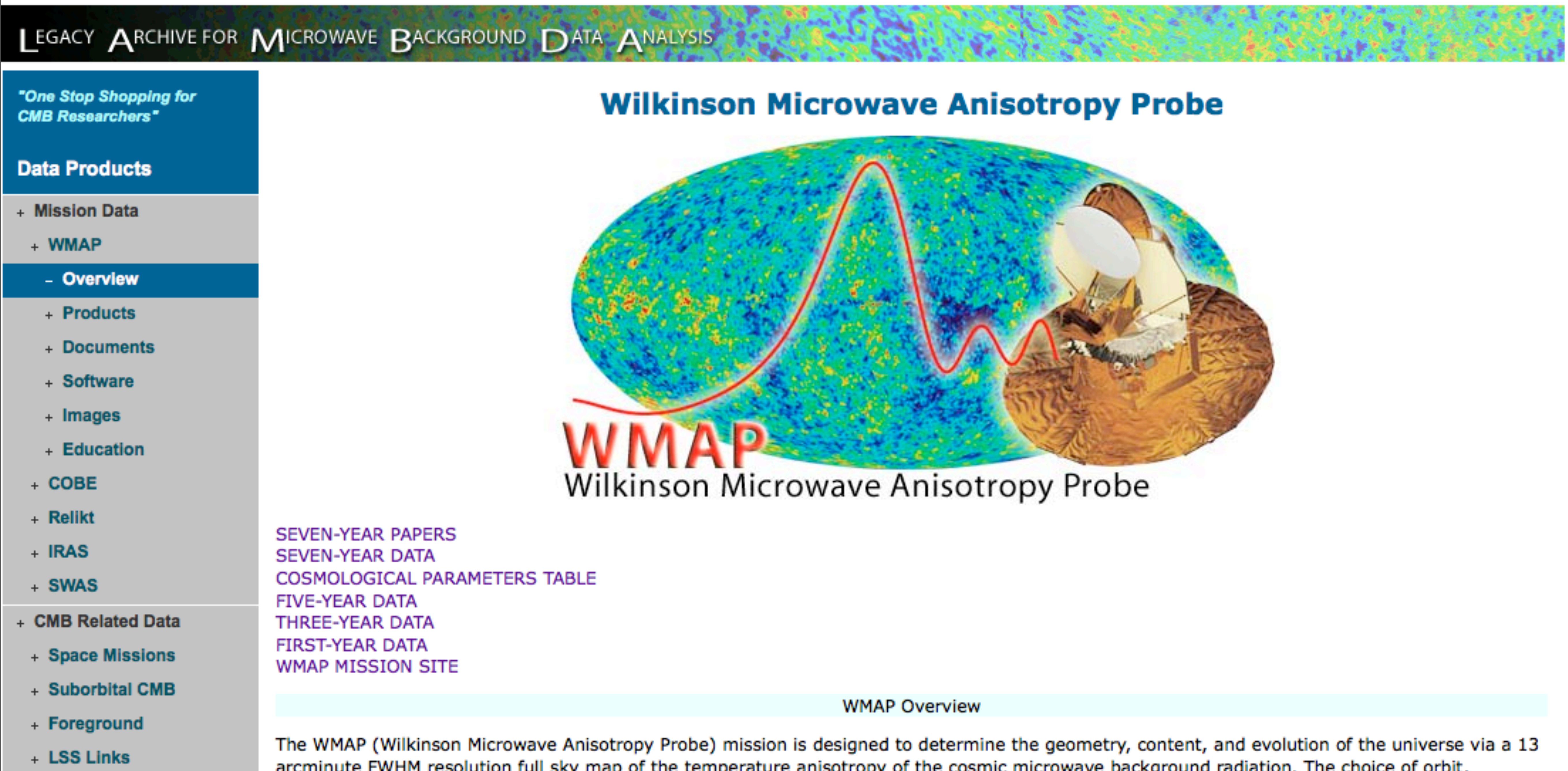

SECONDARY temperature anisotropies

Table 1. Sources of temperature fluctuations.

PRIMARY	Gravity	
	Doppler	
	Density fluctuations	
	Damping	
	Defects	Strings
		Textures
SECONDARY	Gravity	Early ISW
		Late ISW
		Rees-Sciama
		Lensing
	Local reionization	Thermal SZ
		Kinematic SZ
	Global reionization	Suppression
		New Doppler
		Vishniac
"TERTIARY" (foregrounds & headaches)	Extragalactic	Radio point sources
		IR point sources
	Galactic	Dust
		Free-free
		Synchrotron
	Local	Solar system
		Atmosphere
		Noise, *etc.*

Integrated Sachs-Wolfe effect

Temperature anisotropies due to density change and associated gravitational potential (scaler perturbations) at a given point **x** along the direction **n**

Large-scale (linear) anisotropies:

$$\frac{\Delta T}{T}(\vec{n}) \approx \phi_e(\vec{n}) + \int_e^o \frac{\partial \phi}{\partial t} dt + \vec{n} \cdot (\vec{v}_o - \vec{v}_e) + \left(\frac{\Delta T}{T}(\vec{n})\right)_e$$

SW	ISW	Doppler	Acoustic Oscillations
(grav.pot @ decoupling)	(grav.pot evolution)	(motion emitters @ dec)	(photon-baryon @ dec)

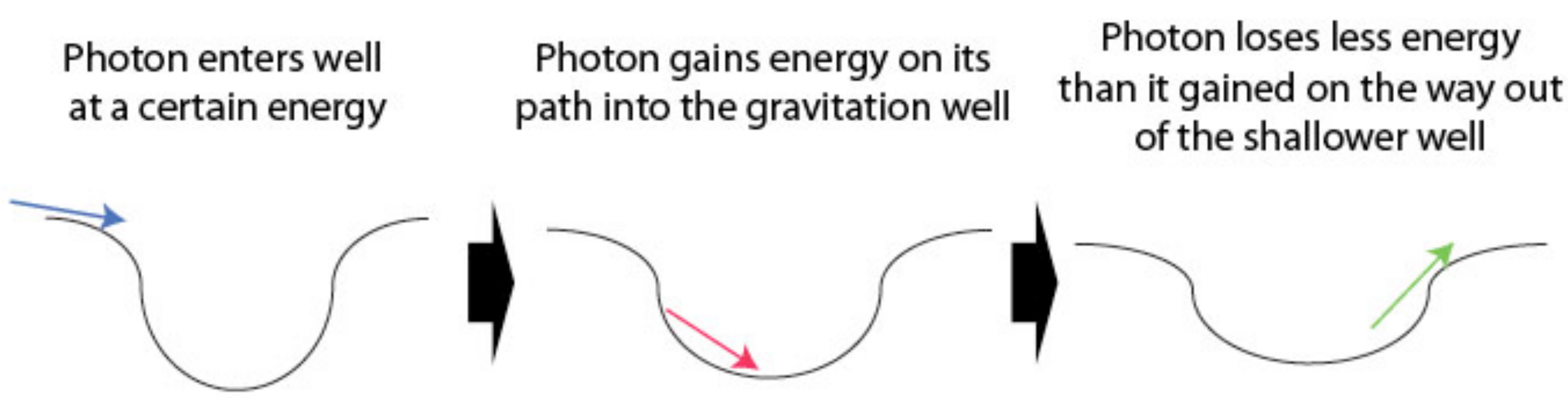

Gravitational well of galaxy supercluster - the depth shrinks as the universe (and cluster) expands

Integrated Sachs-Wolfe effect

- The early ISW effect is caused by the small but non-negligible contribution of photons to the density of the universe

- The late ISW effect:

- Gravitational blueshift on infall does not cancel redshift on climb-out

- Contraction of spatial metric doubles the effect: $\Delta T/T \sim 2\Delta\Phi$

- Effect of potential hills and wells cancel out on small scales

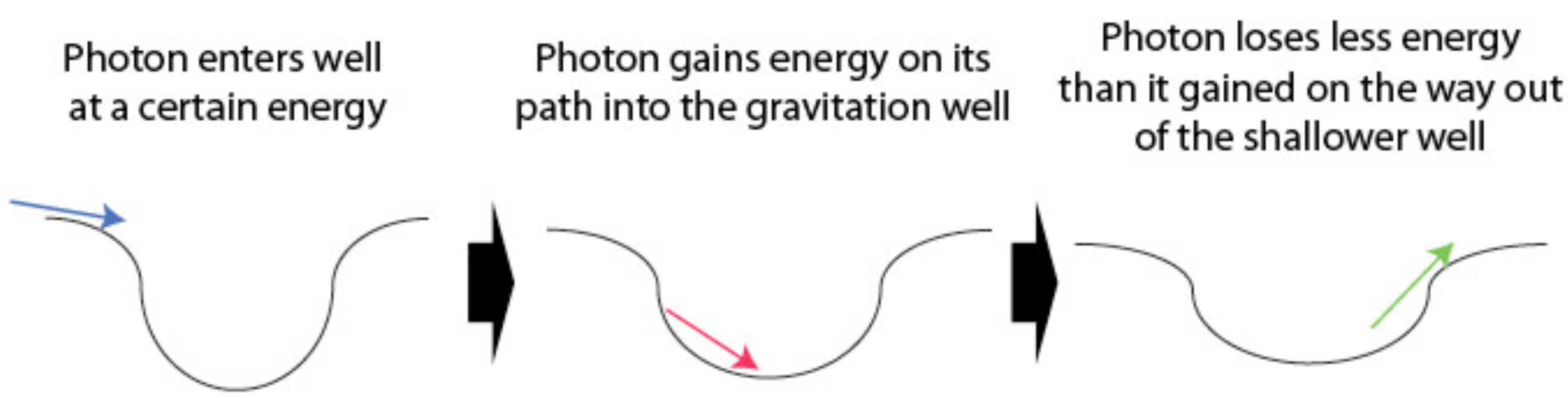

Gravitational well of galaxy supercluster - the depth shrinks as the universe (and cluster) expands

Integrated Sachs-Wolfe effect

ISW effect measures the evolution of ϕ along photon path

$$\Delta_T^{ISW}(\hat{n}) = 2\int dz \frac{d\phi(\hat{n},z)}{dz} \propto \int \mathrm{d}\chi\, a^2 H(a) \frac{\mathrm{d}}{\mathrm{d}a}\frac{D_+}{a}\,\Phi$$

EdS universe : $\boldsymbol{\delta \propto t^{2/3} \propto a}$ **for** $\boldsymbol{\delta << 1}$

$\Omega_m = 1, \Omega_\Lambda = 0, \Omega_k = 0$

ϕ=const *(linear growth = expansion rate)*

E '=E ⟹ No ISW effect

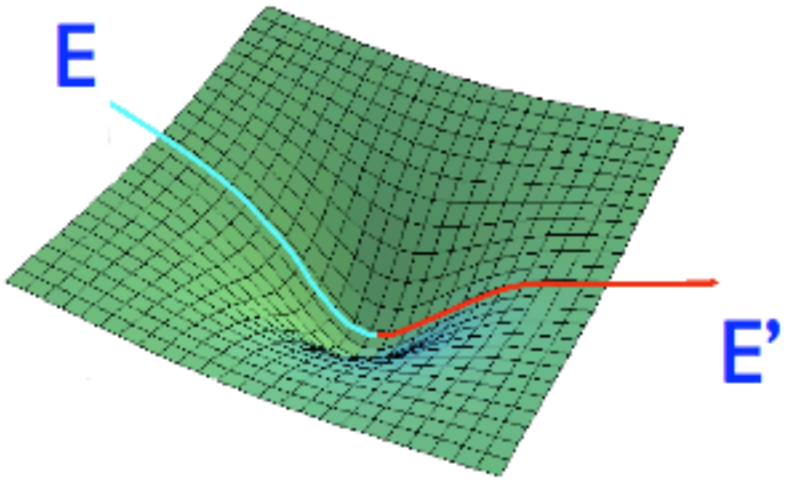

Flat Dark-energy dominated universe (LCDM) :

$\Omega_\Lambda \neq 0, \Omega_k = 0$

ϕ≠const *(linear growth < expansion rate)*

E'>E ⟹ non-zero ISW effect!

detection of ISW effect (in flat FRW universe)⇔ evidence for dark-energy

(Crittenden & Turok 95)

ISW effect as Dark Energy probe

The ISW effect constraints the dynamics of acceleration, be it from dark energy, non-flat geometry, or non-linear growth.

Cosmic evolution of dark energy is parametrized by $w(a) \equiv p_{DE}/\rho_{DE}$
For a cosmological constant, w=–1. In general, $\rho_{DE} \sim a^{-3(1+w)}$

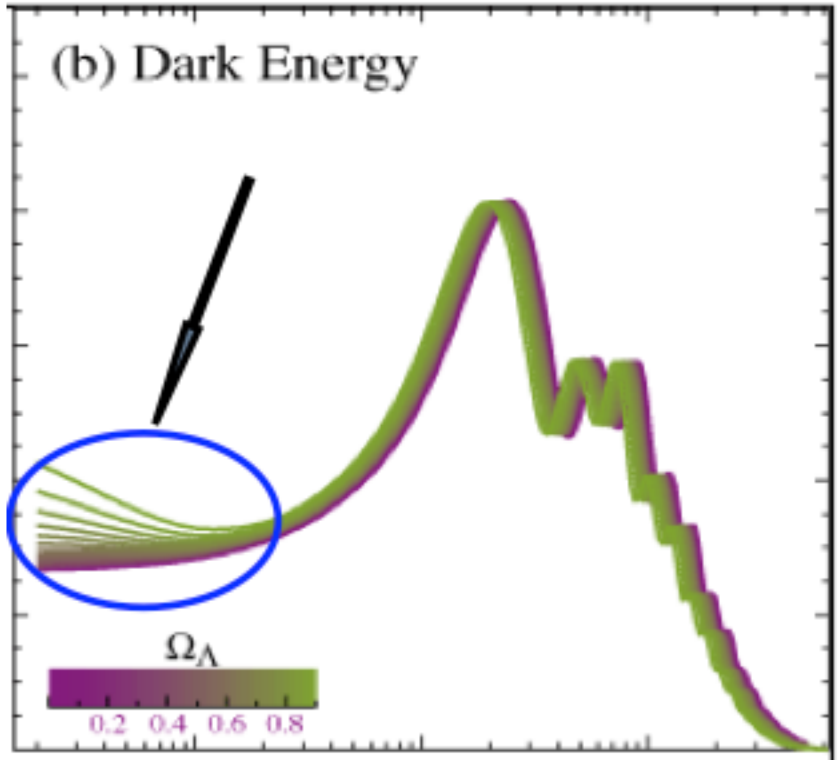

- Linear regime - Integrated Sachs-Wolfe effect (ISW) (Sachs & Wolfe 1967)
- Non-linear regime - Rees-Sciama effect (RS) (Rees & Sciama 1968)

In the absence of curvature, measurement of ISW is measurement of DE.

Cosmic variance problem

Primary anisotropies (SW+acoustic peaks) largely dominate the ISW signal

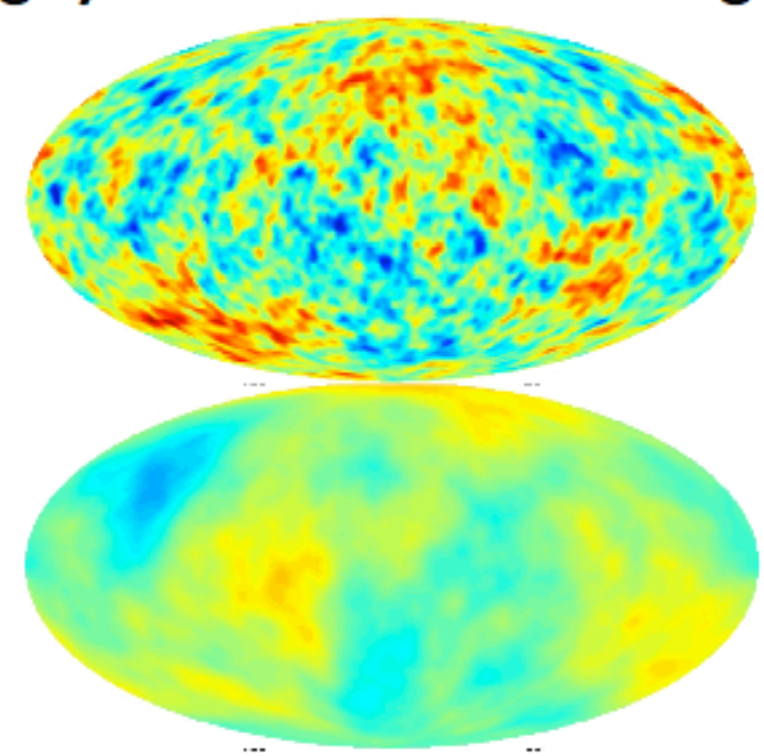

primary
(z~1000)

ISW
(z<3)

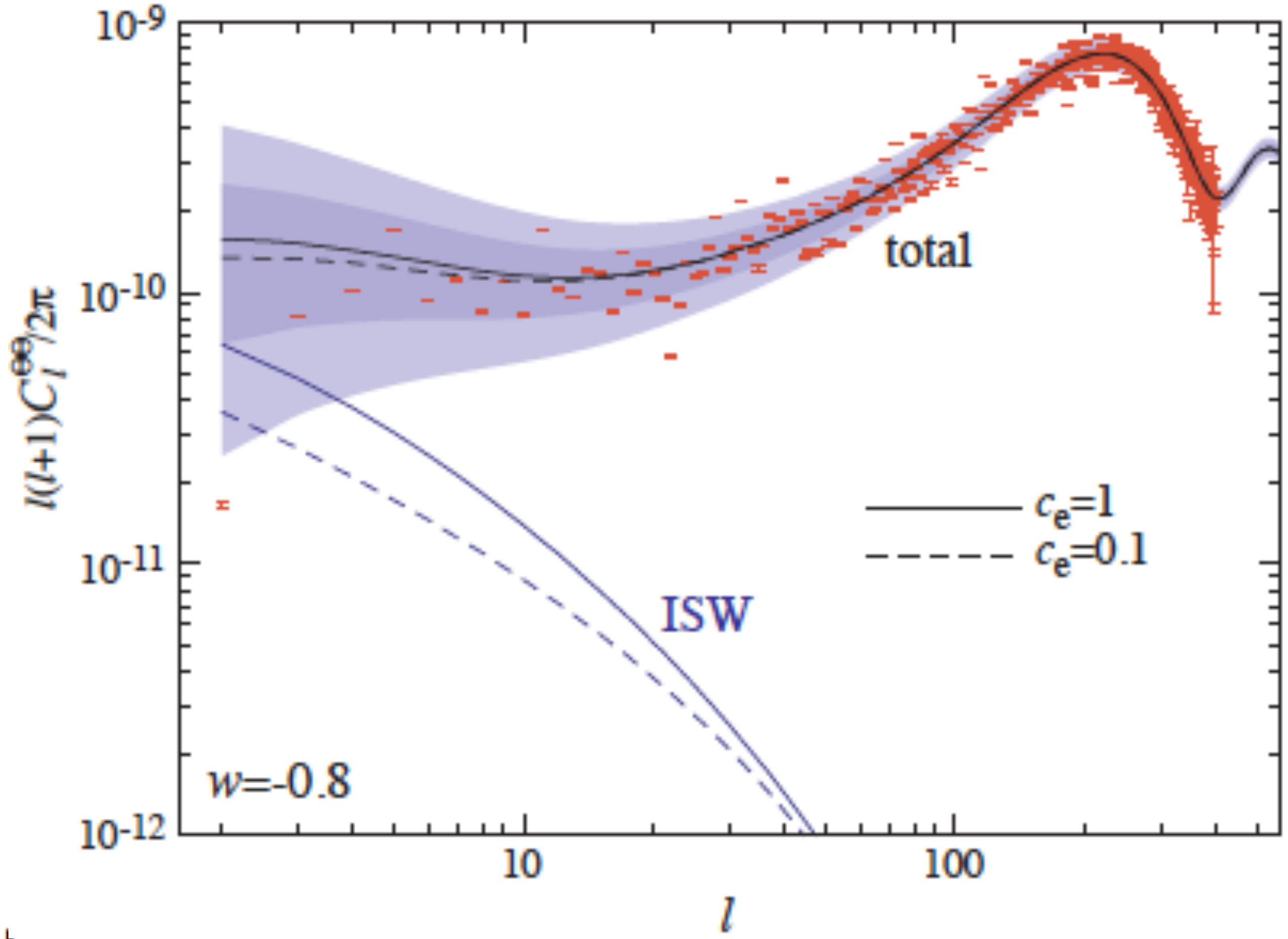

Large-scale anisotropies are dominated by cosmic variance (impossible to extract the ISW signal from CMB maps alone)

Cosmic variance problem

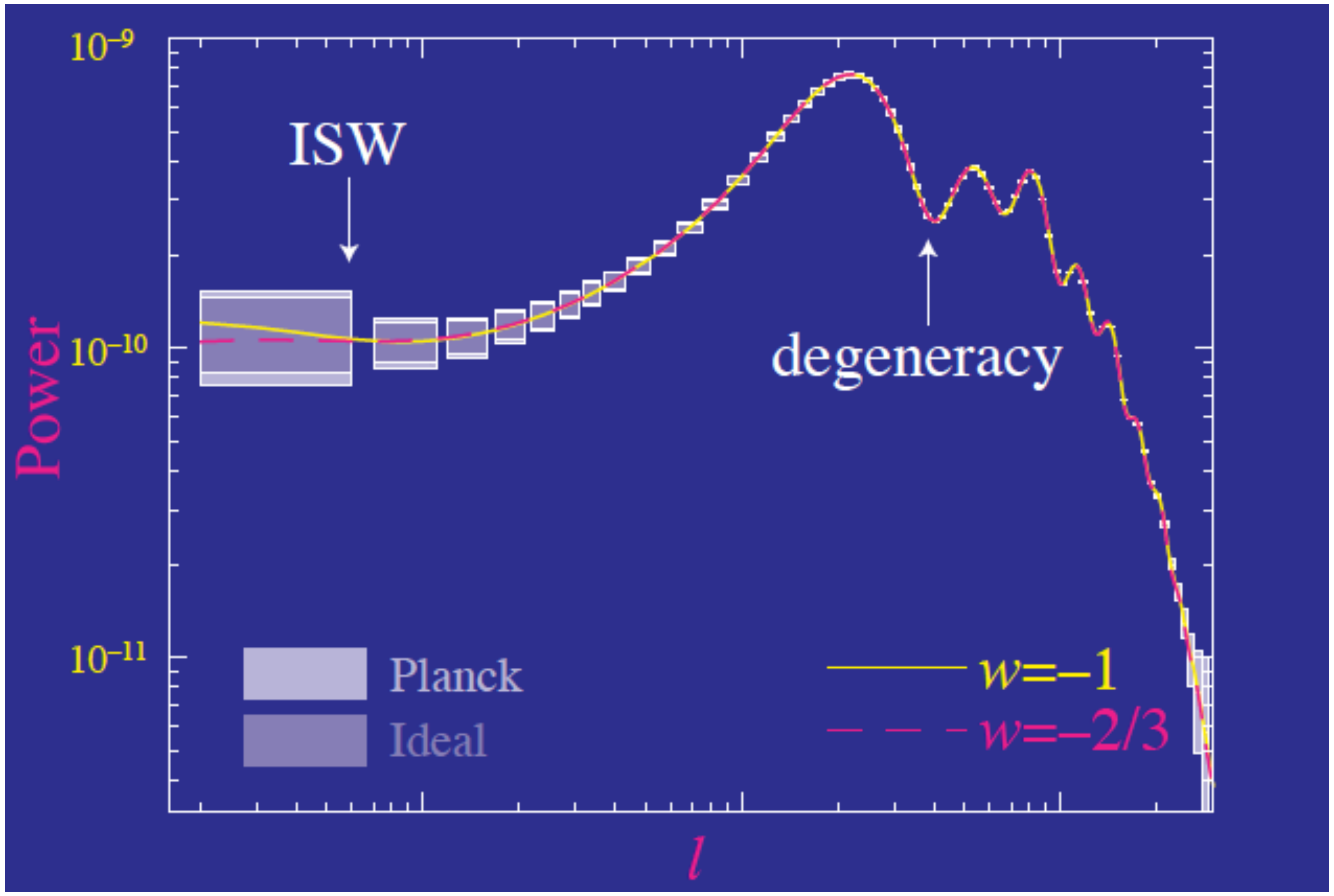

thermal SZ effect—ISW cross-correlation
(Creque-Serbinowski et al. 2016)

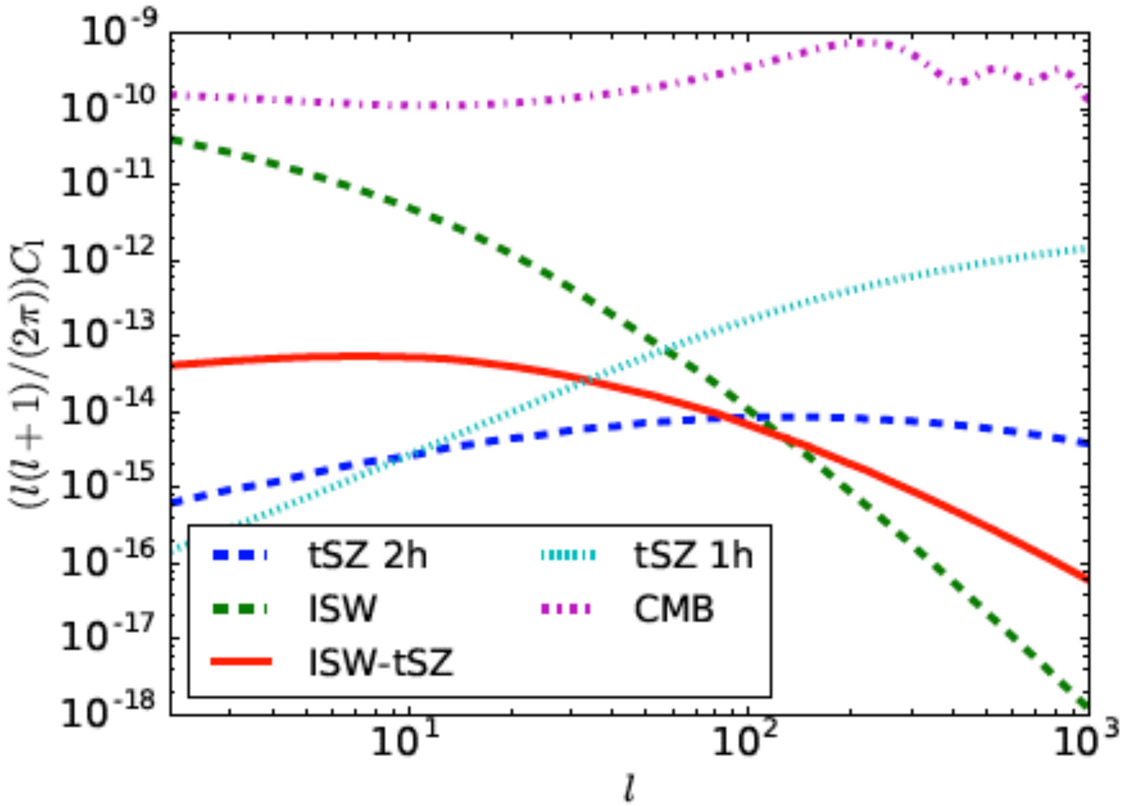

FIG. 1. The ISW power spectrum $C_l^{\rm isw}$ (green) and the two-halo contribution $(y, 2h)$ to C_l^{yy} (blue) are shown in dashed lines, while C_l^{yT} is shown in solid red. The one-halo contribution $(y, 1h)$ to C_l^{yy} is dotted. The CMB power spectrum is shown dot-dashed for comparison.

Solution: Cross-correlate with other probes of dark energy, which has large sky coverage (e.g. optical, X-ray or radio surveys of galaxies, tSZ signal)

ISW optical-survey correlation

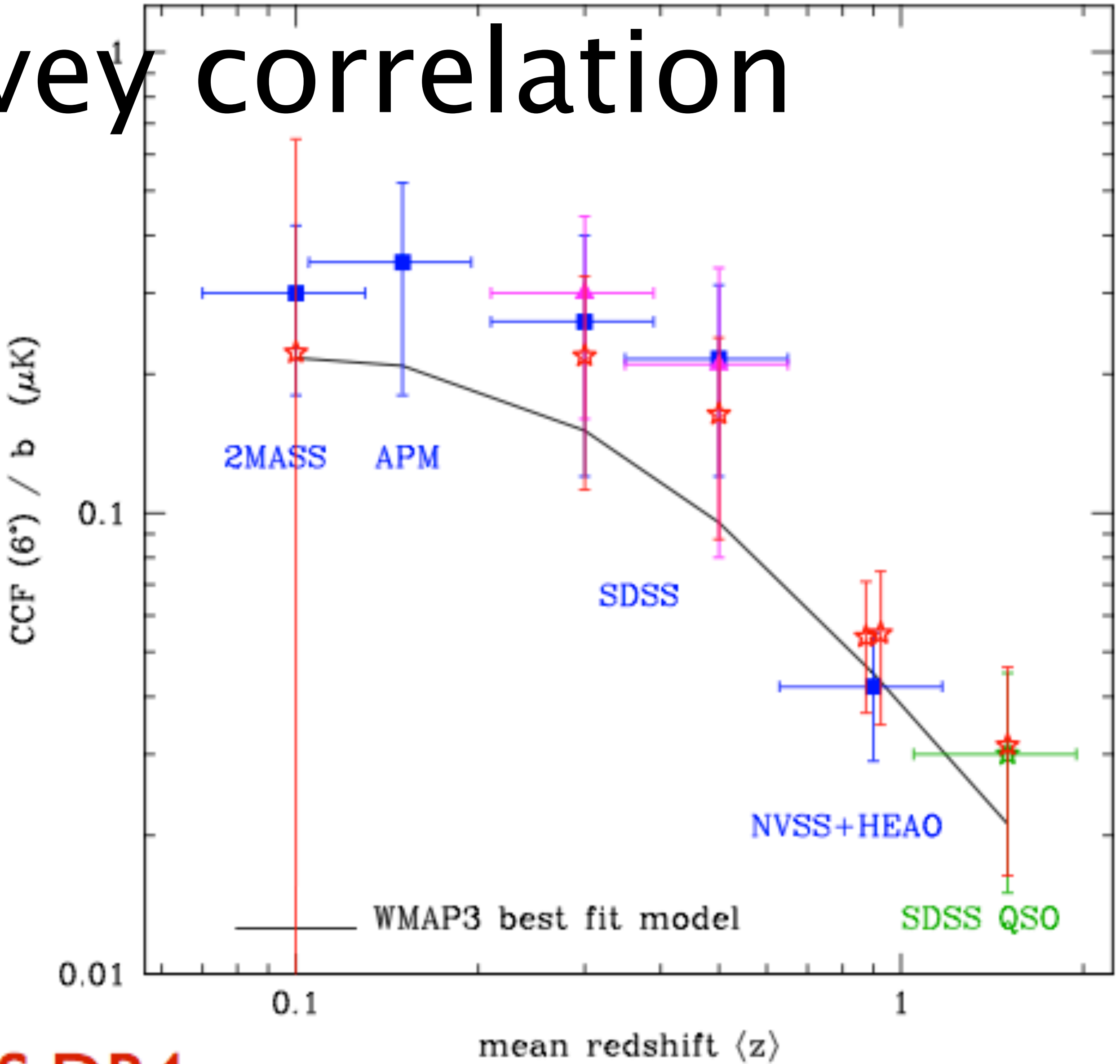

Cosmological Constraints

- each *individual* detection points to a DE dominated universe, $\Omega_\Lambda \approx 0.7 - 0.8$
- all ISW data *combined* reject null detection with $P \simeq 99.997\%$
- all ISW + SNIa $\Omega_\Lambda = 0.71 \pm 0.13$ and $\Omega_m = 0.29 \pm 0.04$.

CMB-LSS cross-correlations: WMAP3-SDSS DR4

(Cabre et al, astro-ph/0603690)

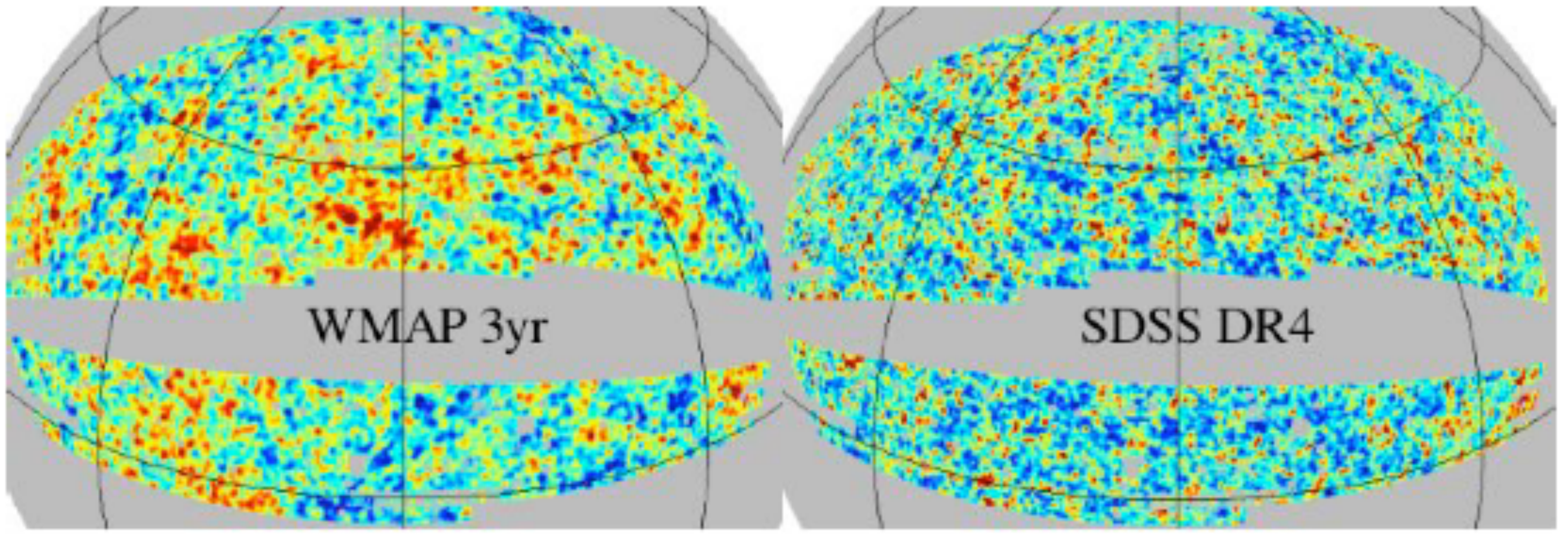

SECONDARY temperature anisotropies

Table 1. Sources of temperature fluctuations.

PRIMARY	Gravity	
	Doppler	
	Density fluctuations	
	Damping	
	Defects	Strings
		Textures
SECONDARY	Gravity	Early ISW
		Late ISW
		Rees-Sciama
		Lensing
	Local reionization	Thermal SZ
		Kinematic SZ
	Global reionization	Suppression
		New Doppler
		Vishniac
"TERTIARY" (foregrounds & headaches)	Extragalactic	Radio point sources
		IR point sources
	Galactic	Dust
		Free-free
		Synchrotron
	Local	Solar system
		Atmosphere
		Noise, *etc.*

ΔT from reionization

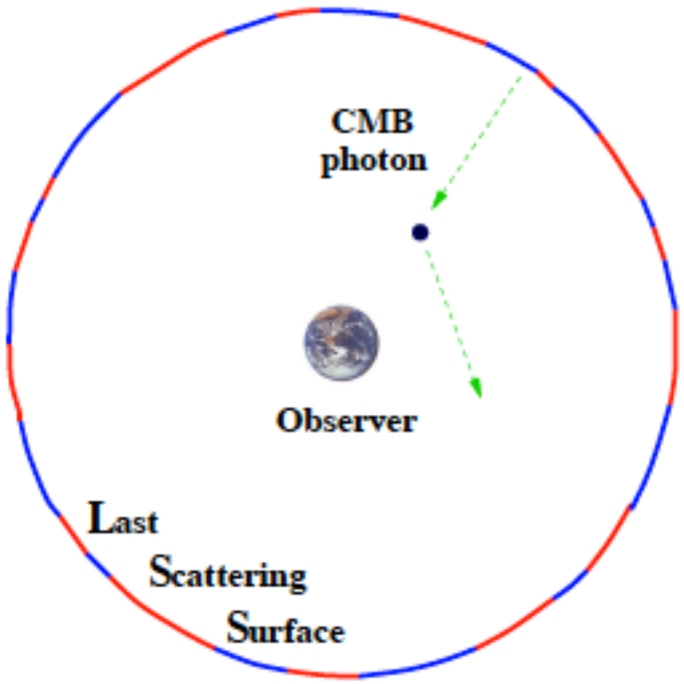

$$\frac{\Delta T}{T_0}(\theta) = e^{-\tau}\ \frac{\Delta T}{T_0}(\theta)\Big|_{orig.} + \frac{\Delta T}{T_0}(\theta)\Big|_{new}$$

"suppression (blurring)" & "generation"

Re-scattering of CMB photons damps anisotropy power (ΔT^2) as $e^{-2\tau}$, with τ the optical depth to Thomson scattering.

For τ = 0.095, this means a 20% reduction from initial power.

New perturbations are generated on small scales due to the bulk motion of electrons in over-dense regions (Ostriker-Vishniac effect)

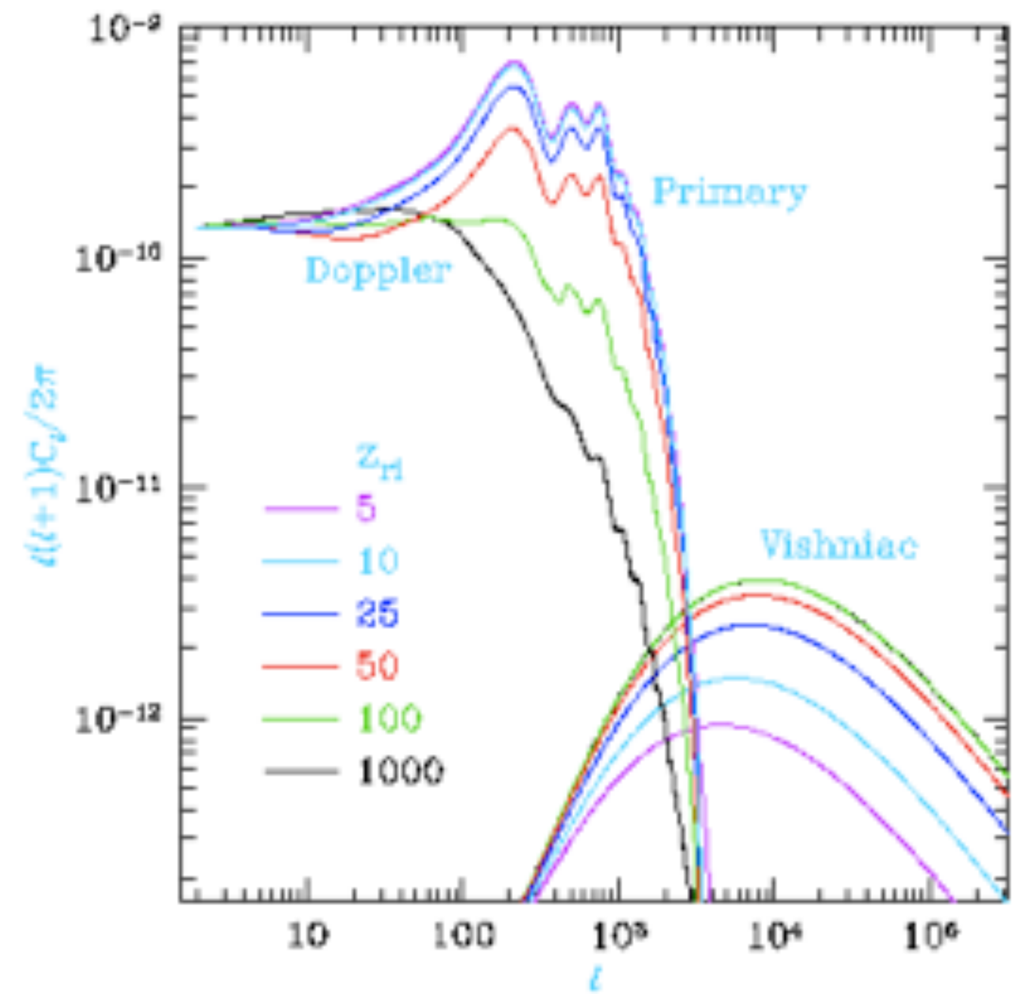

Other small effects..

Resonant scattering by atoms and molecules (CMB spectroscopy!)

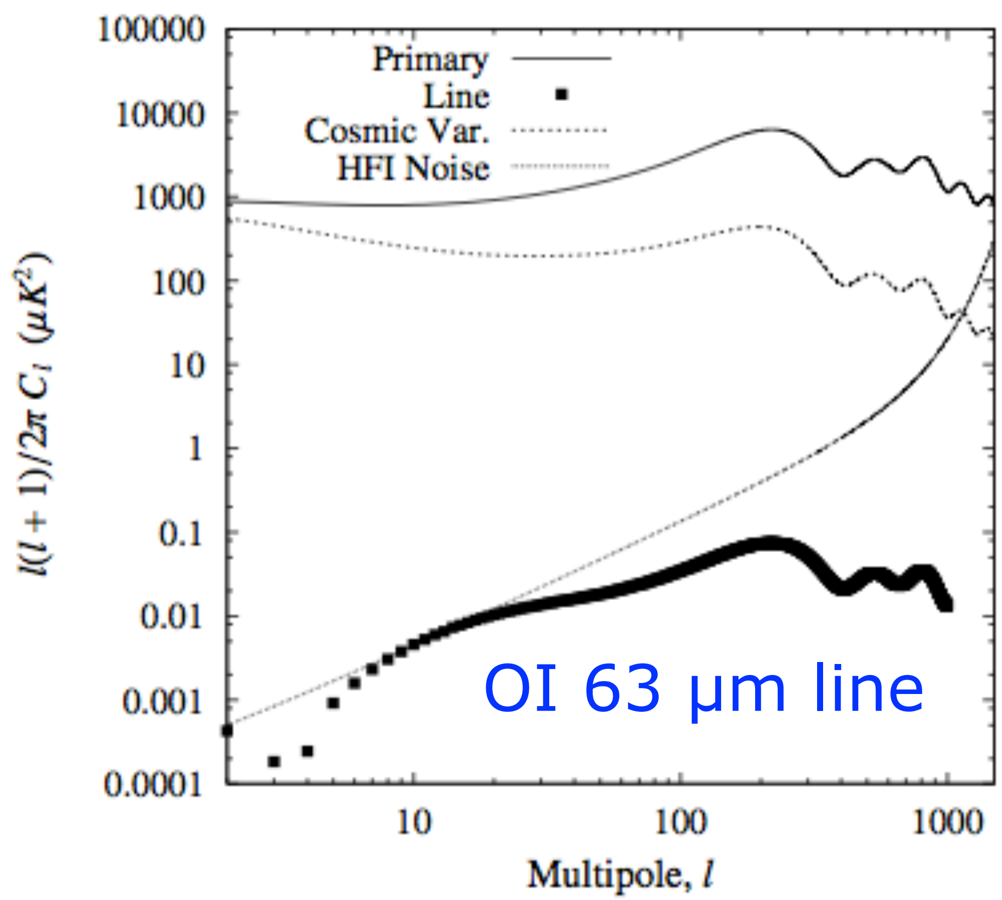

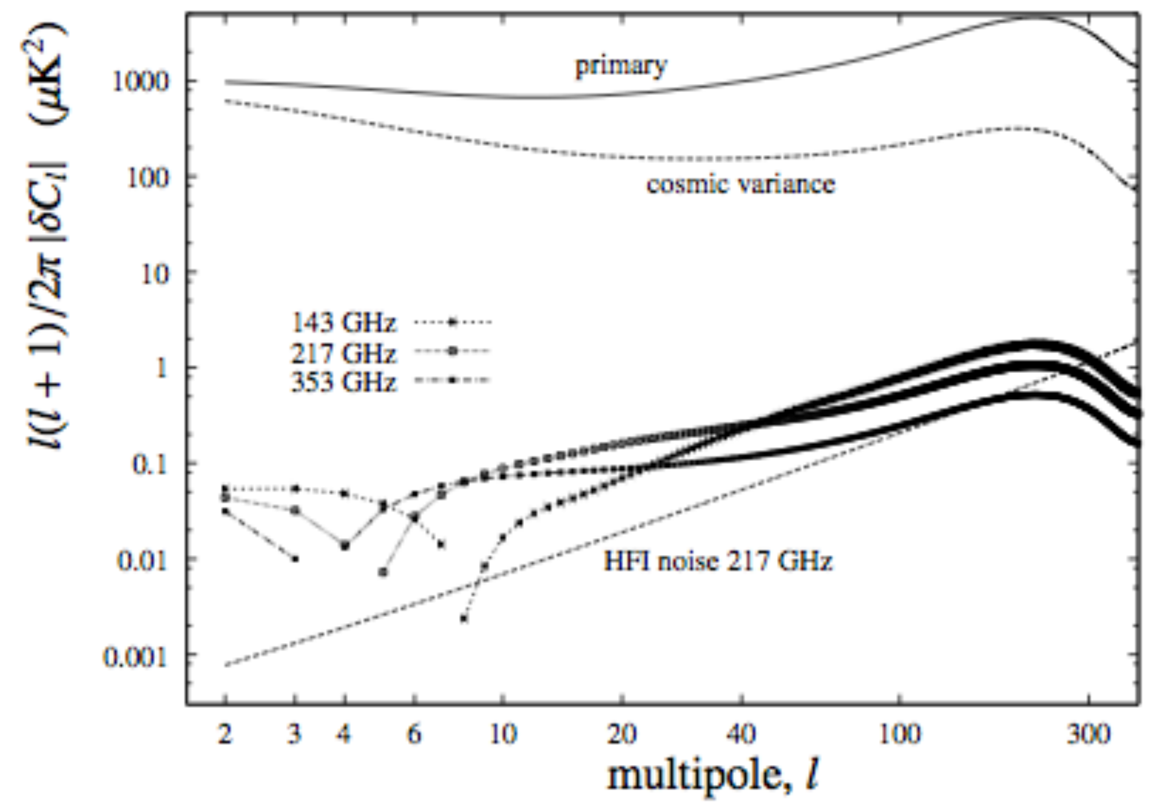

Basu, Hernandez-Monteagudo & Sunyaev 2004

$$\frac{\delta T}{T_0}(\boldsymbol{n}, z=0) = (1-\tau_{X_i})\,\frac{\delta T}{T_0}(\boldsymbol{n}, z_{X_i}) + \tau_{X_i}\,\frac{\delta T}{T_0}\bigg|_{\text{new}}^{\text{lin}}(\boldsymbol{n}, z_{X_i}) + O\left[\tau_{X_i}^2\right].$$

$$\Rightarrow$$

$$\delta C_l \equiv C_l^{X_i} - C_l = \tau_{X_i}\cdot C_1 + \tau_{X_i}^2\cdot C_2 + O\left(\tau_{X_i}^3\right).$$

Lensing of the CMB power

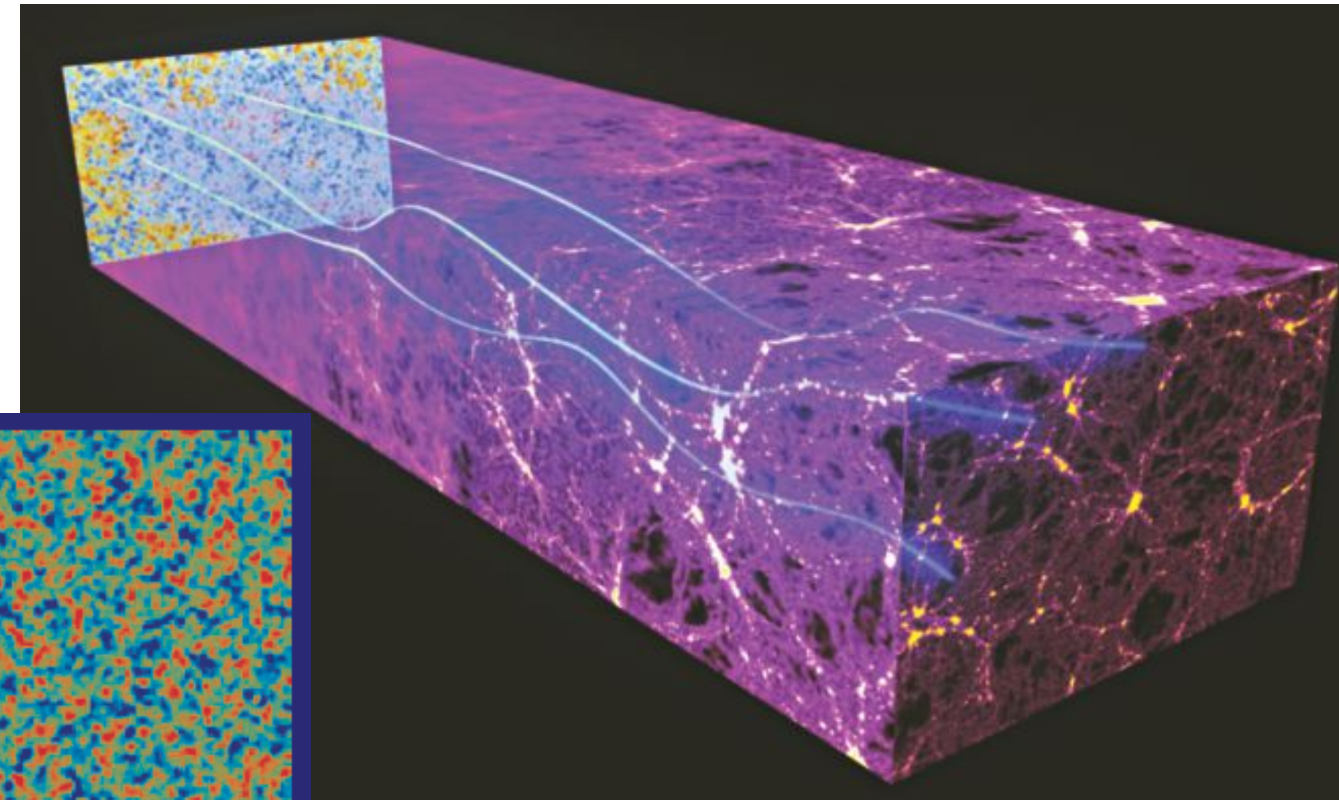

CMB photons get deflected by the intervening large scale structure.

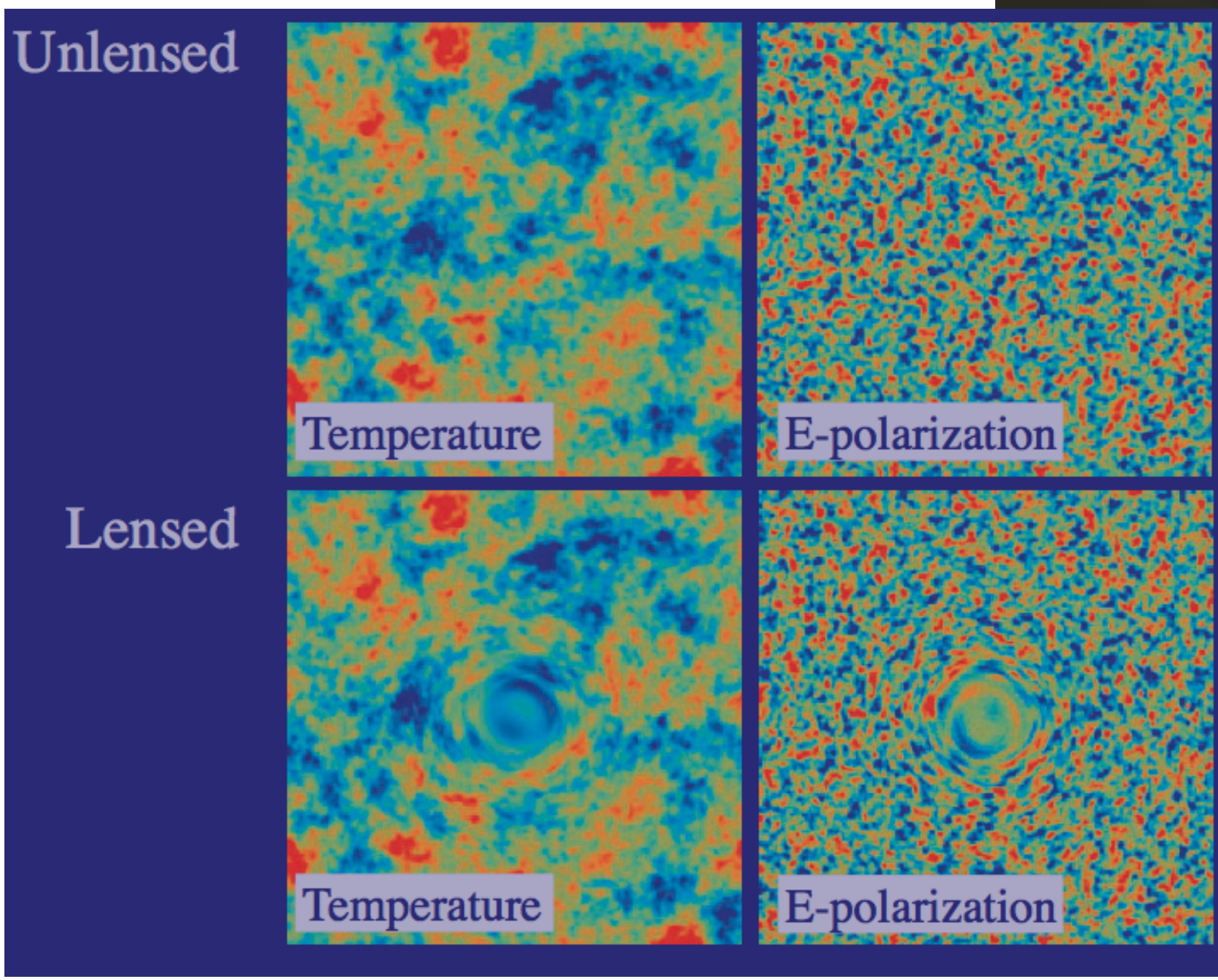

One result of CMB lensing is blurring of temperature anisotropies, as the angular scales associated with the peaks are distorted.

Another result is the mixing of different polarization modes (E modes into B modes).

Lensing of the power spectrum

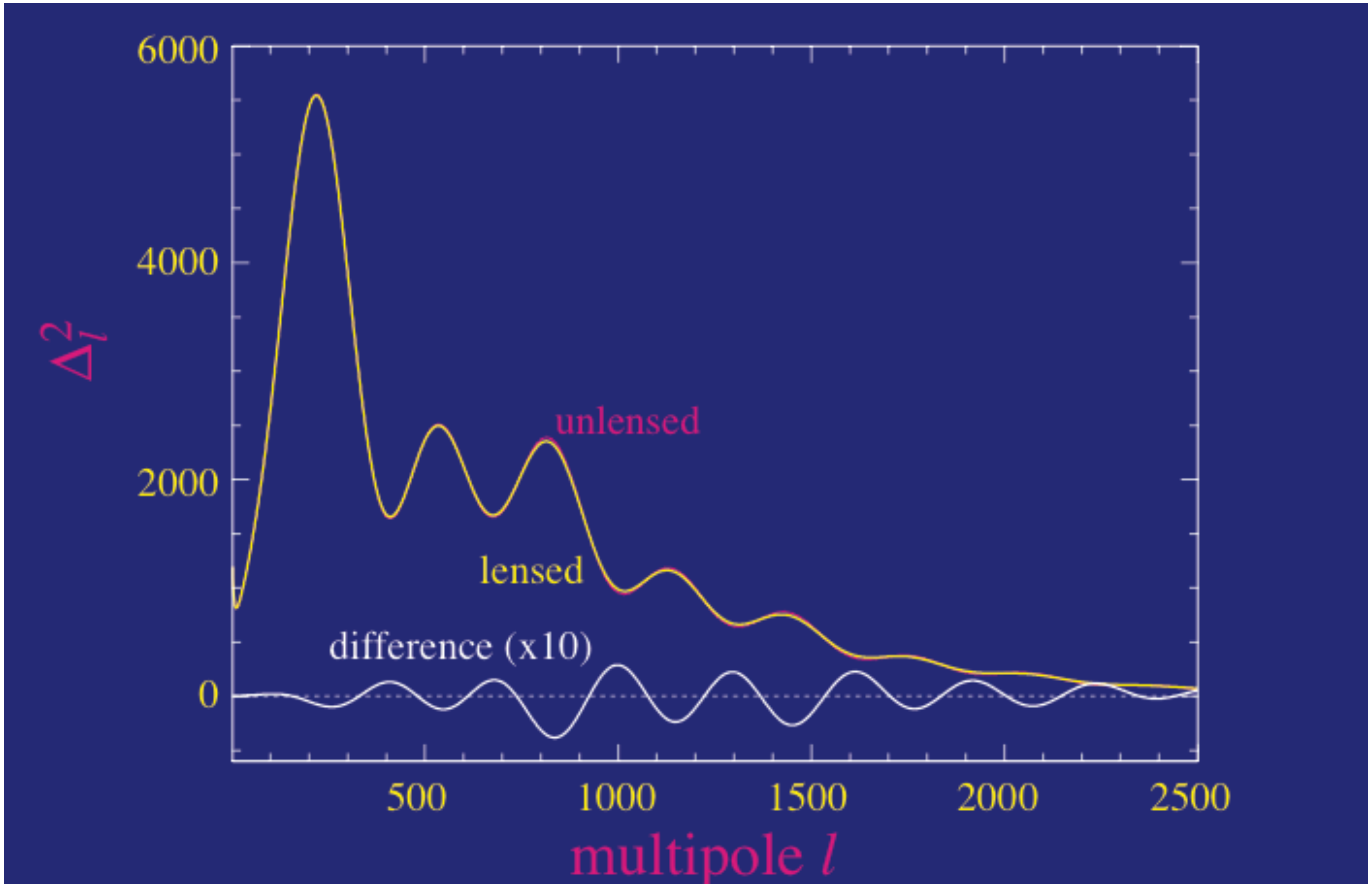

Lensing smooths the temperature power spectrum (and E mode polarization) with a width Δl~60

This is a small, subtle effect, reaching ~10% in the damping tail. However, it is easier to measure at large angles (Planck) due to low foregrounds.

CMB lensing measurements

$$\phi(\hat{\mathbf{n}}) = 2\int \frac{dz}{H(z)} \frac{D_A(D_s - D)}{D_A(D)\, D_A(D_s)} \Phi(D_A \hat{\mathbf{n}}, D)$$

$$x(\hat{\mathbf{n}}) \rightarrow x(\hat{\mathbf{n}} + \nabla\phi)$$

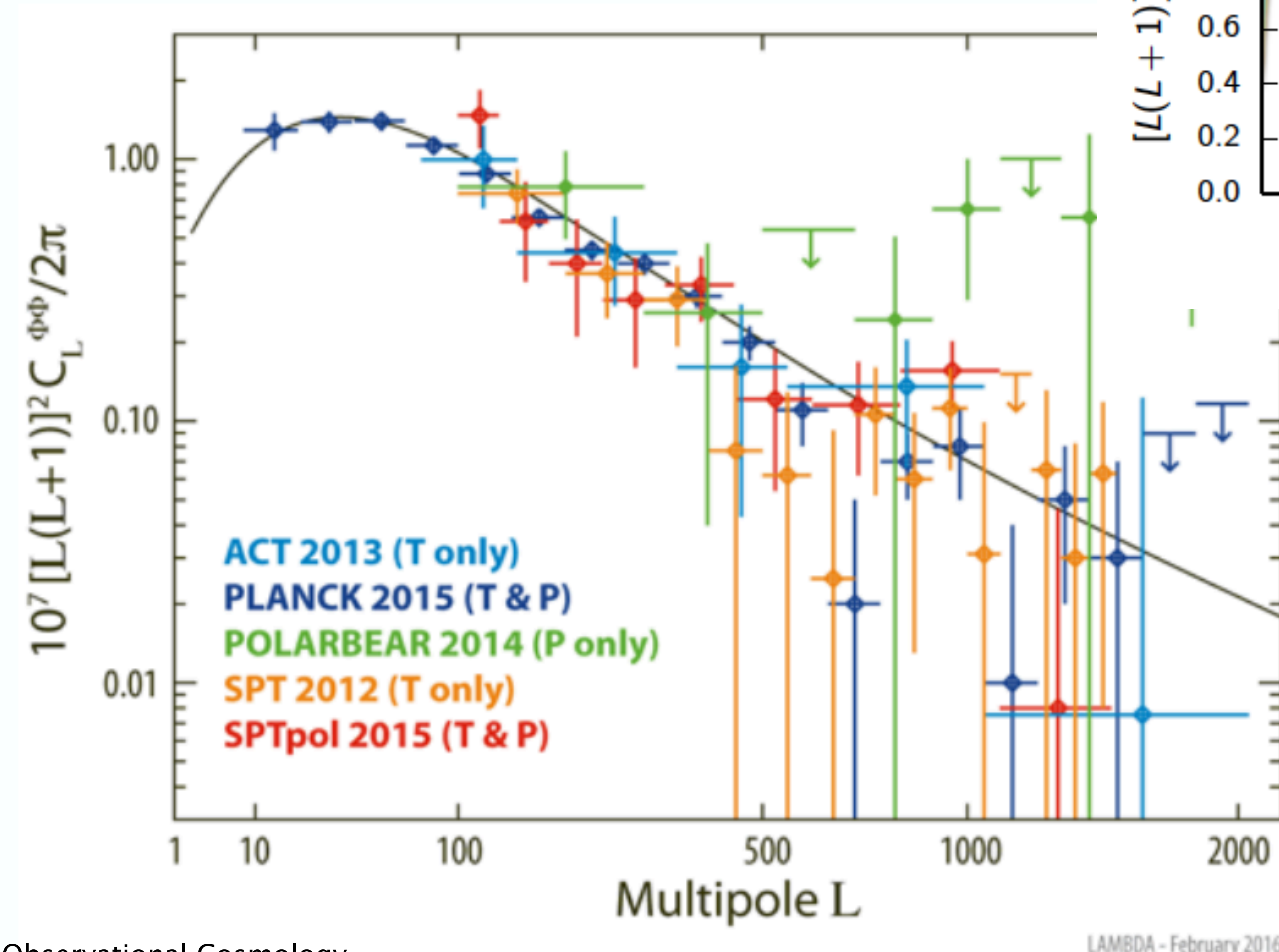

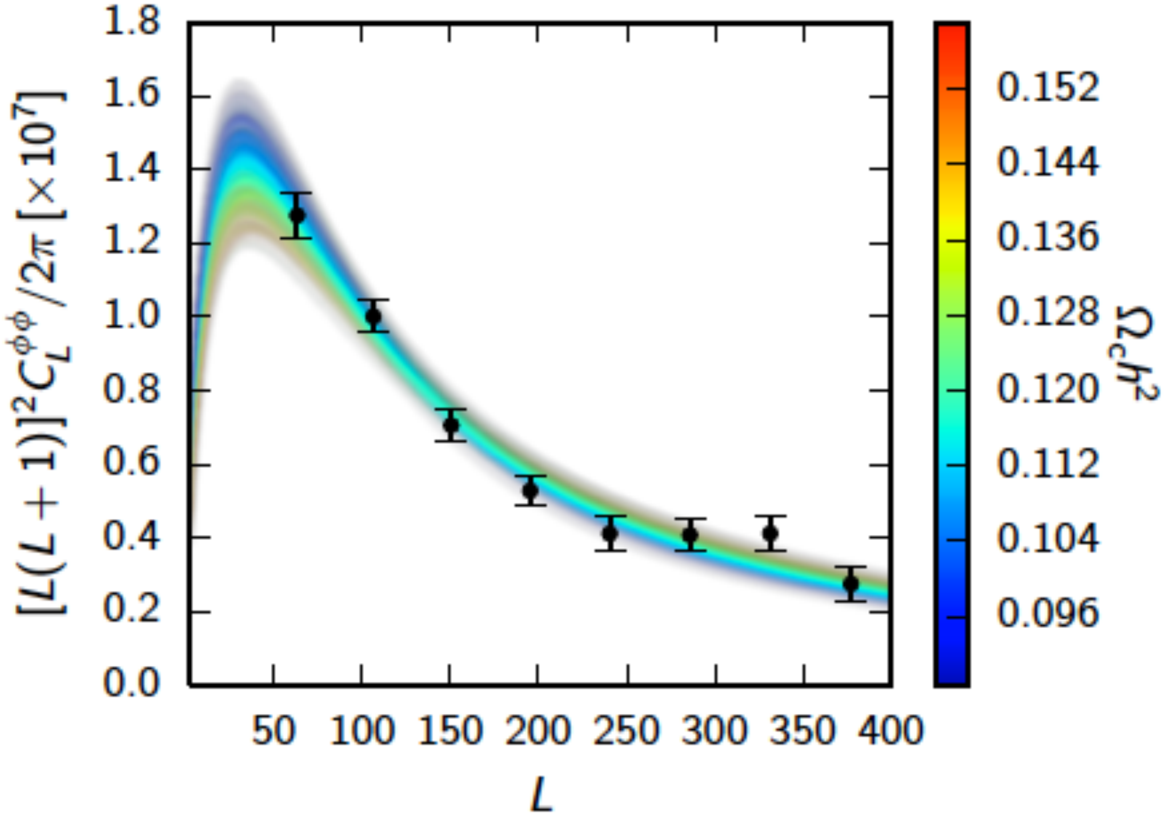

Planck 2015 results

CMB lensing measurements

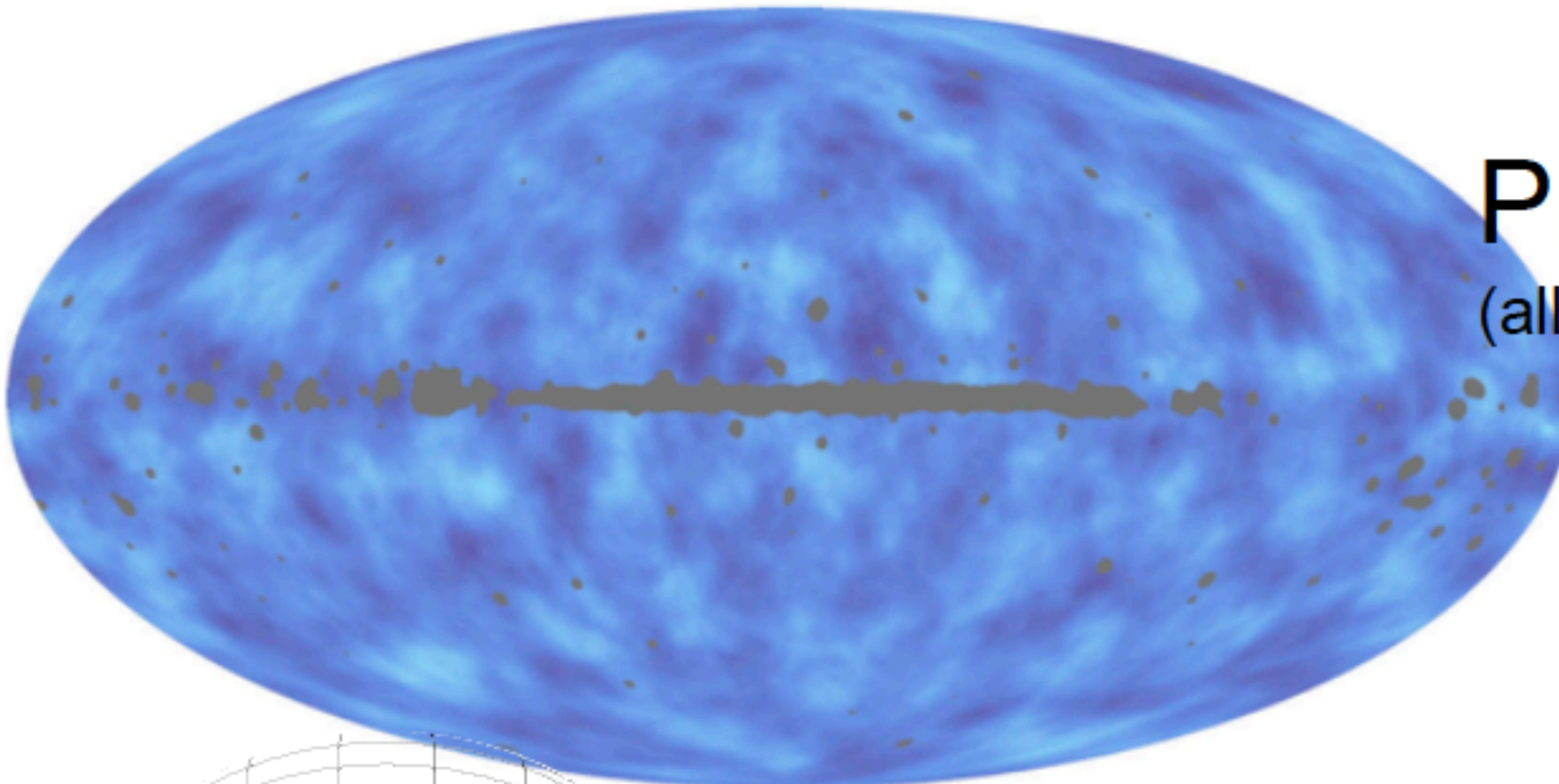

Planck
(all-sky)

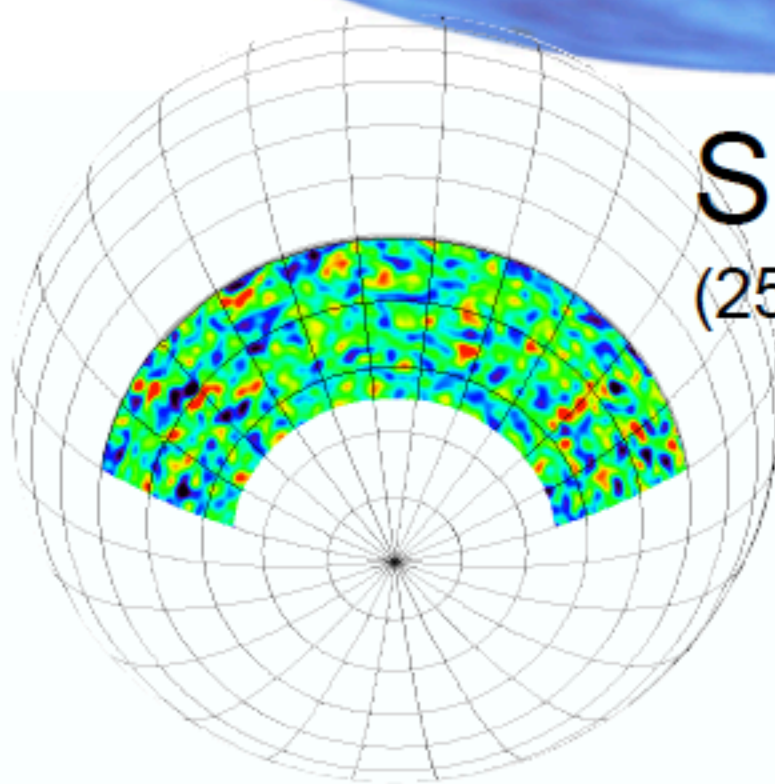

SPT
(2500 sq deg)

SPT-Pol
(100 sq deg)

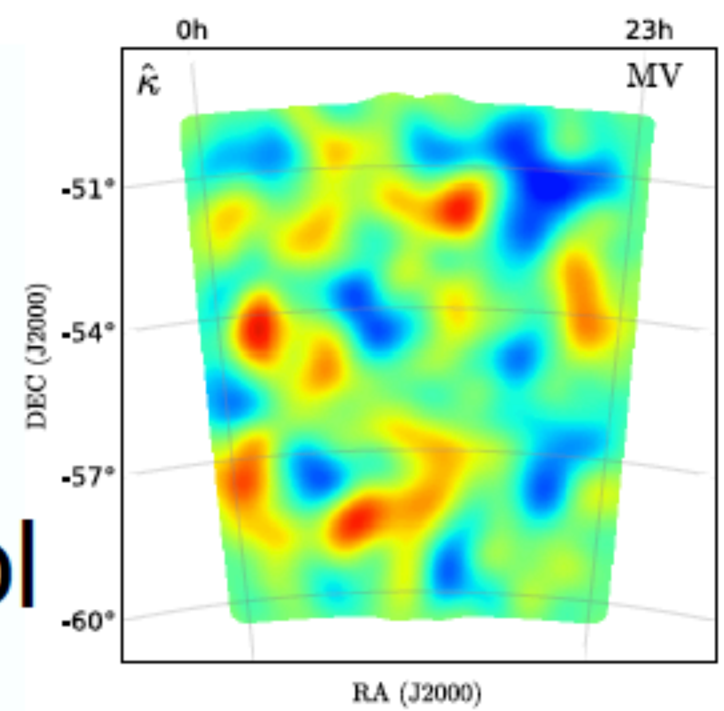

Power at small angular scales

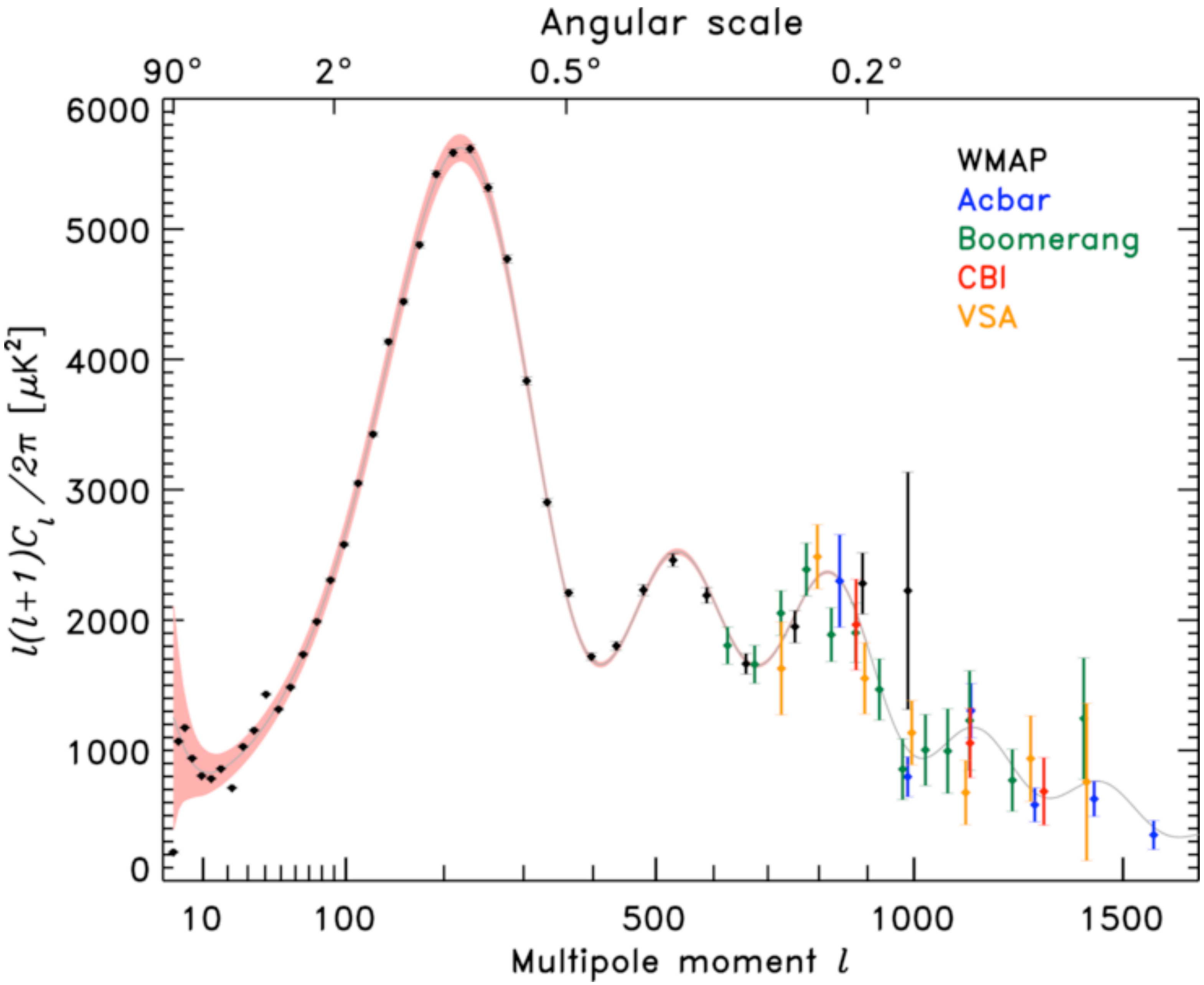

The signal is actually C_l — our power spectrum plots boosts the apparent variance at large l by a factor l^2 ! Observations at high-l therefore requires far greater sensitivity.

Recent large-ℓ measurements

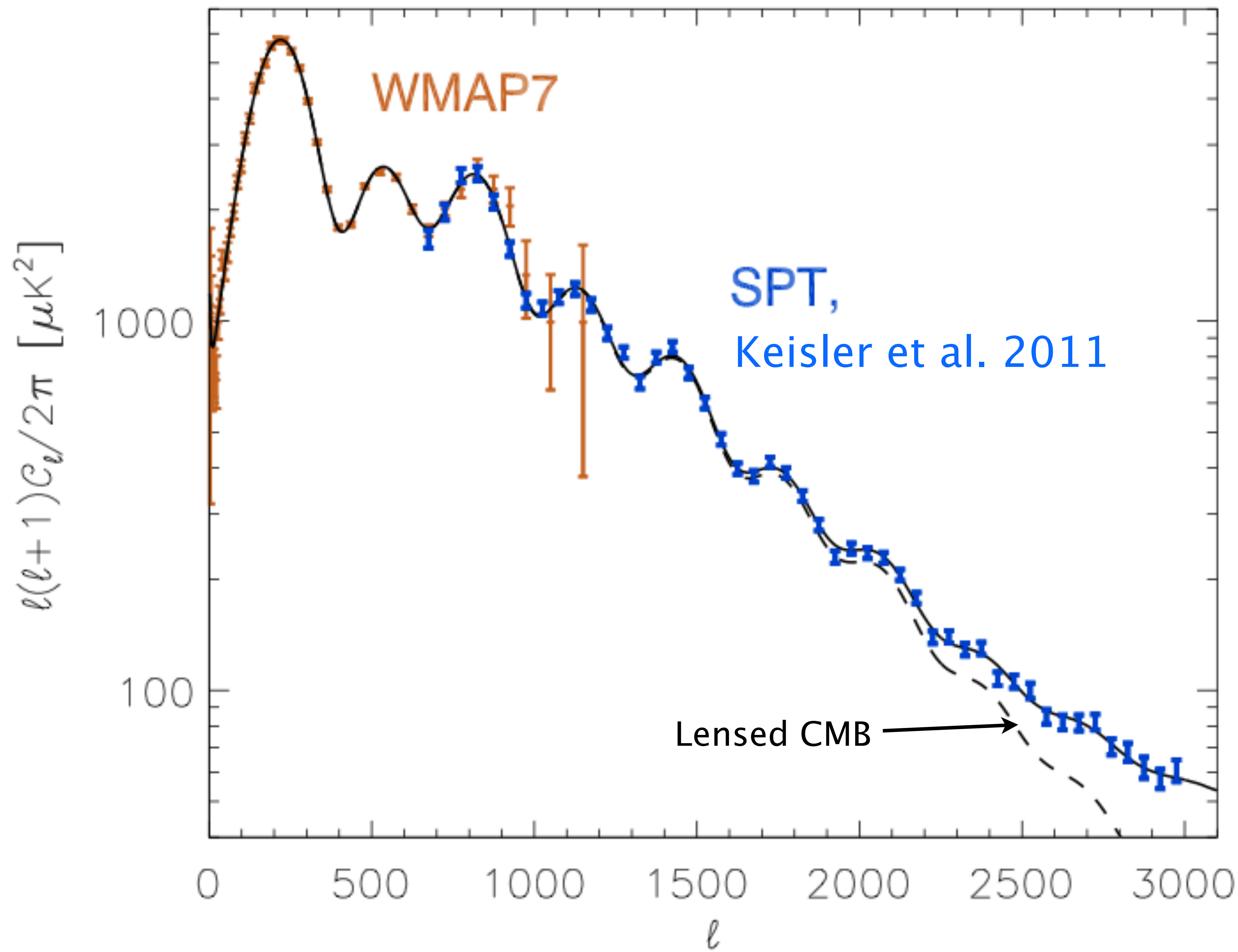

Local y-distortion: thermal SZ effect

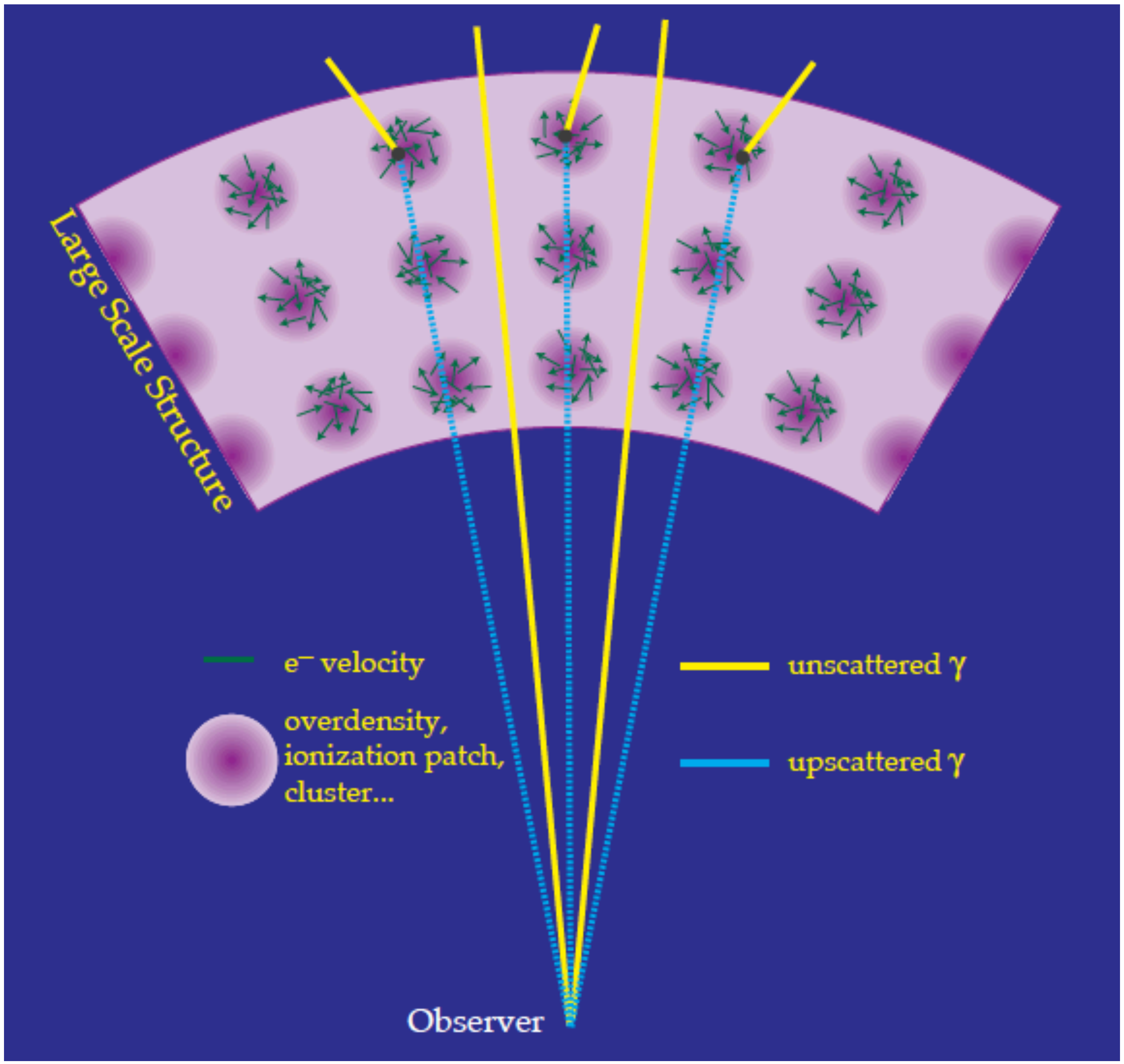

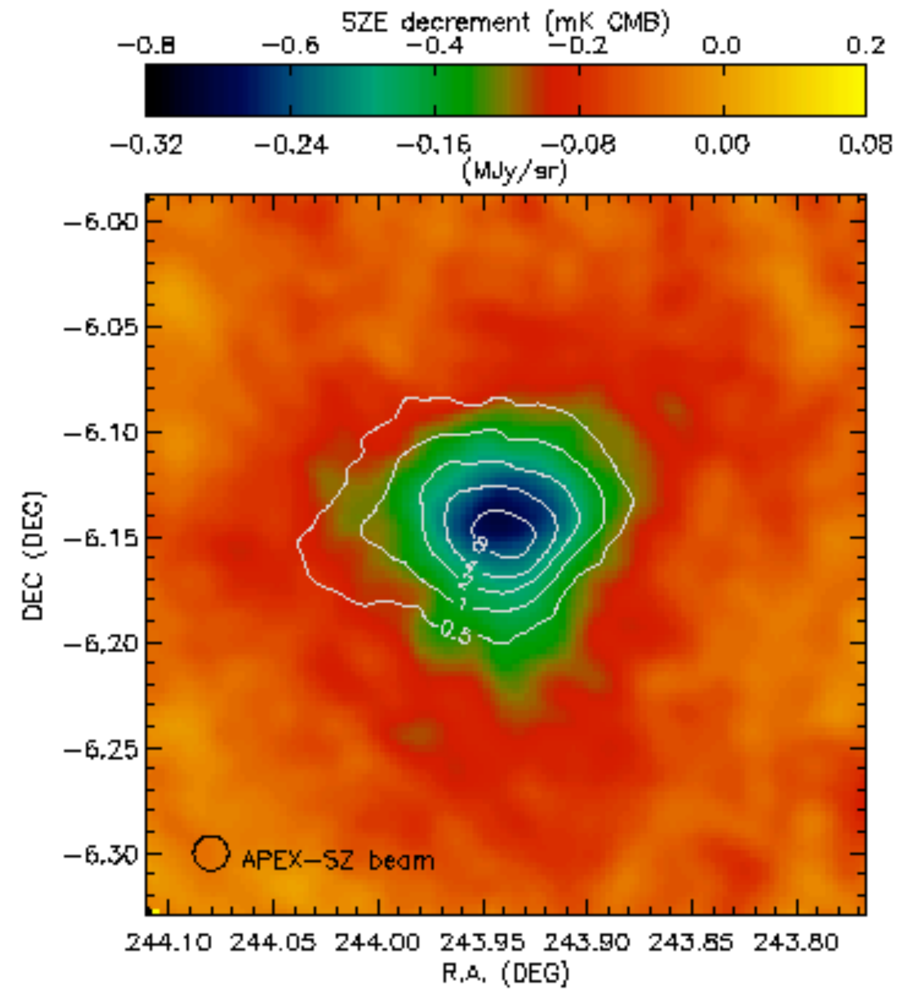

$$\frac{\Delta T}{T_{\rm CMB}} = -2y$$

$$y = \int n_{\rm e}(r)\sigma_{\rm T}\frac{k_{\rm B}T_{\rm e}(r)}{m_{\rm e}c^2}dl$$

tSZ power spectrum

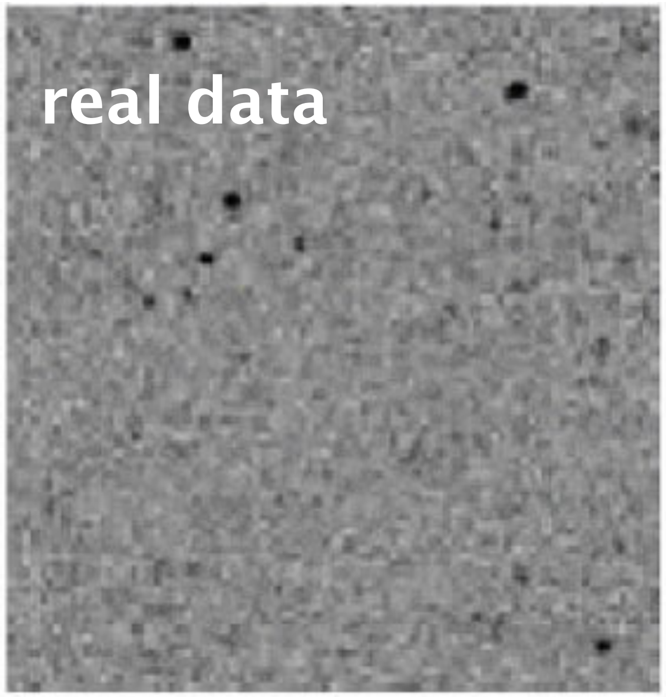

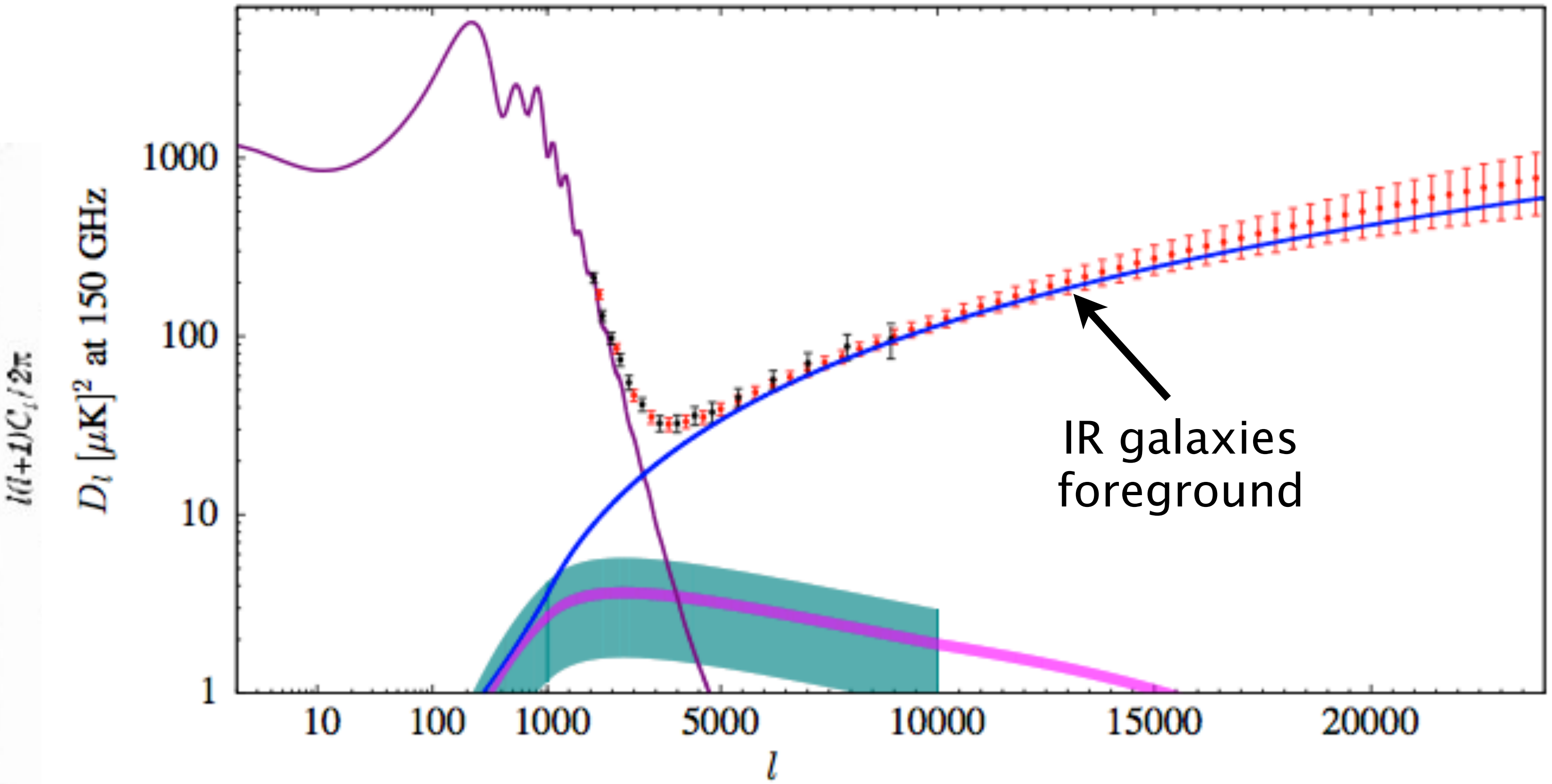

Ramos-Ceja, Basu et al. 2014

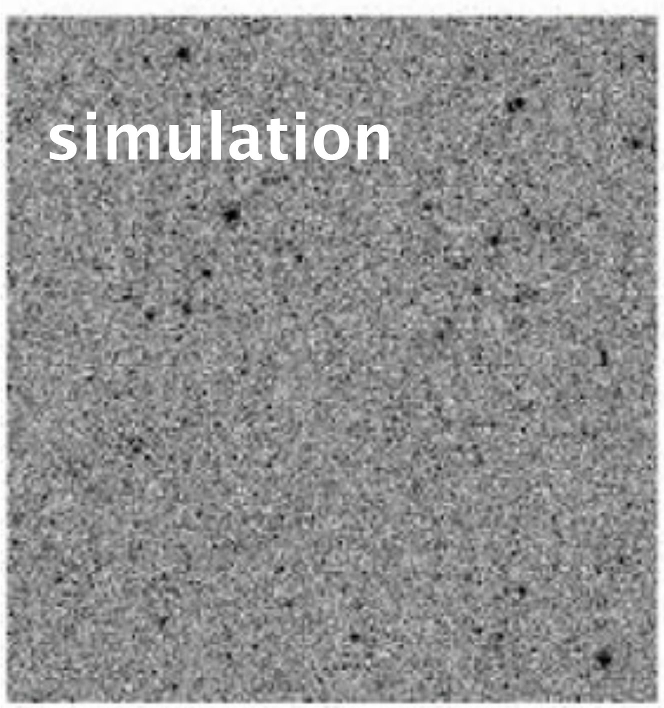

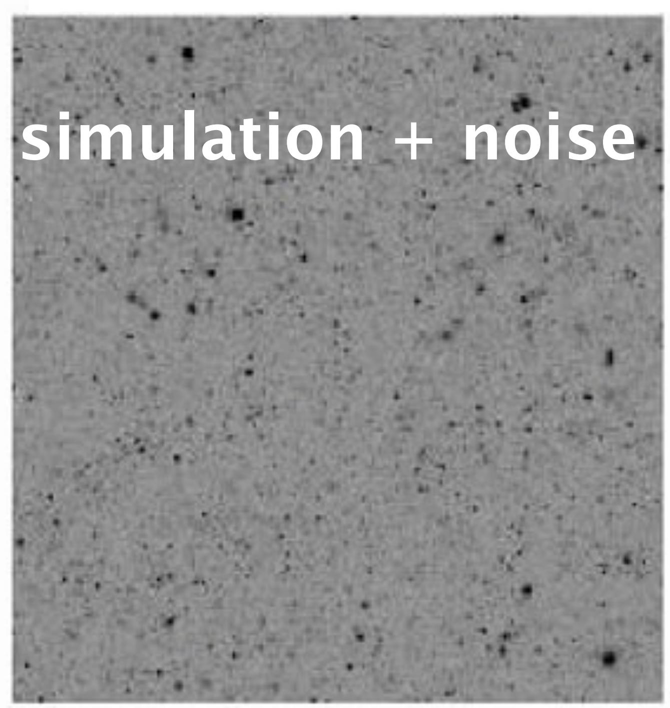

Simulation and observation of high-resolution CMB sky at 150 GHz.

Clusters in the SZ effect show up as dark shadows!

SZ power spectrum

SZ power spectrum is a powerful probe of cosmology, primarily through its strong dependance on σ_8

$$\frac{l(l+1)C_l}{2\pi} \simeq 330\ \mu\mathrm{K}^2 \sigma_8^7 \left(\frac{\Omega_b h}{0.035}\right)^2$$

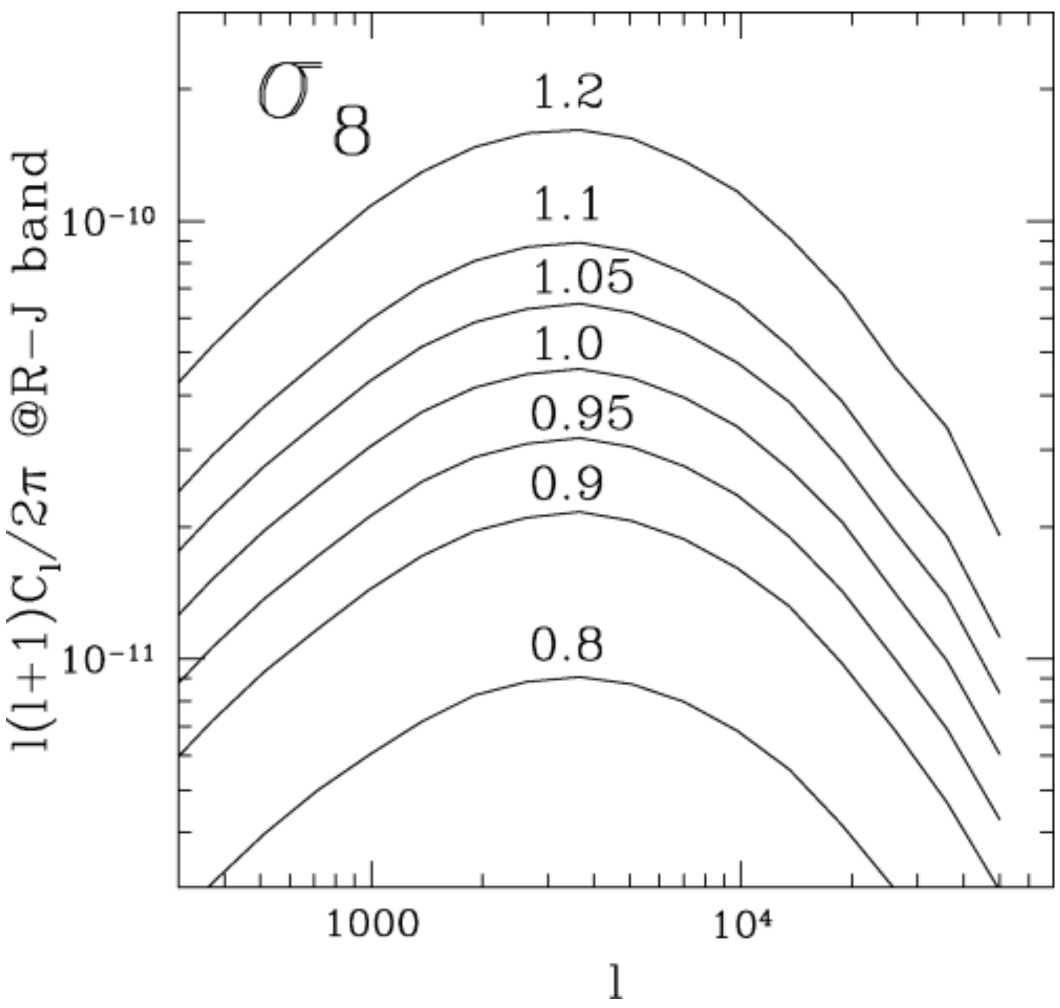

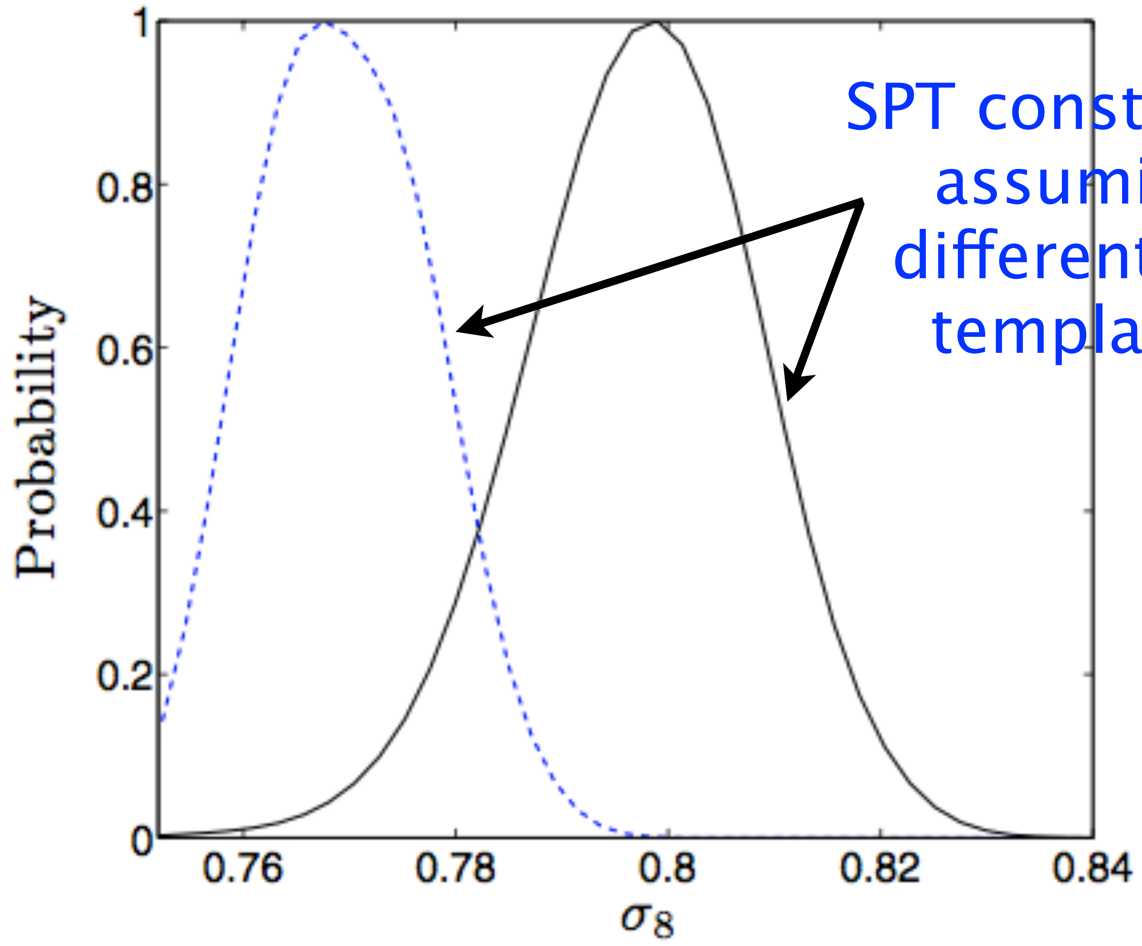

SPT constraints assuming different tSZ templates

kSZ effect from reionization

Anisotropies at ell ≈ 1000 – 10000 receives a substantial contribution from kSZ anisotropy due to patchy reionization ("patchy kSZ"), which arises again from $n_{e} * v_{pec}$ but, during this epoch, the fluctuations in n_e are fractionally large due to the inhomogeneous nature of reionization. The amplitude of the power spectrum of patchy kSZ scales with the duration of the epoch of reionization (EoR), but there is much more information about the bubble size and velocity field during reionization to be obtained if the power spectrum's shape (and possibly the higher moments of the field) can be measured.

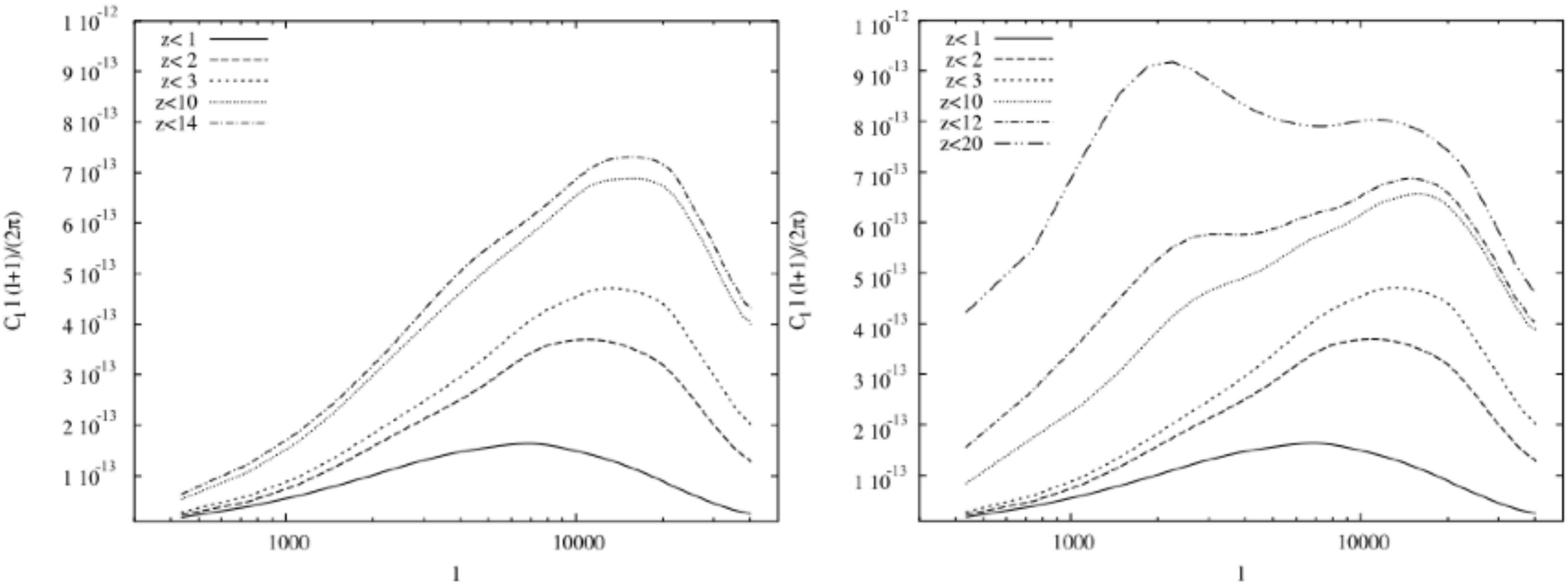

Figure 15: Contributions to the kSZ power spectrum. Left: a model in which ionization occurs instantanously, thus giving only the homogeneous kSZ contribution. Right: a model with extended reionization, receiving contributions from both homogeneous and patchy kSZ. It is clear that homogeneous kSZ dominates at higher multipoles while patchy kSZ dominates at lower multipoles. The patchy kSZ contribution is primarily sourced by z > 10, while the homogeneous kSZ spectrum receives essentially all of its contribution from z < 10. Figures taken from Zahn et al. (2005).

How to go further with CMB?

Cosmic Variance

› We only have one realization (our sky), i.e., one event.

› TT at small l (incl. first peak) is now cosmic variance limited.

To go further:

› TT at large l

› Polarization

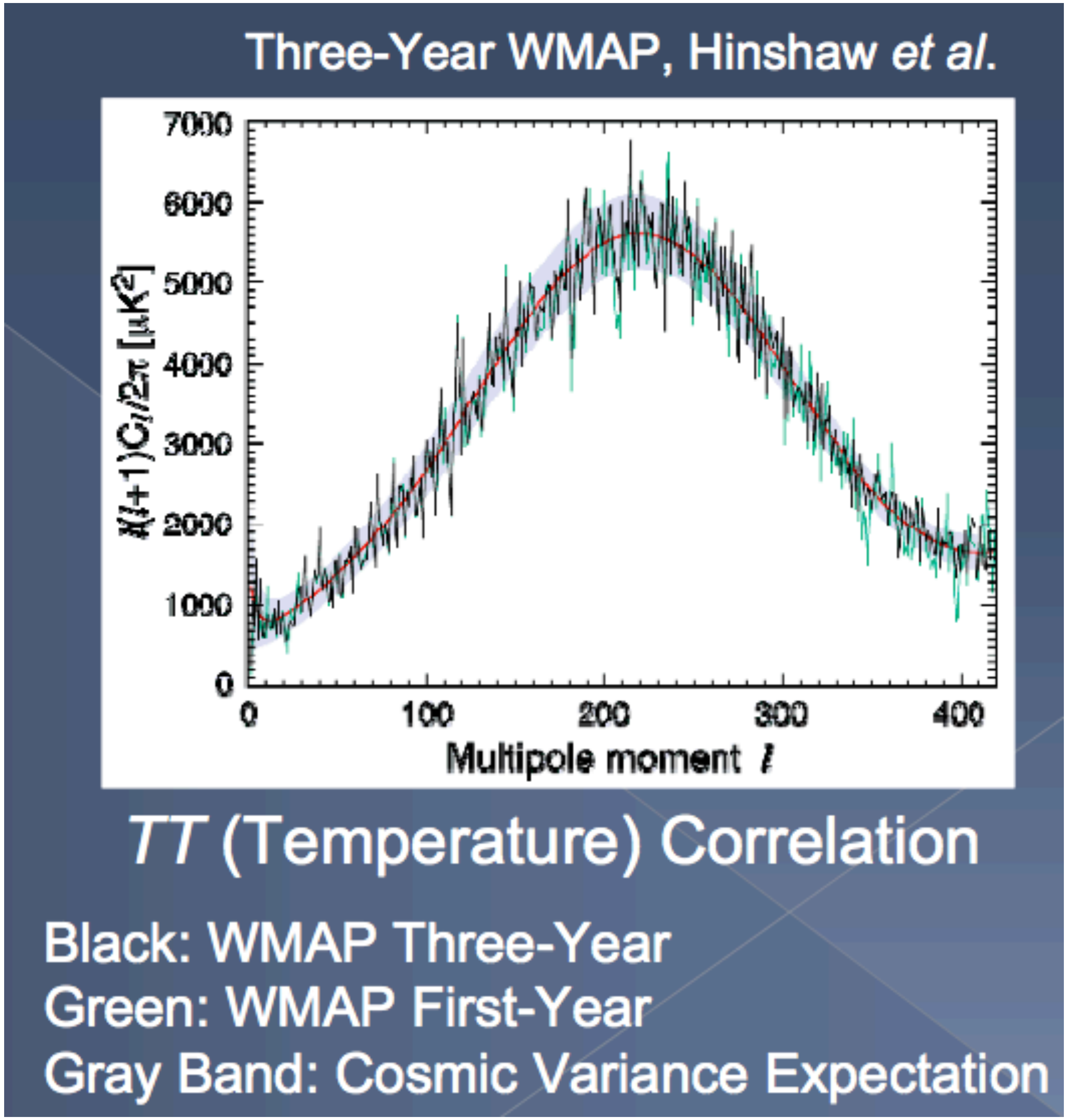

Polarization of the CMB

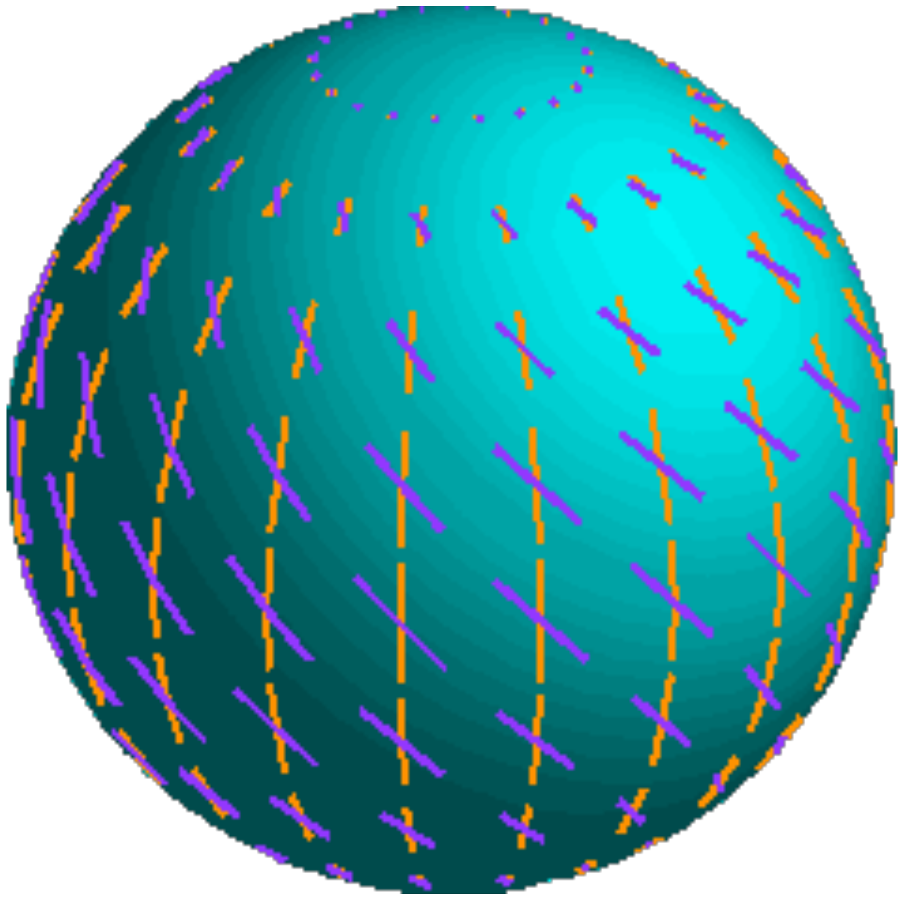

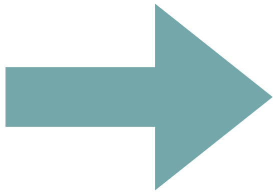

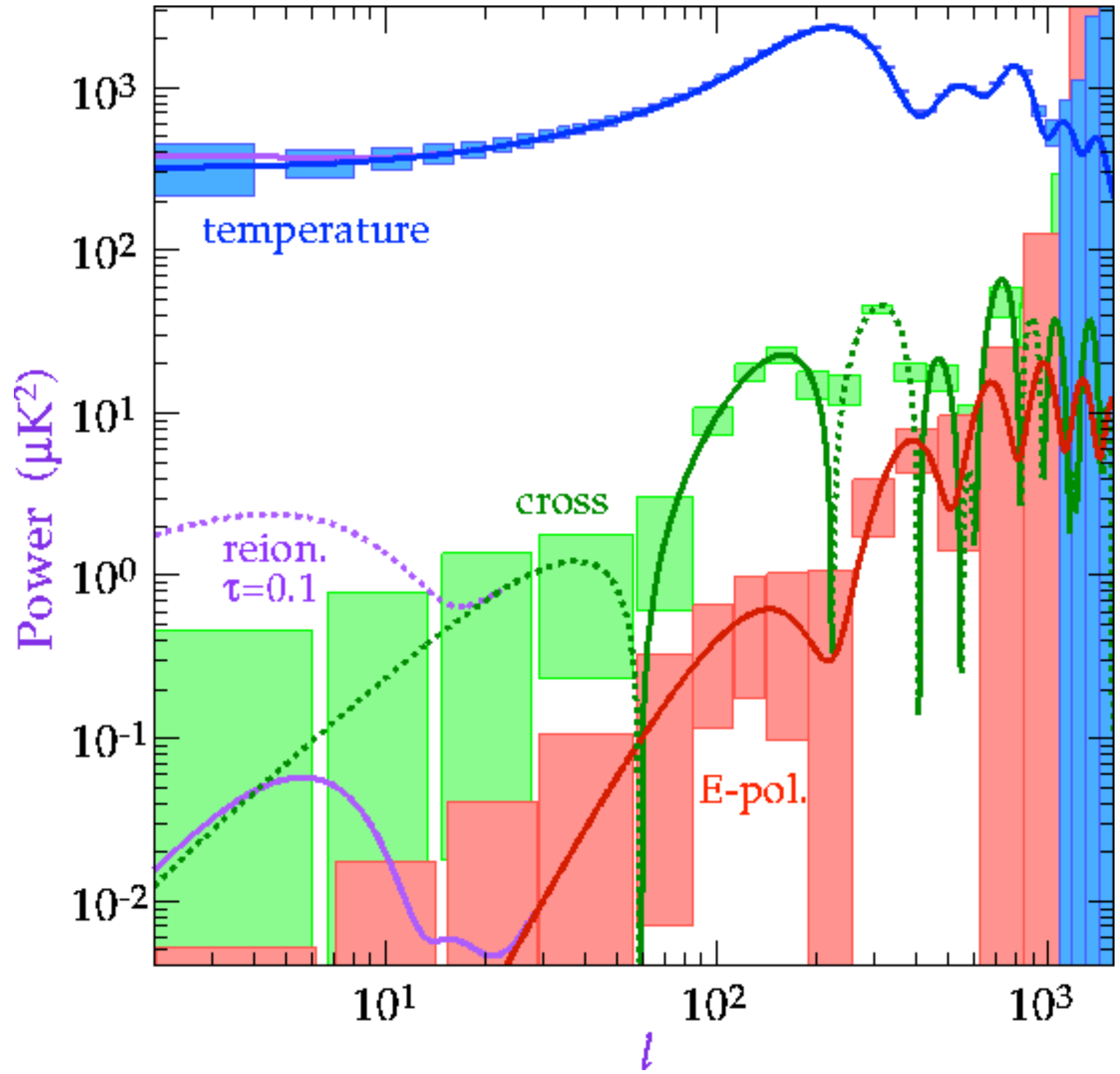

Polarization of the CMB

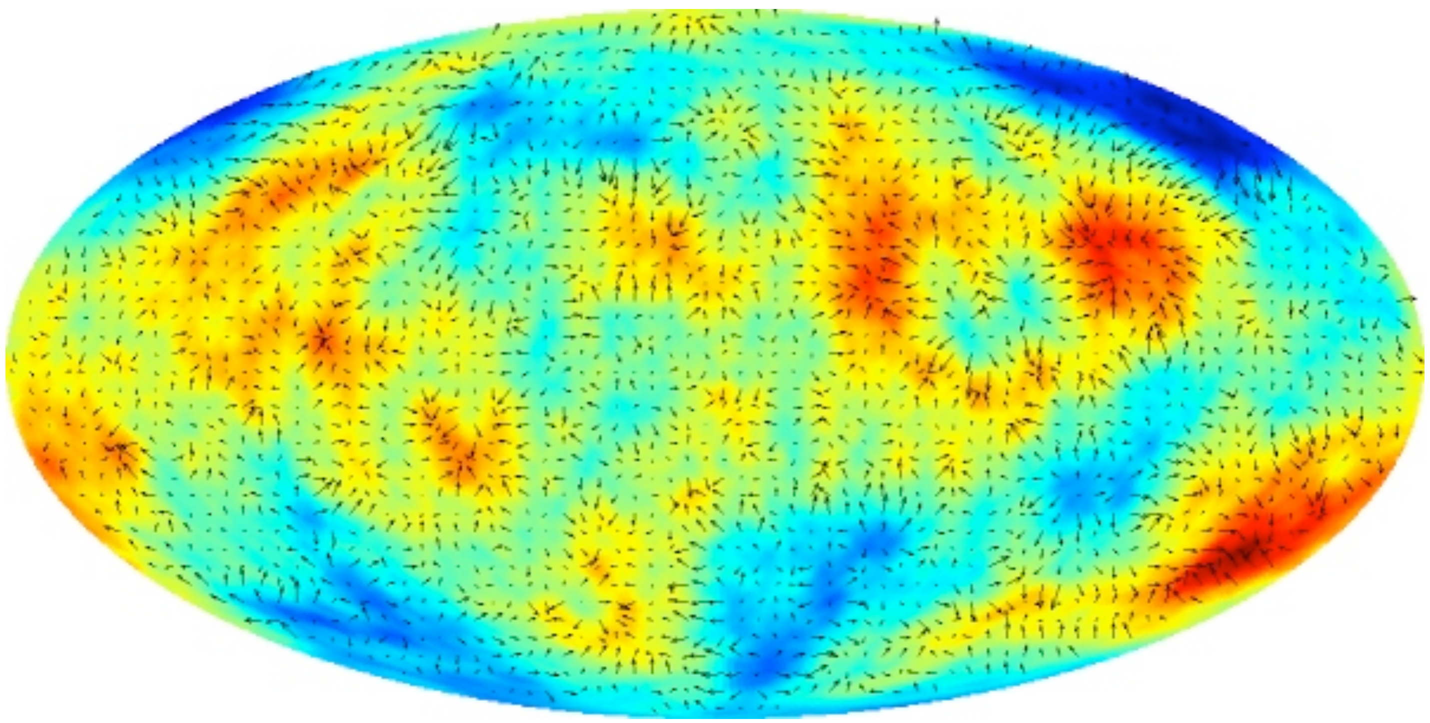

CMB radiation is linearly polarized, which means that at each point on the sky we have a vector orthogonal to the direction of CMB propagation.

Mathematically, this is a spin 2 field on a sphere:

$$(Q \pm \mathrm{i}U)(\vec{n}) = \sum_{l \geqslant 2,\ |m| \leqslant l} a_{\pm 2lm \pm 2} Y_l^m(\vec{n}).$$

Stokes parameters formalism

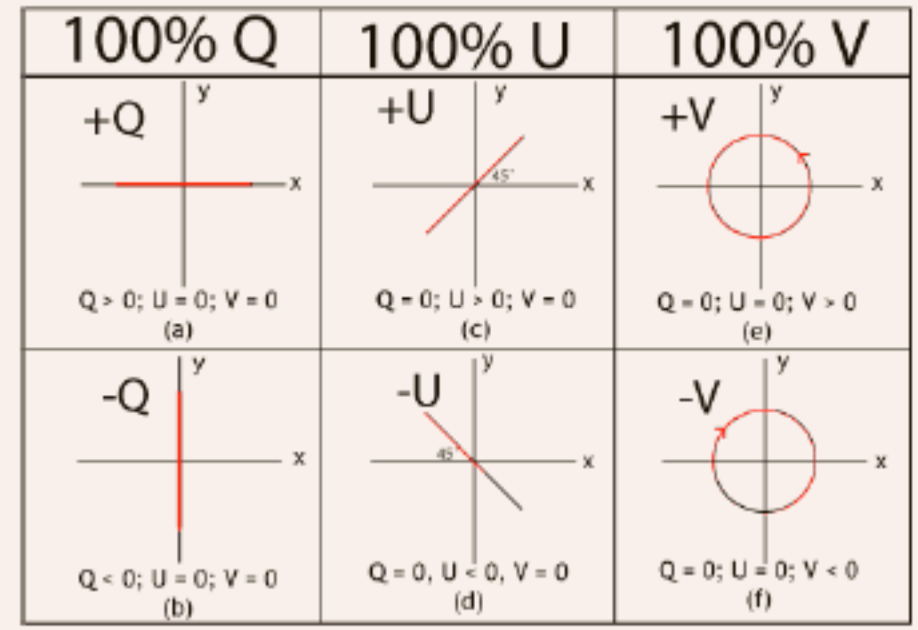

$$\left\{ \begin{matrix} I \\ Q \\ U \\ V \end{matrix} \right\}$$

- ★ I, *intensity*
- ★ Q, U, *linear polarization*
- ★ V, *circular polarization*

★*in the case of the CMB,* $V = 0$

E and B modes

Two flavors of CMB polarization:

Density perturbations: curl–free, “E–mode”
Gravity waves: curl, “B–mode”

E-mode
(“gradient-like”)

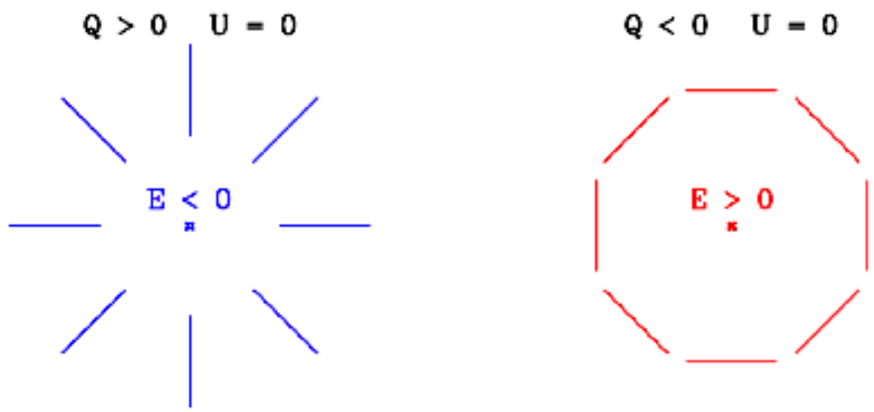

B-mode
(“curl-like”)

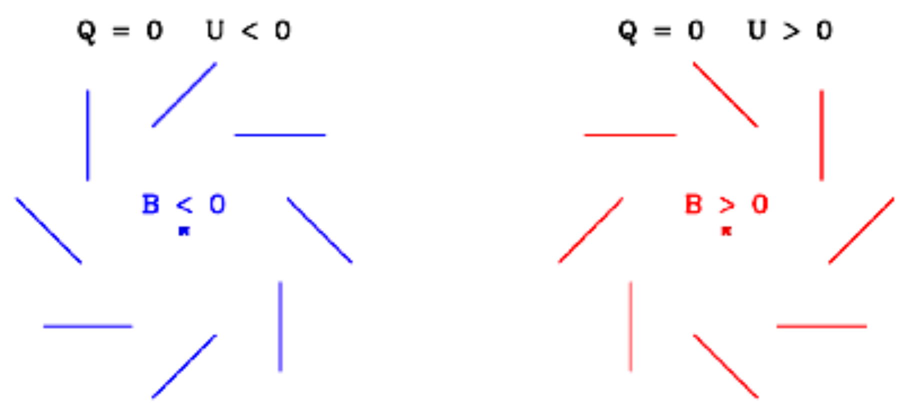

- We can break down the polarization field into two components which we call E and B modes. This is the spin–2 analog of the gradient/curl decomposition of a vector field.
- E modes are generated by density (scalar) perturbations via Thomson scattering.
- Additional vector modes are created by vortical motion of the matter at recombination – this is small
- B modes are generated by gravity waves (tensor perturbations) at last scattering or by gravitational lensing (which transforms E modes into B modes along the line of sight to us) later on.

E and B modes: 2D vector analogy

The Helmholtz's Theorem on Vector Fields

Helmholtz's theorem is also called as the fundamental theorem of vector calculus. It is stated as

"A sufficiently smooth, rapidly decreasing vector field in three dimensions can be decomposed into the sum of a solenoidal (divergence-less) vector field and an irrotational (curl-less) vector field."

The theorem is also called as Helmholtz decomposition, it breaks a vector field into two *orthogonal* components.

$$\mathbf{F} = -\nabla\Phi + \nabla \times \mathbf{A}$$

Instead of decomposing the vector field into E and B modes, one could also use the original Stokes Q and U parameters, but the disadvantage is that the distinction between Q and U depends on the choice of the coordinate frame.

E and B modes

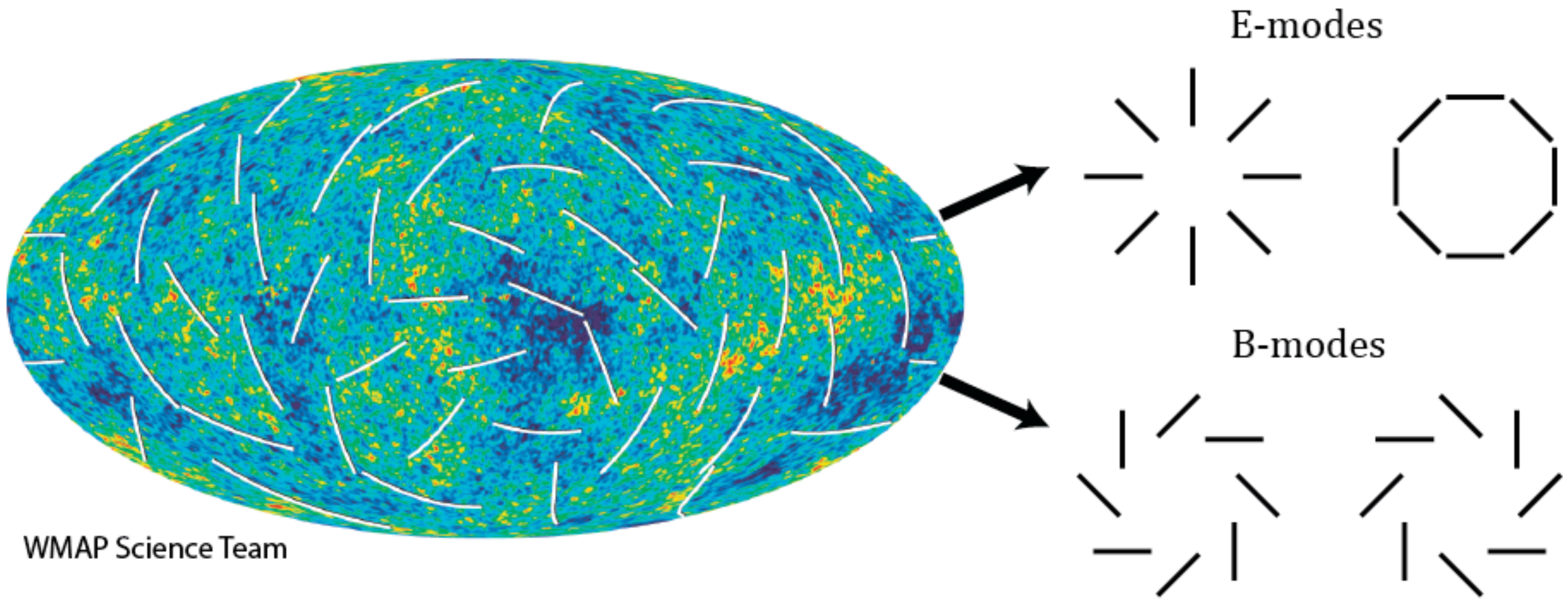

WMAP Science Team

Projection of the polarization in the spinned spherical harmonics space

$$(Q \pm iU)(\mathbf{n}) = \sum_{\ell,m} a_{\pm 2\ell m} \cdot_{\pm 2} Y_{\ell m}(\mathbf{n})$$

*Construction of the **E** and **B** observables*

[Seljak & Zaldarriaga 1997]

$$a^E_{\ell m} = -\frac{a_{2\ell m} + a_{-2\ell m}}{2}$$

$$E(\mathbf{n}) \equiv \sum_{\ell,m} a^E_{\ell m} Y_{\ell m} = \int w(\mathbf{n}-\mathbf{n}') Q_r(\mathbf{n}') d\mathbf{n}'$$

$$a^B_{\ell m} = i\,\frac{a_{2\ell m} - a_{-2\ell m}}{2}$$

$$B(\mathbf{n}) \equiv \sum_{\ell,m} a^B_{\ell m} Y_{\ell m} = \int w(\mathbf{n}-\mathbf{n}') U_r(\mathbf{n}') d\mathbf{n}'$$

★*new observables independent of the chosen frame*

★ $E = f(Q_r)$, $B = f(U_r)$

Ob

(Credit: Jonathan Aumont)

Quadrupole + Thomson scattering

Polarization is induced by Thomson scattering, either at decoupling or during a later epoch of reionization.

For scattering at Θ=π/2 only one component of the initially unpolarized radiation field gets scattered.

$$P(\theta, \phi) \propto 1 - \cos^2\theta$$

$$\frac{d\sigma}{d\Omega} = \left(\frac{e^2}{4\pi mc^2}\right)^2 |\hat{\epsilon} \cdot \hat{\epsilon}'|^2$$

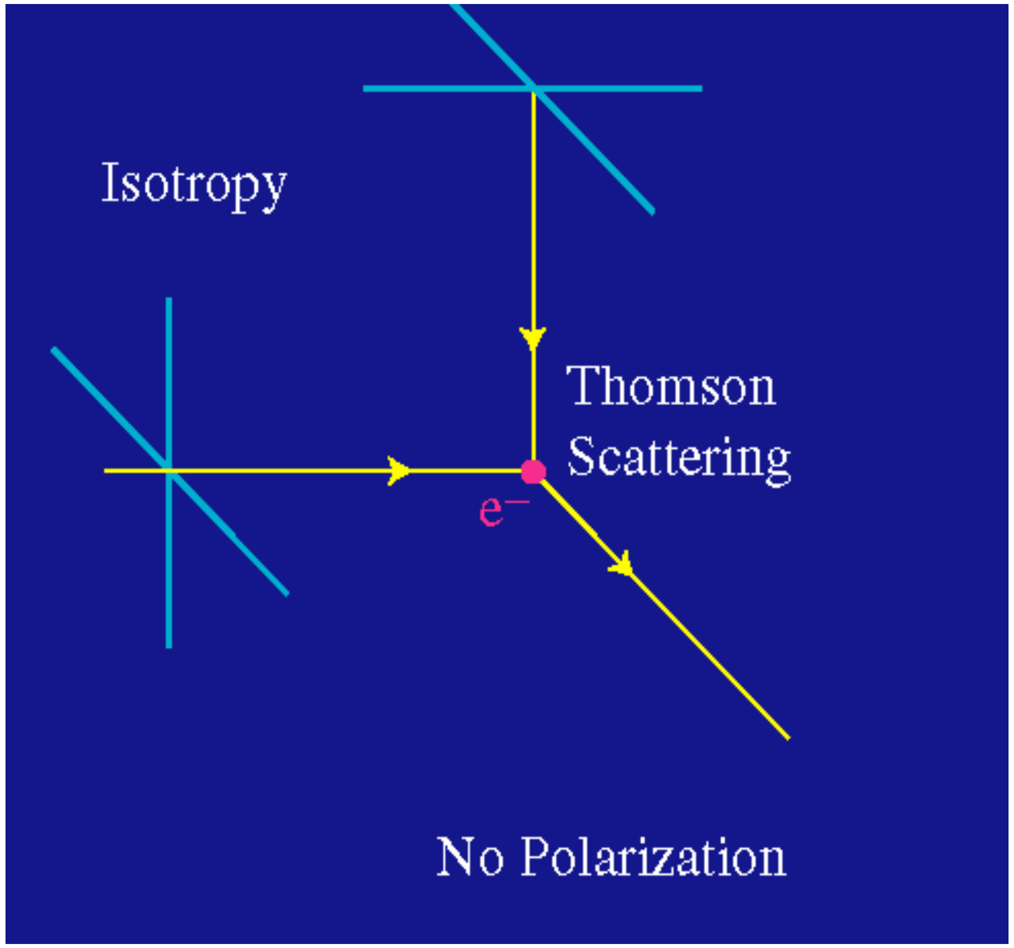

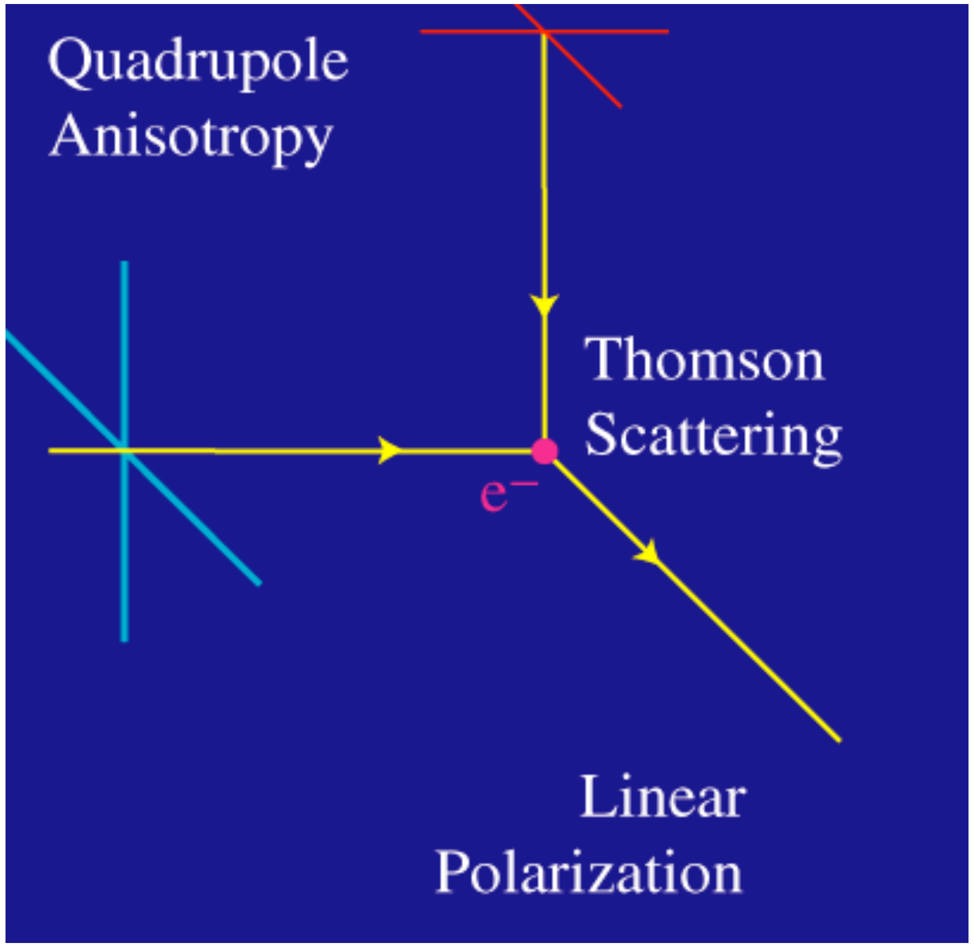

What causes the CMB quadrupole?

Two things:

"Normal" CDM: Density perturbations at z=1100 lead to velocities that create local quadrupoles seen by scattering electrons.

=> E-mode polarization ("grad")

Gravity waves: create local quadrupoles seen by the scattering electrons.

=> B-mode polarization ("curl")

The problem of understanding the polarization pattern of the CMB thus reduces to understanding the quadrupole temperature fluctuations at the *instant of last scattering*.

From velocity gradients to polarization

Velocity gradients in the photon-baryon fluid lead to a quadrupole component of the intensity distribution, which, through Thomson scattering, is converted into polarization!

(See Zaldarriaga, astro-ph/0305272)

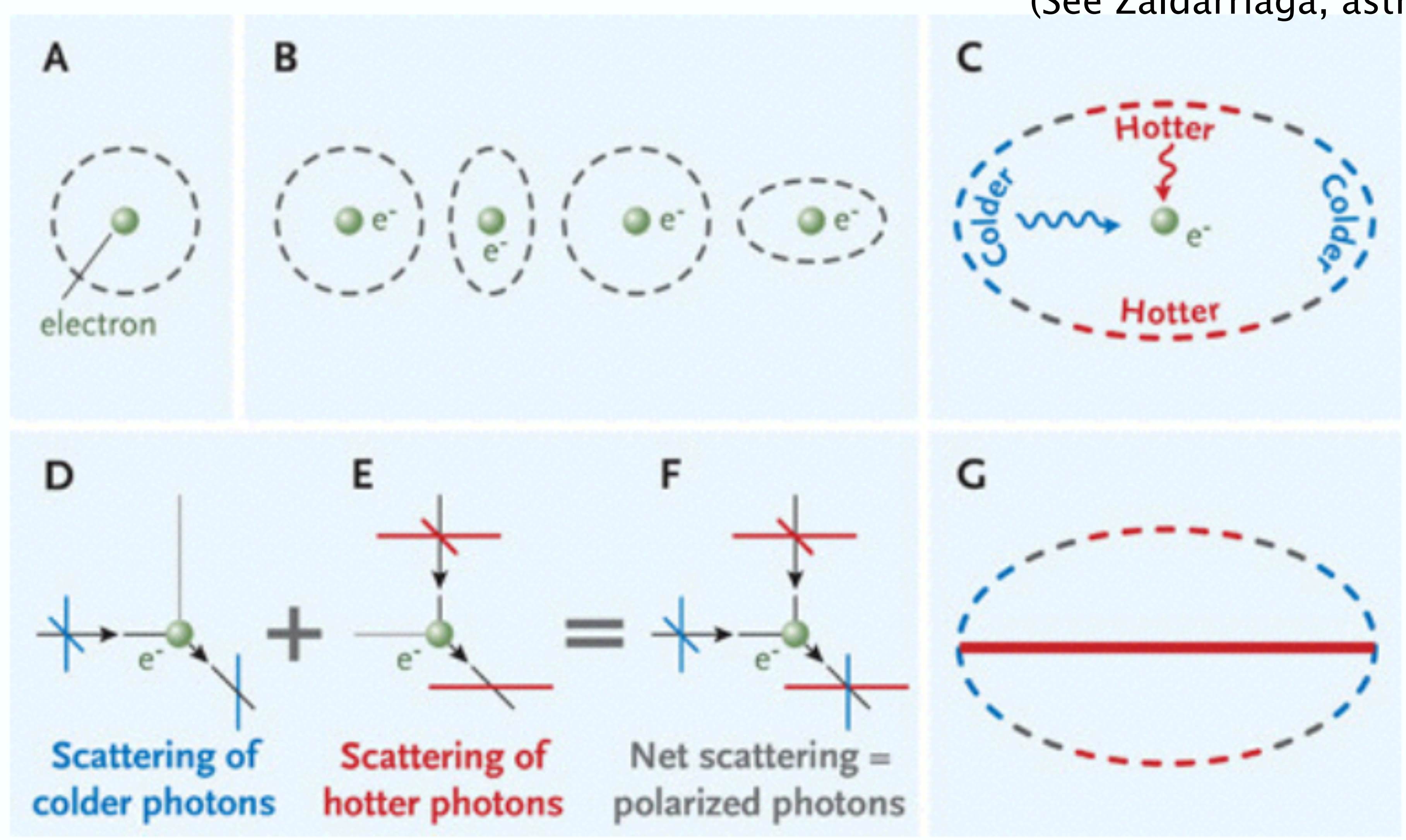

When gravity overwhelms pressure, matter flows towards the overdense regions. But these overdense regions are also colder initially, as photons must climb out of the potential well. Hence flows are established from hot to cold regions locally, and these velocity gradients create the polarization signal.

Polarization from the last scattering

We saw that polarization pattern created at the last scattering can only come from a quadrupole temperature anisotropy present at that epoch.

In terms of multipole decomposition of a radiation field in terms of spherical harmonics, $Y_{lm}(\theta,\varphi)$, the five quadrupole moments are represented by $l = 2$; $m = 0, \pm 1, \pm 2$.

The orthogonality of the spherical harmonics guarantees that no other moment can generate polarization from Thomson scattering!

The problem of understanding the polarization pattern of the CMB thus reduces to understanding the quadrupolar temperature fluctuations at the epoch of last scattering.

Polarization patterns

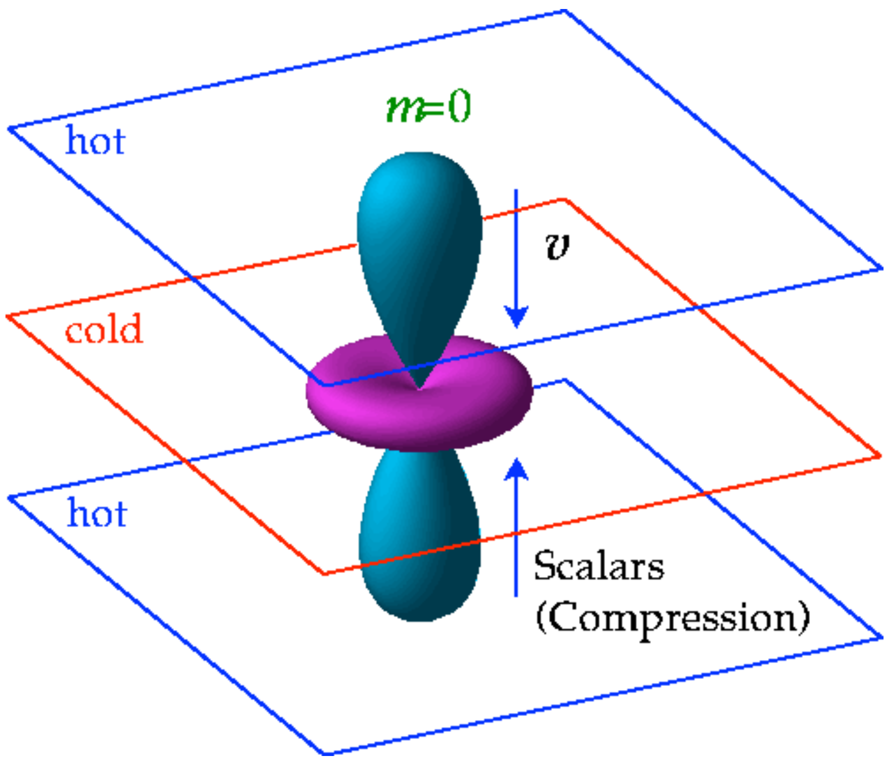

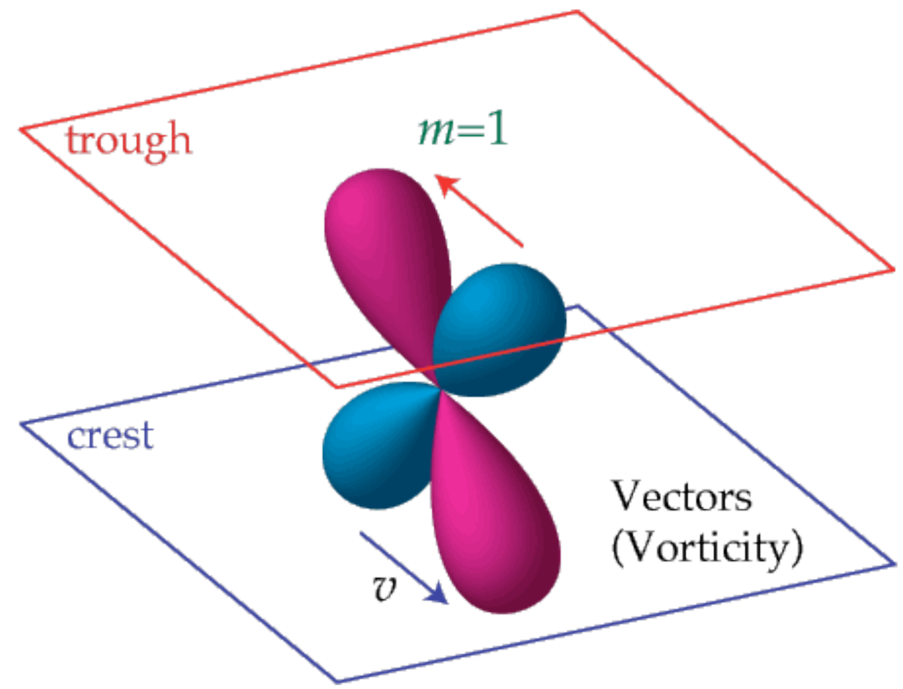

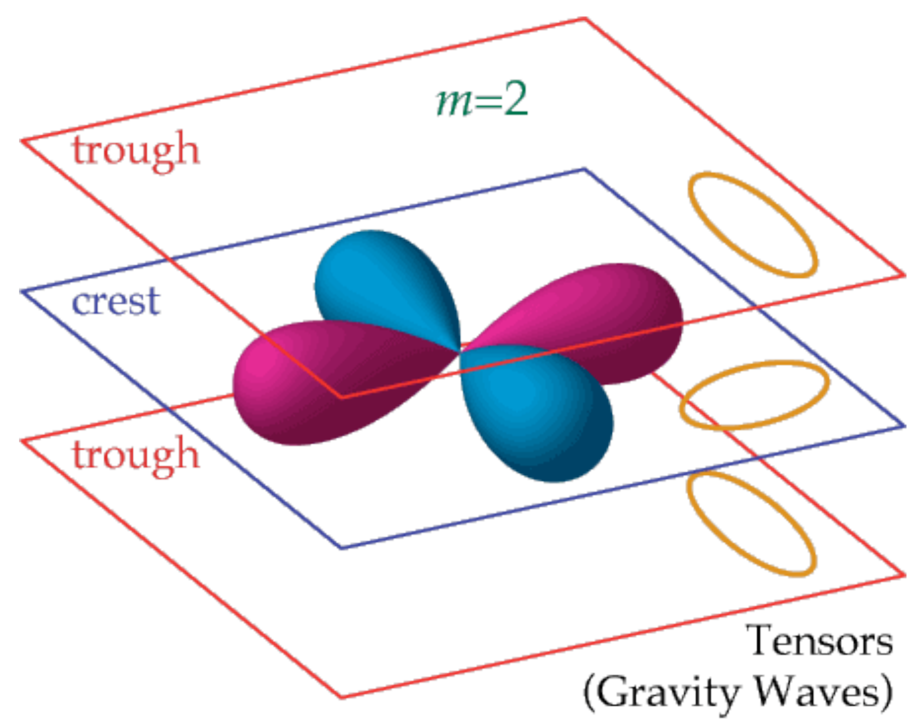

There are three sources to the quadrupole temperature anisotropy at recombination:

- scalers (m=0) for velocity perturbation
- vectors (m=1) for vorticity *(negligible)*
- tensors (m=2) for gravity waves

Visualization of the polarization pattern

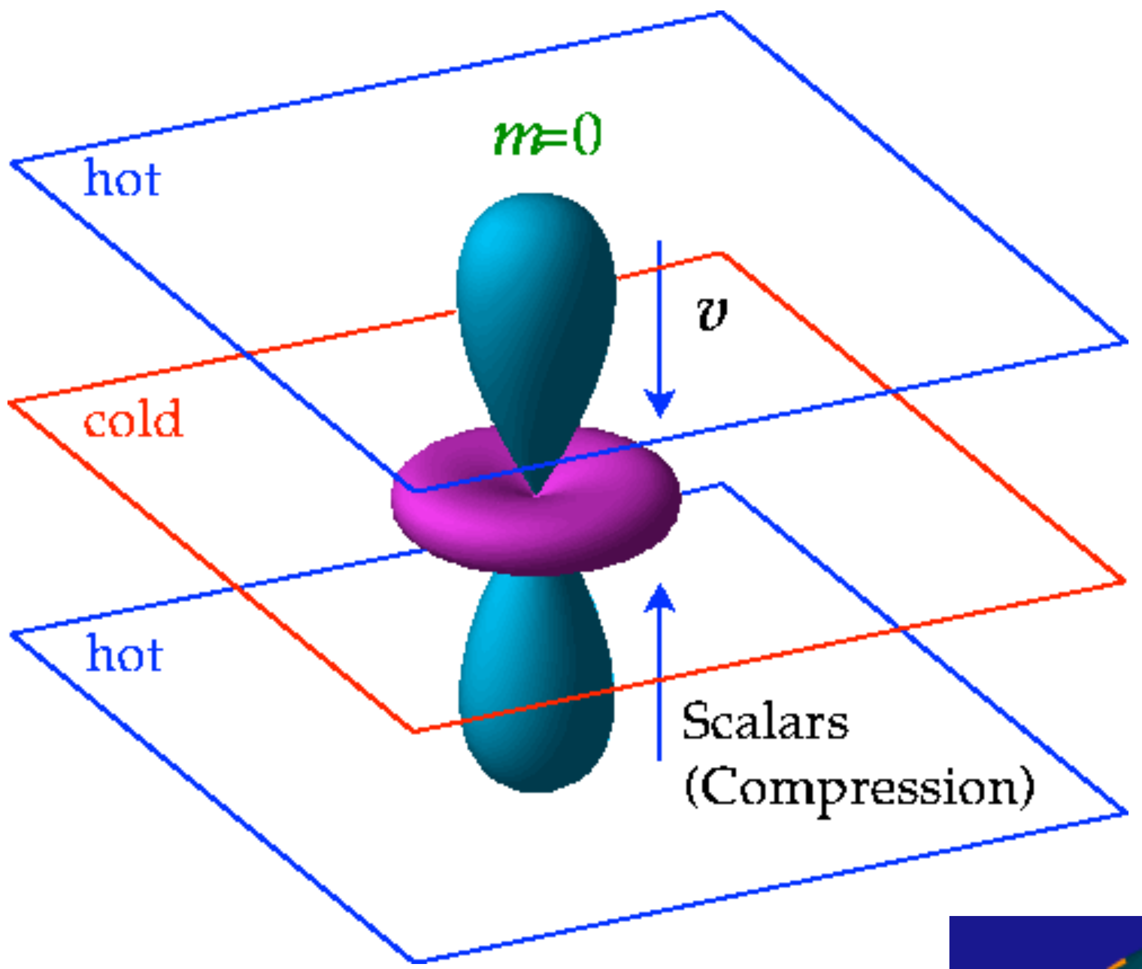

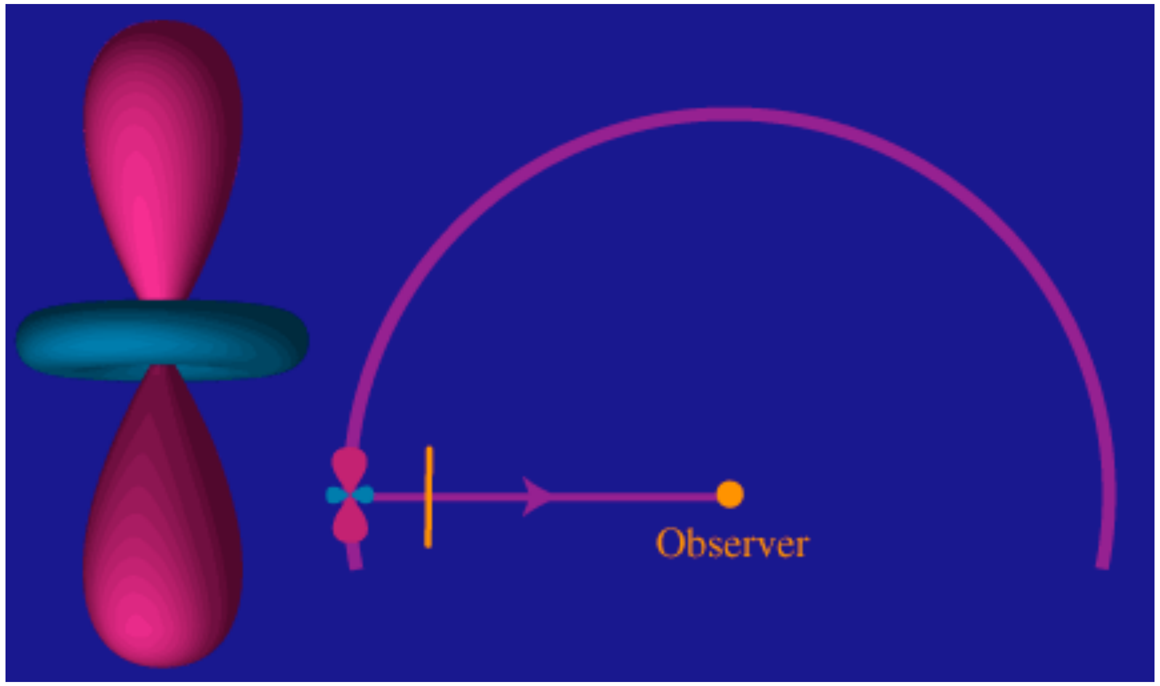

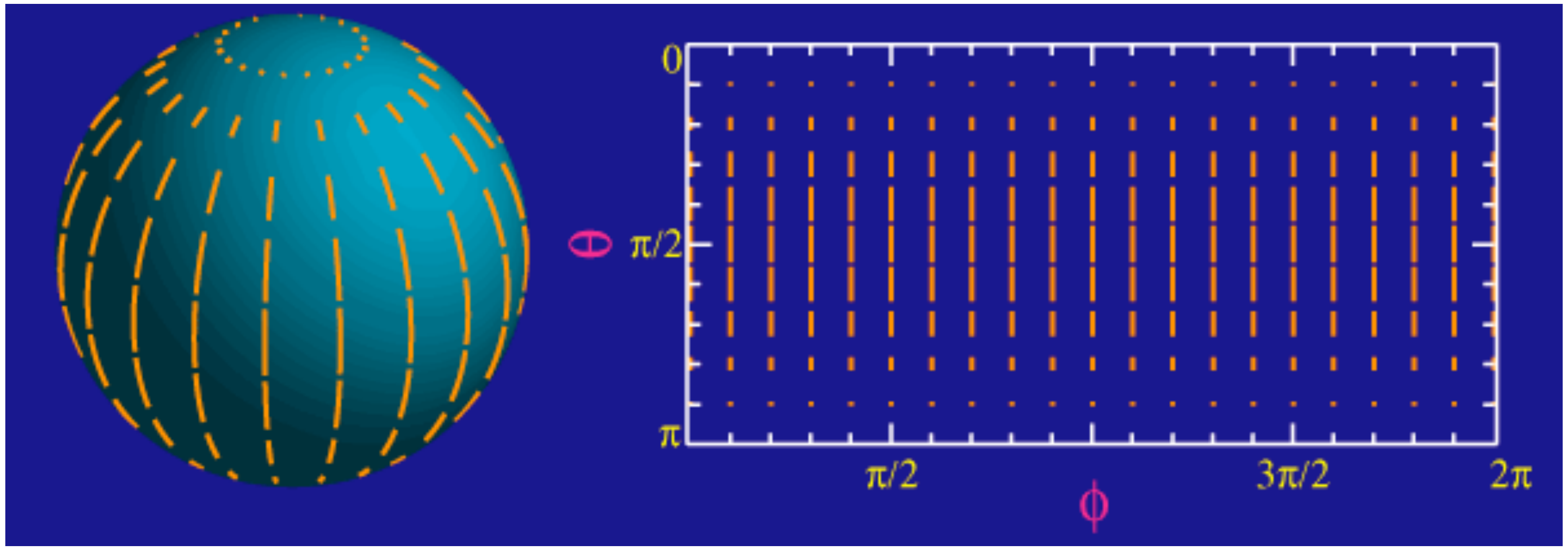

The scaler quadrupole moment, l=2, m=0. Note the azimuthal symmetry in the transformation of this quadrupole anisotropy into linear polarization.

Polarization patterns

Animations by Wayne Hu. Thick and thin lines are E and B-mode patterns.

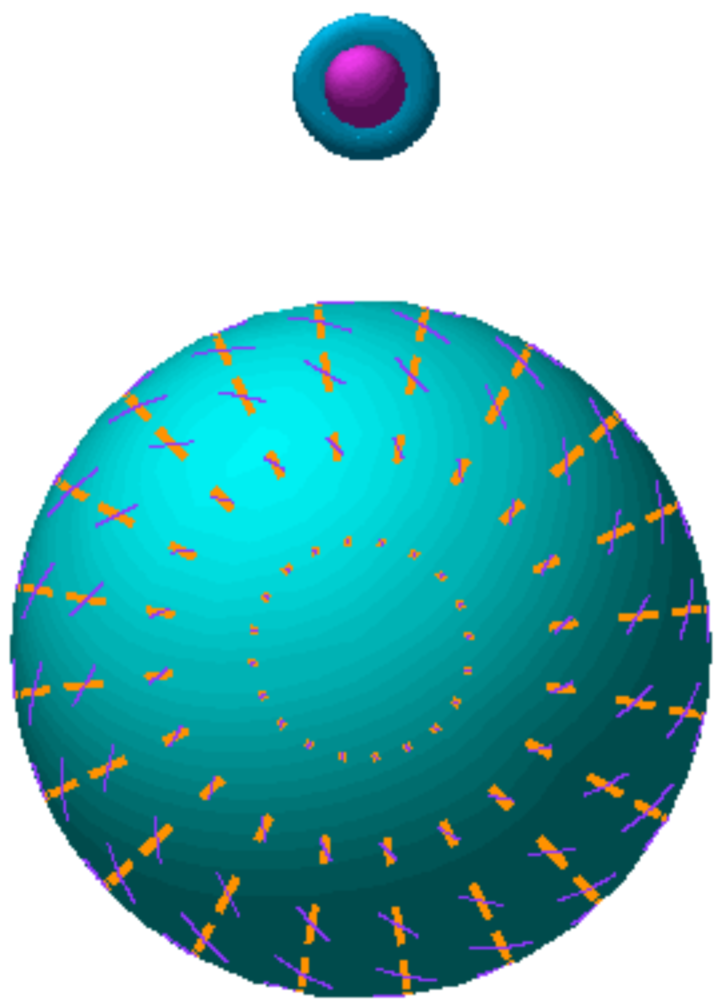

Scaler mode
(l=2, m=0)

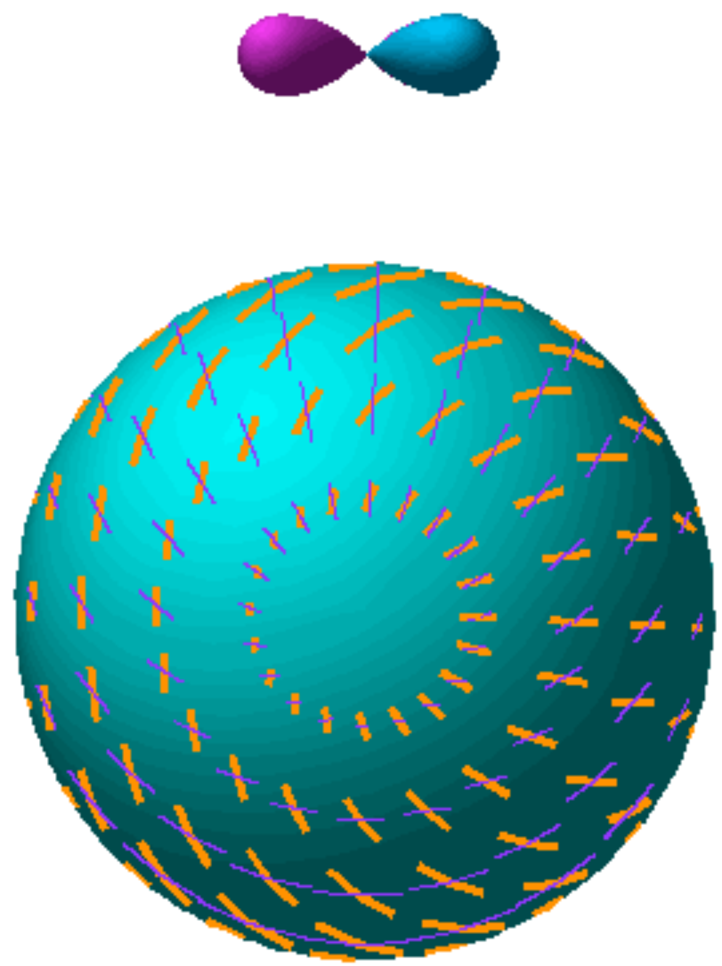

Vector mode
(l=2, m=±1)
(negligible)

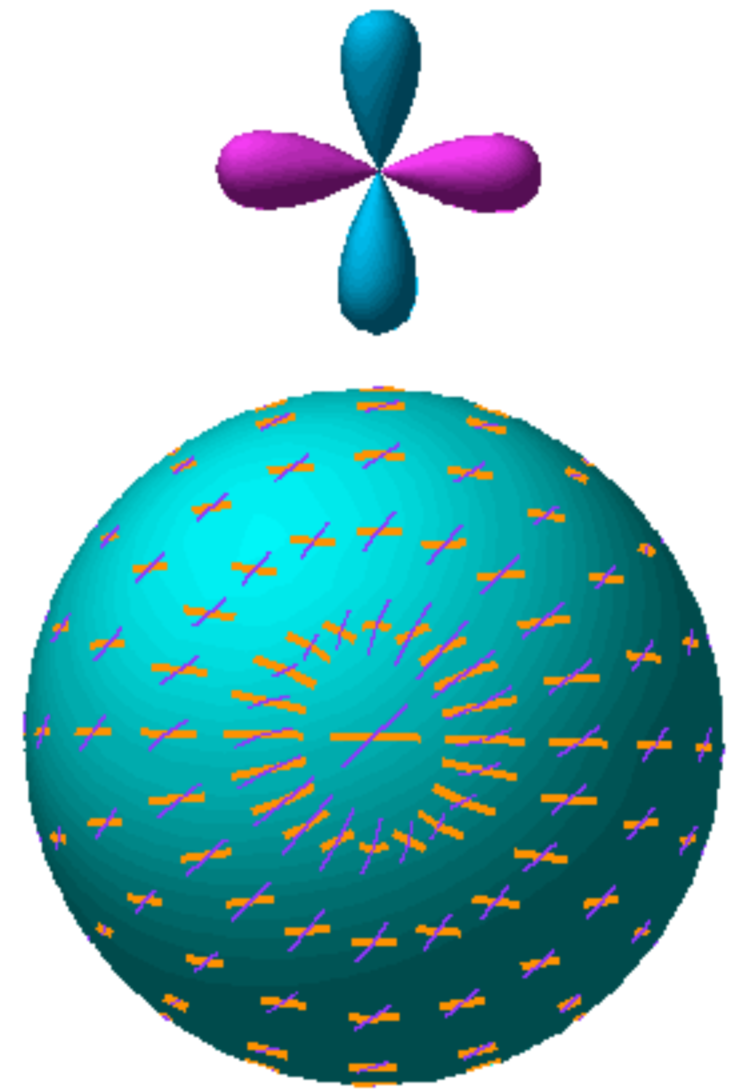

Tensor mode
(l=2, m=±2)

Parity of E & B modes

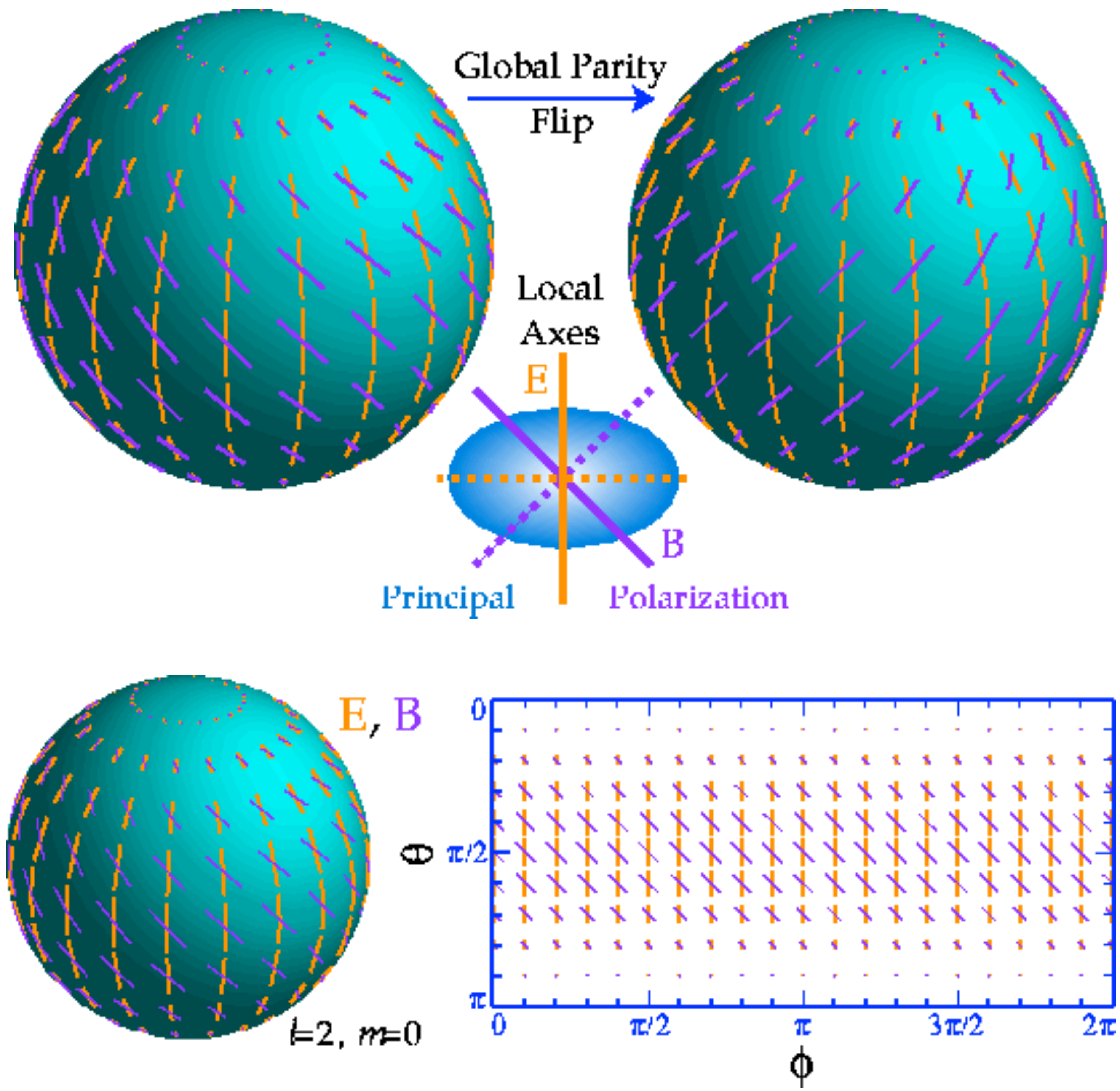

Polarization power spectra

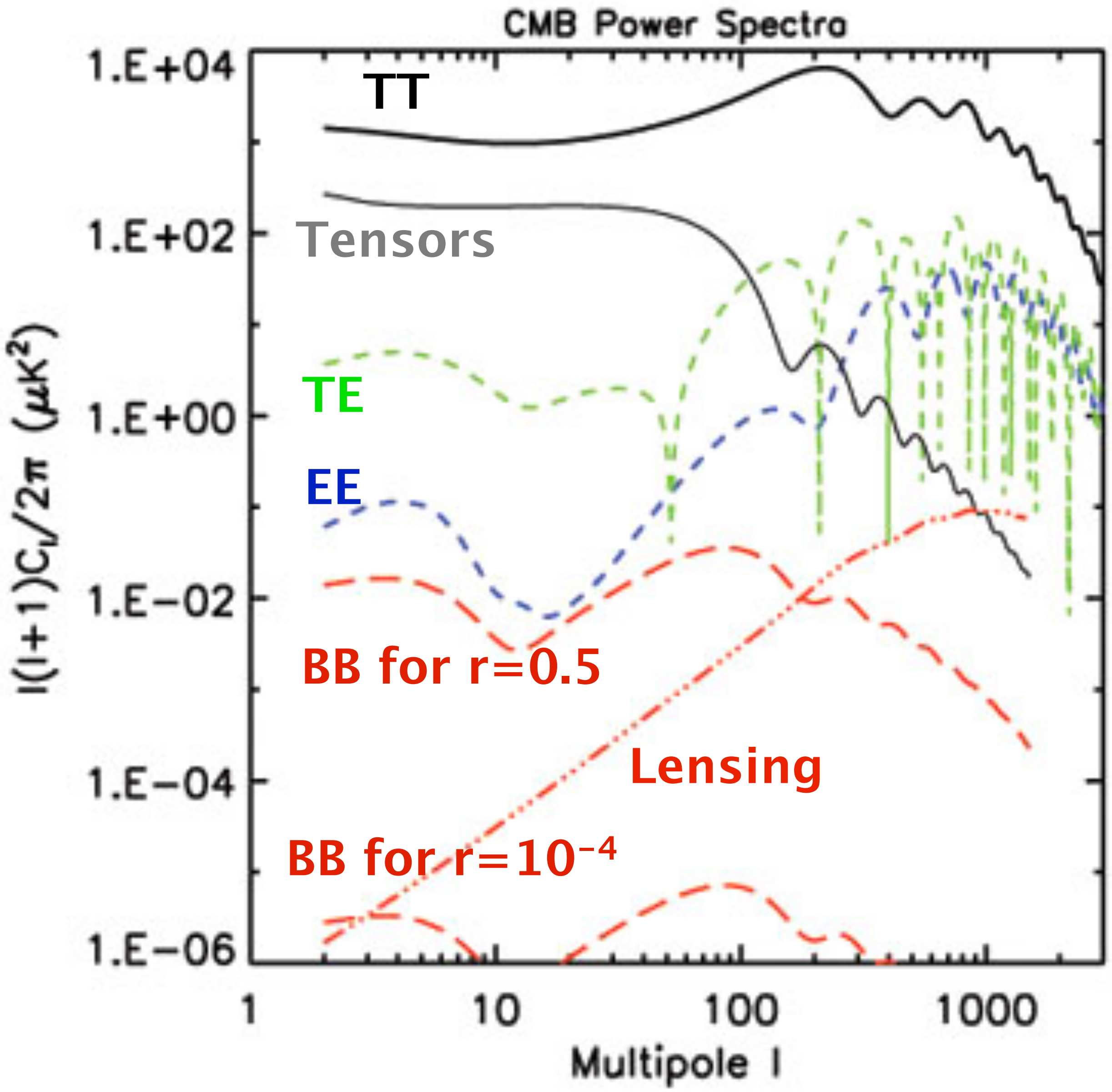

r = T/S: Tensor to scaler ratio, generated by the primordial gravity waves at last scattering

E & B modes have different reflection properties ("parities"):

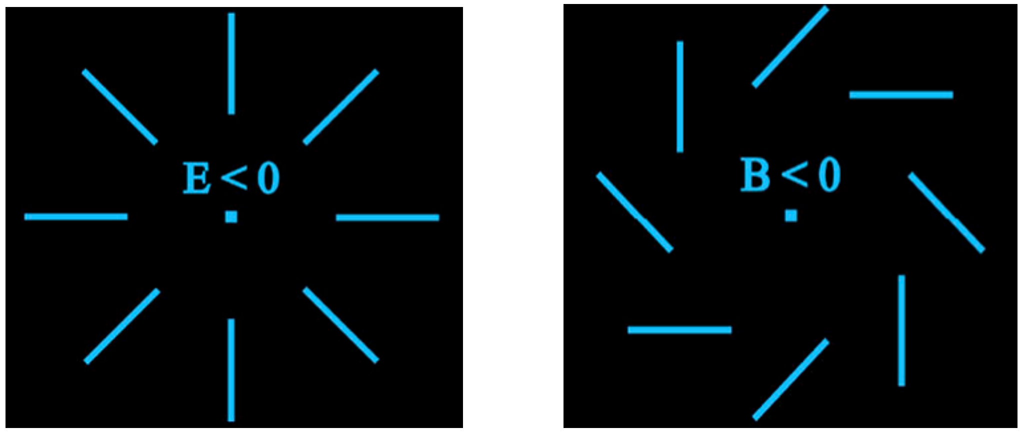

Parity: $(-1)^l$ for E and $(-1)^{l+1}$ for B (here l=2) ⇒ **B has negative parity**

The cross-correlation between B and E or B and T vanishes (unless there are parity-violating interactions), because B has opposite parity to T or E.

We are therefore left with 4 fundamental observables.

Detecting polarization is difficult!

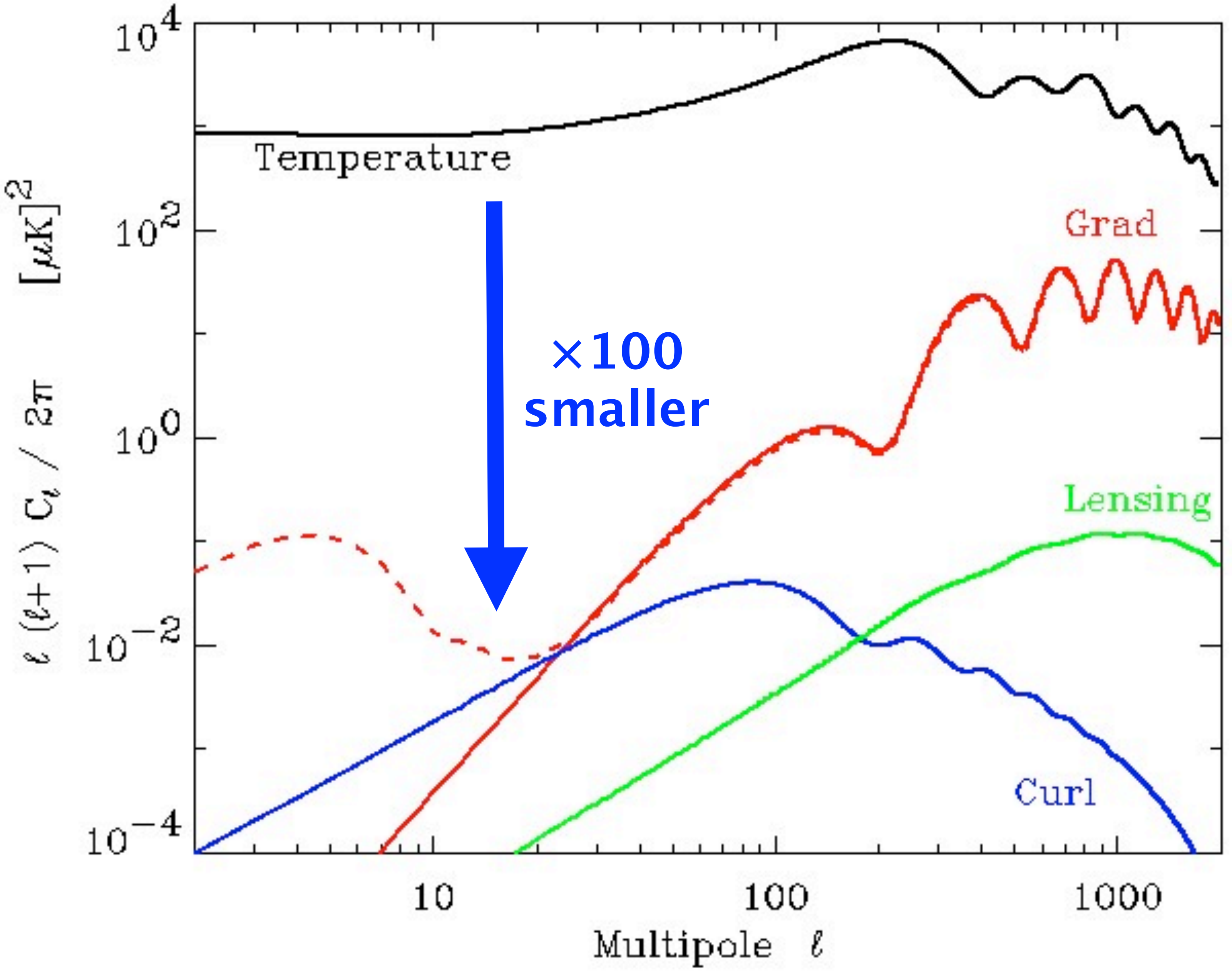

Polarization signal amplitude is much smaller than the temperature, since it requires a scattering event and hence can only be produced in optically thin condition.

Power spectra of CMB temperature anisotropies (black), grad polarization (red), and curl polarization due to the GWB (blue) and due to the lensing of the grad mode (green), all assuming a standard CDM model with T/S = 0.28. The dashed curve indicates the effects of reionization on the grad mode for $\tau = 0.1$.

Polarization power spectra

The polarization power also exhibits acoustic oscillations since the quadrupole anisotropies that generate it are themselves formed from the acoustic motion of the fluid.

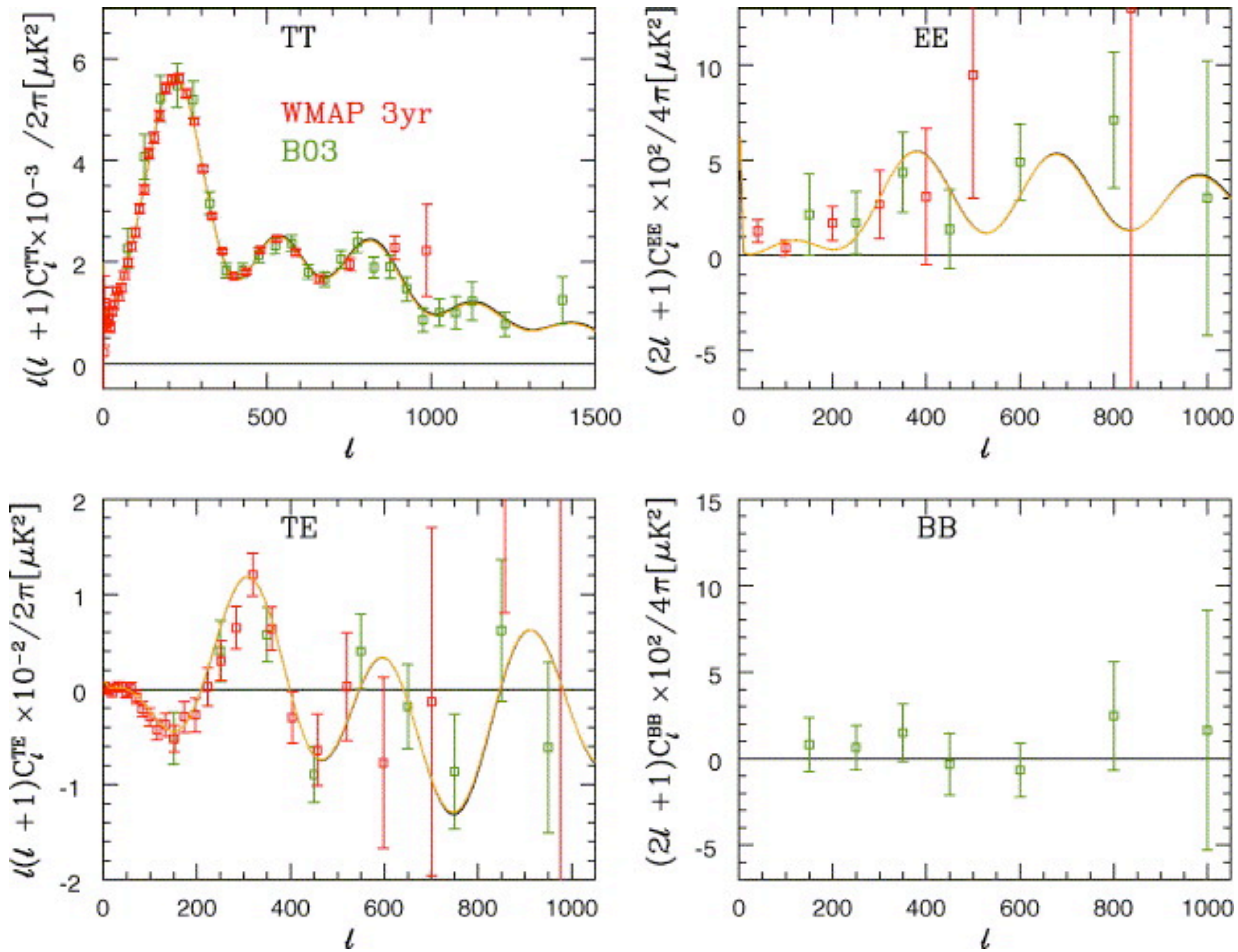

The EE peaks are out of phase with TT peaks since scaler perturbation effect is maximum when the velocity field is maximum.

Shape of the power spectra

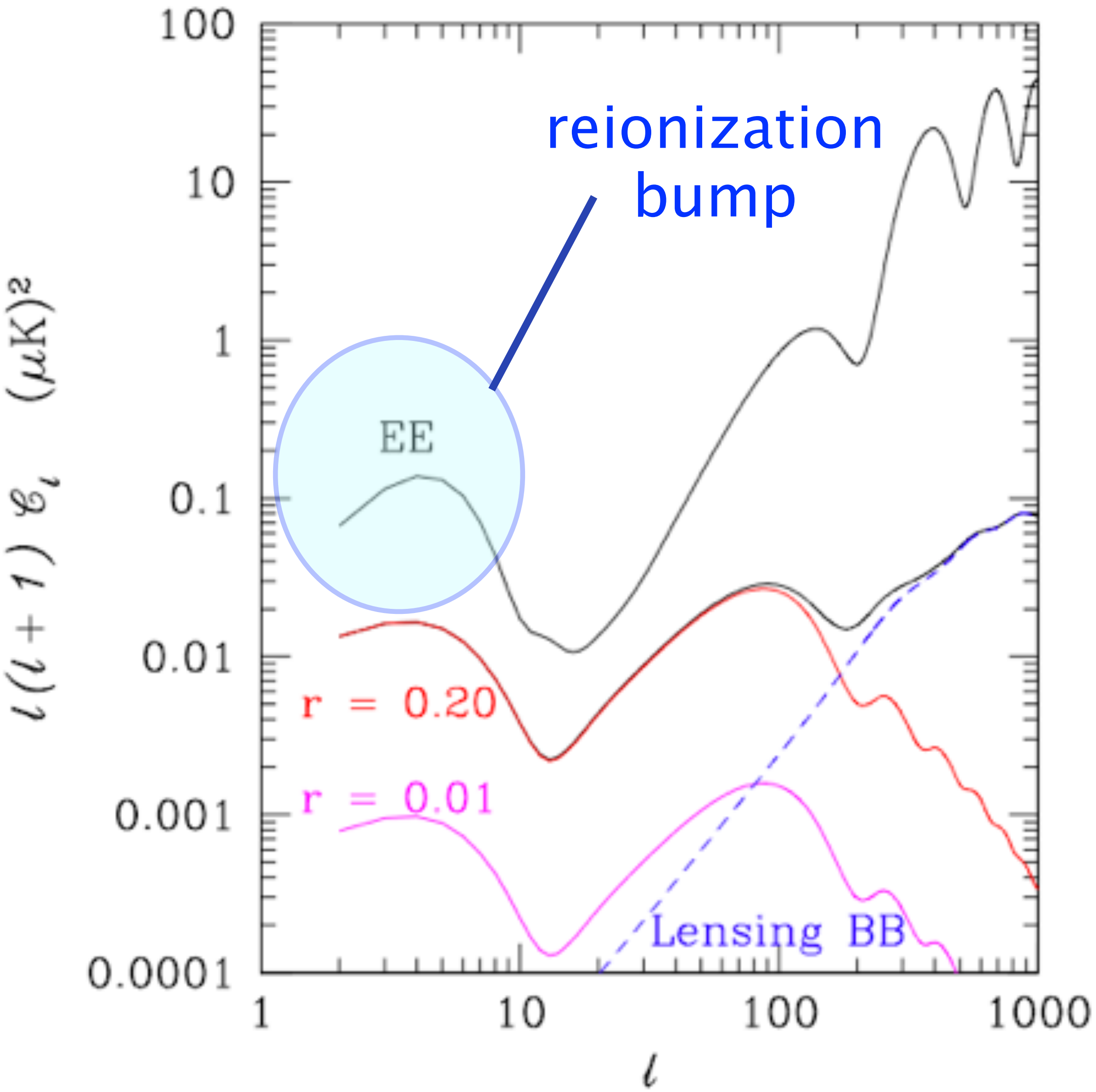

- Primordial E-mode signal peaks at small scales, corresponding to the width of the epoch of last scattering
- The primordial B-mode signal (due to a stochastic background of gravitational waves) dominates only at large angular scales
- On similarly large angular scales, the E-mode polarization signal is dominated by *secondary fluctuations imprinted by reionization*
- The lens-generated signal grows at smaller scales (turning E modes into B modes!)

Shape and amplitude of EE are predicted by ΛCDM.

Shape of BB is predicted "scale-invariant gravity waves".

Amplitude of BB is model dependent, and not really constrained from theory.
Measuring this amplitude would provide a direct handle of the energy scale of inflation!

EE power spectrum

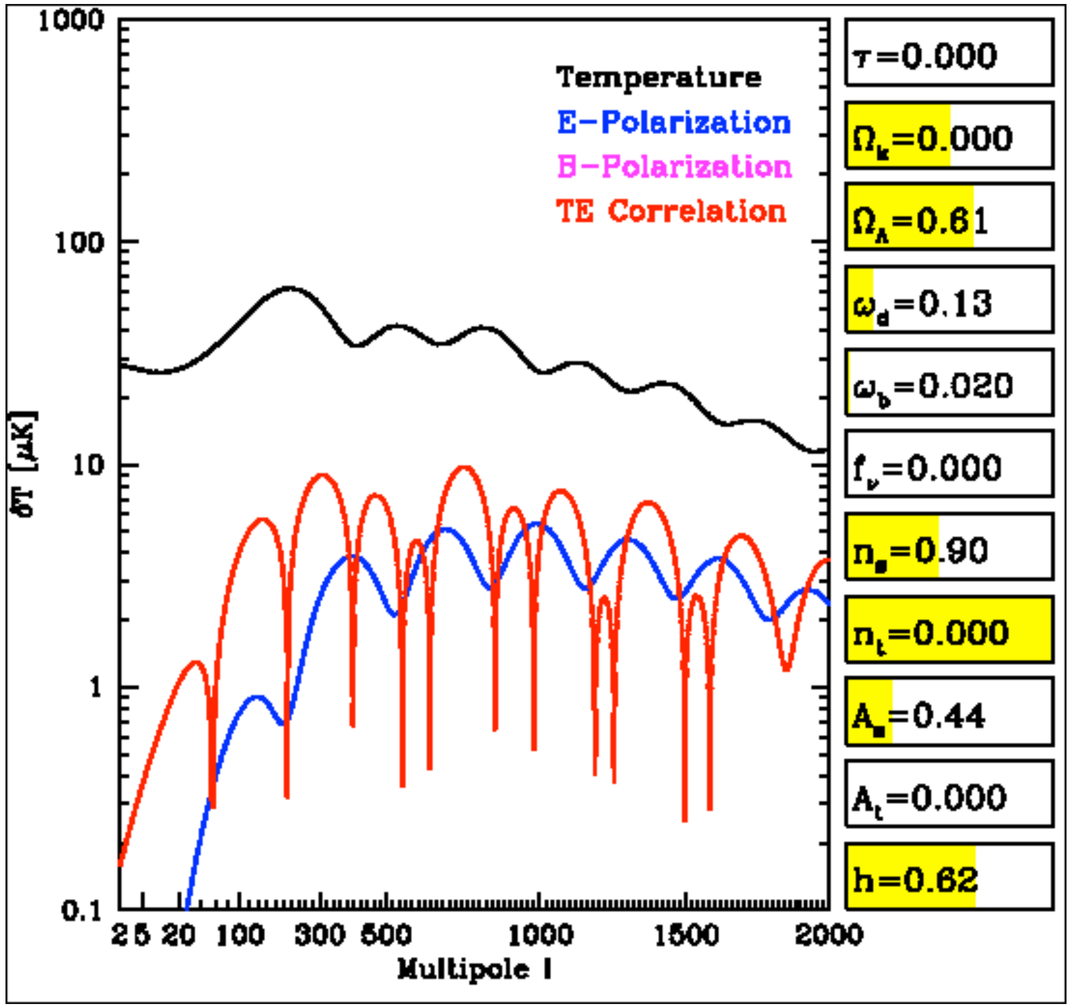

MCMC simulations from K. Vanderlinde

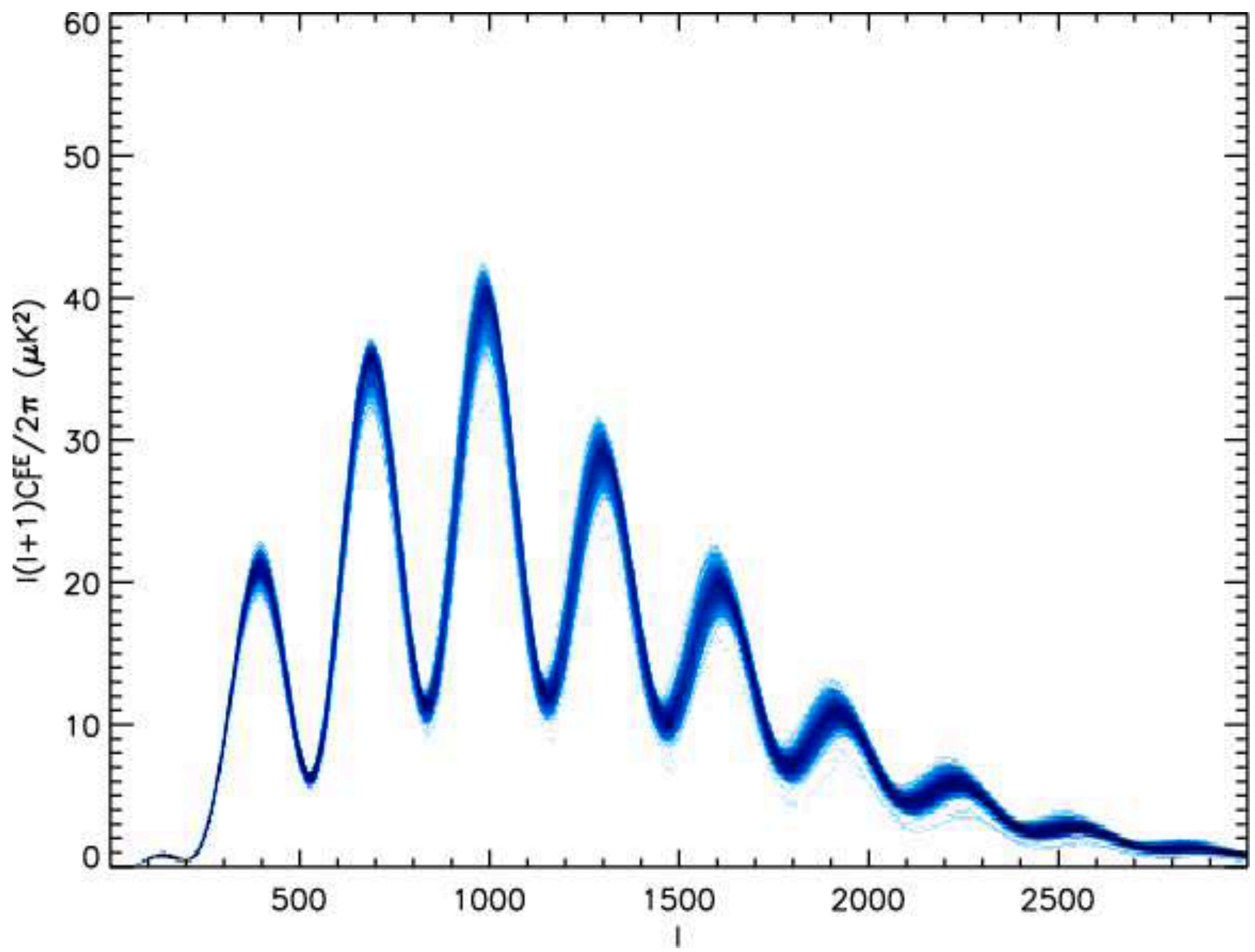

The intermediate to small scale EE polarization signal is sensitive only to the physics at the epoch of last scattering (unlike TT which can be modified).

The EE spectrum is already well constrained from the cosmological models, but it provides additional checks and helps to break some degeneracies.

BB spectrum uncertainties

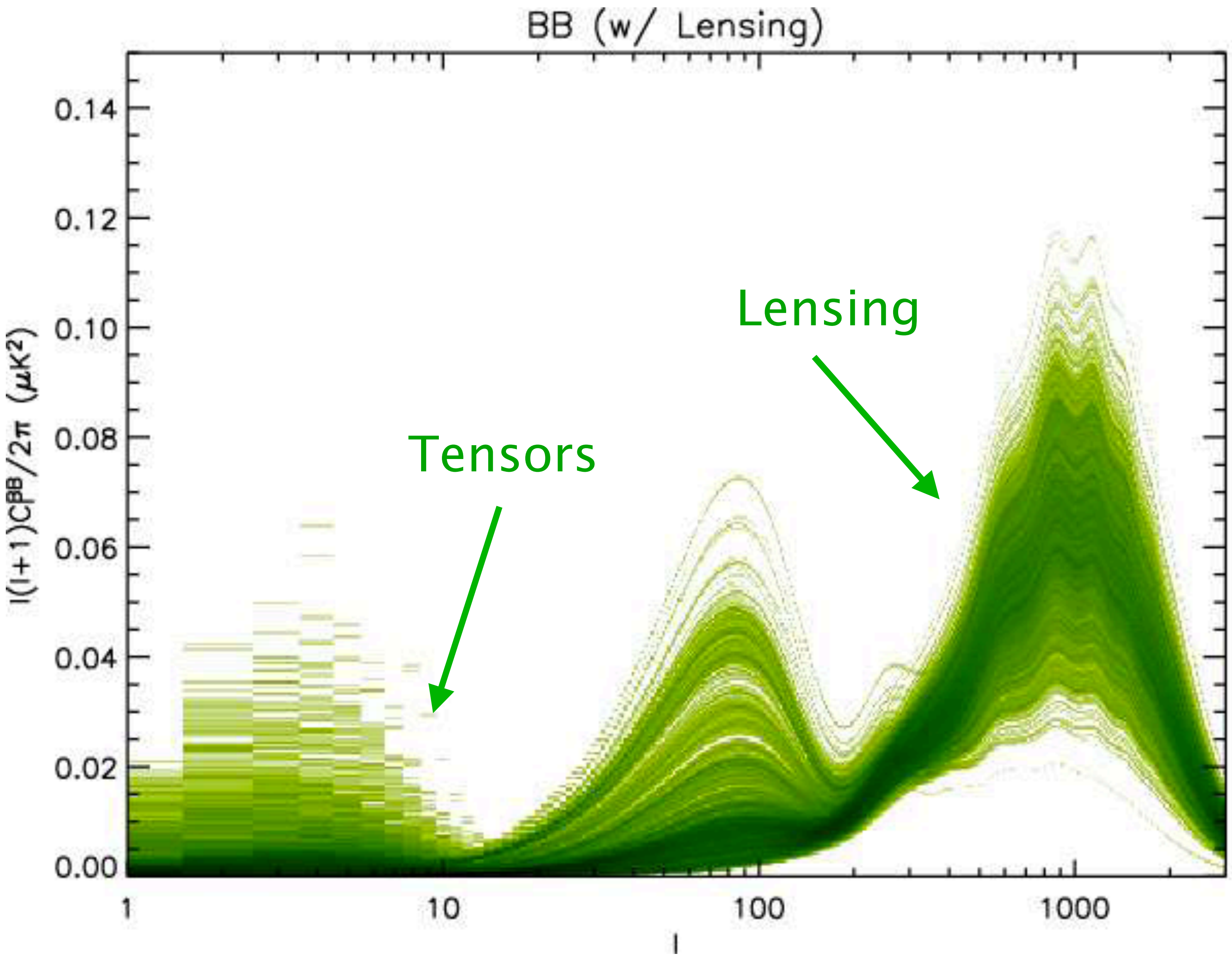

MCMC simulations from K. Vanderlinde

BB mode can tell us about a lot of new physics (energy scale at inflation, neutrino mass, etc.), but its prediction is still very uncertain.

Latest (2015) Planck+BICEP results put *r<0.08* at 95% confidence.

Scaler-to-Tensor ratio

1. Scaler power spectrum

The scaler perturbations are Gaussian, so all information about them is contained in the two-point correlation function:

$$\langle \mathcal{R}(\mathbf{k})\mathcal{R}^*(\mathbf{k}')\rangle = \frac{P(k)}{(2\pi)^3}\delta(\mathbf{k}-\mathbf{k}'),$$

The mean square value of the initial perturbation amplitude is

$$\langle \mathcal{R}^2(\mathbf{x})\rangle = \langle \int e^{i\mathbf{k}\mathbf{x}} R(\mathbf{k}) d^3k \int e^{-i\mathbf{k}'\mathbf{x}} R^*(\mathbf{k}') d^3k' \rangle = \int d^3k \frac{P(k)}{(2\pi)^3} = \int_0^\infty \frac{dk}{k}\mathcal{P}(k),$$

Where $\mathcal{P}(k) = k^3 P(k)/(2\pi^2)$ is also called the power spectrum, and is approximated as follows:

$$\mathcal{P}_s(k) = A_s \left(\frac{k}{k_*}\right)^{n_s-1}$$

In 1960's, Zel'dovich and Harrison independently predicted the flat spectrum of perturbations (i.e. $n_s = 1$). The WMAP5 values for a fixed $k_* = 500\ \mathrm{Mpc}^{-1}$ are:

$$A_s = (2.46 \pm 0.09)\cdot 10^{-9},$$
$$n_s = 0.960 \pm 0.014.$$

Scaler-to-Tensor ratio

2. Inflation and tensor power spectrum

Actually, the derivation of approximately flat power spectrum does not depend on whether we deal with scalar or tensor fields. So inflation also generates tensor perturbations (transverse traceless perturbations of spatial metric h_{ij}, i.e. gravitational waves).

We have the same picture for tensor perturbations: primordial perturbations are Gaussian random field with almost flat power spectrum. In this case we have

$$\mathcal{P}_T(k) = A_T \left(\frac{k}{k_*}\right)^{n_T} .$$

It is convenient to introduce the parameter $r = \mathcal{P}_T/\mathcal{P}_s$ which measures the ratio of tensor to scalar perturbations.

For simple inflation theories with power-law potentials (last slide), prediction is $r \sim 0.1 - 0.3$

➜ **these are now practically ruled out by Planck data**

Scaler-to-Tensor ratio

3. Inflation and the spectral index, n_s

Inflation occurs if the universe is filled with a scalar field φ, which has non-vanishing scalar potential V(φ). The homogeneous field φ then satisfies the equation

$$\ddot{\varphi} + 3H\dot{\varphi} = -\frac{dV}{d\varphi}. \qquad\qquad a(t) \propto \exp\left(\int H dt\right), \quad H \approx \text{const.}$$

For a relatively flat potential (dV/dφ small), the acceleration term can be neglected. The Friedmann equation in this case is $H^2 = 8\pi/3\ G\ V(\varphi)$. So if φ varies slowly, then V(φ) and thus H also varies slowly, and the parameters of inflation are almost time independent *(slow-roll inflation)*.

Yet, the parameters are not *exactly* time-independent at inflation, so the predicted value of the spectral tilt (n_s – 1) is small but non-zero. It can be positive or negative, depending on the scalar potential V(φ). In particular, it is negative for the simplest power-law potentials like

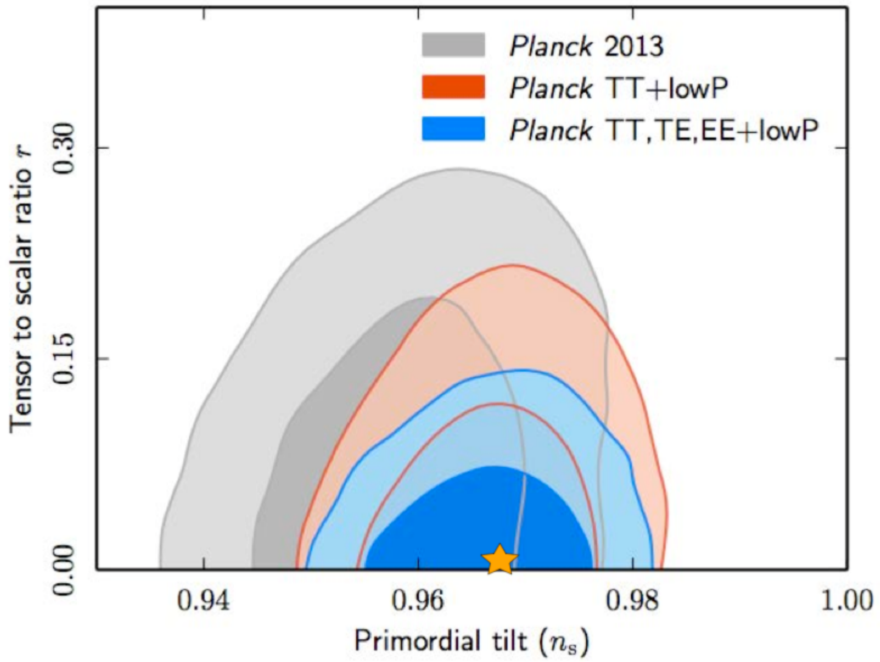

$$V(\varphi) = \frac{m^2}{2}\varphi^2 \quad \text{or} \quad V(\varphi) = \frac{\lambda}{4}\varphi^4.$$

Here one can have a very simple relation (for specific slow-roll inflation models):

$$r = -8n_s$$

Detection of E-mode polarization

- The DASI experiment at the South Pole was the first to detect E-mode CMB polarization
- It was followed by WMAP's measurement of $C^{TE}(l)$ for $l<500$
- Both the BOOMERANG and the CBI experiments have reported measurements of C^{TT}, C^{TE}, C^{EE} and a non-detection of B modes
- E-mode has also been measured by CAPMAP and Maxipol
- B-mode polarization has not been detected yet (current noise level for ground-based experiment is below 1 μK in Q and U))

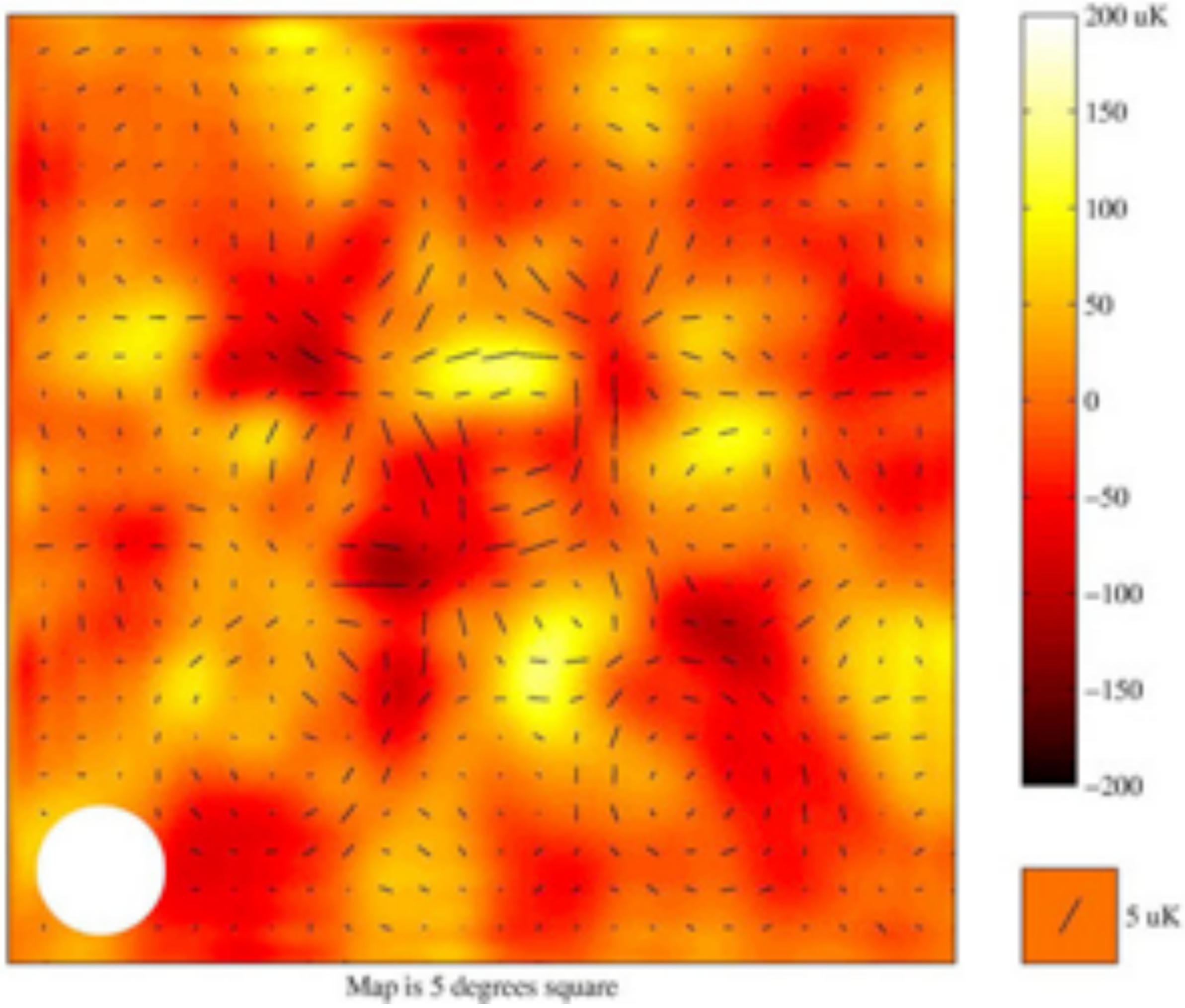

DASI collaboration, 2002

WMAP measurement of E-mode

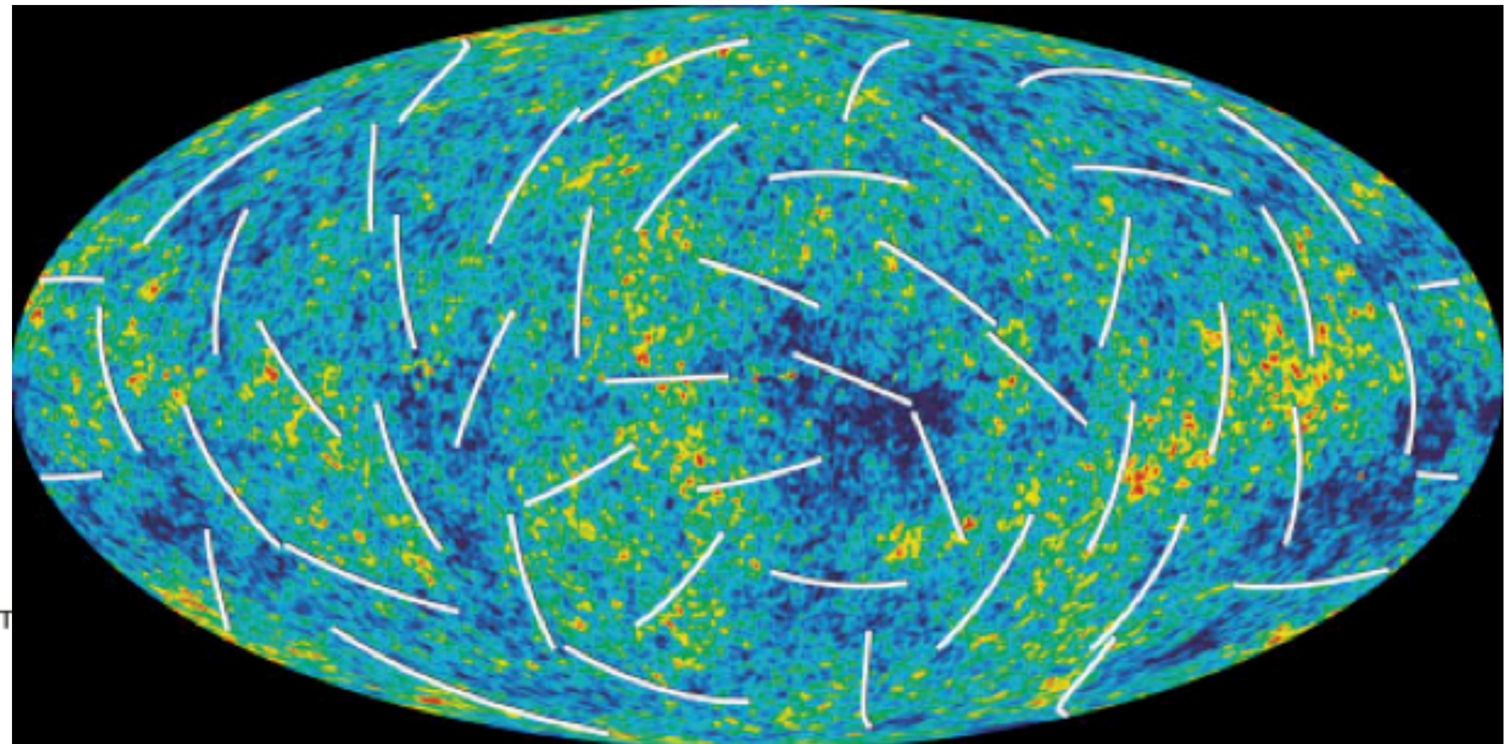

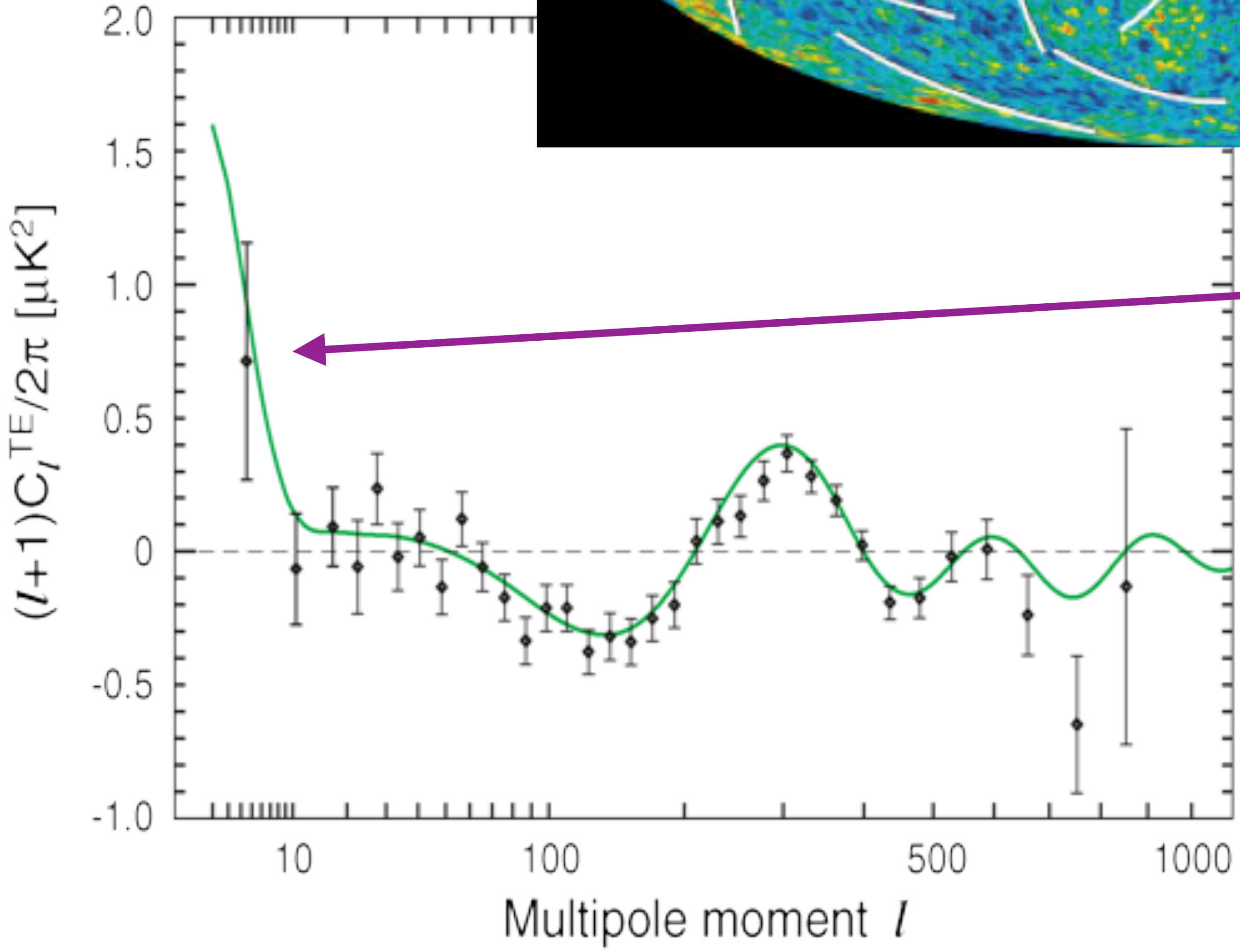

Re-scattering of the CMB photons during and after reionization added to the polarized power on large angular scales

(scale comparable to the horizon, H^{-1}, at the epoch of scattering)

Measurements of Planck TE, EE

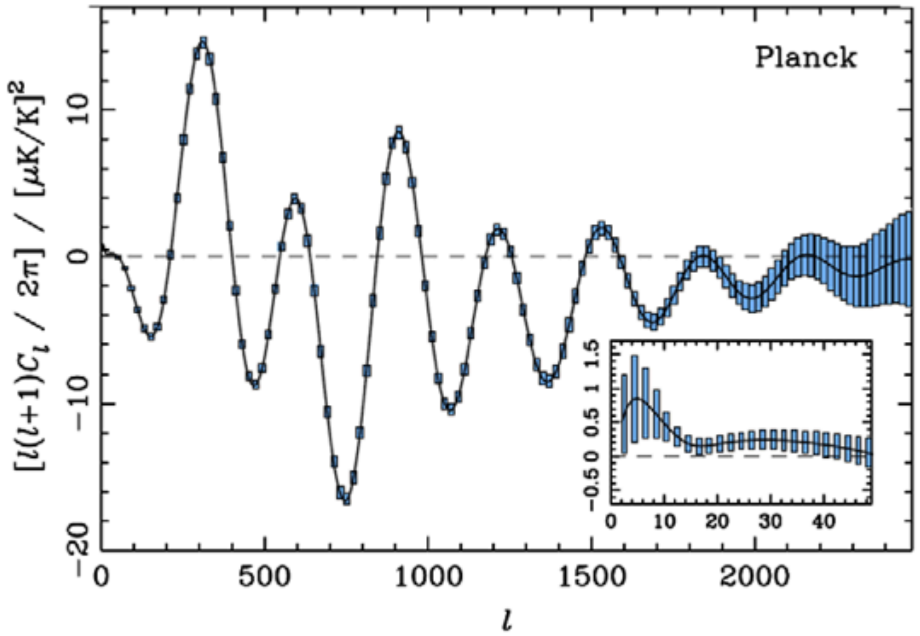

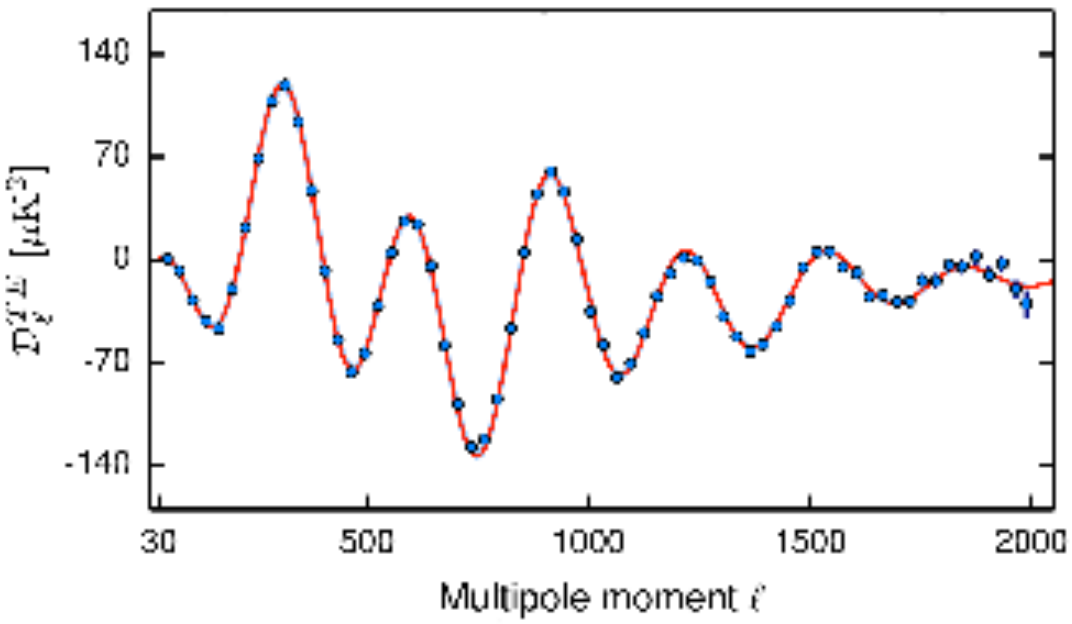

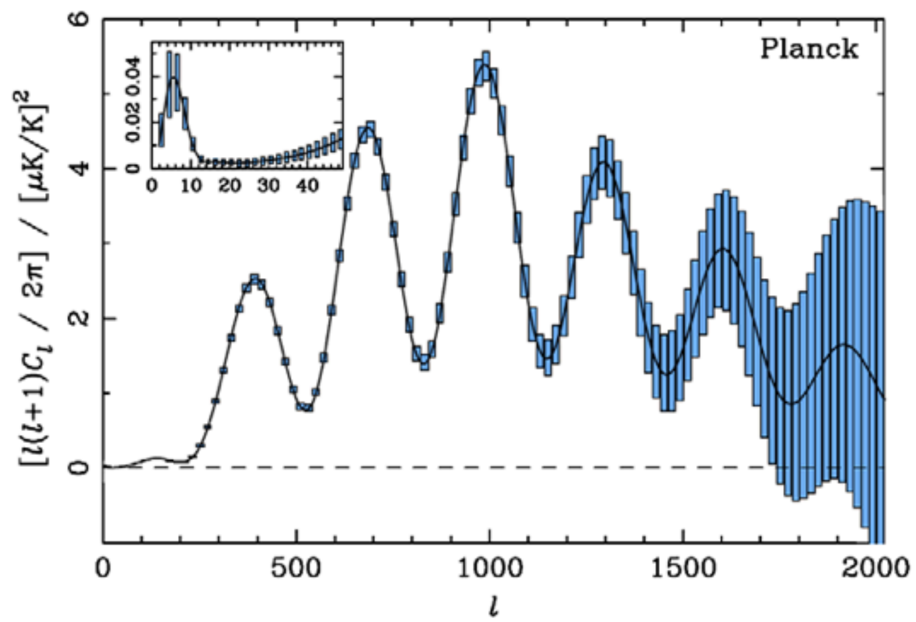

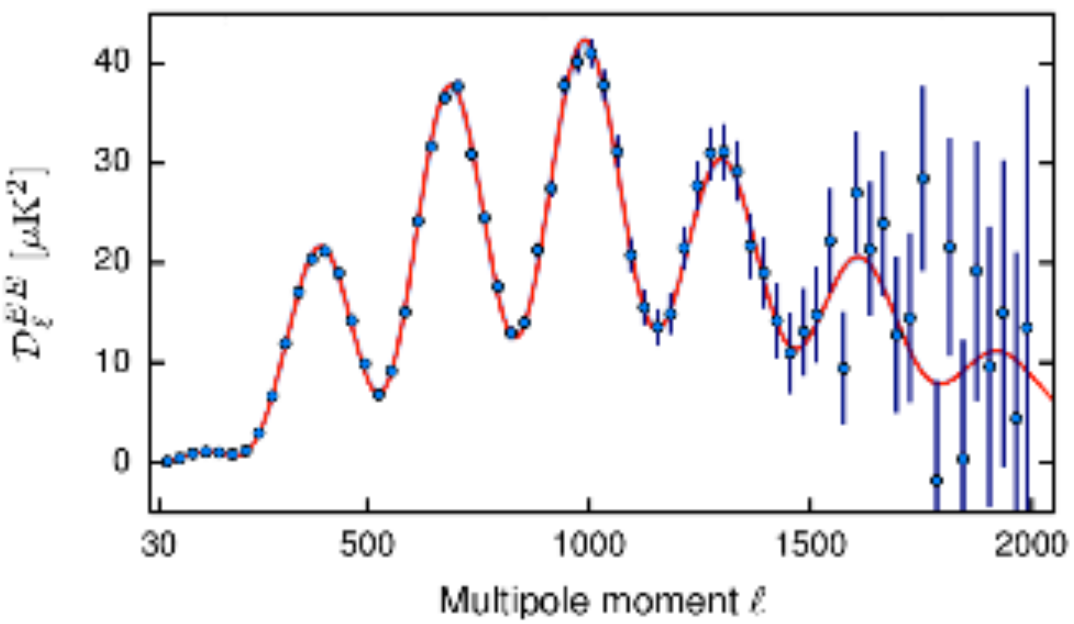

Prediction (Planck bluebook)

Measurements (Planck 2015)

Planck limits from Temperature data

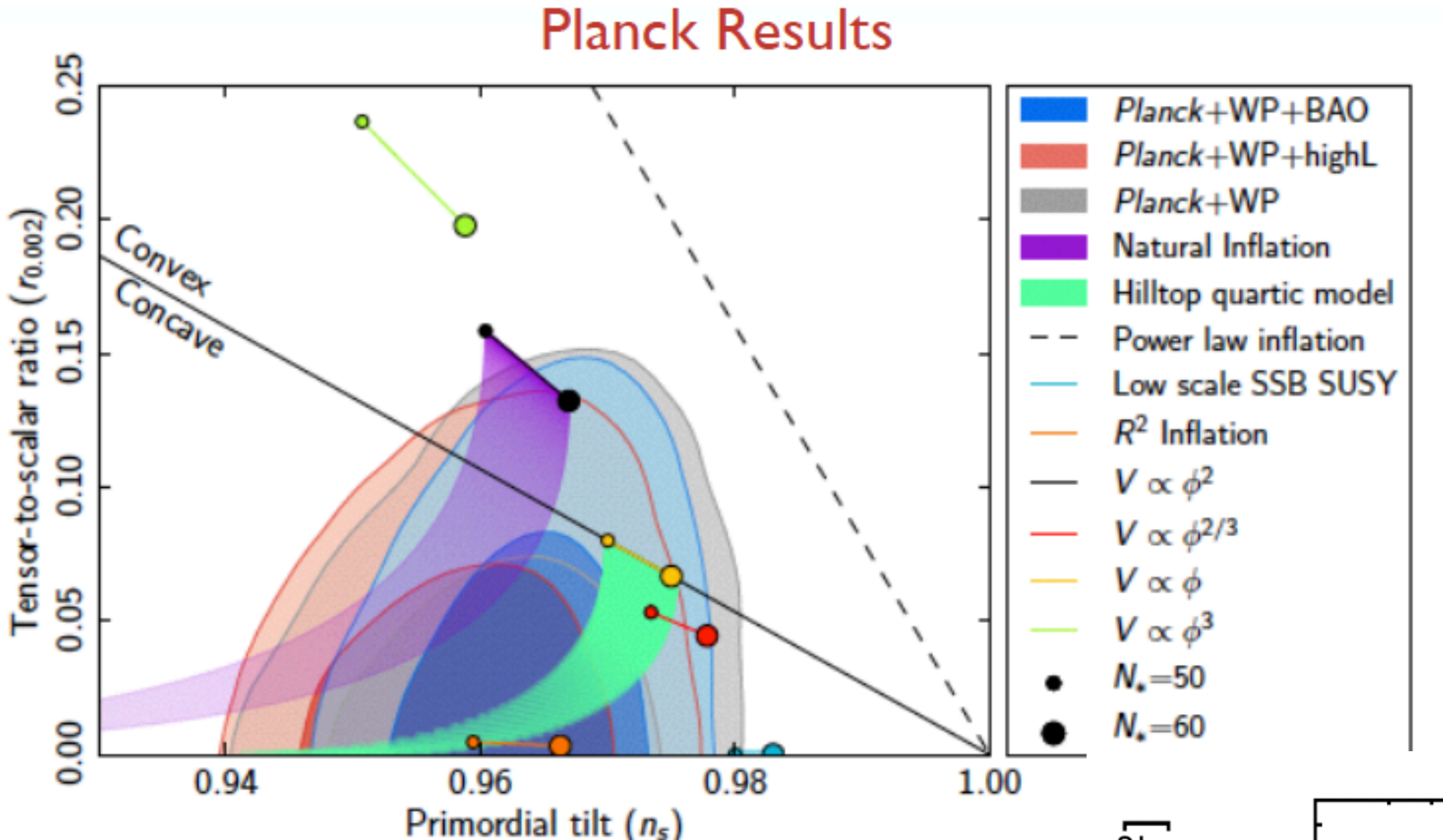

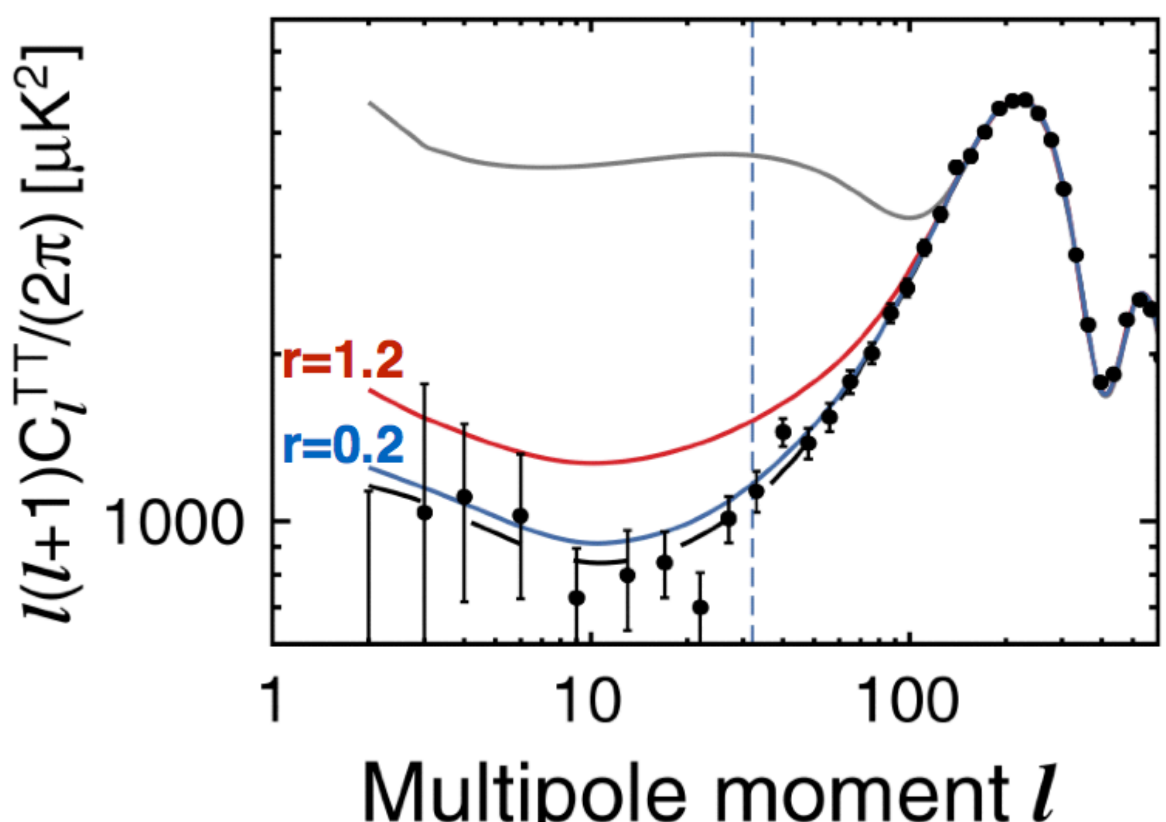

From precise TT measurements, Planck could already exclude a lot of parameter space.

Other measurements of EE, BB

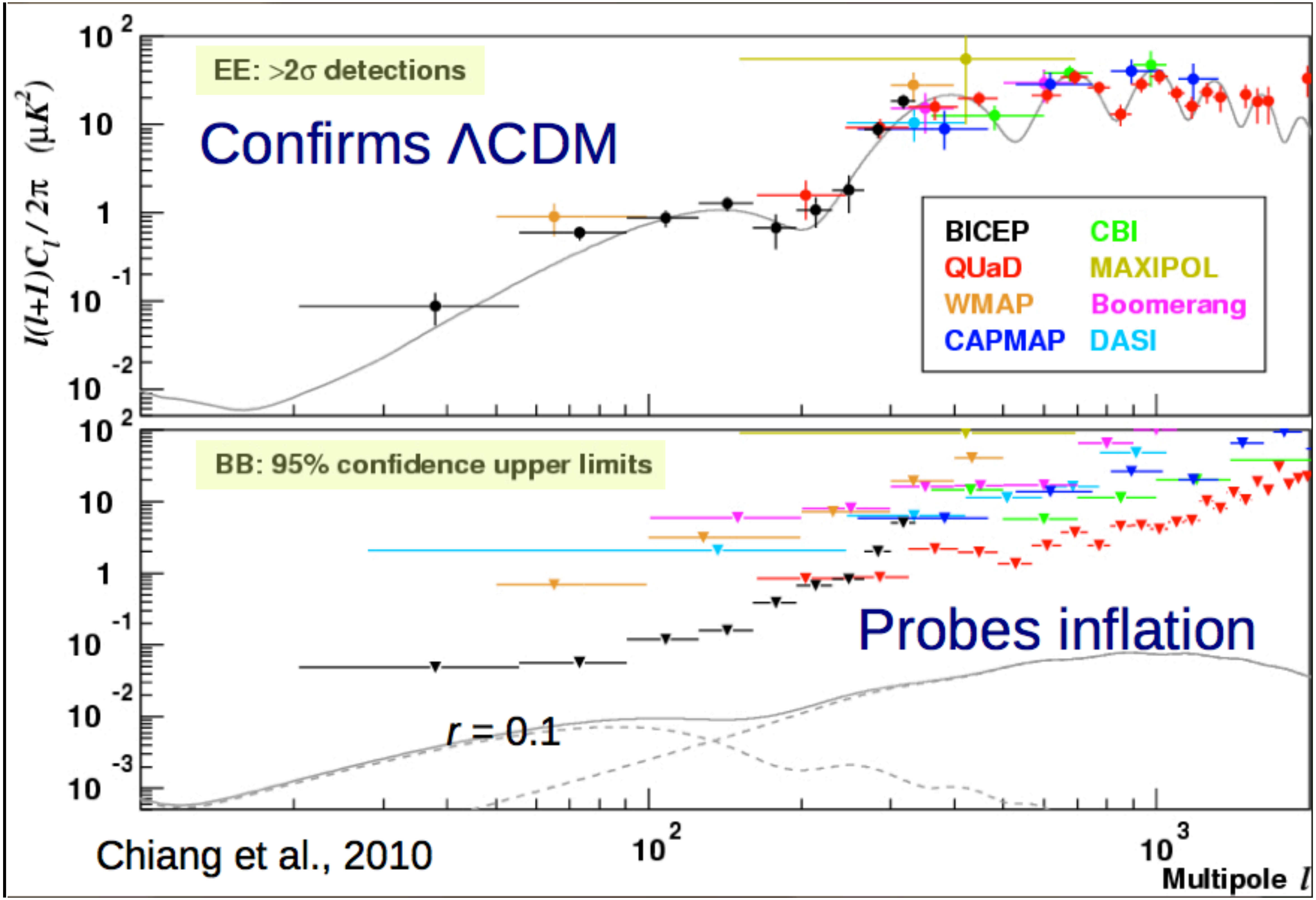

BICEP-2 result in 2014

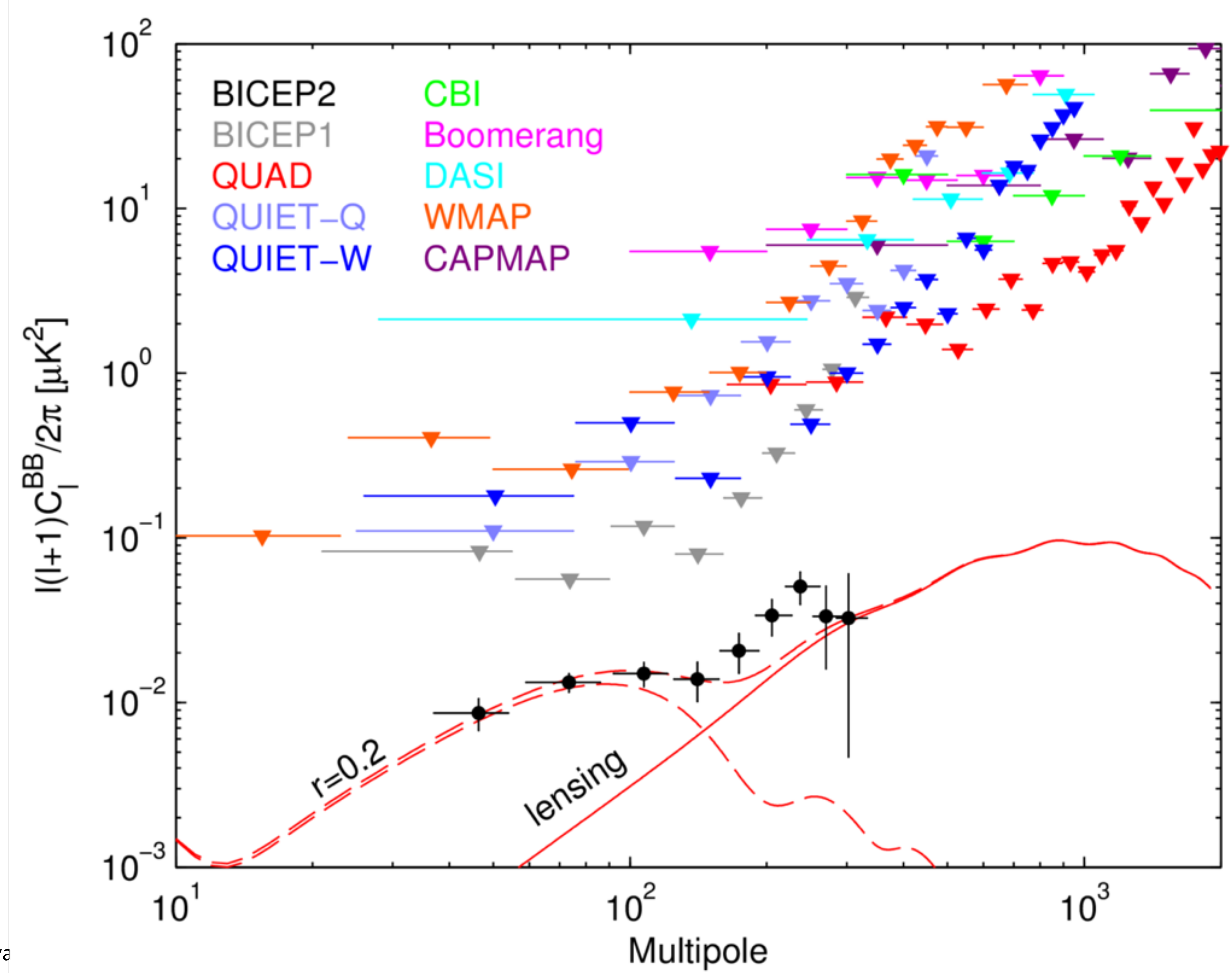

BICEP-2 observation of the CMB

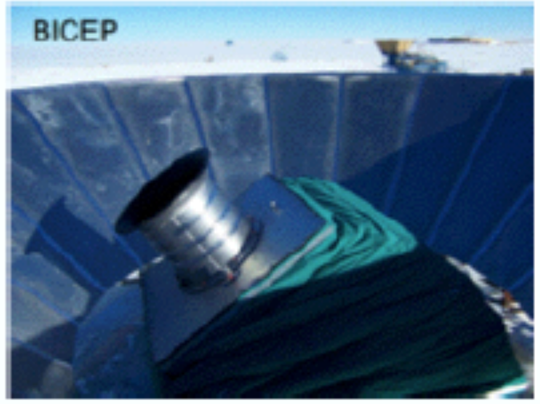

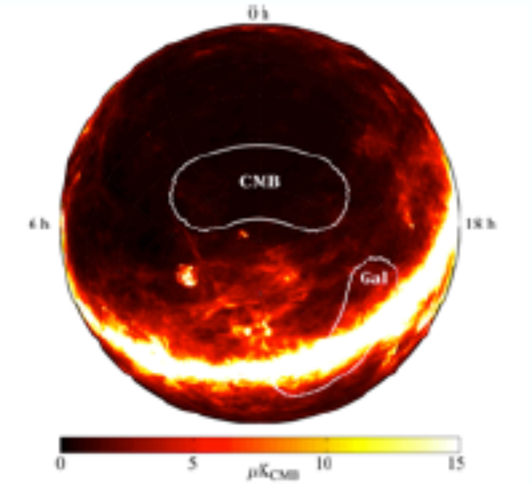

- Small telescope at South Pole
- 512 bolometers at 150 GHz
- Observed 380 square degrees for three years (2010 - 2012)
- Previous BICEP1 at 100 and 150 GHz (2006-2008)
- Current: Keck Array = 5 x BICEP2 at 150 GHz (2011 - 2013) and additional detectors at 100 and 220 GHz (2014 onwards)

BICEP-2 observation of the CMB

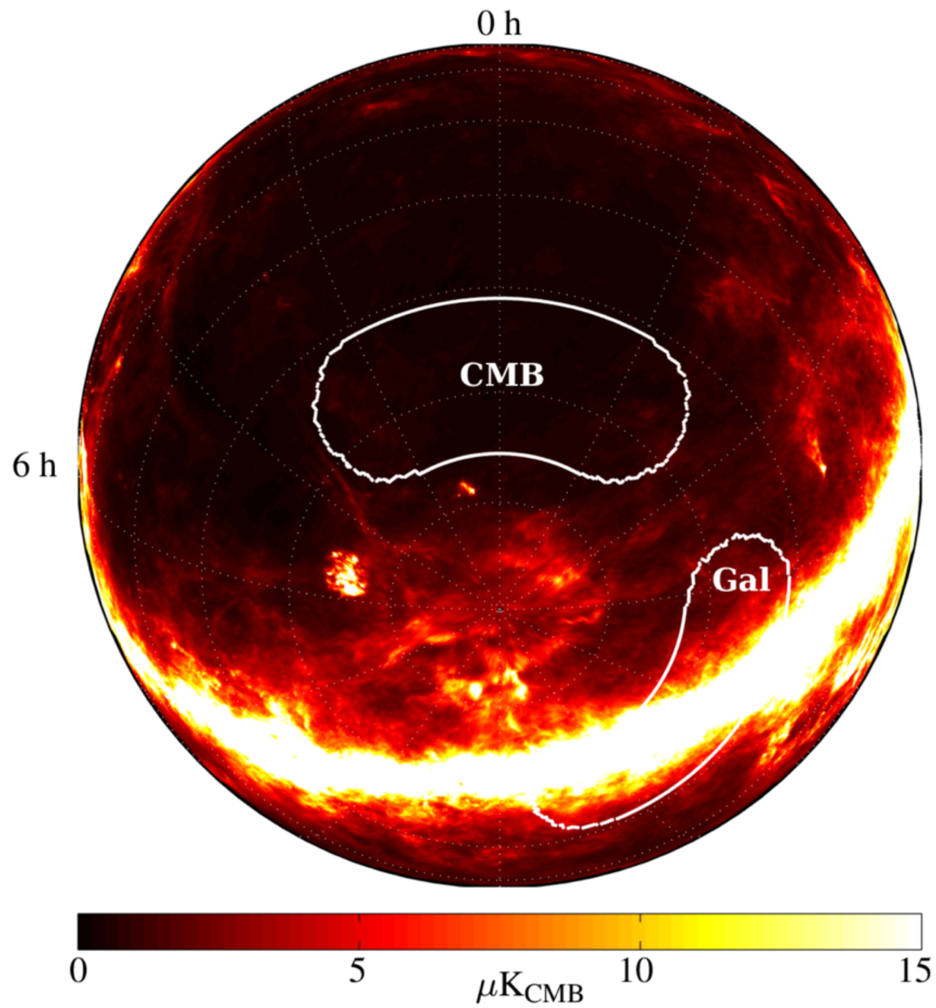

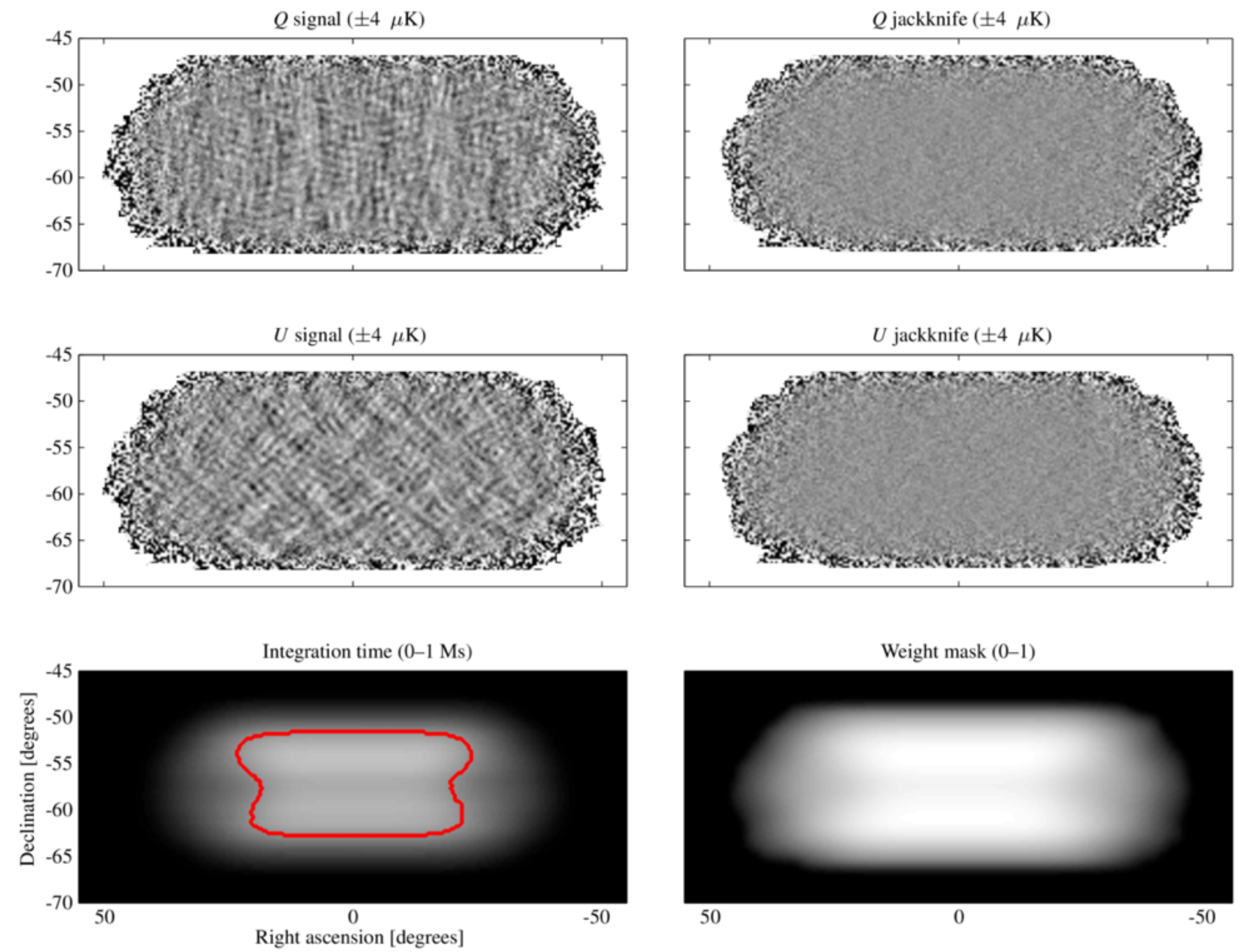

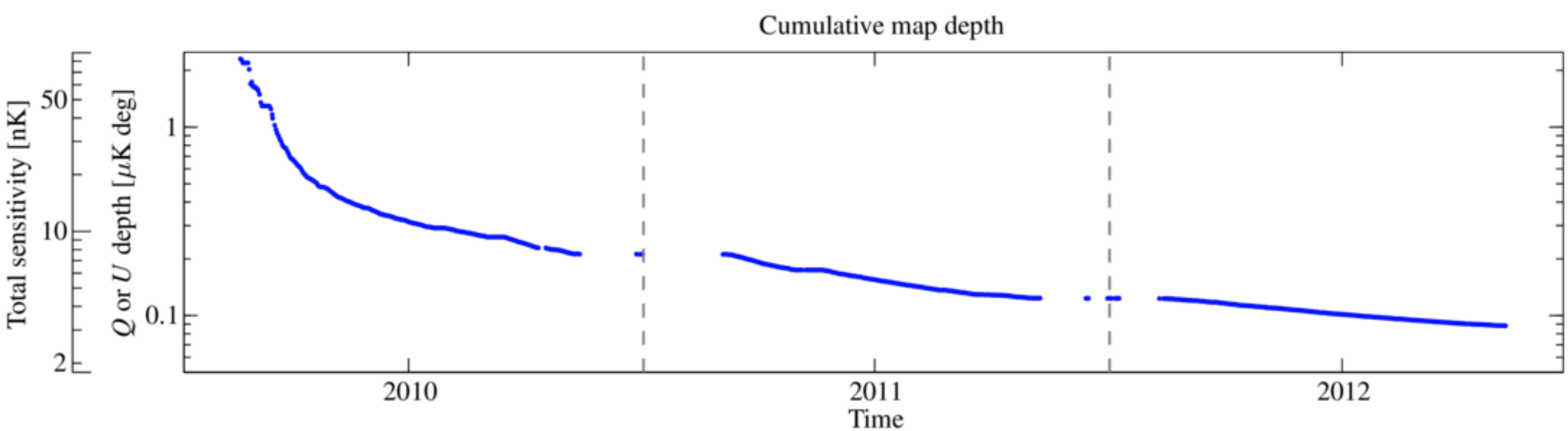

BICEP2 E- and B-mode CMB maps

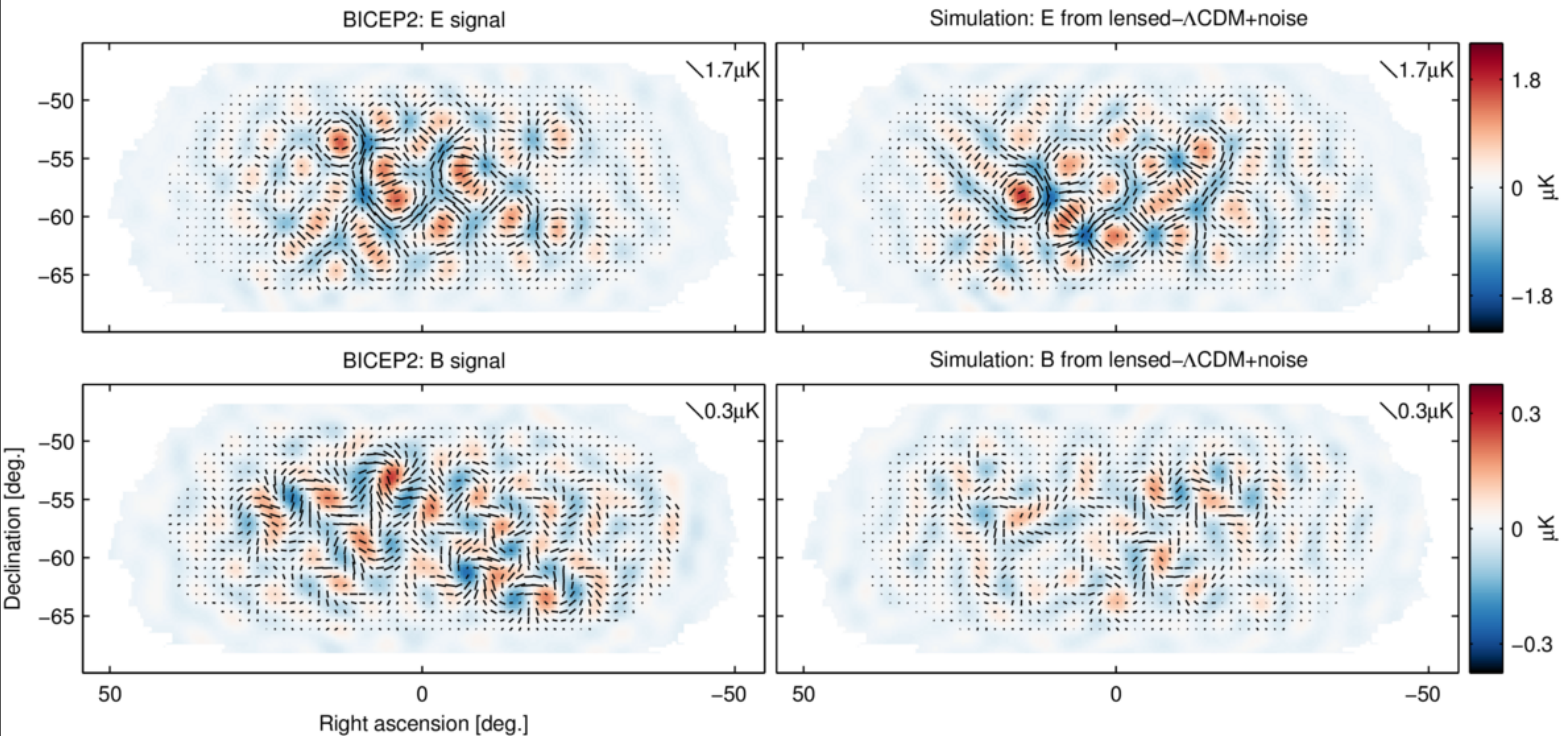

BICEP2 power-spectra and null tests

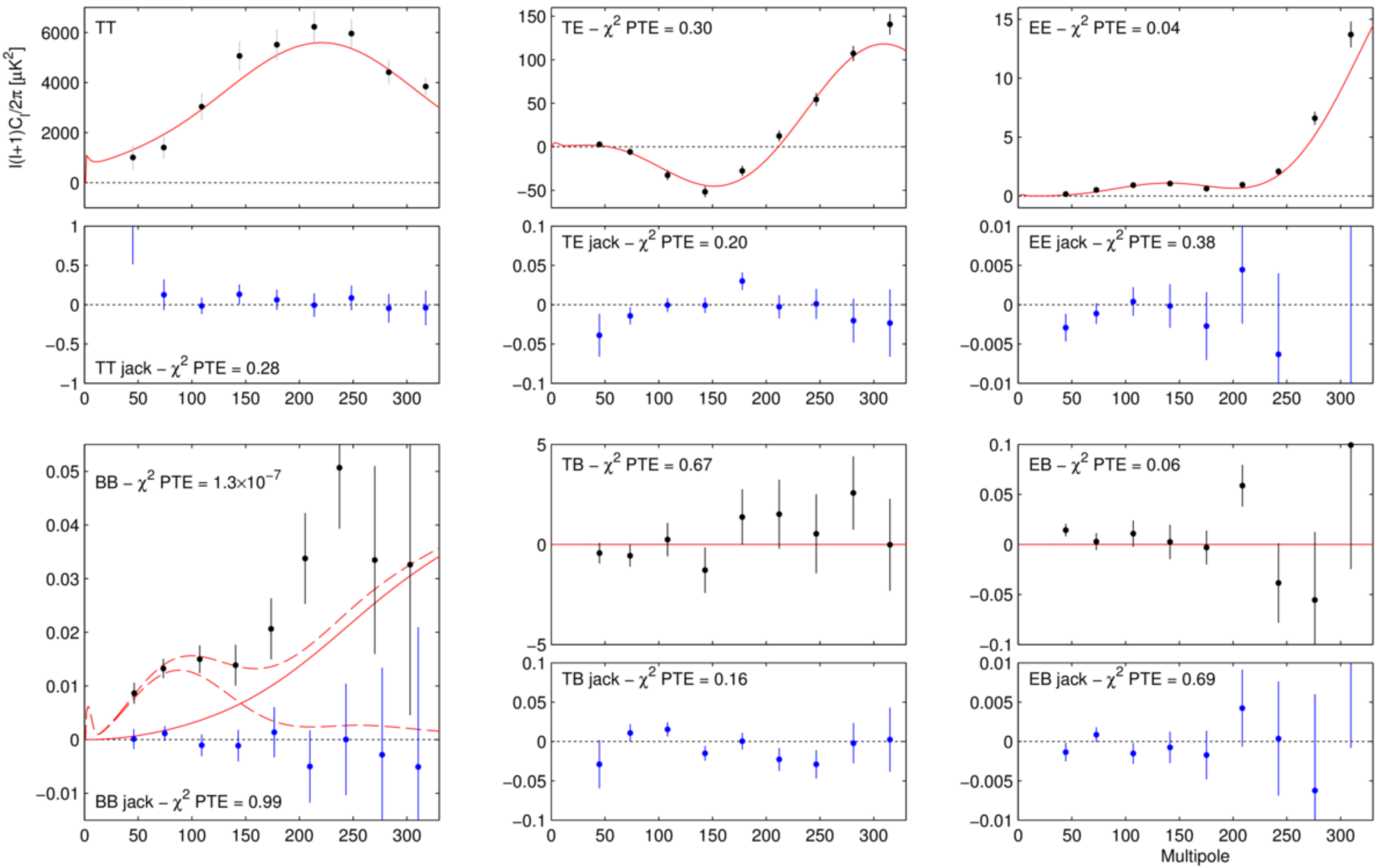

BICEP2 scaler-to-tensor ratio

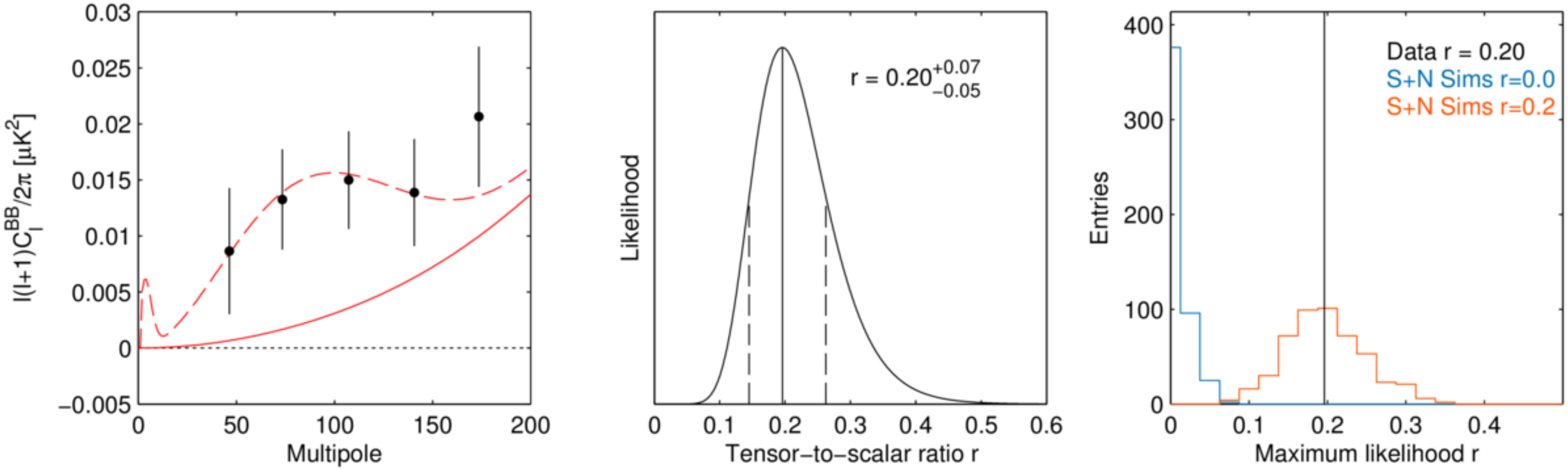

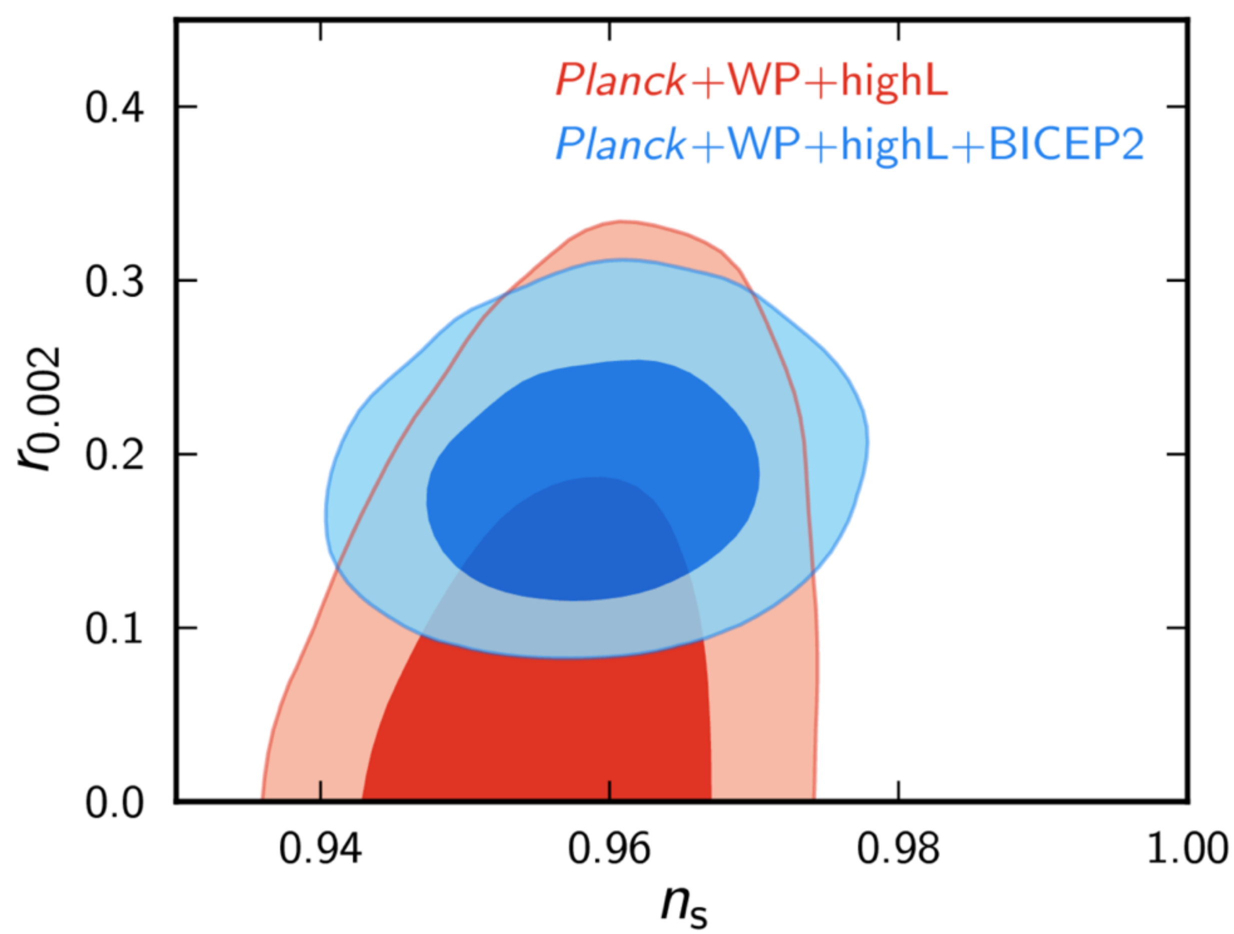

Comparison with Planck 2013 result → a clear tension!

Then... proved wrong by *Planck*!

Planck Collaboration XXX (2014)

Dust polarization at high galactic latitudes

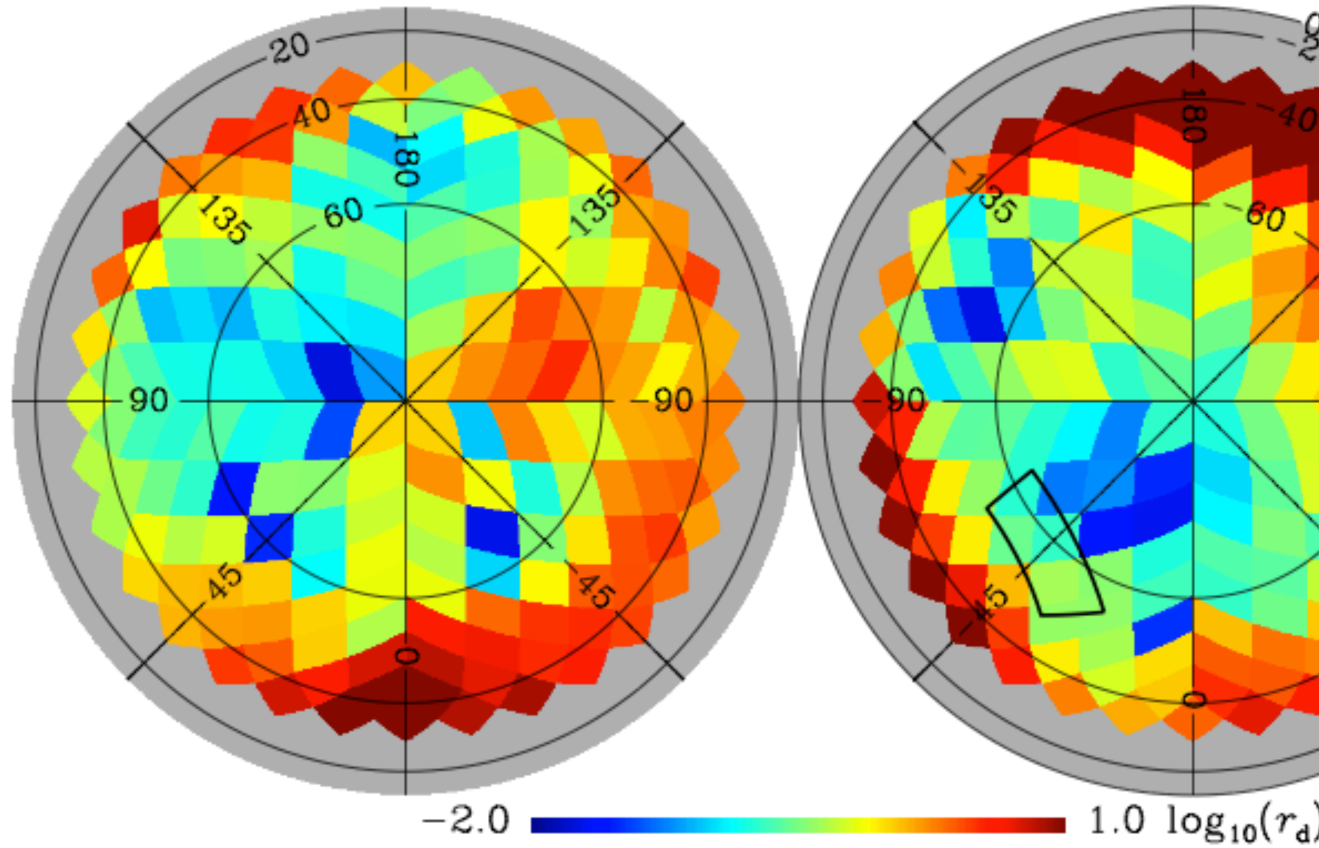

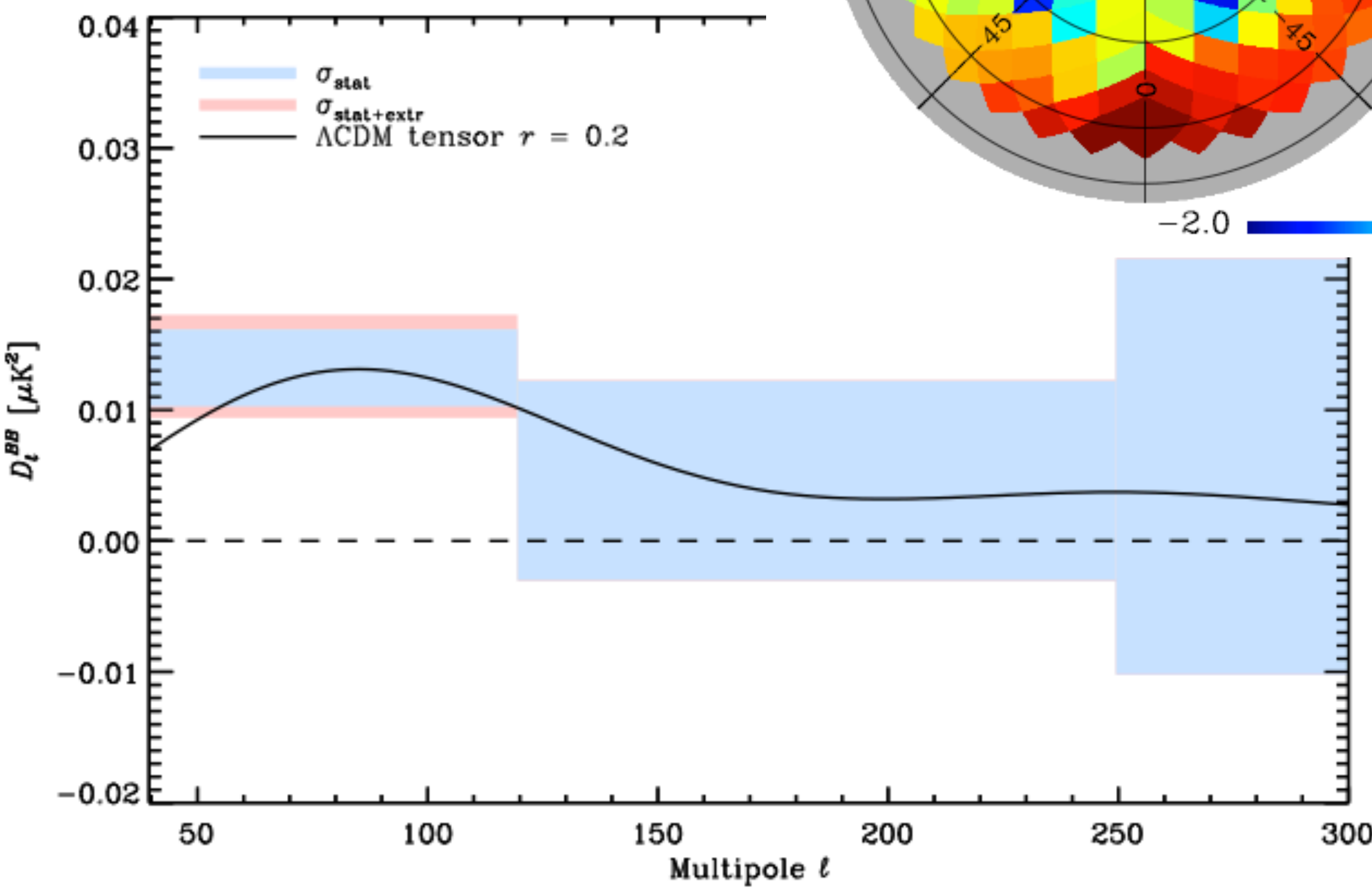

BICEP-2 severely underestimated the dust polari- -zation power at low multipoles

Planck's view of the BICEP2 field

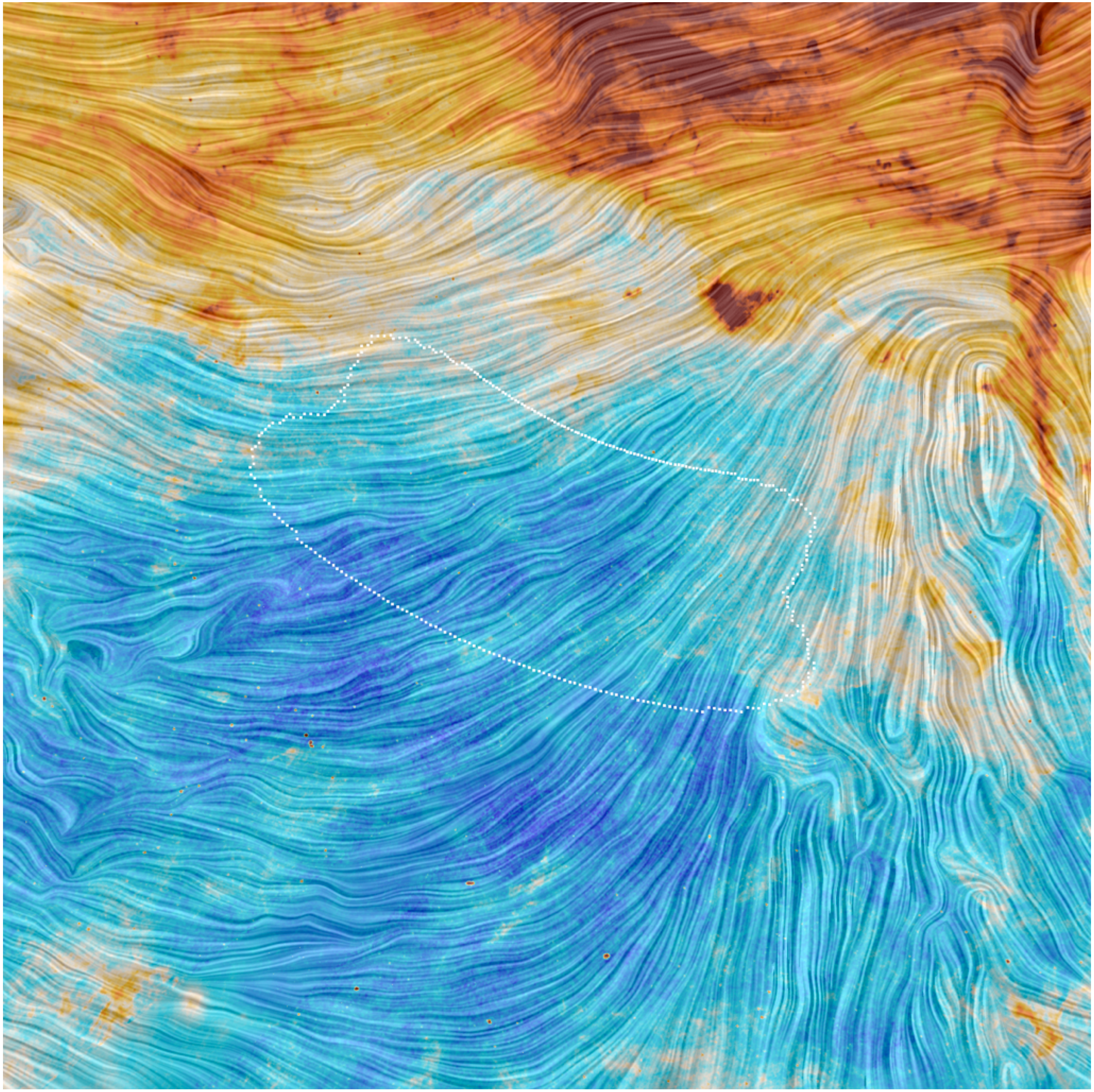

colors → dust intensity

"engravings" → magnetic fields

Planck results on the B-mode

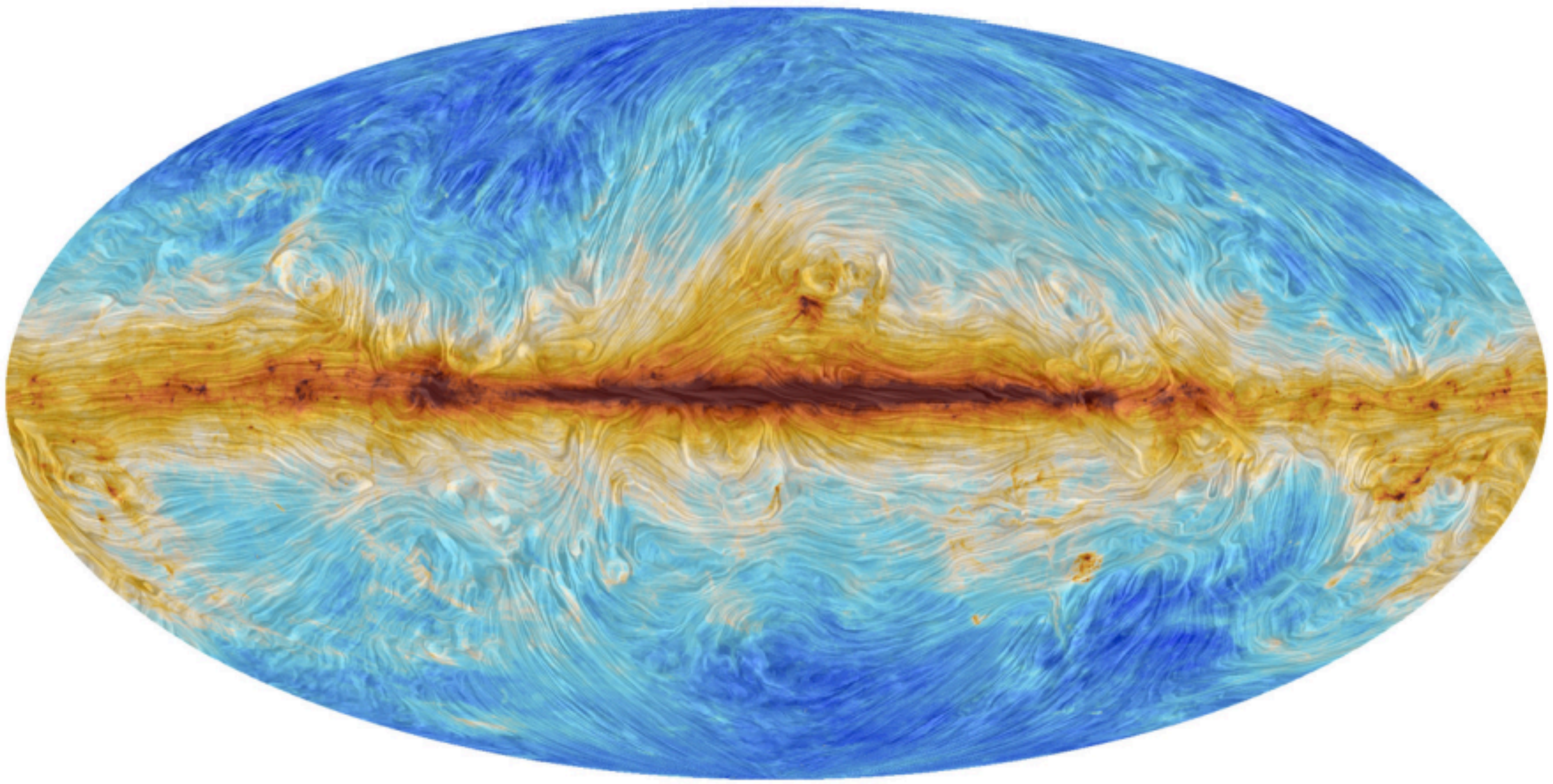

Dust polarization map
(Planck collaboration 2015)

Lensing B-mode
(Planck collaboration 2015)

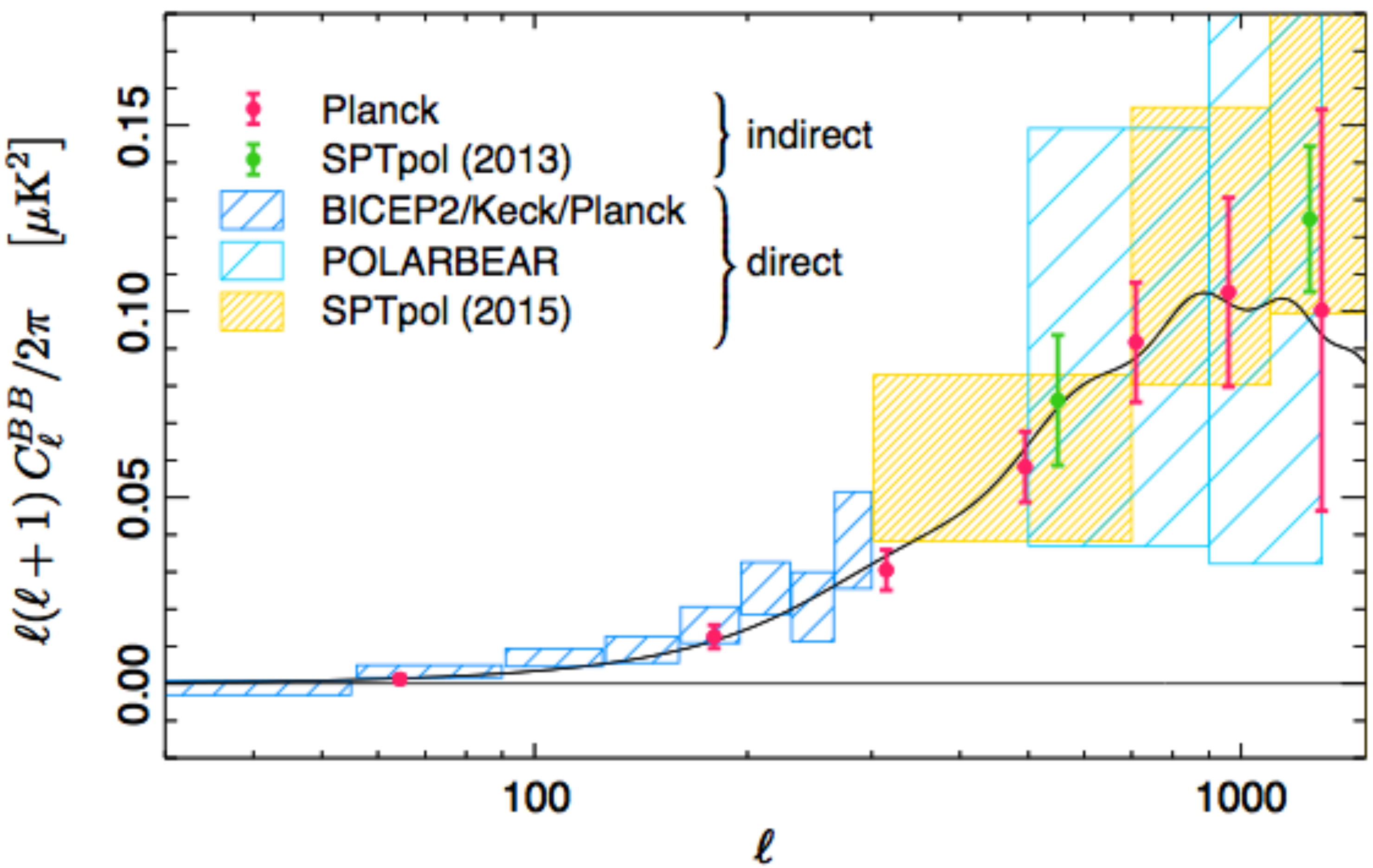

Planck 2015 + BICEP2

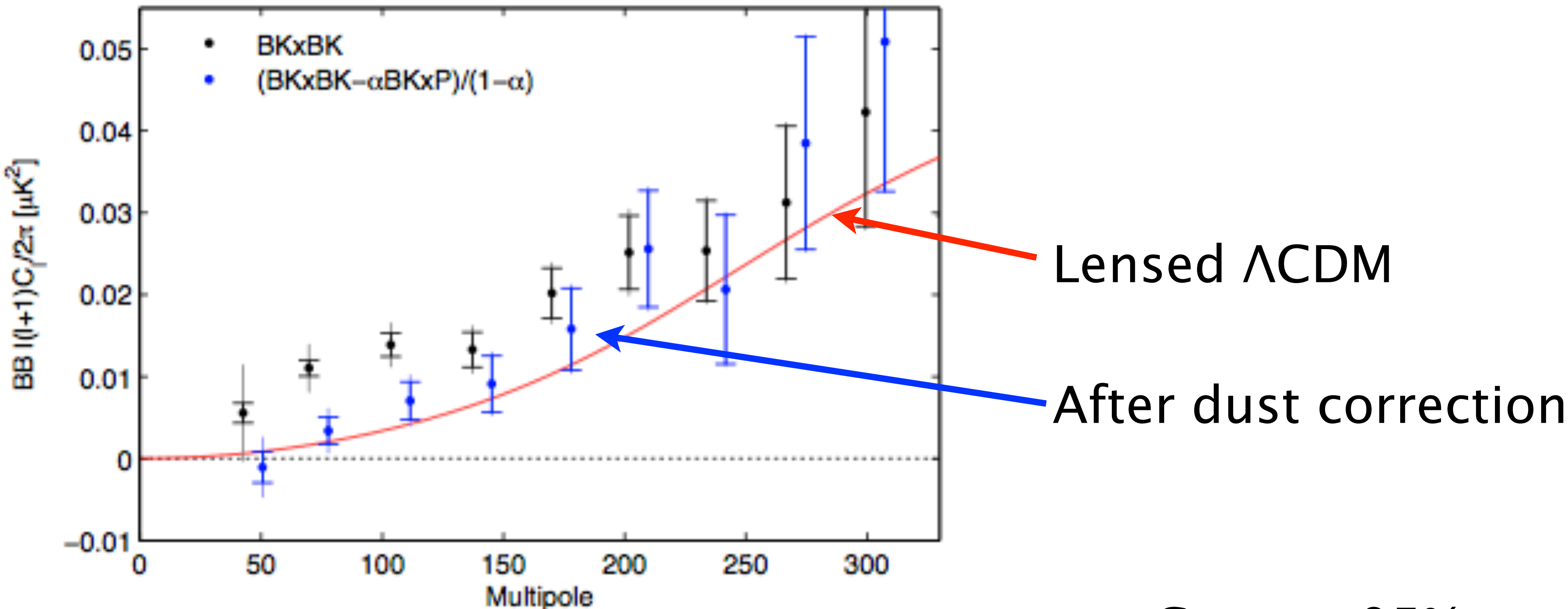

BICEP2 + Planck joint analysis (2015)

Current 95% upper limit: $r < 0.08$

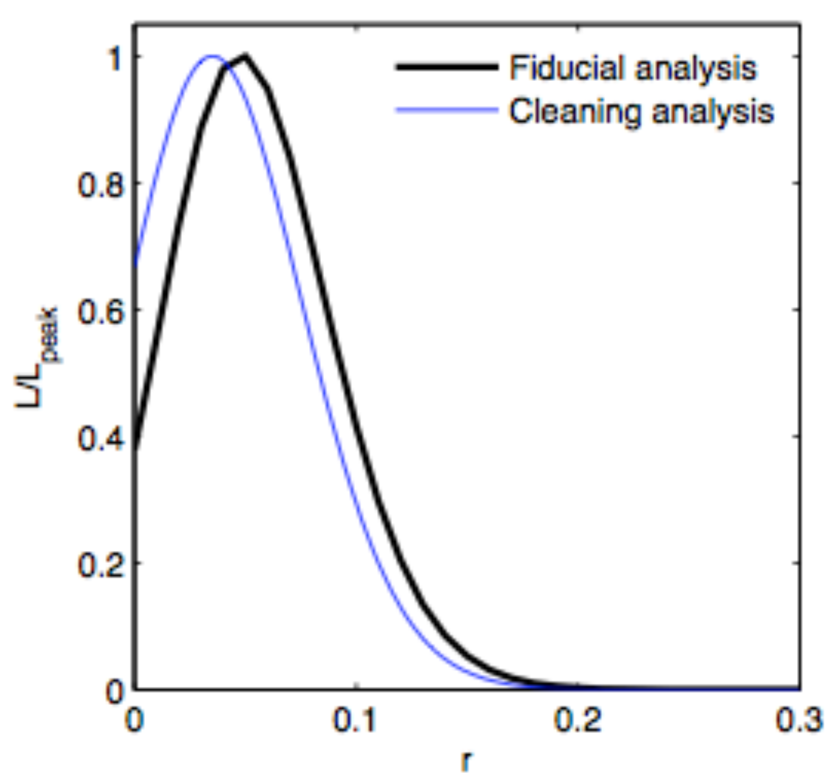

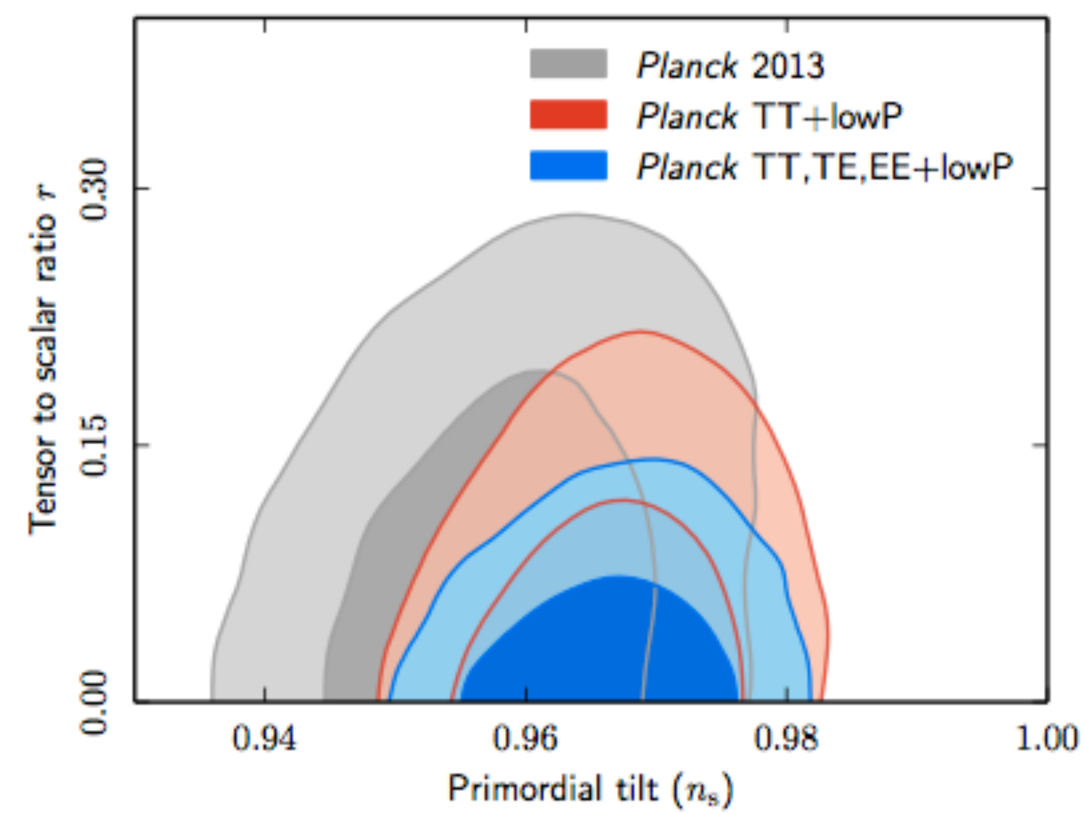

Several new experiments

ACTpol

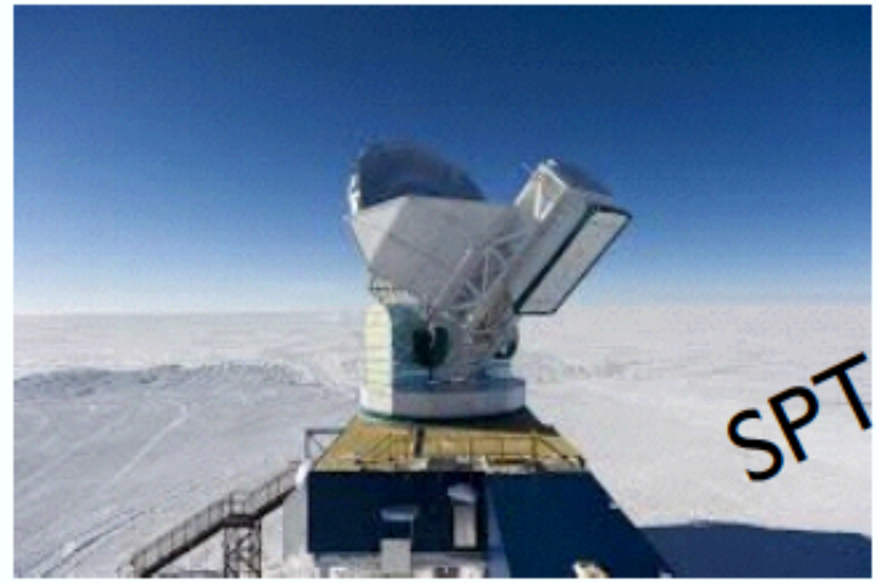

SPTpol

Have broad science range

ABS

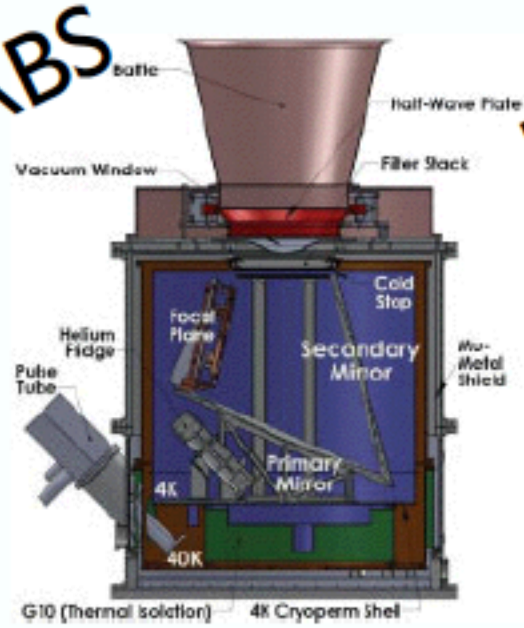

Polarbear

SPIDER

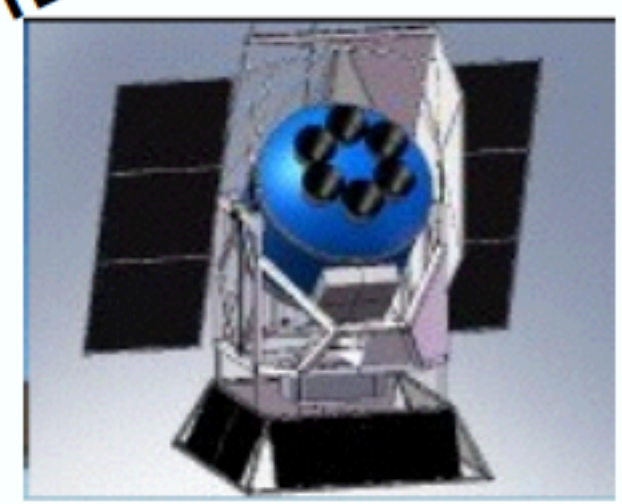

Dedicated to r

The Planck satellite

Credit: ESA

PLANCK launched May 2009

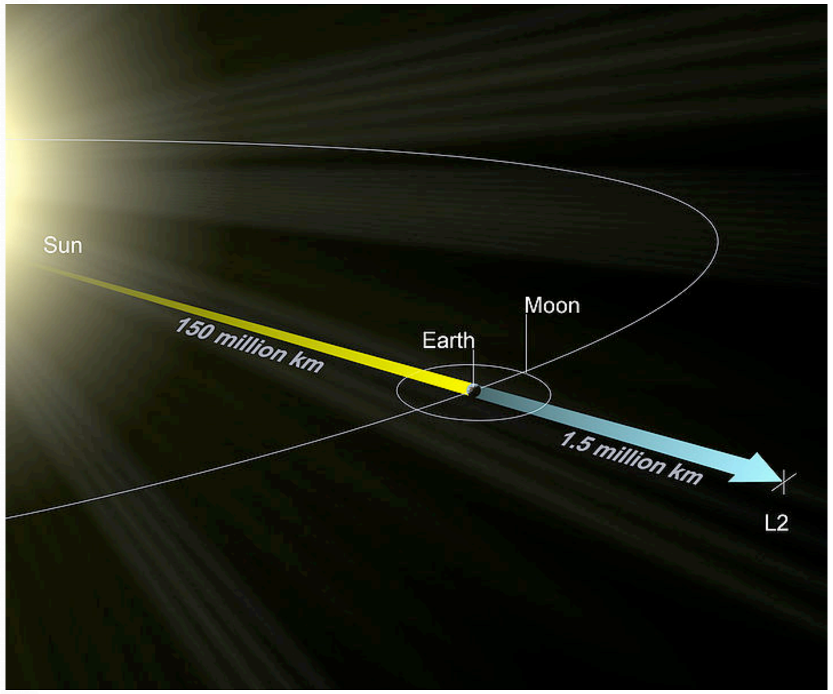

Destination L2: the second Lagrangian point

(getting crowded there!)

Credit: ESA

Planck revolutionizing CMB science

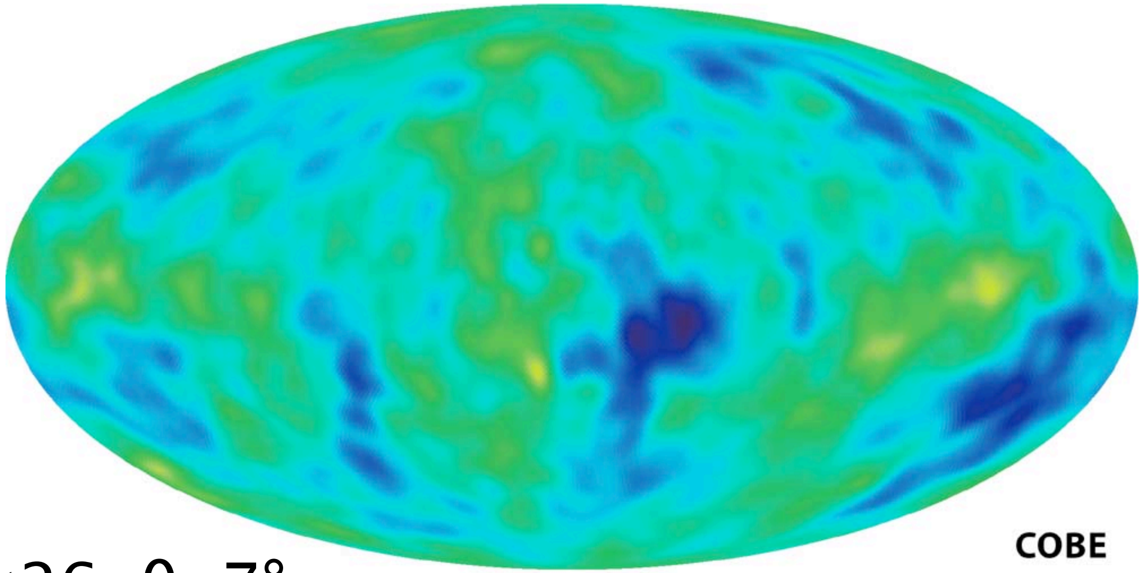

$l<26$, $\theta\sim7°$

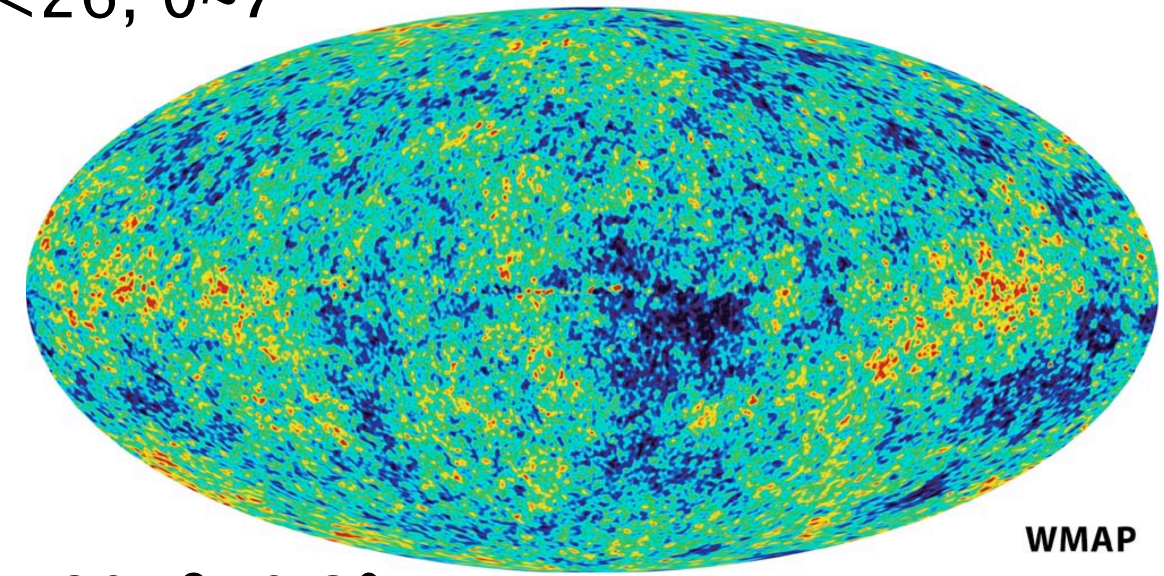

$l<780$, $\theta\sim0.2°$

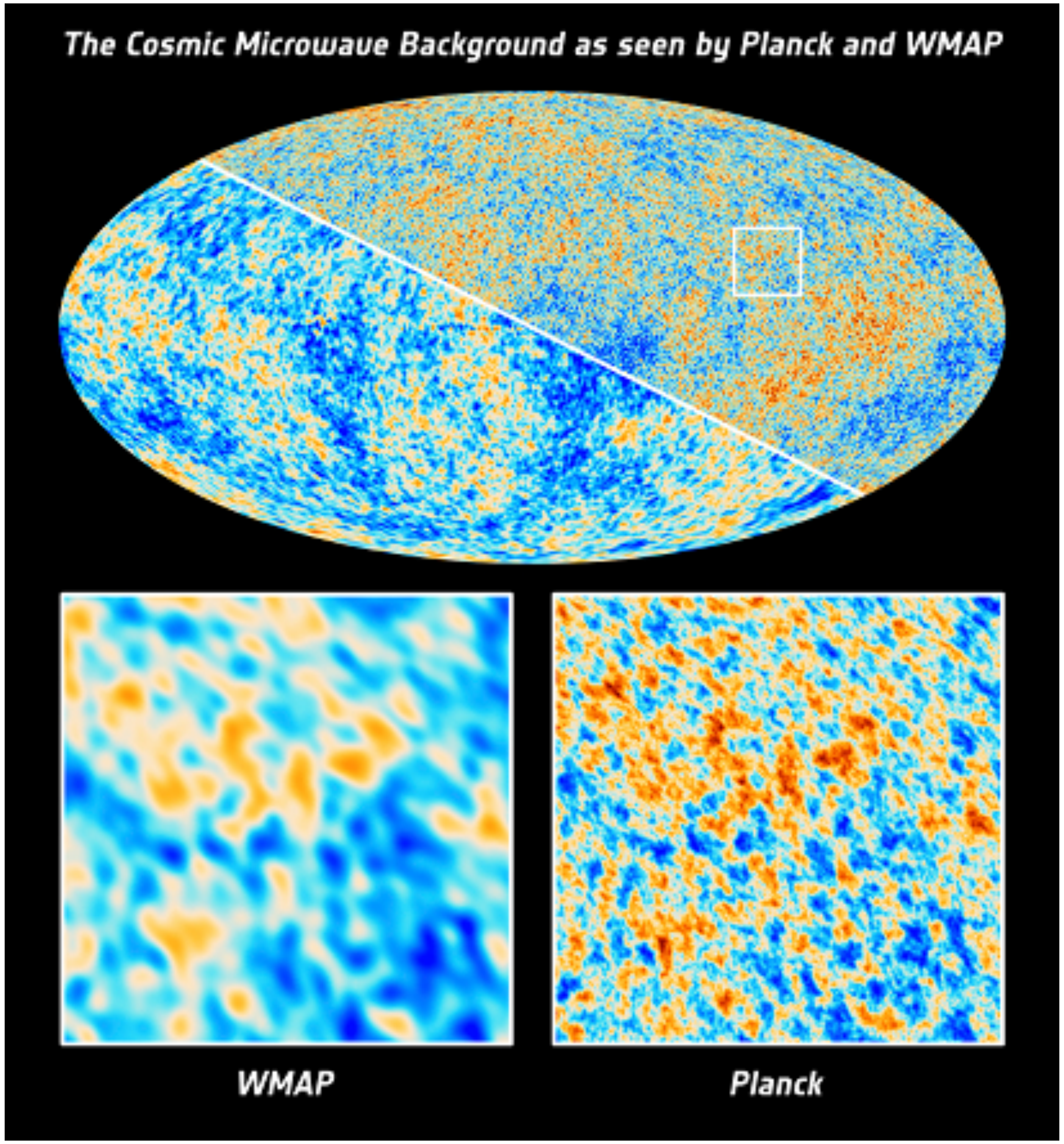

$l<2160$, $\theta\sim0.1°$

CMB sky seen from Planck

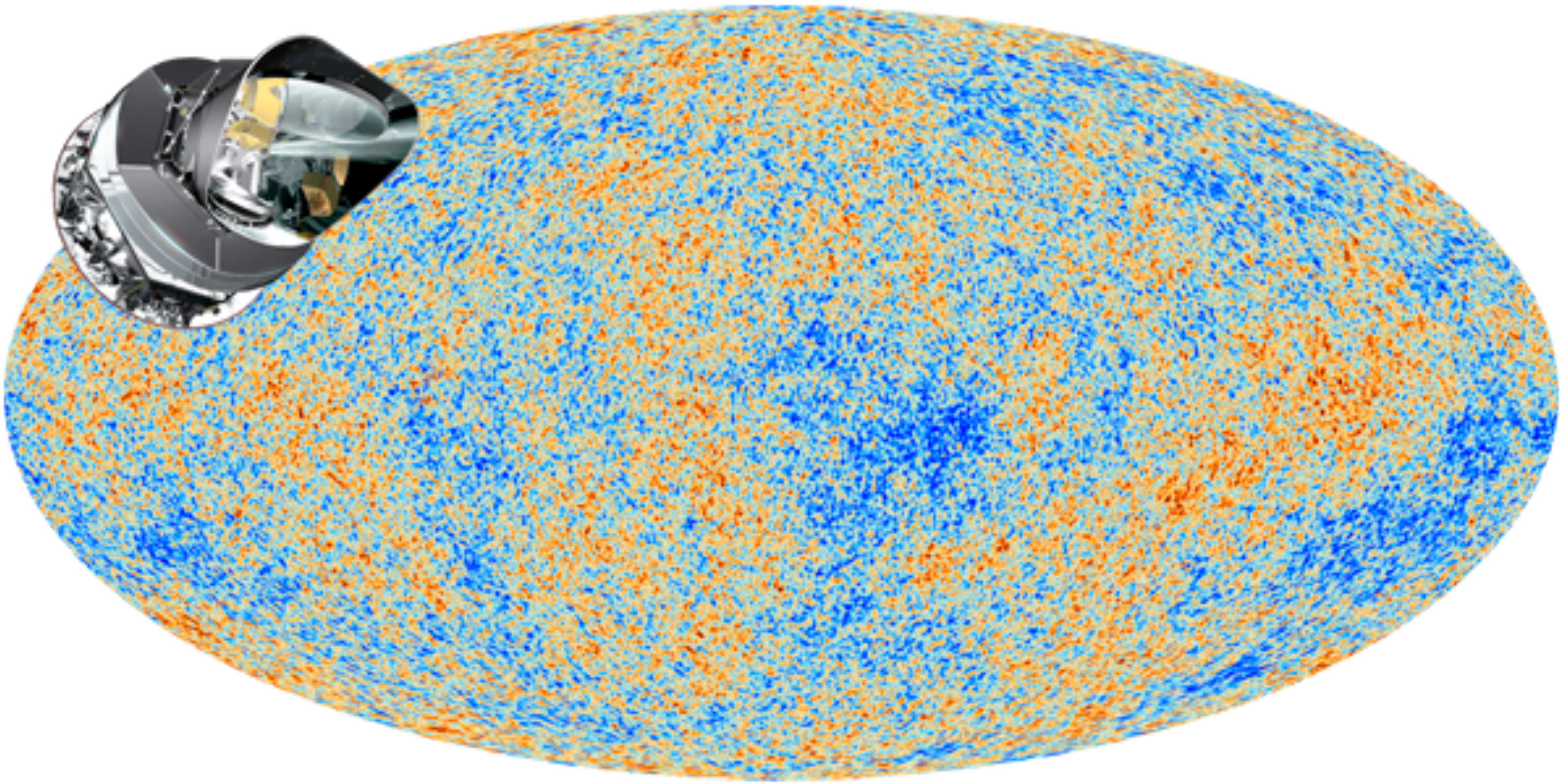

Measurement from Planck, dipole and Galaxy subtracted.

We learned in the last lecture how to do science from this 2D map.

Planck detectors

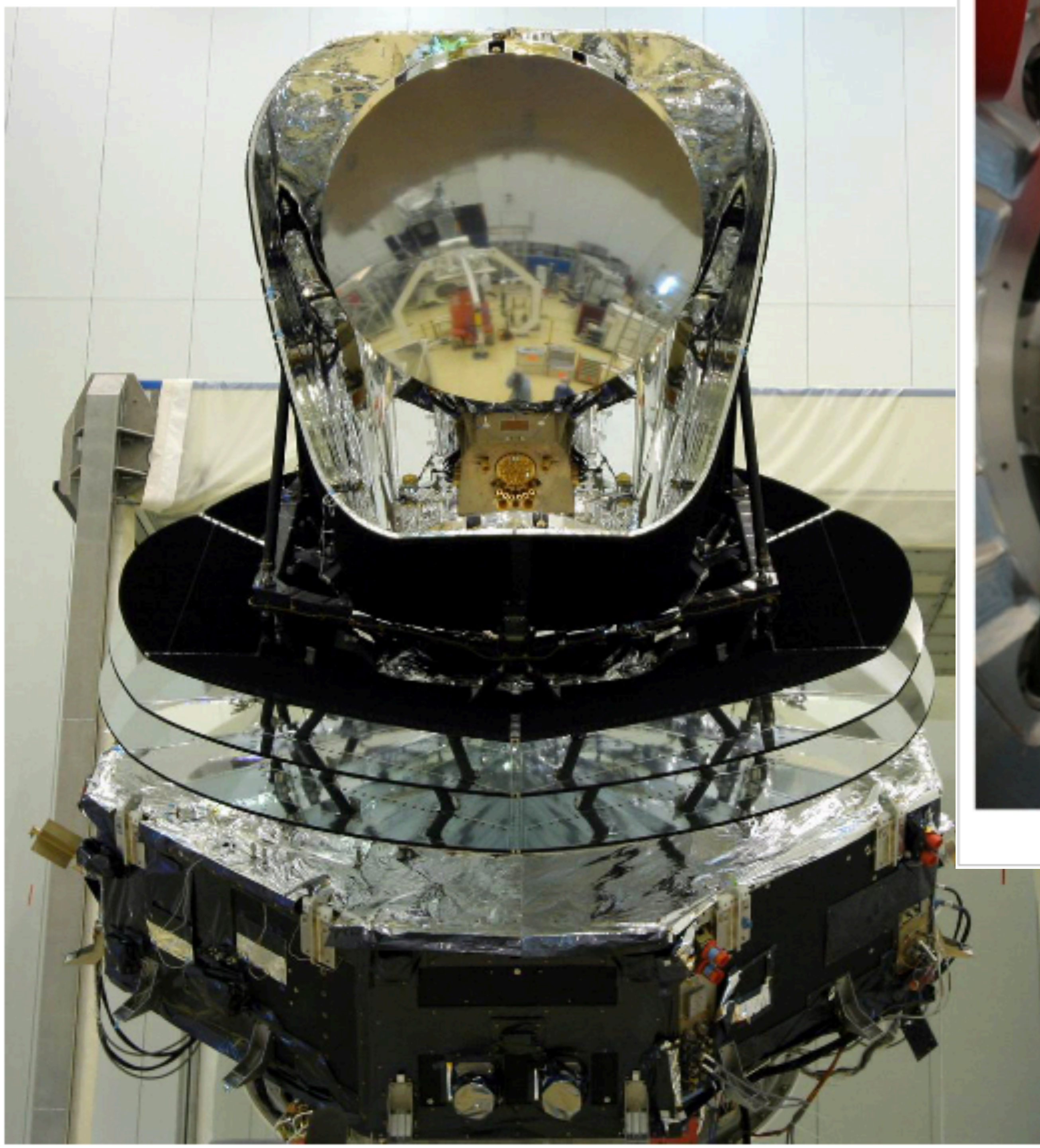

The fully assembled Planck satellite a few days before integration into the Ariane 5 rocket. Herschel is visible by reflection on the primary reflector.

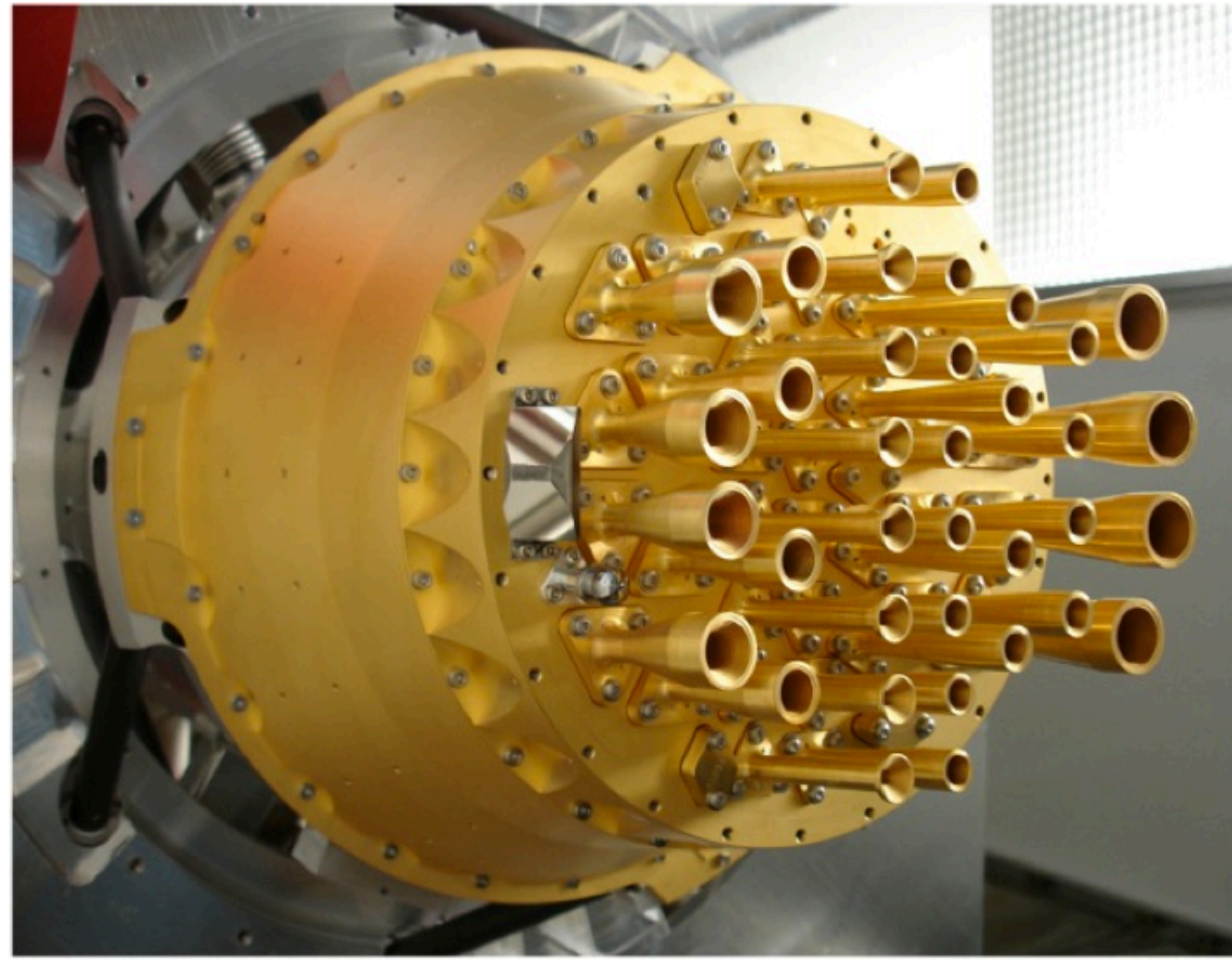

The HFI focal plane optics and 4K thermo-mechanical stage

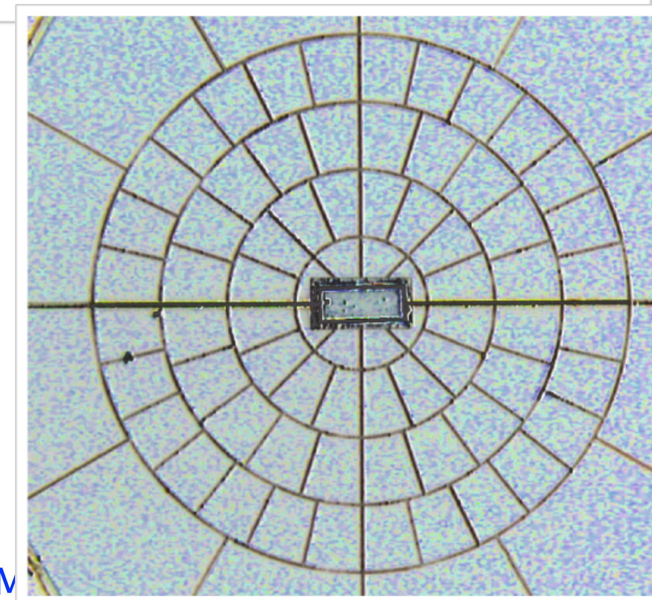

Picture of a Spider Web Bolometer. This a 143 GHz module, The temperature sensor is at the center of the absorbing grid.

Planck detectors

Instrument Characteristic	LFI			HFI					
Detector Technology	HEMT arrays			Bolometer arrays					
Center Frequency [GHz]	30	44	70	100	143	217	353	545	857
Bandwidth ($\Delta\nu/\nu$)	0.2	0.2	0.2	0.33	0.33	0.33	0.33	0.33	0.33
Angular Resolution (arcmin)	33	24	14	10	7.1	5.0	5.0	5.0	5.0
$\Delta T/T$ per pixel (Stokes I)[a]	2.0	2.7	4.7	2.5	2.2	4.8	14.7	147	6700
$\Delta T/T$ per pixel (Stokes Q & U)[a]	2.8	3.9	6.7	4.0	4.2	9.8	29.8	...	...

[a] Goal (μK/K, 1σ), 14 months integration, square pixels whose sides are given in the row "Angular Resolution".

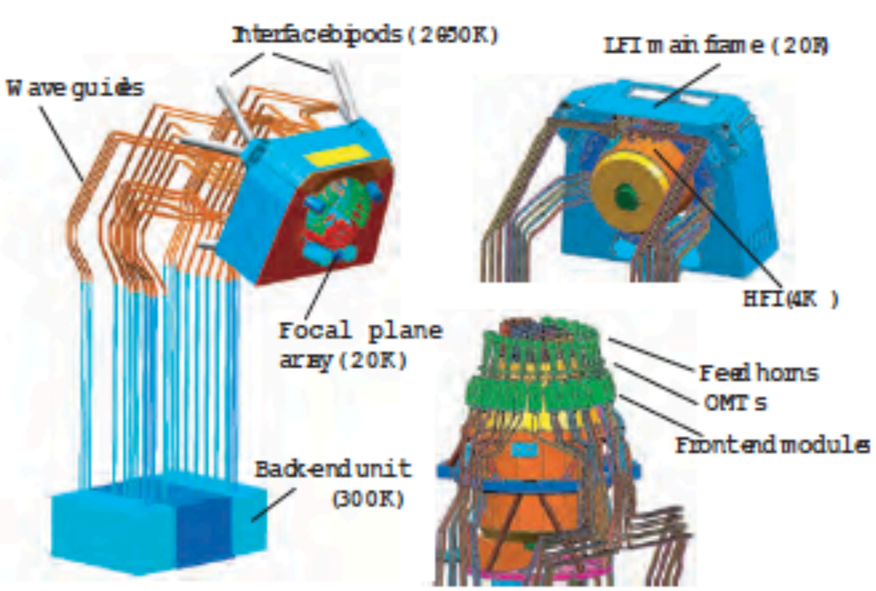

Planck Bluebook

Thales/Alenia Space+ESA

Planck Bluebook

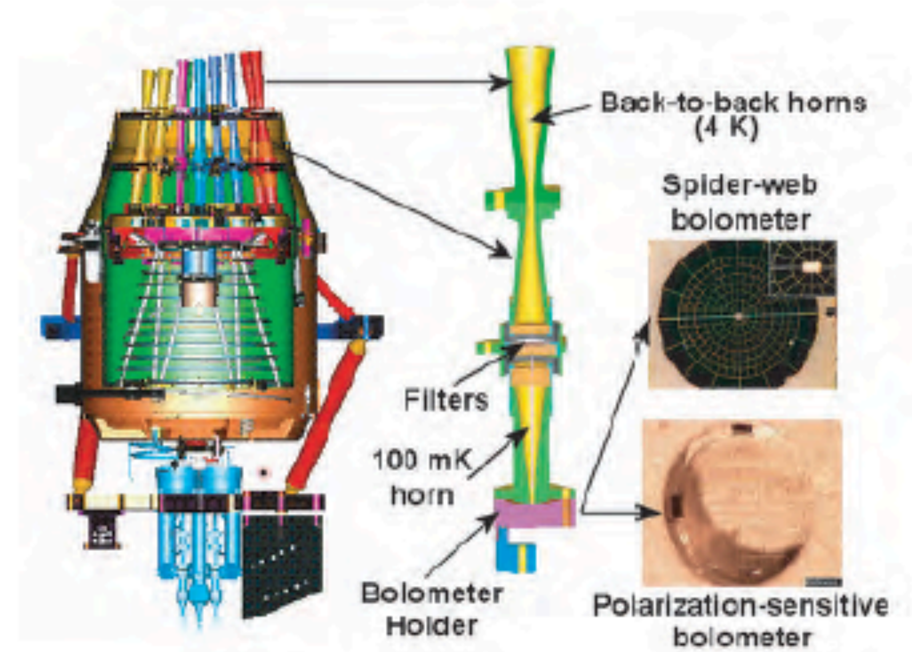

Planck Bluebook

Planck HFI

Center Frequency (GHz)	100	143	217	353	545	857
N Detectors	8	11	12	12	3	4
Resolution (arcmin)	9.5	7.1	4.7	4.5	4.7	4.4
Noise in maps μK_{CMB} deg	1.6	0.9	1.4	5.0	70	1180
Array NET (μK s)	22.6	14.5	20.6	77.3	4.9 (RJ)	2.1 (RJ)

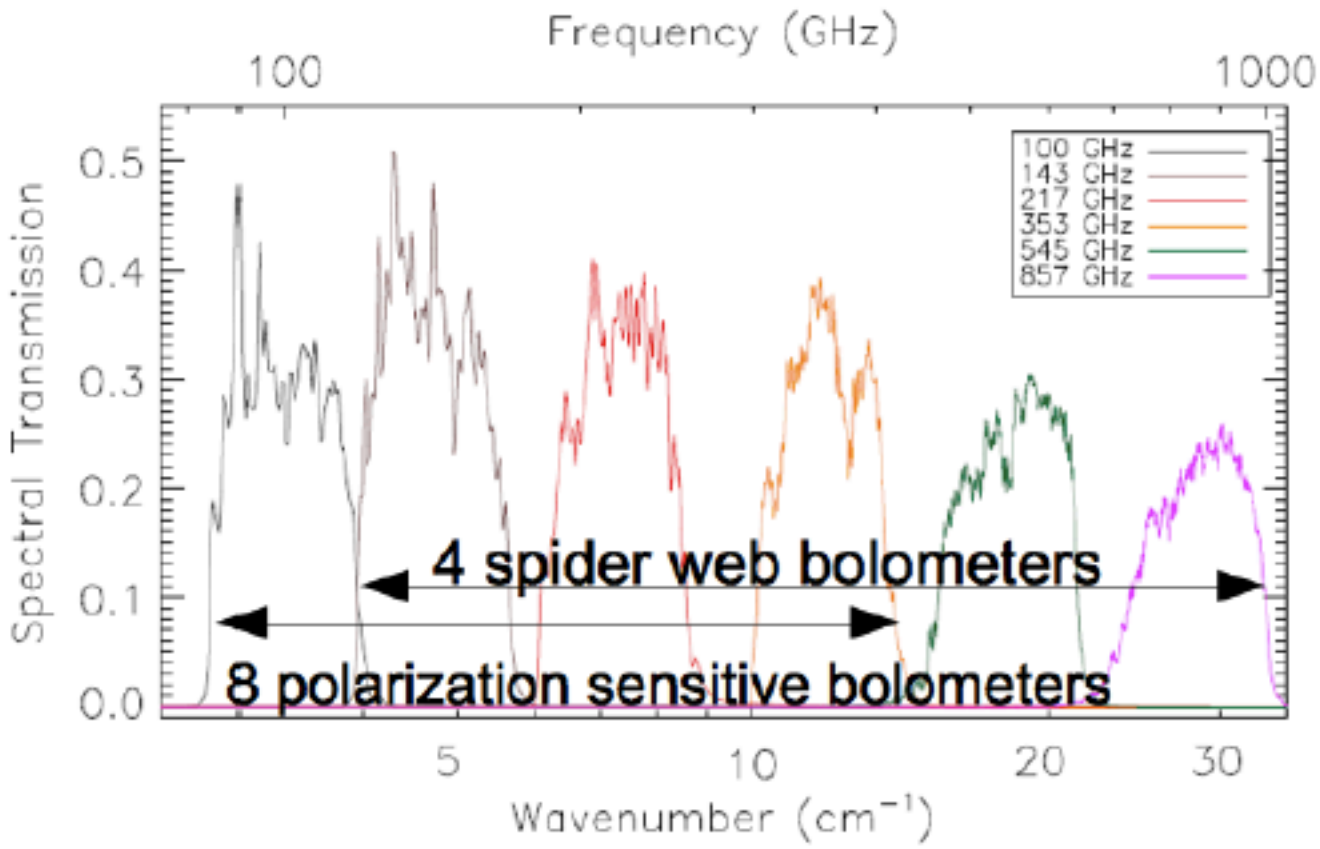

HFI polarization sensitivity

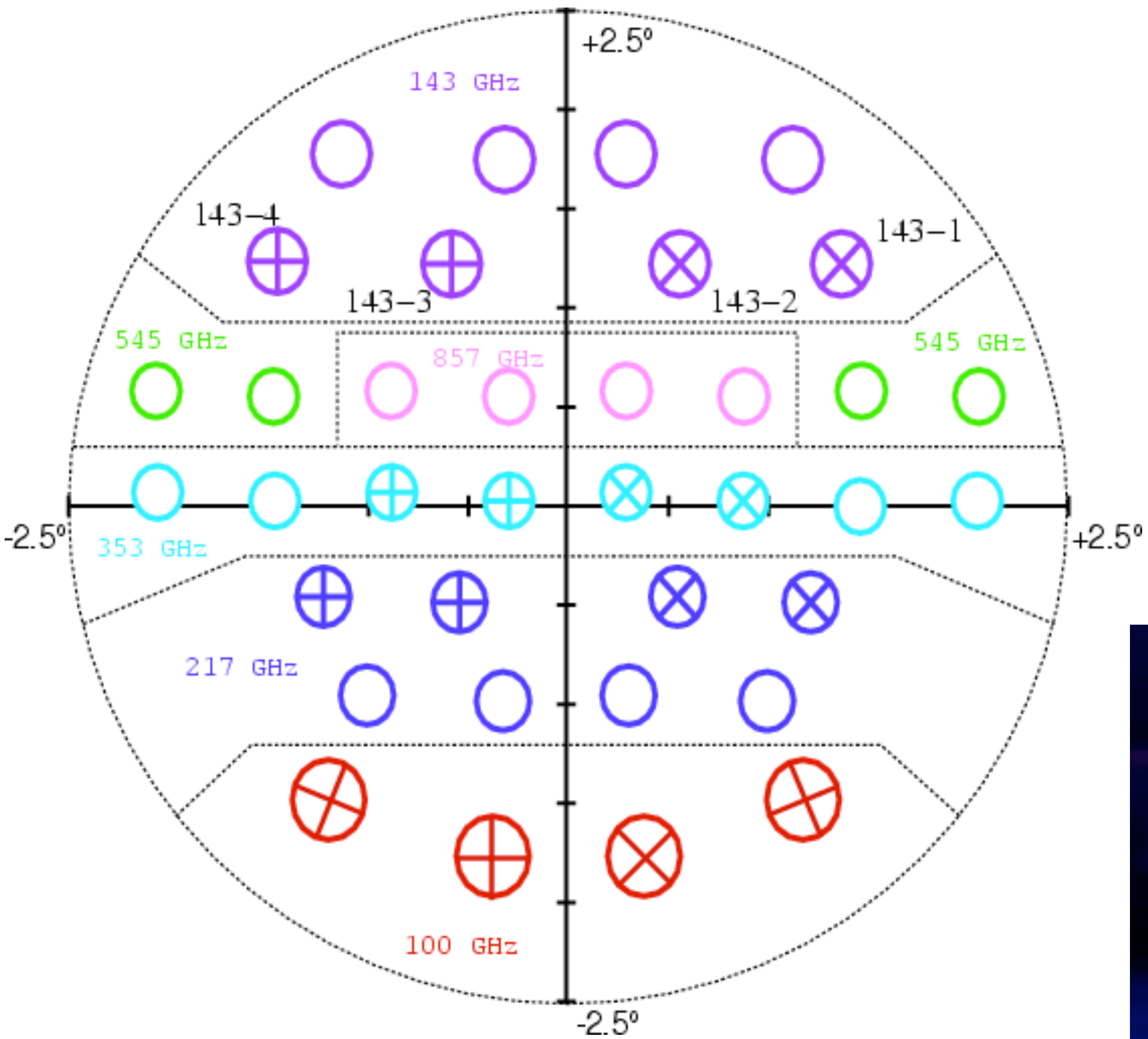

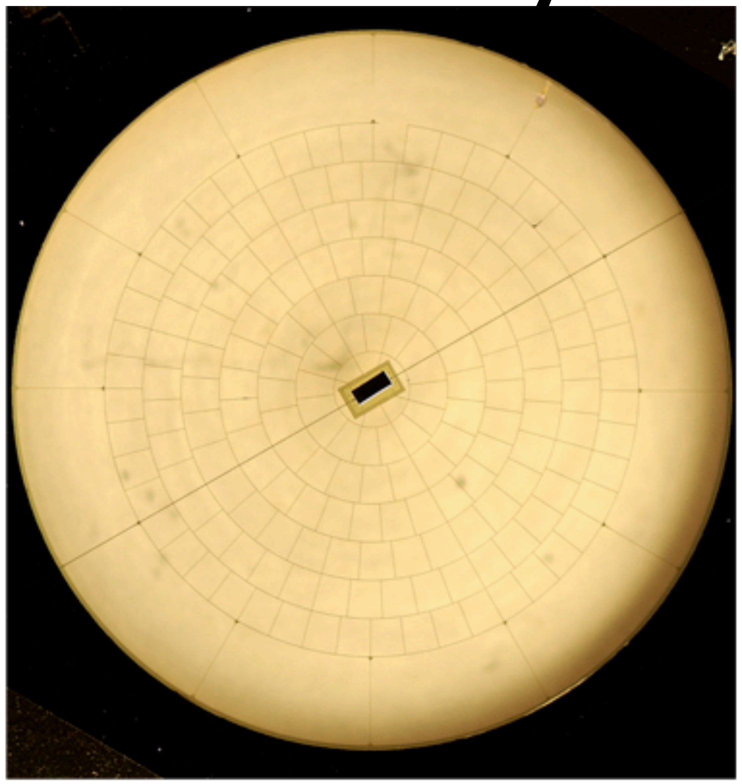

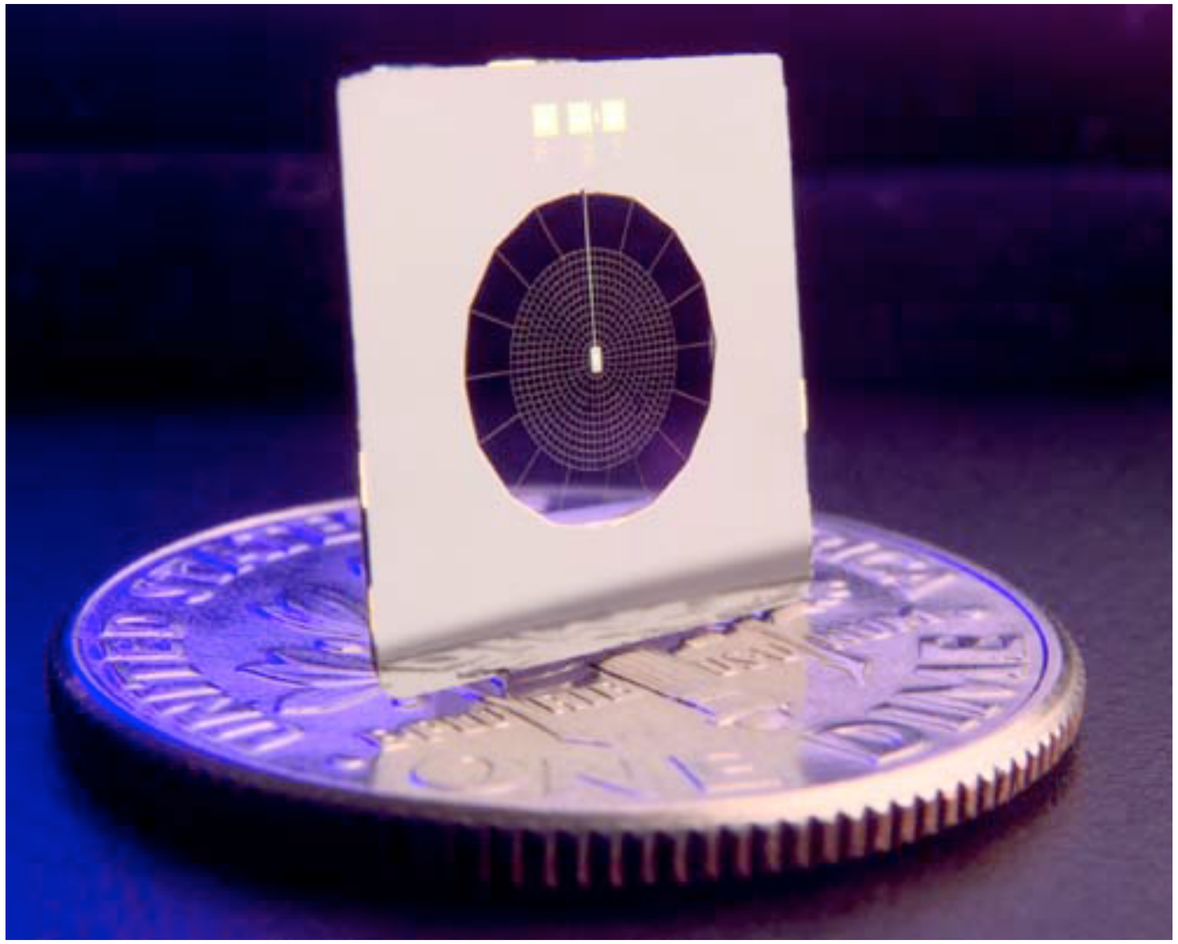

Planck Focal Plane Unit with polarization sensitive bolometers (spiderweb bolometers). Here one has two bolometers back-to-back with orthogonal grids.

Planck scanning strategy

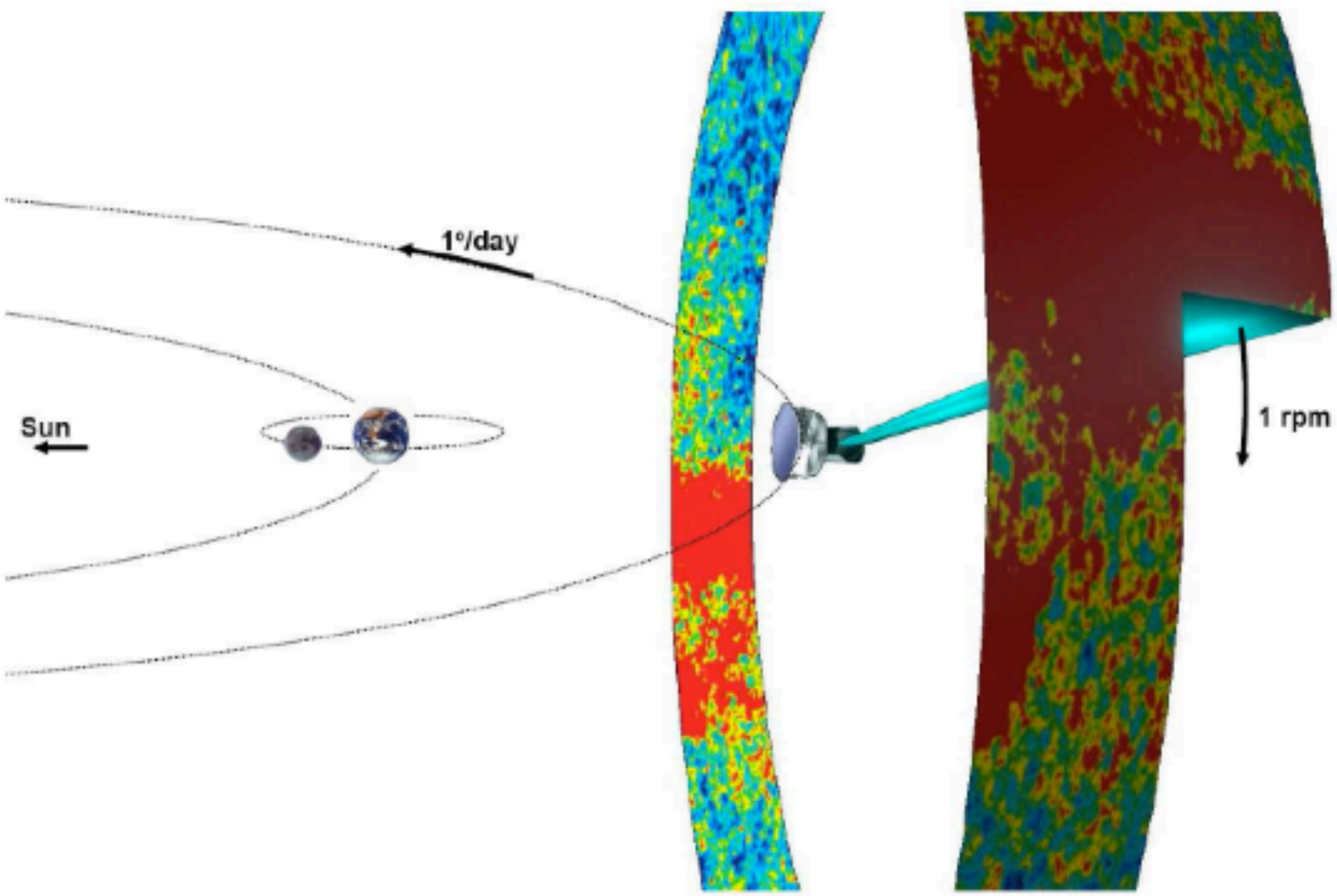

Simplified way to show the Planck scanning strategy, without additional motion of the spin axis

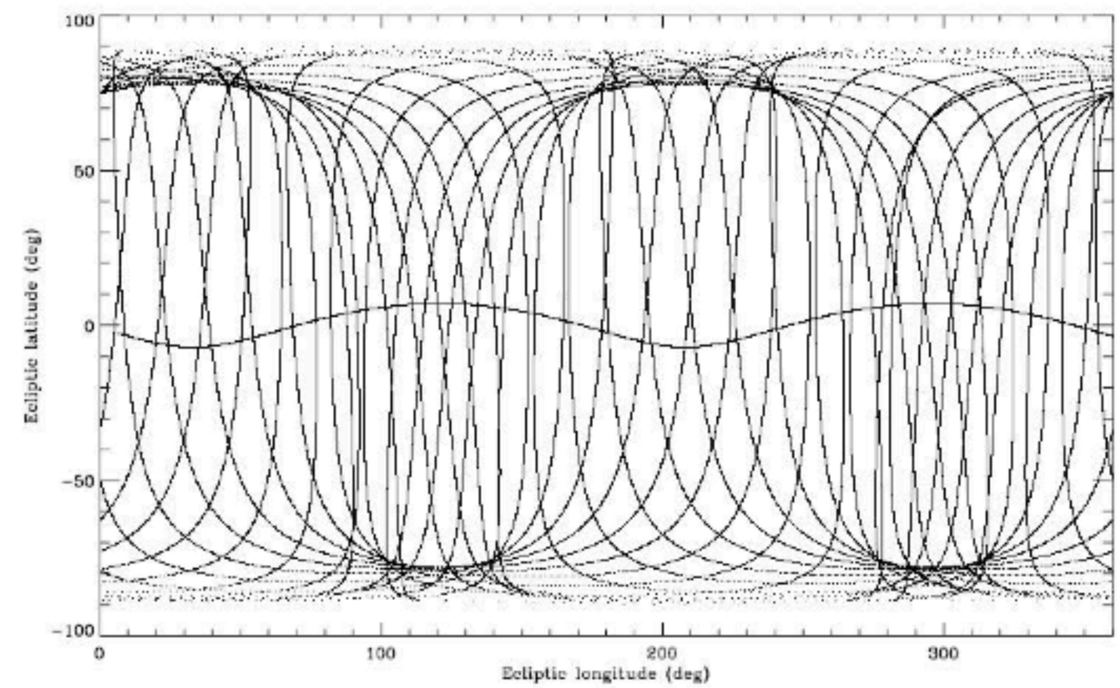

Spin axis path with a 7 degree amplitude cycloidal scanning, from #dupac2005

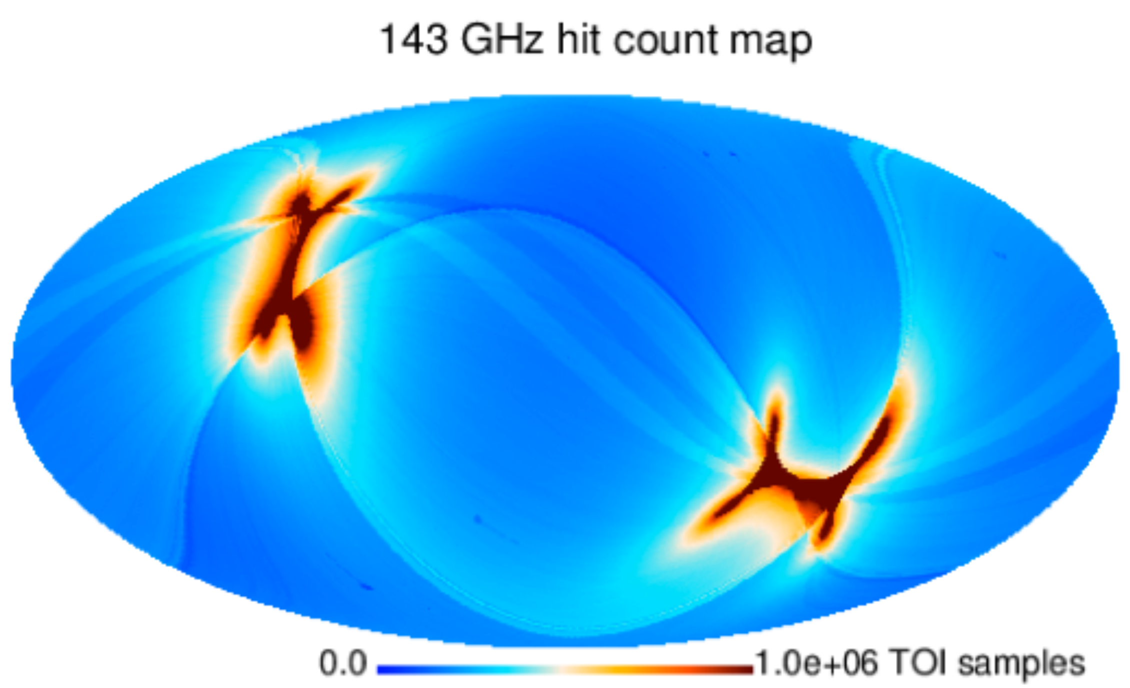

Planck power spectrum

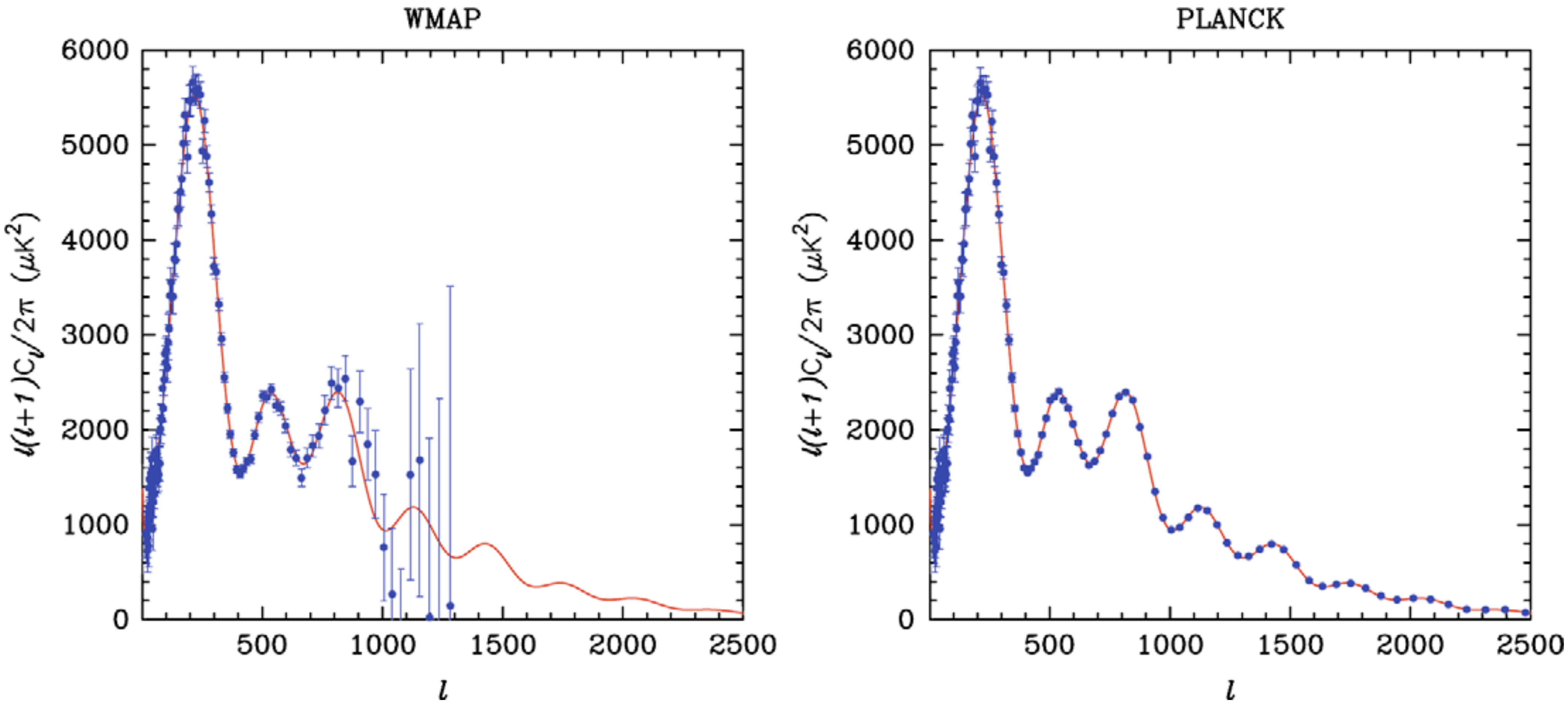

- Much better resolution (5′ compared to 14′ for WMAP), combined with μK sensitivity (about an order of magnitude lower than WMAP at 100 GHz)

- Much wider frequency coverage (30–857 GHz) – better foreground removal

- By-product: all-sky cluster catalogue, radio source catalogue, Galactic foreground maps

Planck power spectrum

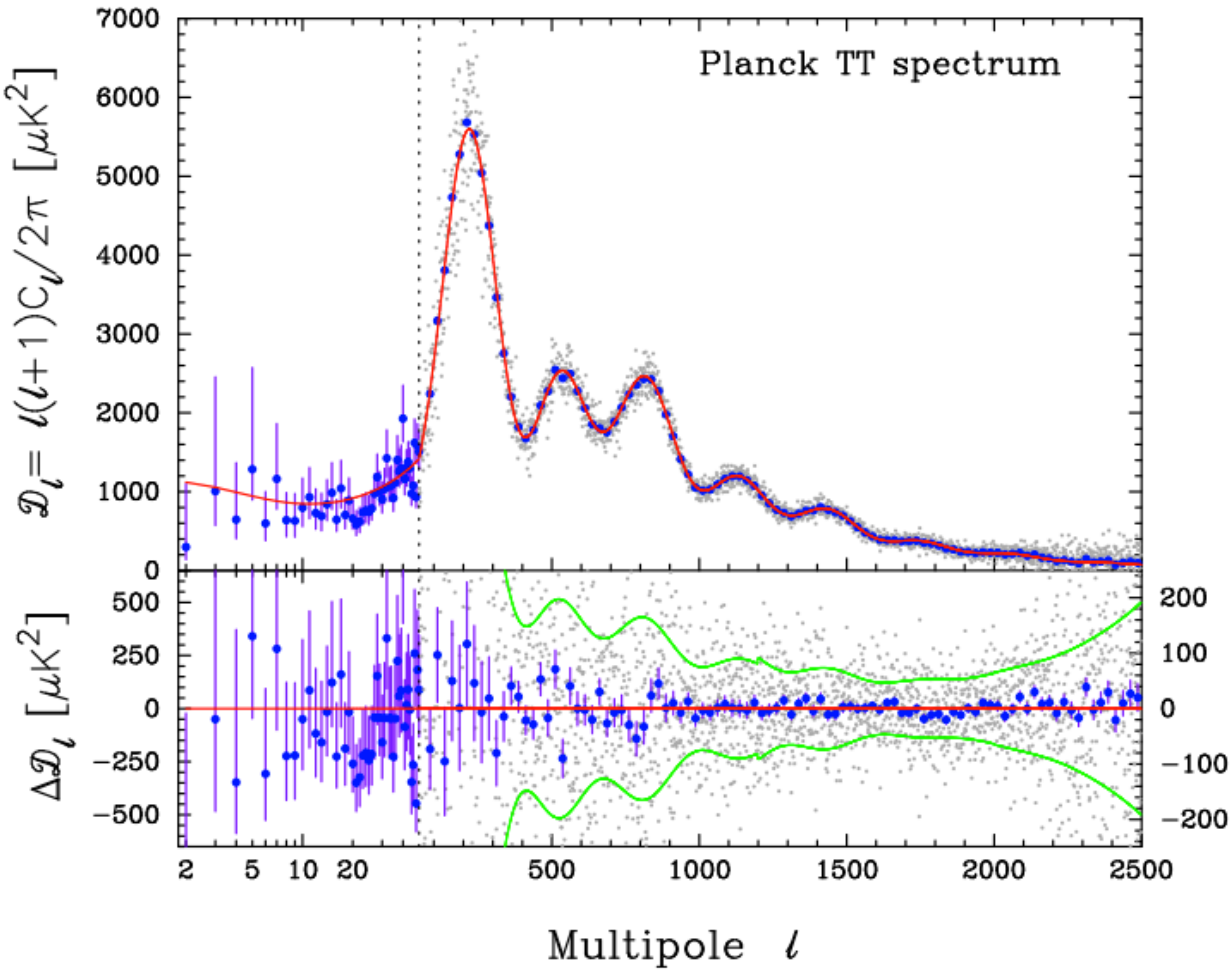

Planck collaboration (2013)

Planck 2013 cosmological parameters

	Planck+WP		*Planck*+WP+highL		*Planck*+lensing+WP+highL		*Planck*+WP+highL+BAO	
Parameter	Best fit	68% limits	Best fit	68% limits	Best fit	68% limits	Best fit	68% limits
$\Omega_b h^2$	0.022032	0.02205 ± 0.00028	0.022069	0.02207 ± 0.00027	0.022199	0.02218 ± 0.00026	0.022161	0.02214 ± 0.00024
$\Omega_c h^2$	0.12038	0.1199 ± 0.0027	0.12025	0.1198 ± 0.0026	0.11847	0.1186 ± 0.0022	0.11889	0.1187 ± 0.0017
$100\theta_{MC}$	1.04119	1.04131 ± 0.00063	1.04130	1.04132 ± 0.00063	1.04146	1.04144 ± 0.00061	1.04148	1.04147 ± 0.00056
τ	0.0925	$0.089^{+0.012}_{-0.014}$	0.0927	$0.091^{+0.013}_{-0.014}$	0.0943	$0.090^{+0.013}_{-0.014}$	0.0952	0.092 ± 0.013
n_s	0.9619	0.9603 ± 0.0073	0.9582	0.9585 ± 0.0070	0.9624	0.9614 ± 0.0063	0.9611	0.9608 ± 0.0054
$\ln(10^{10} A_s)$	3.0980	$3.089^{+0.024}_{-0.027}$	3.0959	3.090 ± 0.025	3.0947	3.087 ± 0.024	3.0973	3.091 ± 0.025
A^{PS}_{100}	152	171 ± 60	209	212 ± 50	204	213 ± 50	204	212 ± 50
A^{PS}_{143}	63.3	54 ± 10	72.6	73 ± 8	72.2	72 ± 8	71.8	72.4 ± 8.0
A^{PS}_{217}	117.0	107^{+20}_{-10}	59.5	59 ± 10	60.2	58 ± 10	59.4	59 ± 10
A^{CIB}_{143}	0.0	< 10.7	3.57	3.24 ± 0.83	3.25	3.24 ± 0.83	3.30	3.25 ± 0.83
A^{CIB}_{217}	27.2	29^{+6}_{-9}	53.9	49.6 ± 5.0	52.3	50.0 ± 4.9	53.0	49.7 ± 5.0
A^{tSZ}_{143}	6.80	...	5.17	$2.54^{+1.1}_{-1.9}$	4.64	$2.51^{+1.2}_{-1.8}$	4.86	$2.54^{+1.2}_{-1.8}$
$r^{PS}_{143\times217}$	0.916	> 0.850	0.825	$0.823^{+0.069}_{-0.077}$	0.814	0.825 ± 0.071	0.824	0.823 ± 0.070
$r^{CIB}_{143\times217}$	0.406	0.42 ± 0.22	1.0000	> 0.930	1.0000	> 0.928	1.0000	> 0.930
γ^{CIB}	0.601	$0.53^{+0.13}_{-0.12}$	0.674	0.638 ± 0.081	0.656	0.643 ± 0.080	0.667	0.639 ± 0.081
$\xi^{tSZ\times CIB}$	0.03	...	0.000	< 0.409	0.000	< 0.389	0.000	< 0.410
A^{kSZ}	0.9	...	0.89	$5.34^{+2.8}_{-1.9}$	1.14	$4.74^{+2.6}_{-2.1}$	1.58	$5.34^{+2.8}_{-2.0}$
Ω_Λ	0.6817	$0.685^{+0.018}_{-0.016}$	0.6830	$0.685^{+0.017}_{-0.016}$	0.6939	0.693 ± 0.013	0.6914	0.692 ± 0.010
σ_8	0.8347	0.829 ± 0.012	0.8322	0.828 ± 0.012	0.8271	0.8233 ± 0.0097	0.8288	0.826 ± 0.012
z_{re}	11.37	11.1 ± 1.1	11.38	11.1 ± 1.1	11.42	11.1 ± 1.1	11.52	11.3 ± 1.1
H_0	67.04	67.3 ± 1.2	67.15	67.3 ± 1.2	67.94	67.9 ± 1.0	67.77	67.80 ± 0.77
Age/Gyr	13.8242	13.817 ± 0.048	13.8170	13.813 ± 0.047	13.7914	13.794 ± 0.044	13.7965	13.798 ± 0.037
$100\theta_*$	1.04136	1.04147 ± 0.00062	1.04146	1.04148 ± 0.00062	1.04161	1.04159 ± 0.00060	1.04163	1.04162 ± 0.00056
r_{drag}	147.36	147.49 ± 0.59	147.35	147.47 ± 0.59	147.68	147.67 ± 0.50	147.611	147.68 ± 0.45

Planck 2013 cosmological results

Planck collaboration (2013)

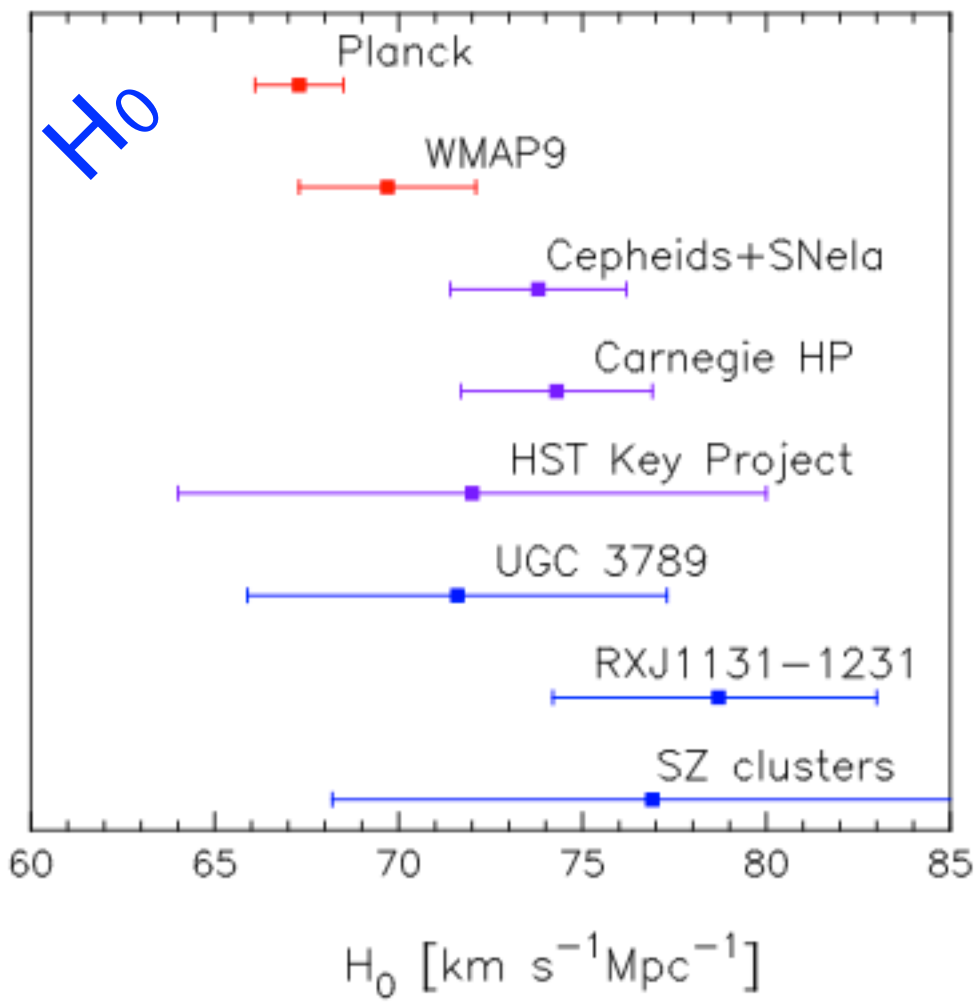

Fig. 16. Comparison of H_0 measurements, with estimates of $\pm 1\,\sigma$ errors, from a number of techniques (see text for details). These are compared with the spatially-flat ΛCDM model constraints from *Planck* and *WMAP*-9.

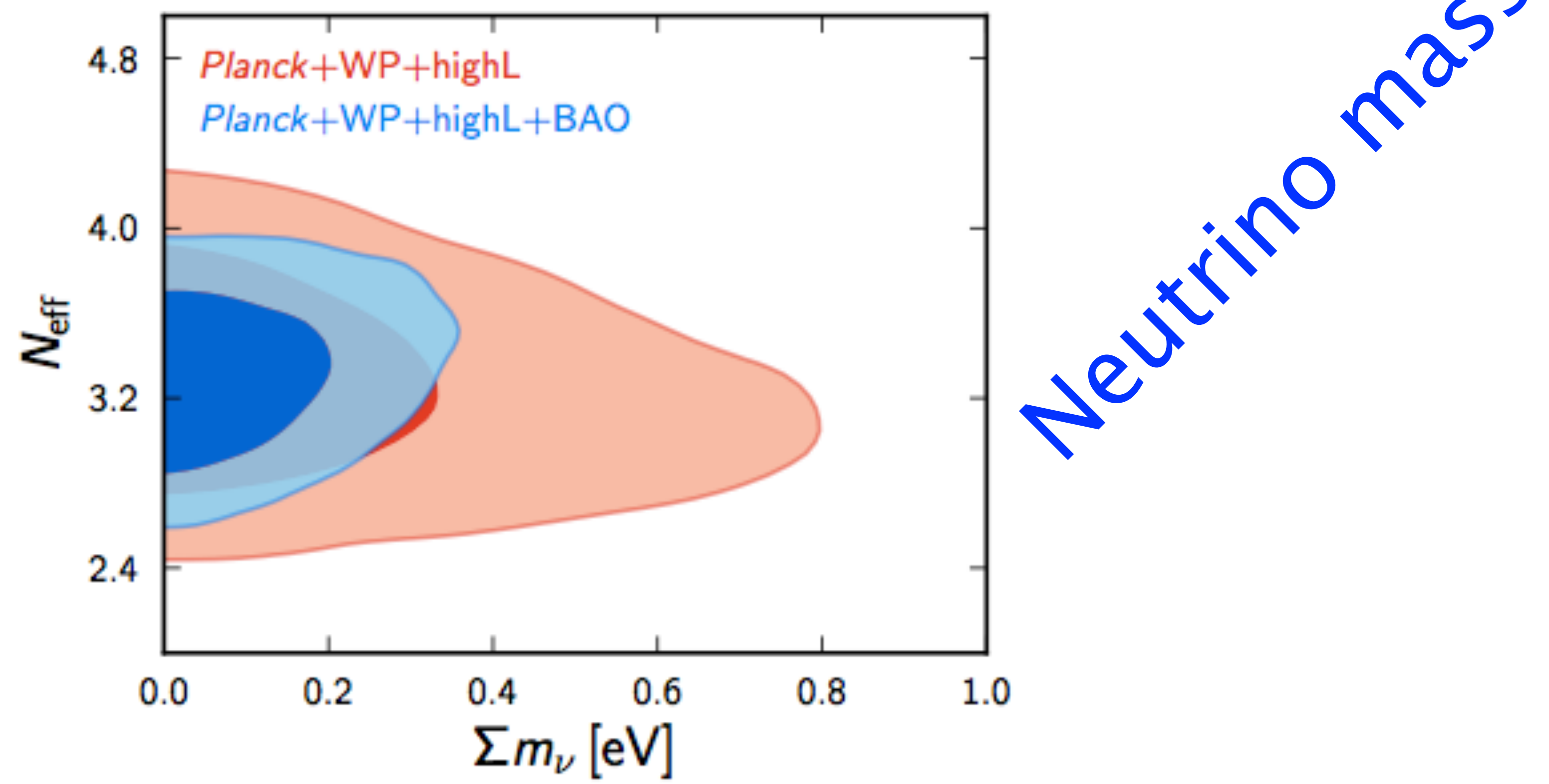

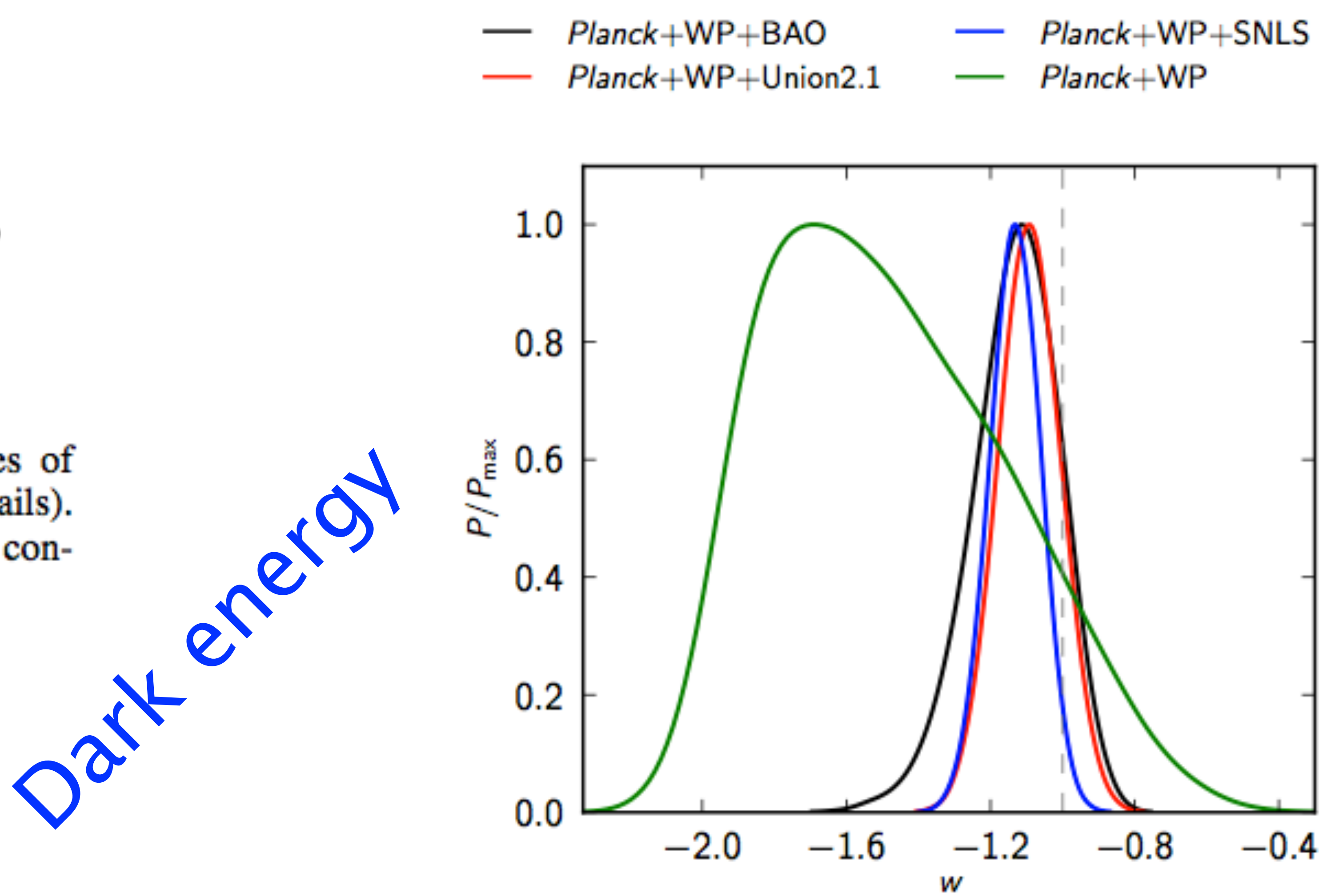

Planck cosmological results

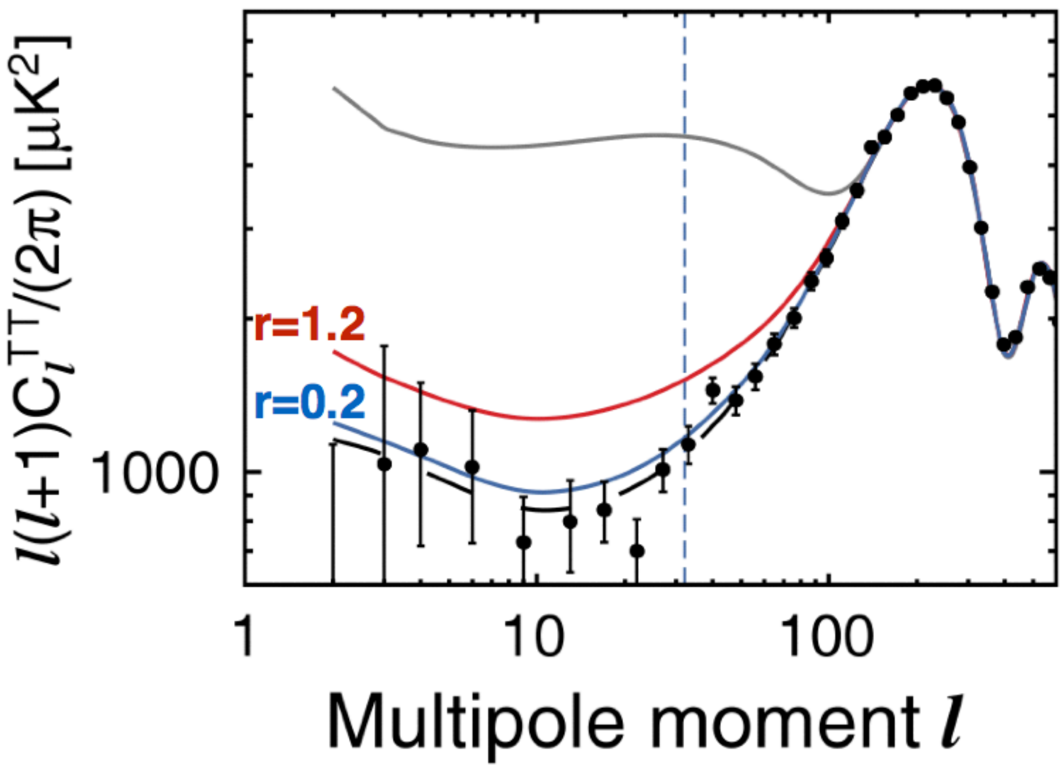

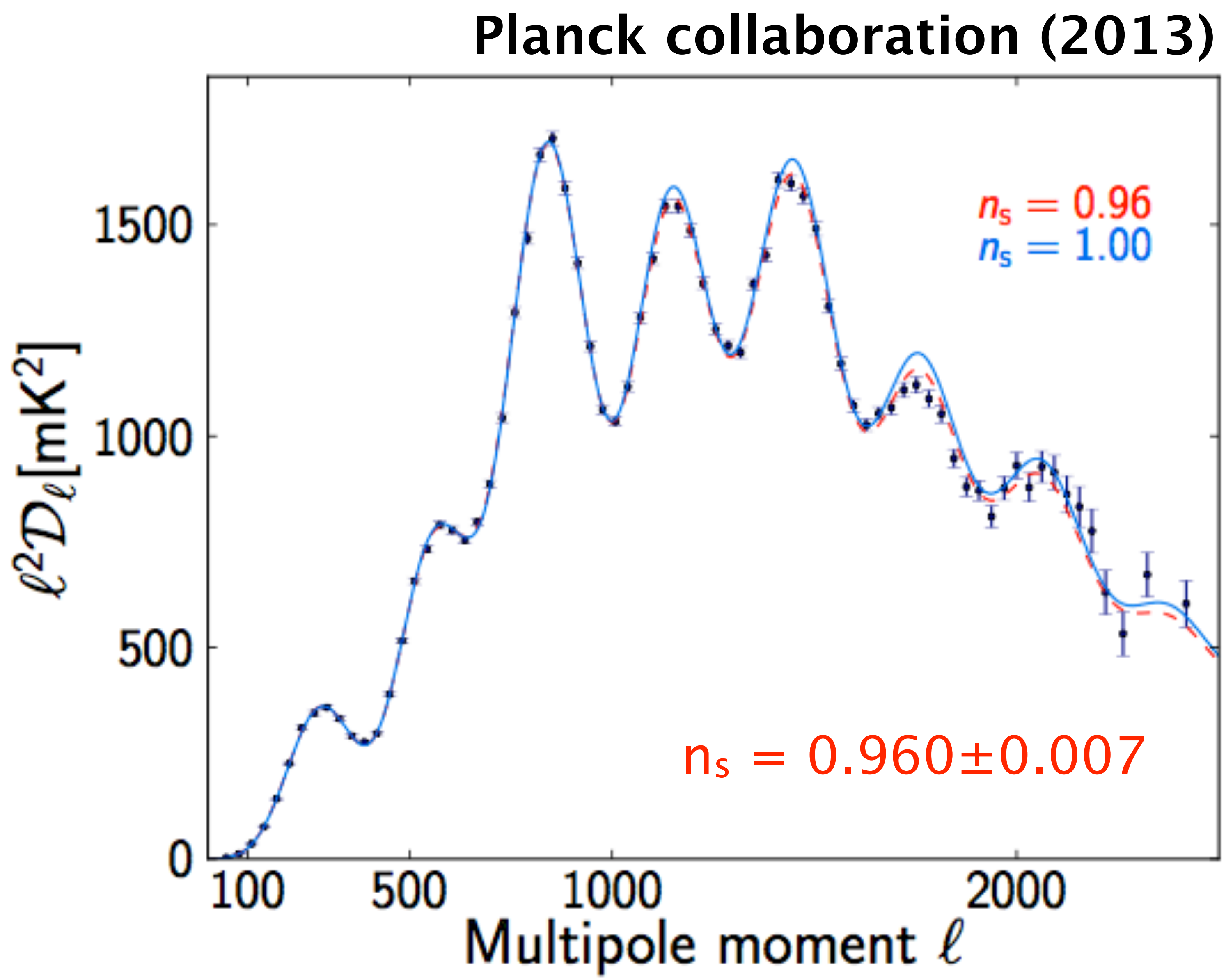

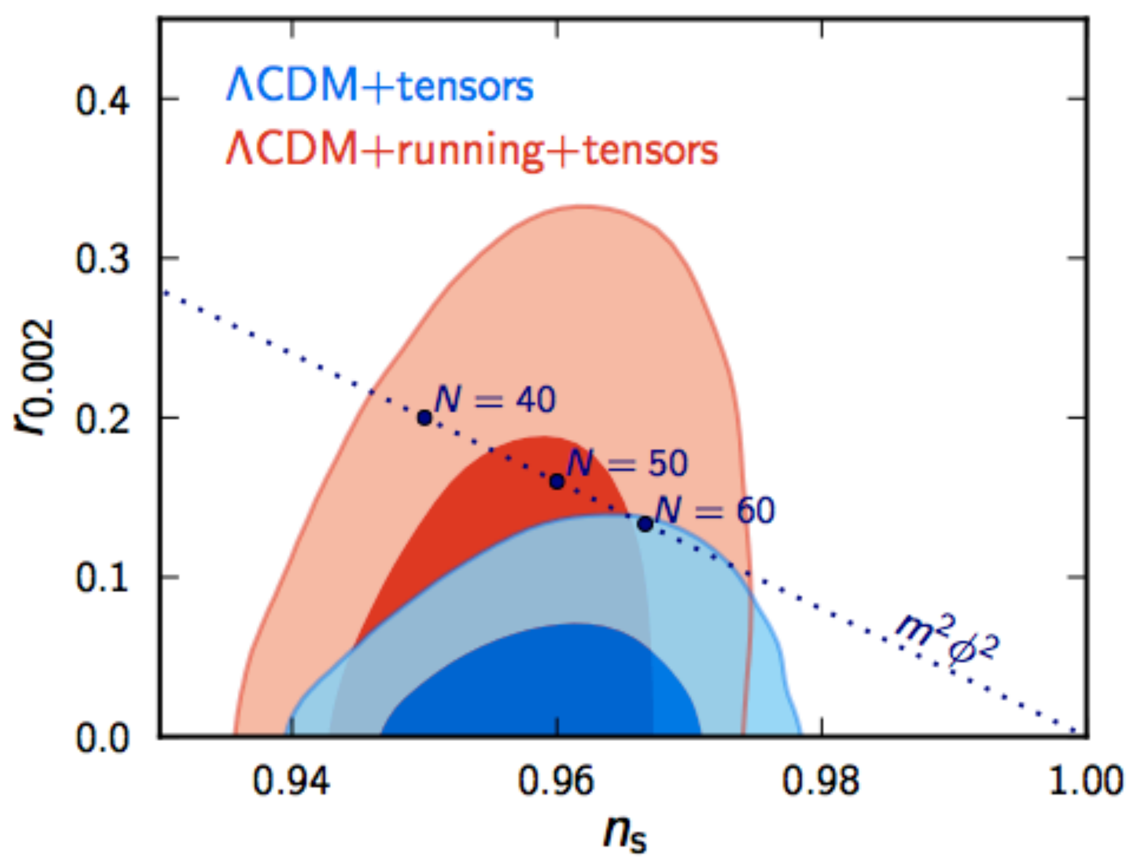

Inflation

Other Planck 2015 results

Mass distribution from CMB lensing

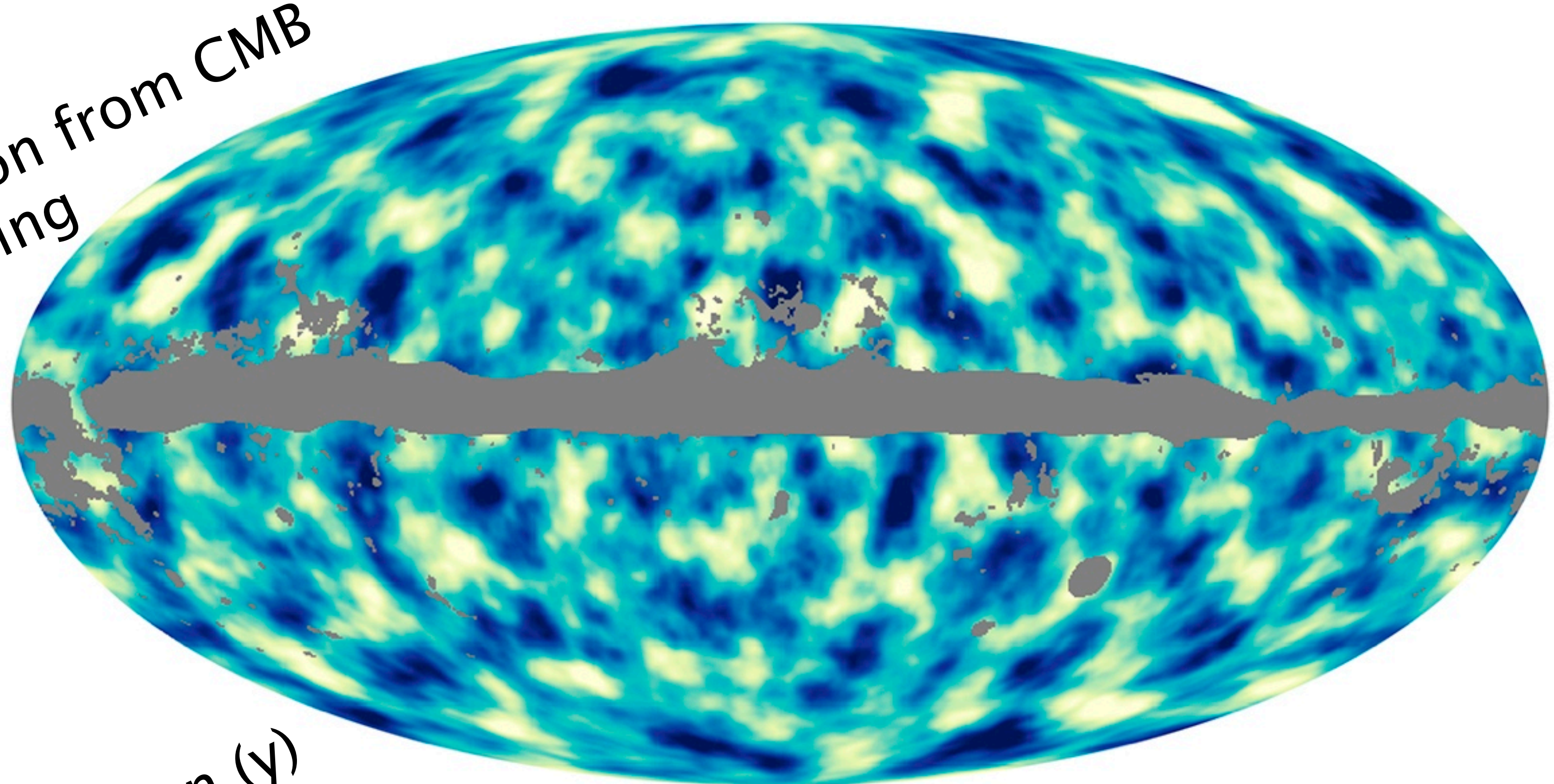

All-sky Comptonization (y) map

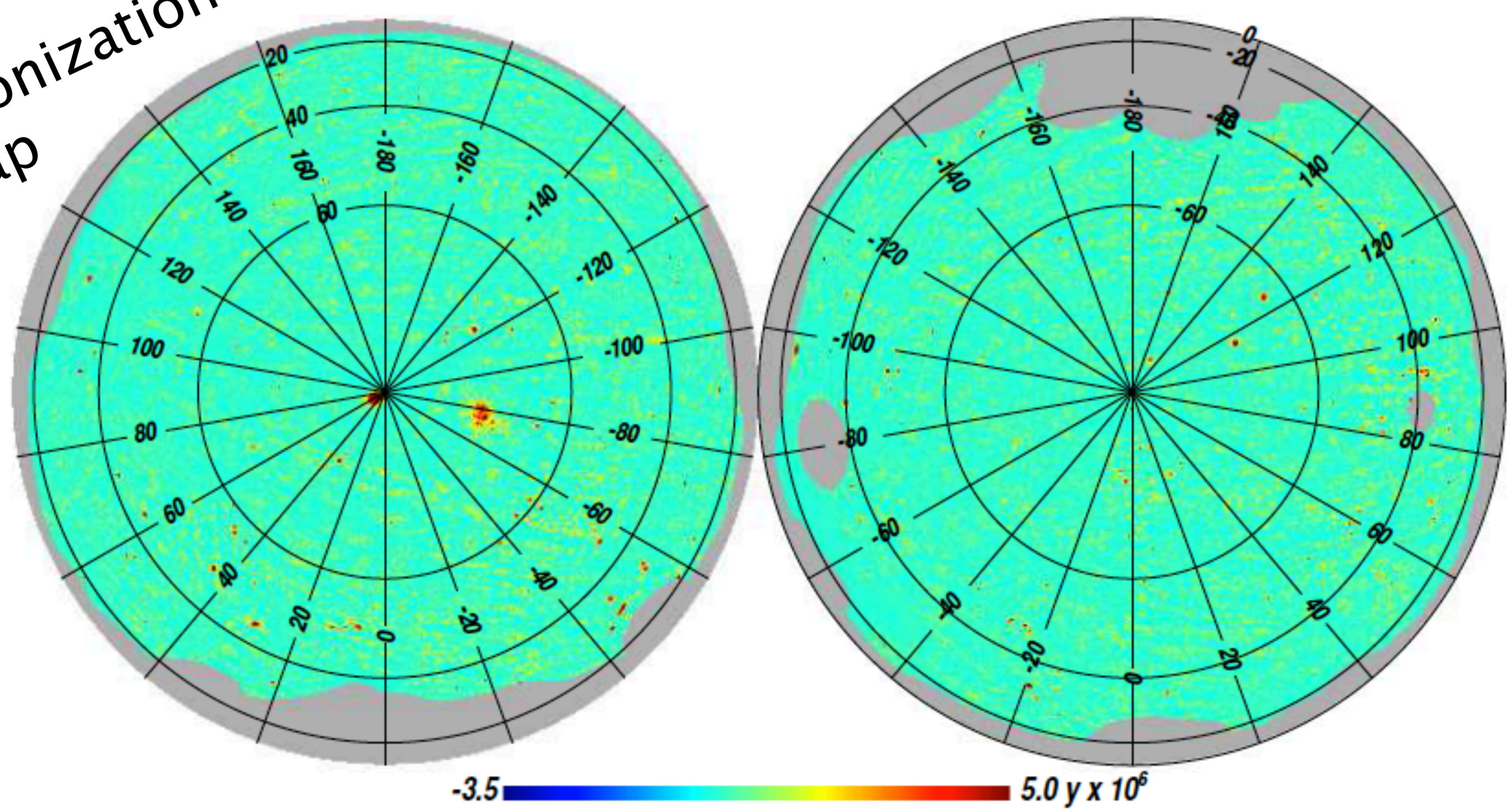

Planck 2015 CMB power spectra

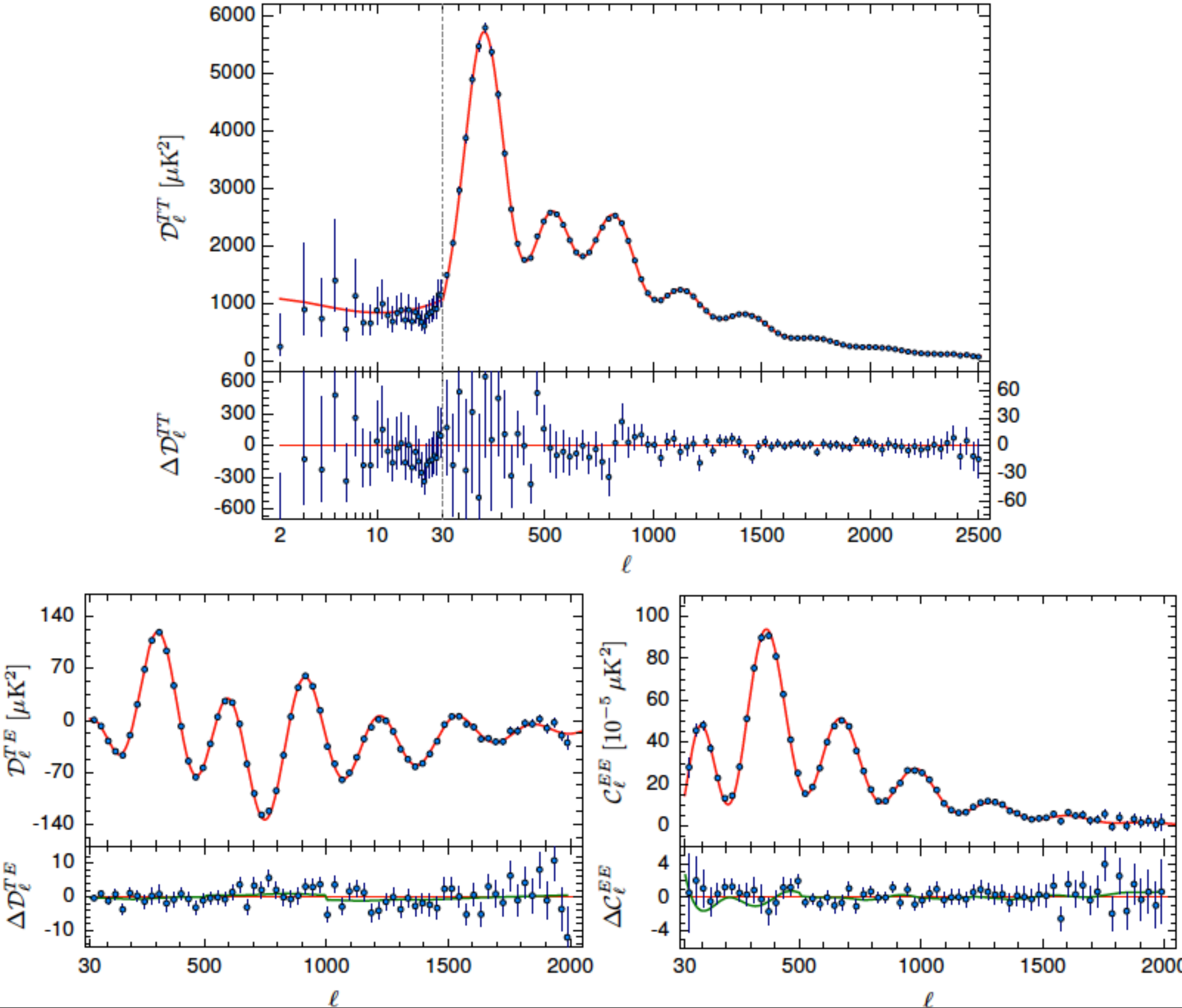

Low multipole “anomaly”

Planck collaboration (2013)

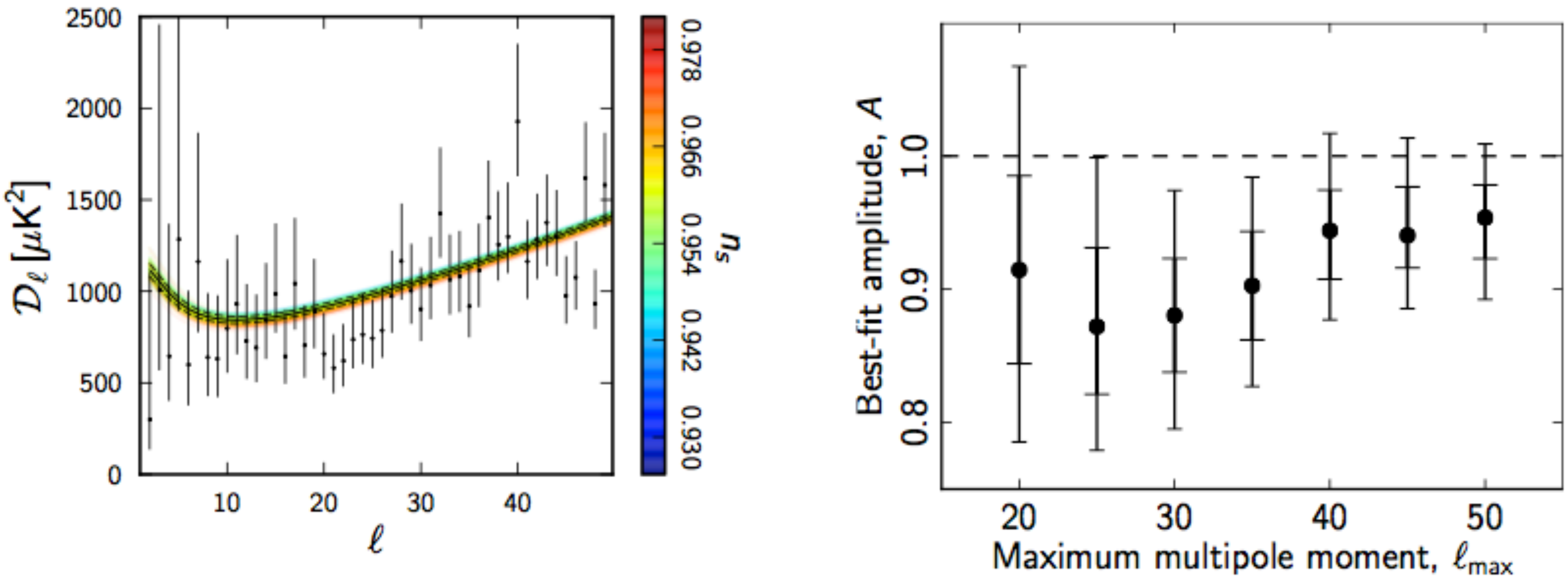

Fig. 39. *Left*: *Planck TT* spectrum at low multipoles with 68% ranges on the posteriors. The “rainbow” band show the best fits to the entire *Planck*+WP likelihood for the base ΛCDM cosmology, colour-coded according to the value of the scalar spectral index n_s. *Right*: Limits (68% and 95%) on the relative amplitude of the base ΛCDM fits to the *Planck*+WP likelihood *fitted only to the Planck TT likelihood* over the multipole range $2 \leq \ell \leq \ell_{max}$.

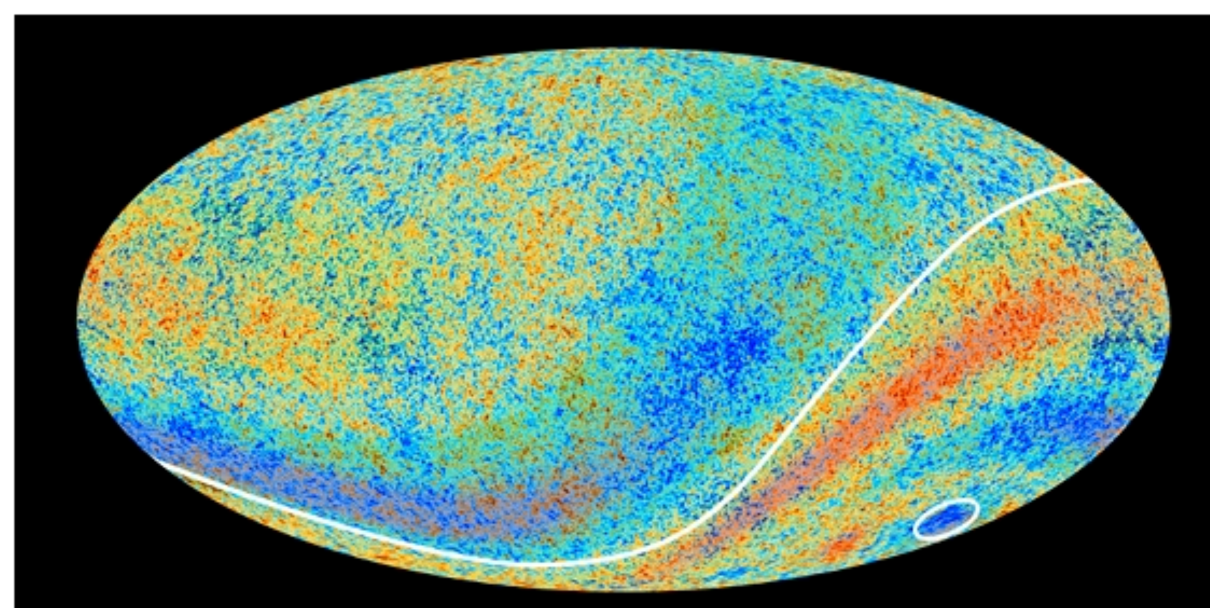

Planck’s anomalous sky: the hemispheric asymmetry and the cold spot. *Credit: ESA and the Planck Collaboration*

Low multipole “anomaly”

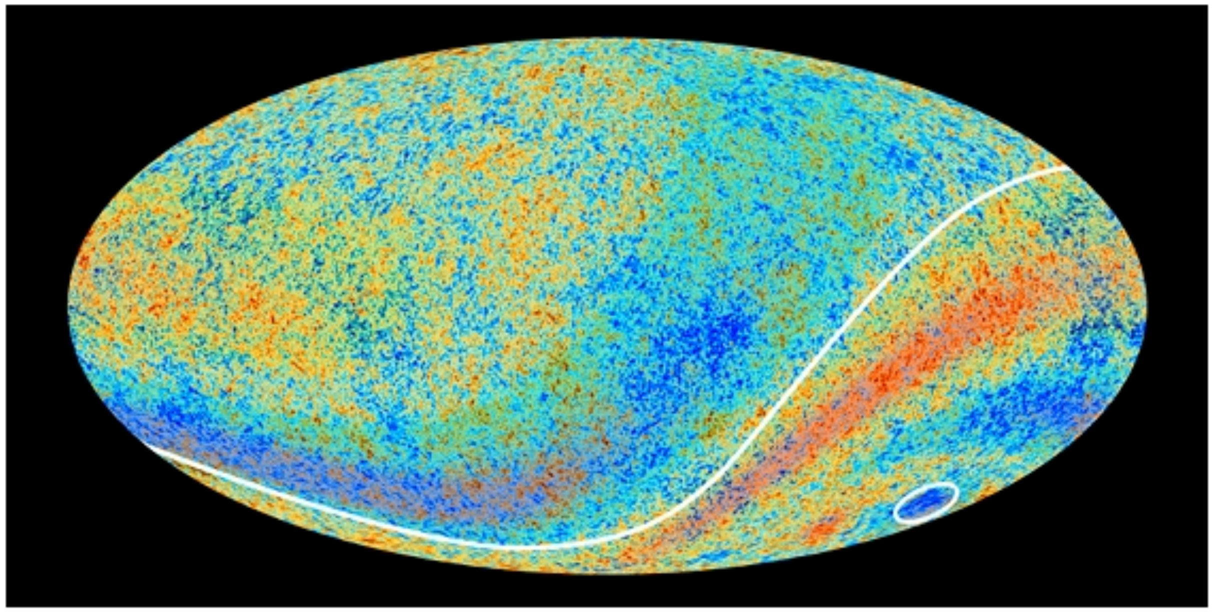

Planck’s anomalous sky: the hemispheric asymmetry and the cold spot. *Credit: ESA and the Planck Collaboration*

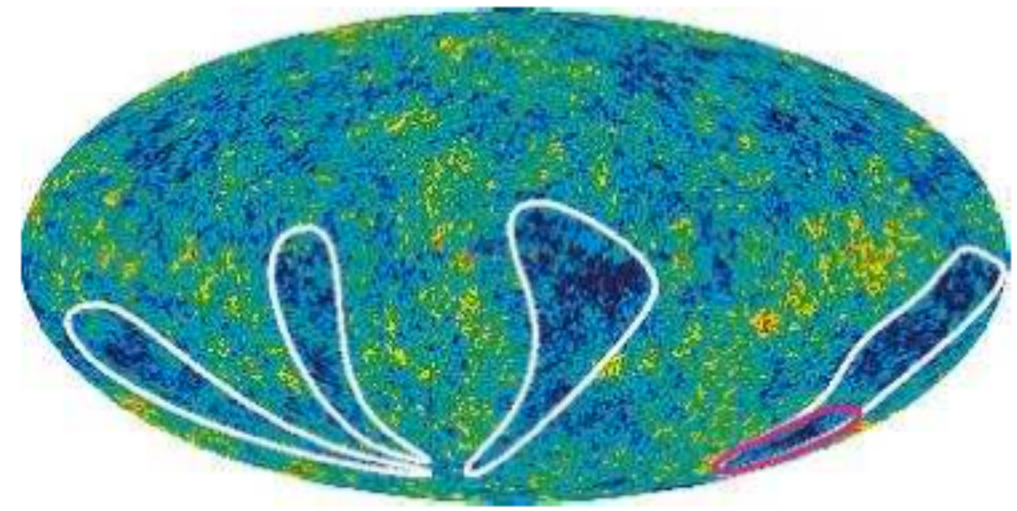

WMAP “fingers”

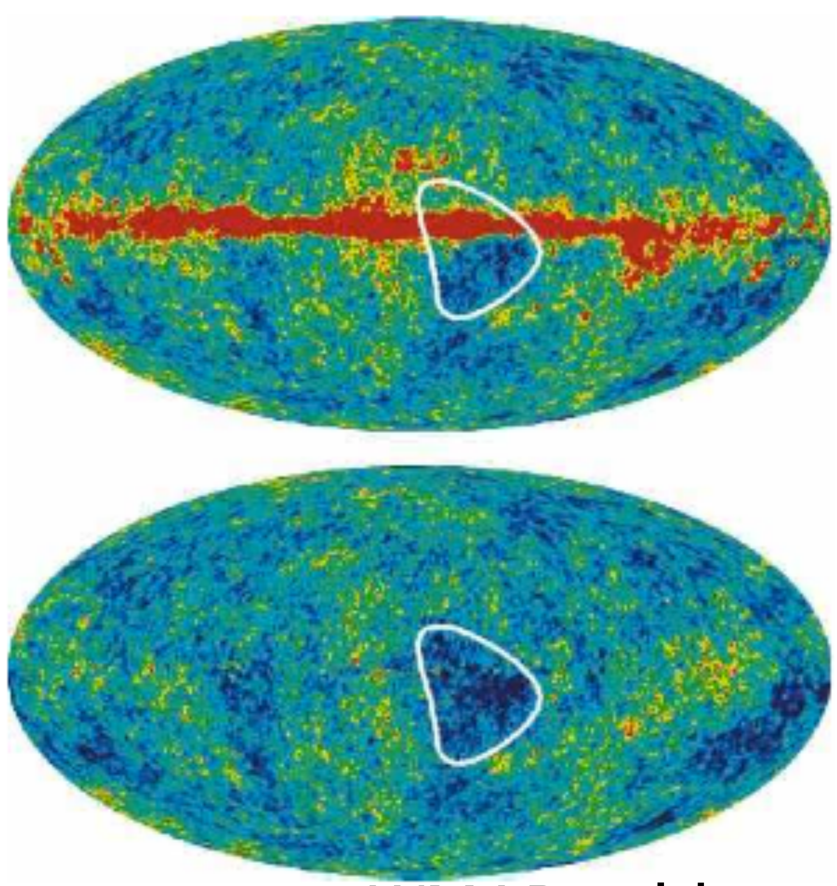

WMAP cold spot

Bennett et al. (2011)

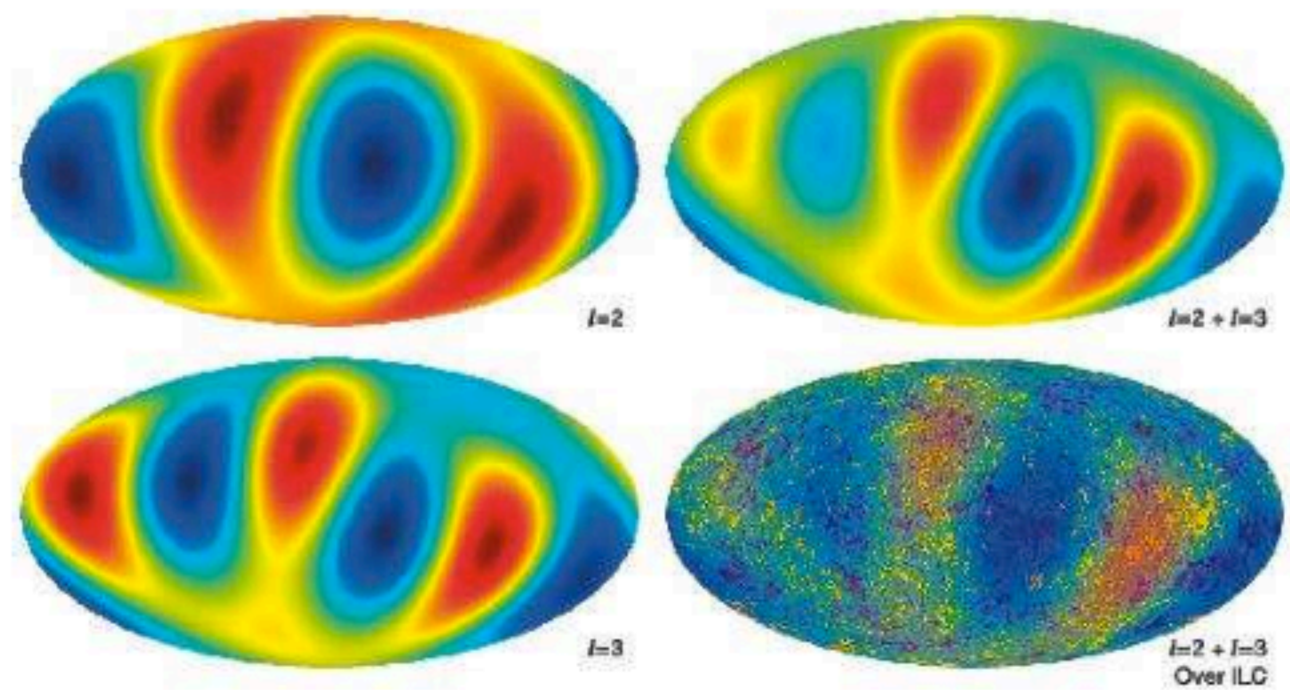

Figure 14. $l = 2$ quadrupole and $l = 3$ octupole maps are added. The combined map is then shown superposed on the ILC map from Figure 2. Note that the quadrupole and octupole components arrange themselves to match the cool fingers and the warm regions in between. The fingers and the alignment of the $l = 2$ and $l = 3$ multipoles are intimately connected.

CMB "anomalies"

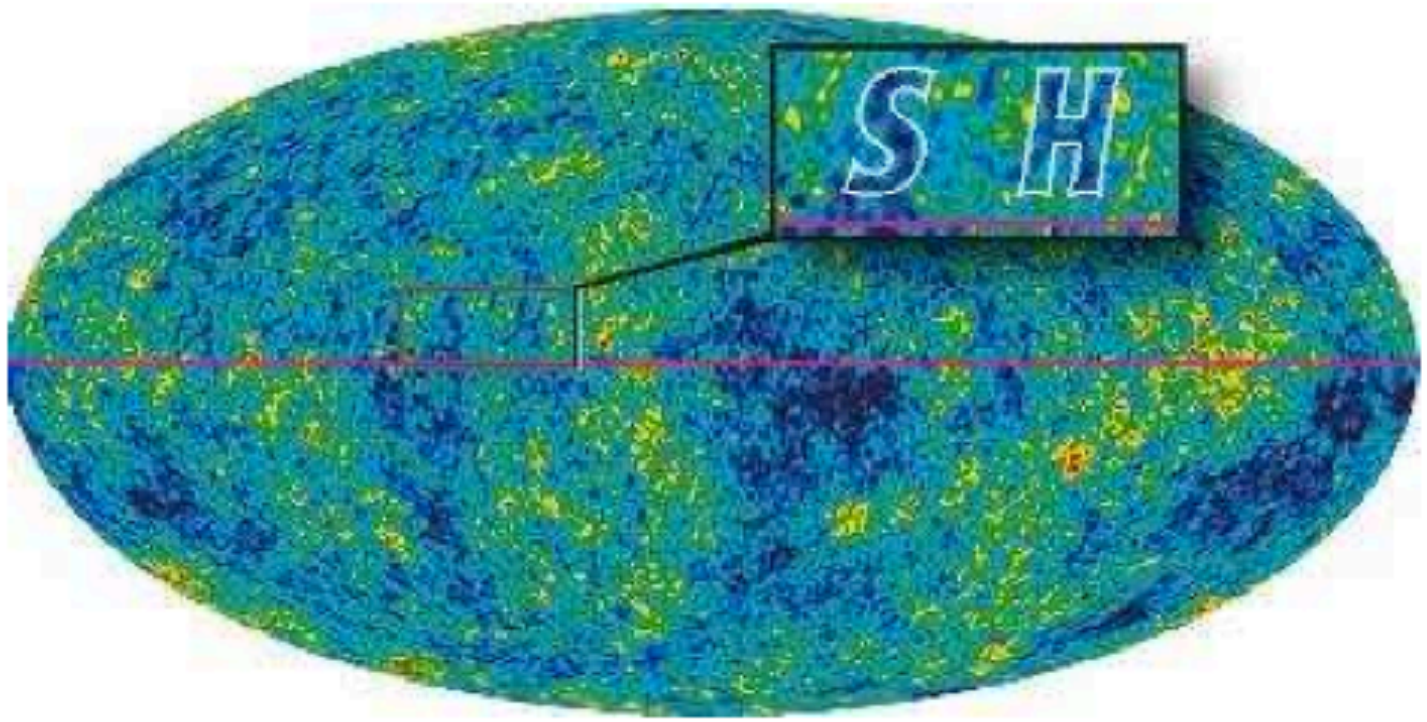

Figure 17. "SH" initials of Stephen Hawking are shown in the ILC sky map. The "S" and "H" are in roughly the same font size and style, and both letters are aligned neatly along a line of fixed Galactic latitude. A calculation would show that the probability of this particular occurrence is vanishingly small. Yet, there is no case to made for a non-standard cosmology despite this extraordinarily low probability event. It is clear that the combined selection of looking for initials, these particular initials, and their alignment and location are all *a posteriori* choices. For a rich data set, as is the case with *WMAP* , there are a lot of data and a lot of ways of analyzing the data. Low probability events are guaranteed to occur. The *a posteriori* assignment of a likelihood for a particular event detected, especially when the detection of that event is "optimized" for maximum effect by analysis choices, does not result in a fair unbiased assessment. This is a recurrent issue with CMB data analysis and is often a tricky issue and one that is difficult to overcome.

WMAP 7 yr data, Bennett et al. (2011)

“pi” in the sky

Ali Frolop & Douglas Scott, arXiv:1603.09073

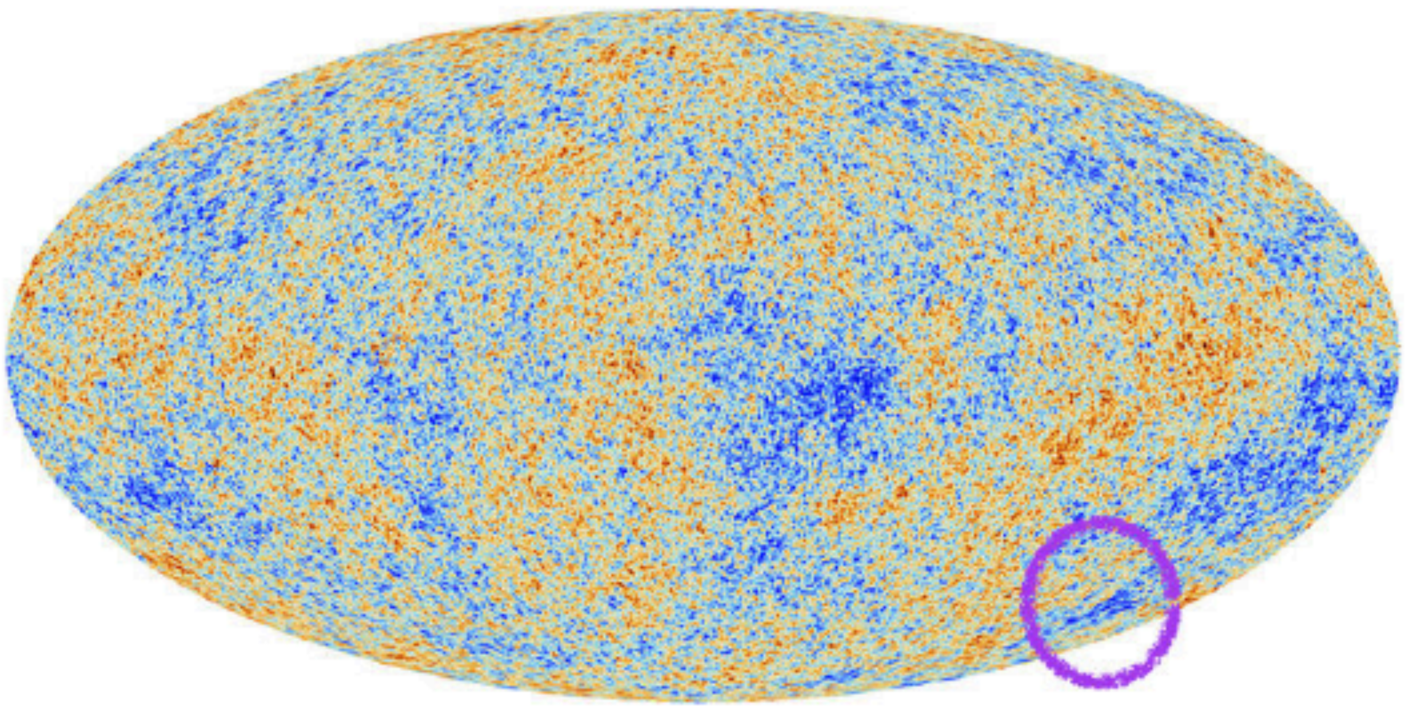

(a)

314159265358979323846264338327950288419716939937510
58209749445923078164062862089986280348253421170679
82148086513282306647093844609550582231725359408128
48111745028410270193852110555964462294895493038196
44288109756659334461284756482337867831652712019091
45648566923460348610454326648213393607260249141273
72458700660631558817488152092096282925409171536436
78925903600113305305488204665213841469519415116094
33057270365759591953092186117381932611793105118548
07446237996274956735188575272489122793818301194912
98336733624406566430860213949463952247371907021798
60943702770539217176293176752384674818467669405132
00056812714526356082778577134275778960917363717872
14684409012249534301465495853710507922796892589235
42019956112129021960864034418159813629774771309960
51870721134999999837297804995105973173281609631859
50244594553469083026425223082533446850352619311881
71010003137838752886587533208381420617177669147303

(b)

“pi” in the sky

Ali Frolop & Douglas Scott, arXiv:1603.09073

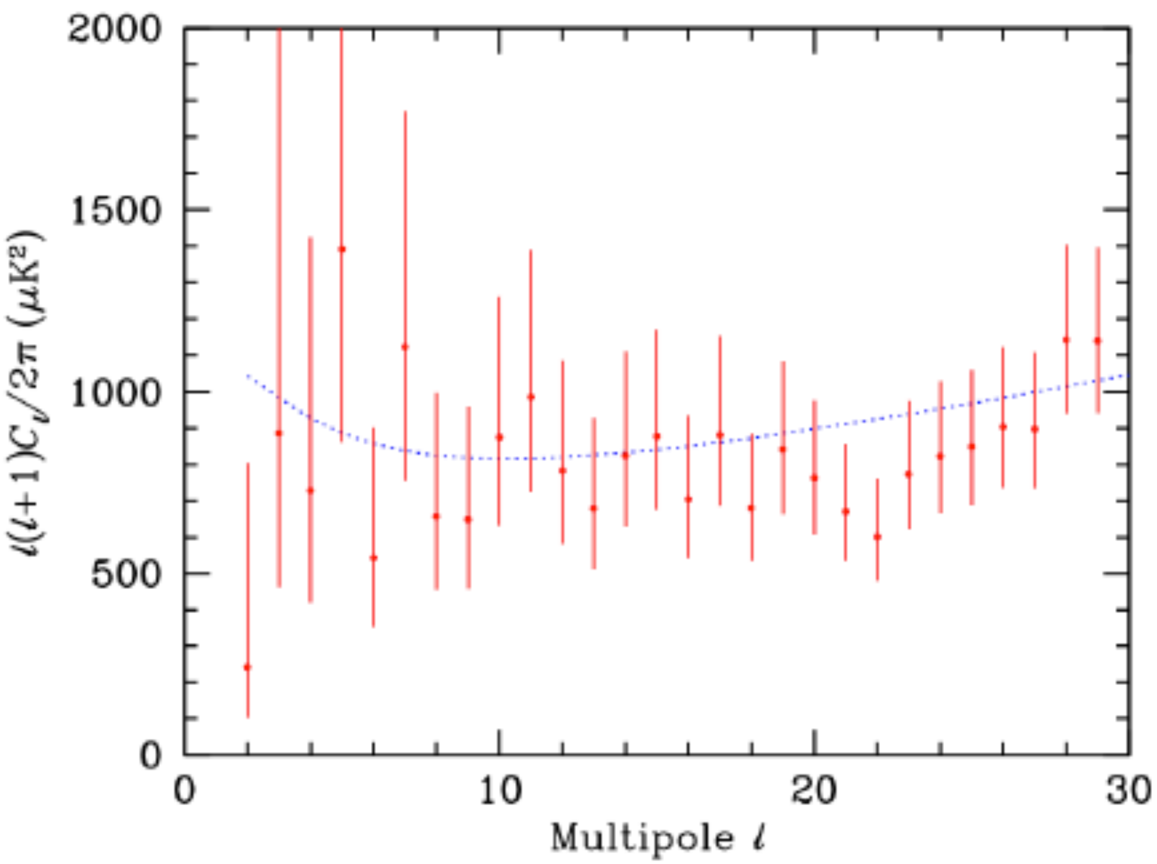

Result from Planck 2015 data, showing the first 30 multipoles. There is a clear asymmetry towards lower values!

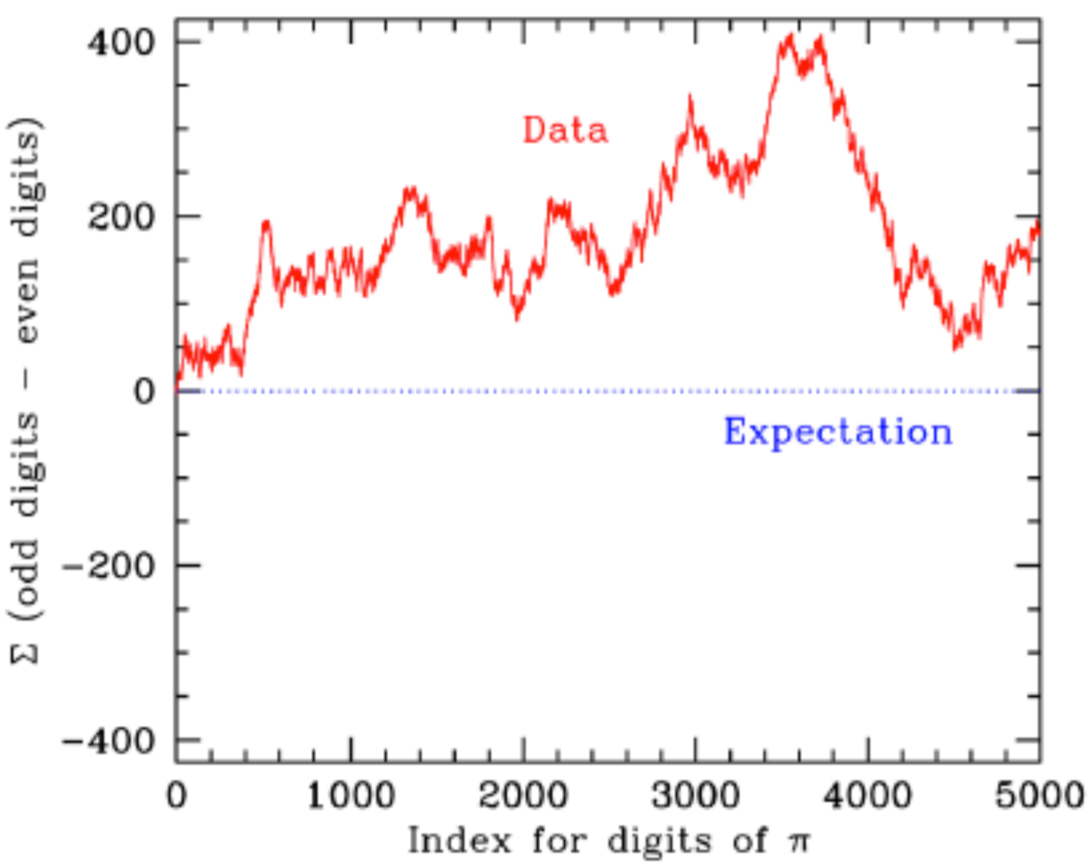

Asymmetry of odd and even digits in π

CMB instrumentation and Map-making

Ground-based measurement

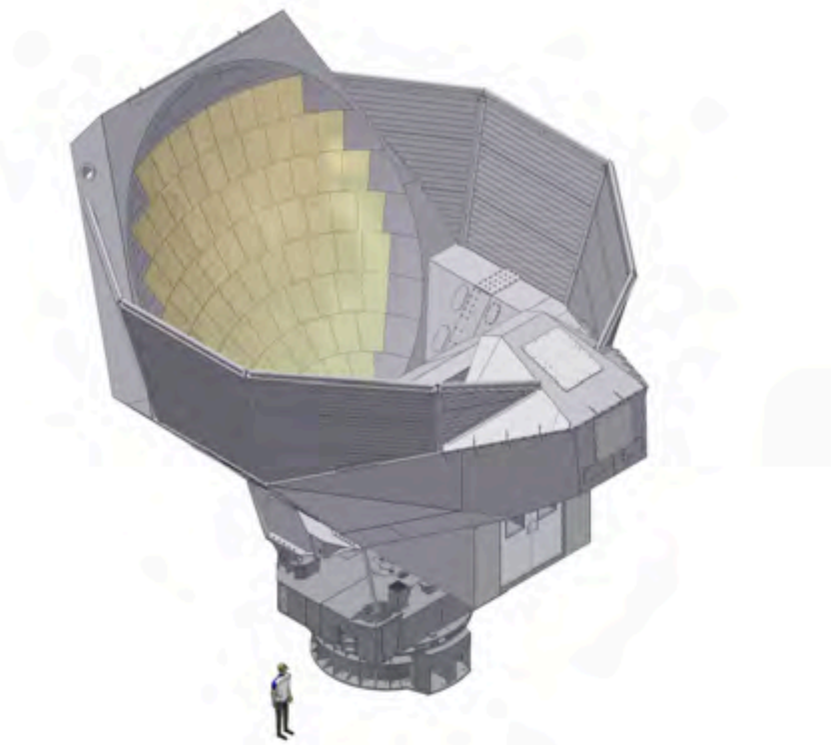

Atacama Cosmology Telescope

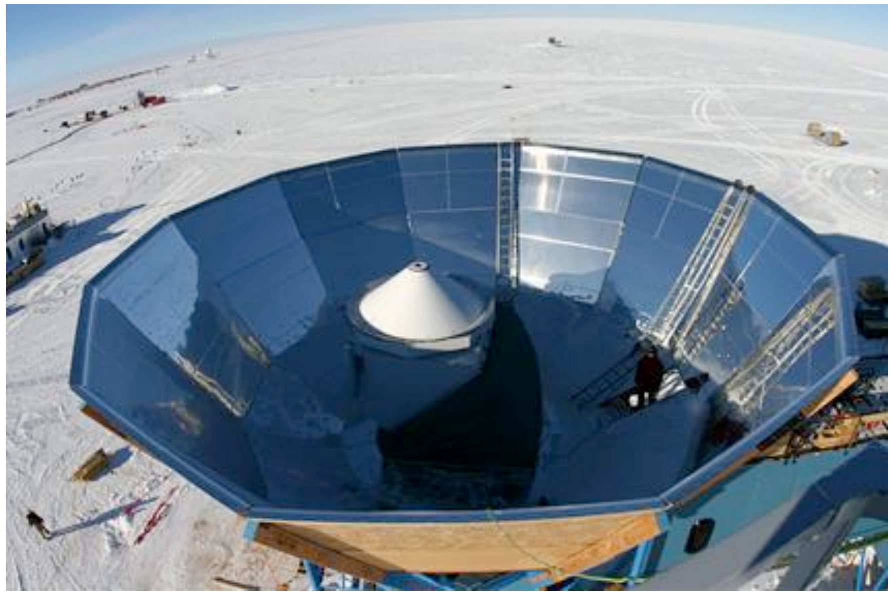

QUaD at south pole

Since 3 K << 300 K, CMB measurements are sensitive to thermal emission from their environments

CMB telescopes are specially designed to be very directional, but 300 K in the sidelobes is always a worry

A receiver has system temperatre T_{sys}

$$T_{sys} = T_{rec} + T_{CMB} + T_{atm} + T_{ground} + \ldots$$

The radiometer equation is: $\delta T = \frac{bT_{sys}}{\sqrt{\Delta\nu\,\tau}}$

CMB flux

Planck spectrum: $$I(\nu,T) = \frac{2h\nu^3}{c^2}\frac{1}{e^{\frac{h\nu}{kT}} - 1}.$$

Example:

- Beam FWHM = 8°, beam aperture = 8 cm^2
- ν_0 = 90 GHz, $\Delta\nu$ = 10 GHz

The CMB flux (2.7K) on the horn is then: **2.5 x 10^{-13} Watts**

Temperature anisotropy: $\sim 10^{-18}$ Watts

Polarization anisotropy: $\leq 10^{-19}$ Watts

CMB receivers

Coherent receivers:

Phase-preserving amplification
Correlation of different polarization

- Correlation/Pseudocorrelation receiver (e.g. WMAP, CAPMAP)
- Interferometer (e.g. DASI, CBI)

Incoherent receivers (bolometers):

Direct detection of radiation,
No phase information kept
Large arrays!

- Bolometers (e.g. ACBAR, Boomerang, BICEP, Clover, Planck)

Interferometers

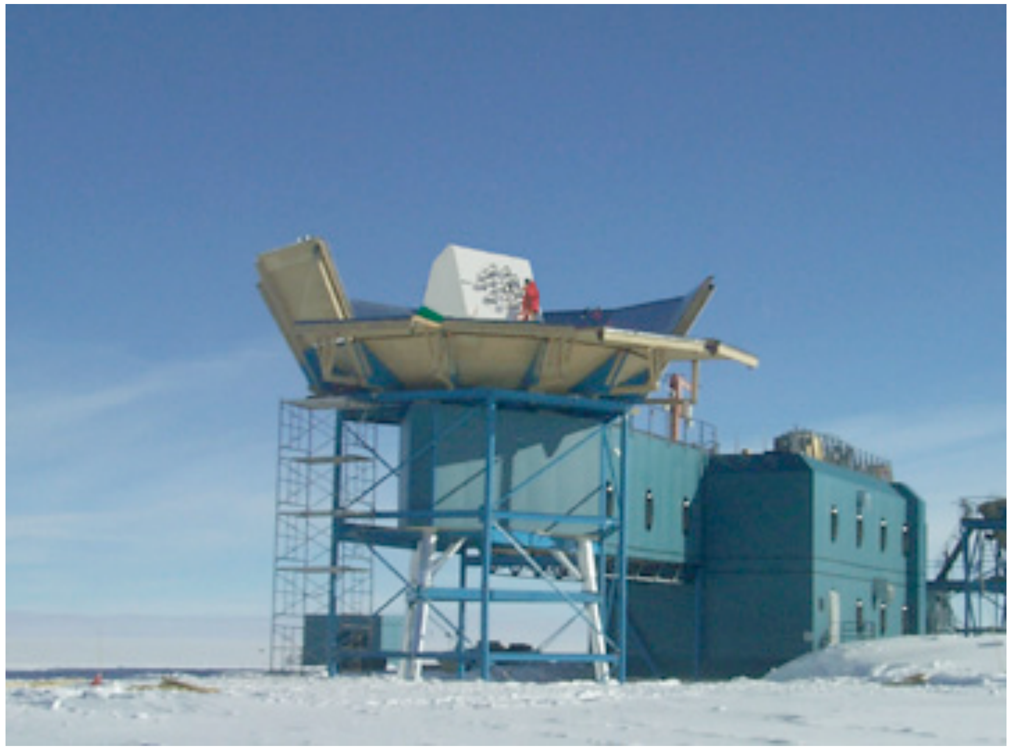

DASI in South Pole

CBI in Atacama desert

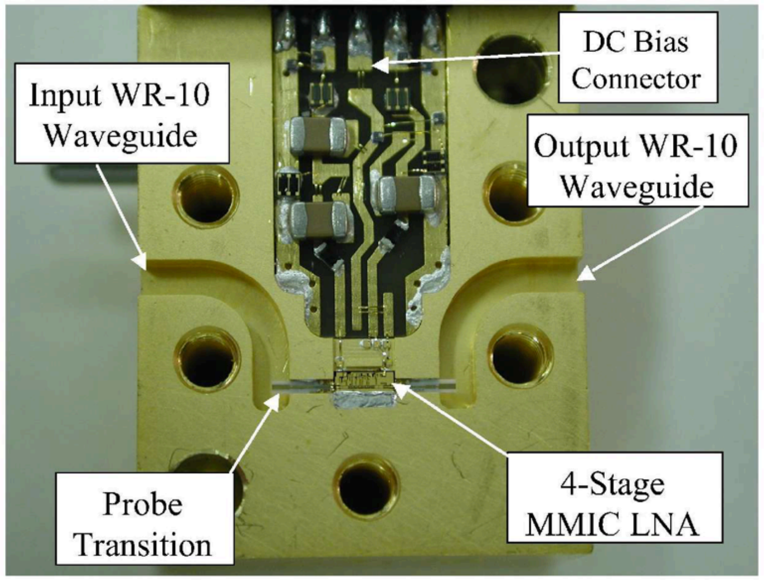

Coherent receivers: Can be configured so that the output is the correlation of two input signals.
HEMT (High Electron Mobility Transistor) allow coherent amplification with low noise and high gain.

Interferometric measurements

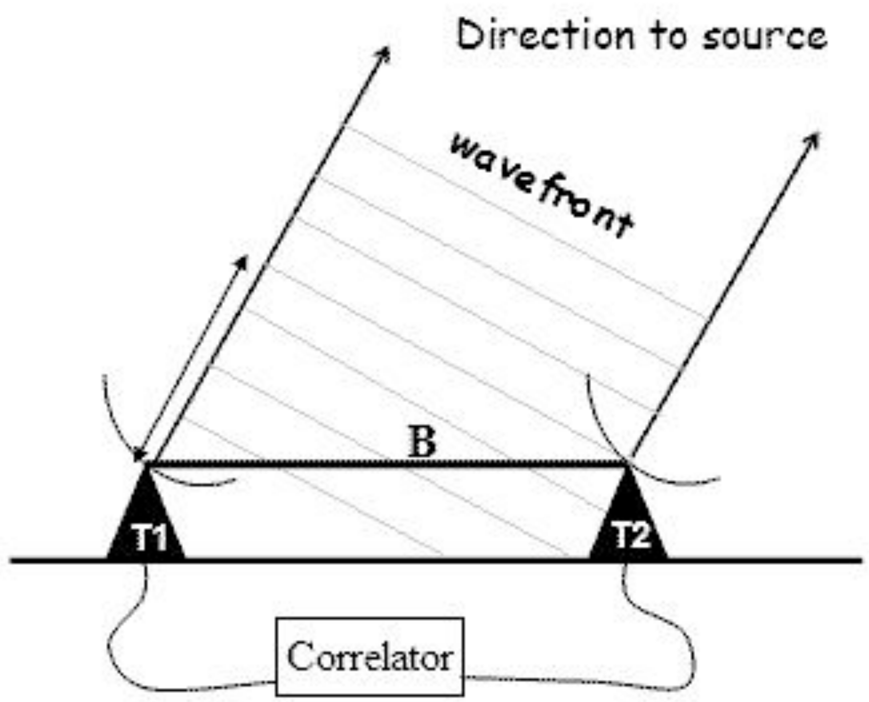

Properties of interferometers that make them ideally suited for CMB observation:

- Automatic subtraction of the mean signal
- Intrinsically stable (no skynoise)
- Beamshape is easy to obtain (and is not as important as in single dish observations)
- Direct measurement of visibilities (which are very nearly the Fourier transform of sky brightness distribution)
- Precision radiometry and polarimetry
- Repeated baselines allow variety of instrumental checks

C(θ) from interferometers

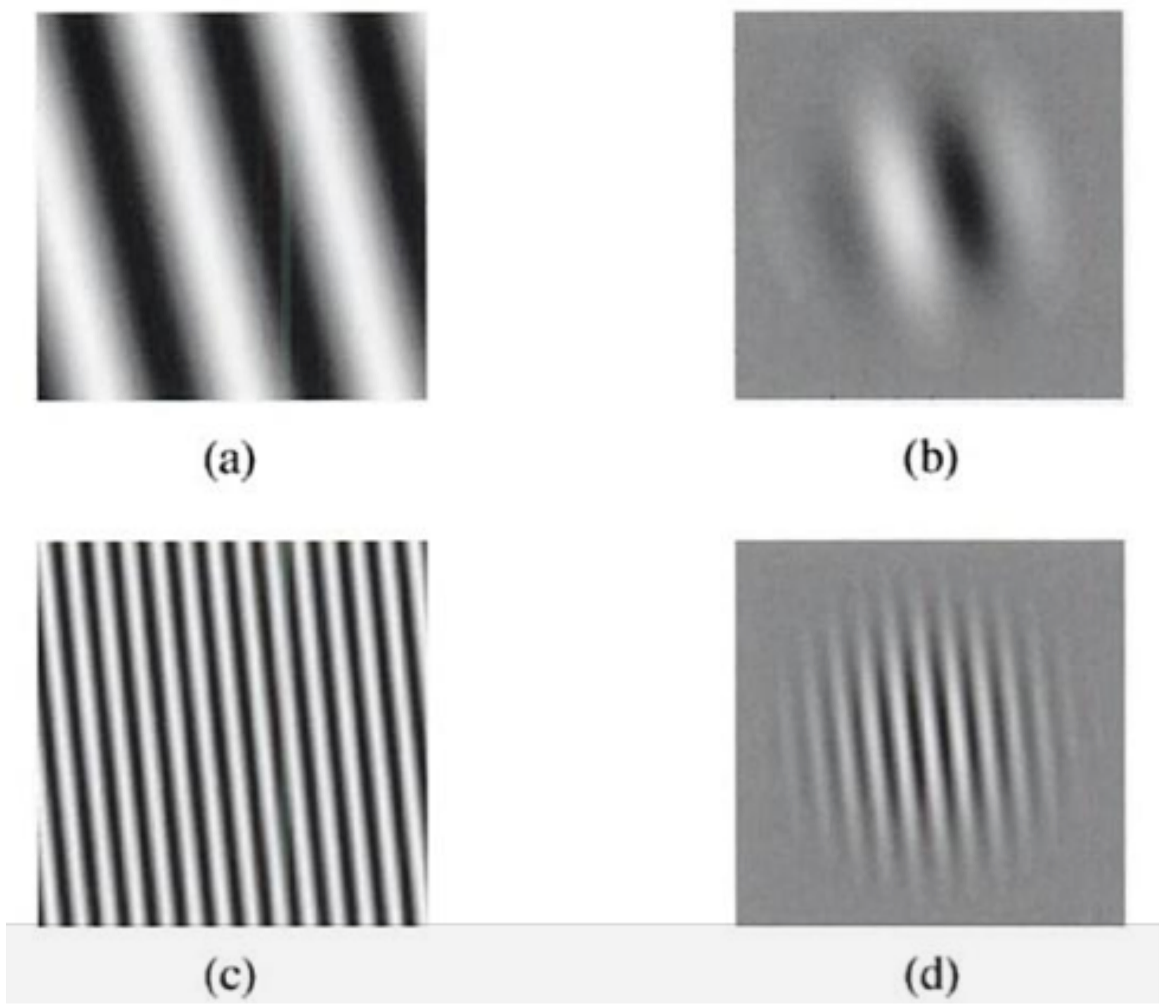

Left: Illustration of two multipole components of sky brightness over a 1.5° × 1.5° field of view. An interferometer measures directly these components multiplied by the primary beam, shown in the right. For CBI, (a) and (b) corresponds to 1-meter baselines, and (c) and (d) represents 5-meter baselines.

Bolometer and HEMT sensitivities

Fluctuations in the arrival rate of CMB photons impose a fundamental limit of ~30 μK√(sec) for detection of a single mode of radiation in a fractional bandwidth of 25% from ~30 to 220 GHz.

	2005[b]		2010[c]	
Freq.	**Bolometer**	**HEMT** $/\sqrt{2}$	**Bolometer**	**HEMT** $/\sqrt{2}$
[GHz]	[$\mu K_{cmb}\sqrt{s}$]	[$\mu K_{cmb}\sqrt{s}$]	[$\mu K_{cmb}\sqrt{s}$]	[$\mu K_{cmb}\sqrt{s}$]
30	–	93	57	48
40	–	115	51	51
60	–	175	44	60
90	67	224	40	75
120	–	–	40	93
150	48	–	43	–
220	68	–	64	–
350	224	–	220	–

(CMB Task Force Report, 2005)

Bolometers (heat detectors)

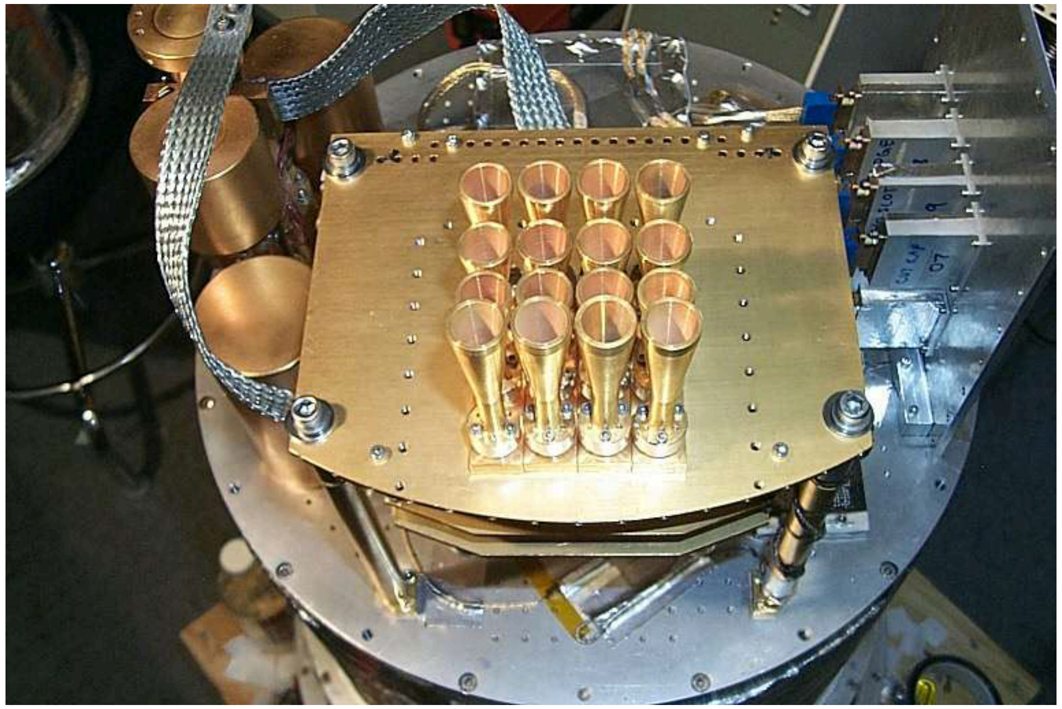

ACBAR

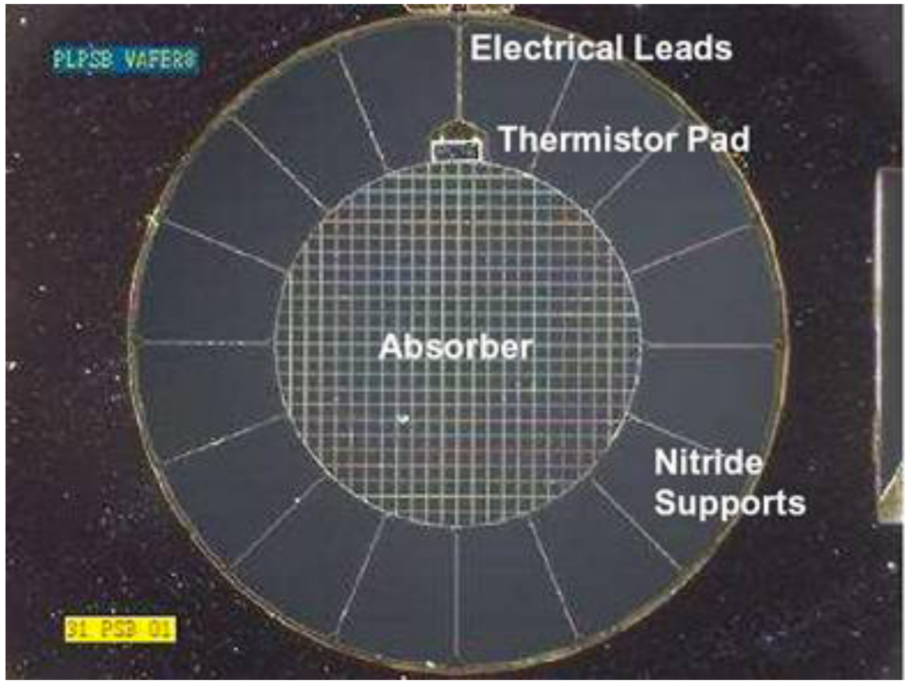

Boomerang

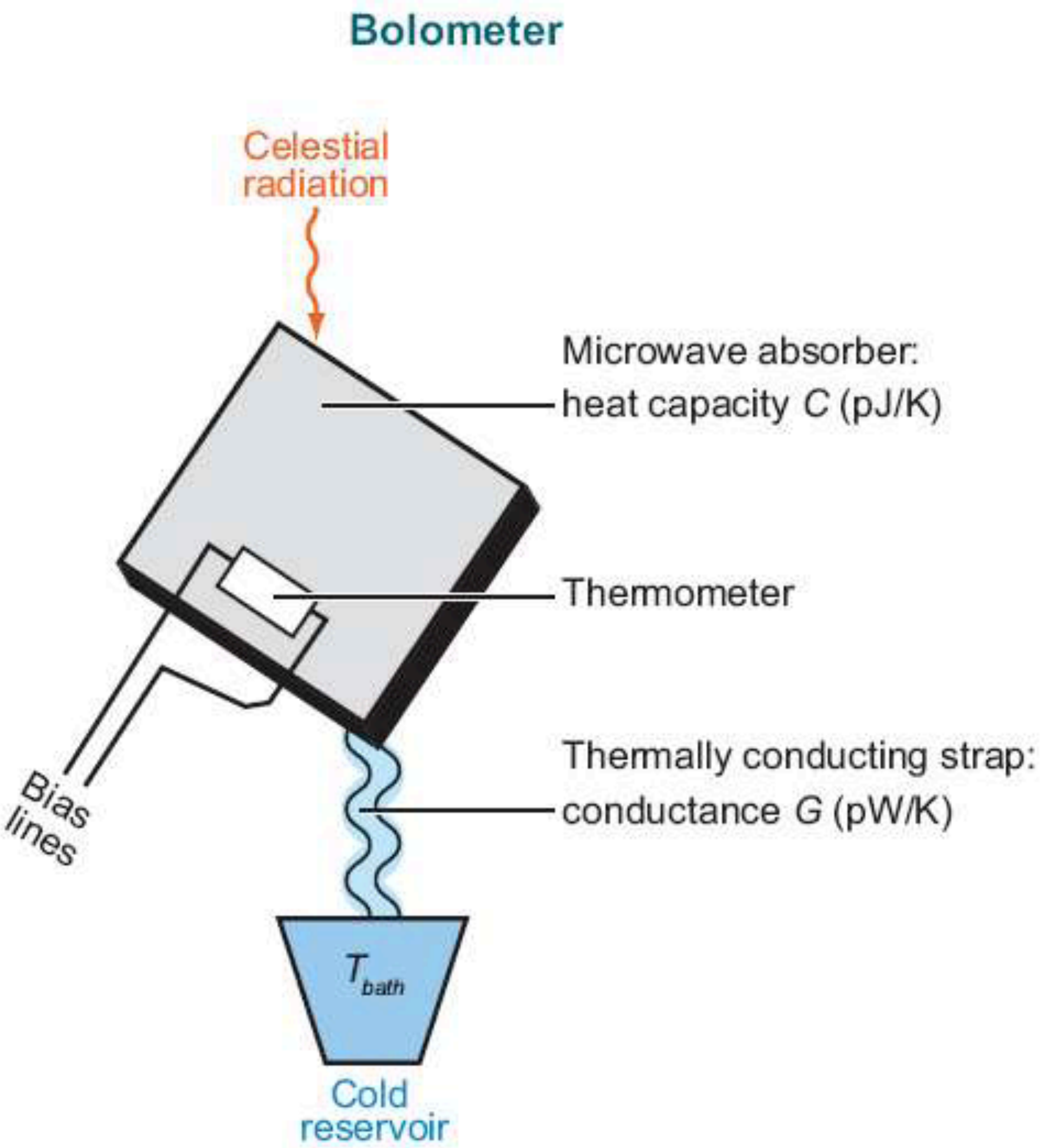

Ground- and space-based experiments

From Delabrouille et al., CORE mission paper

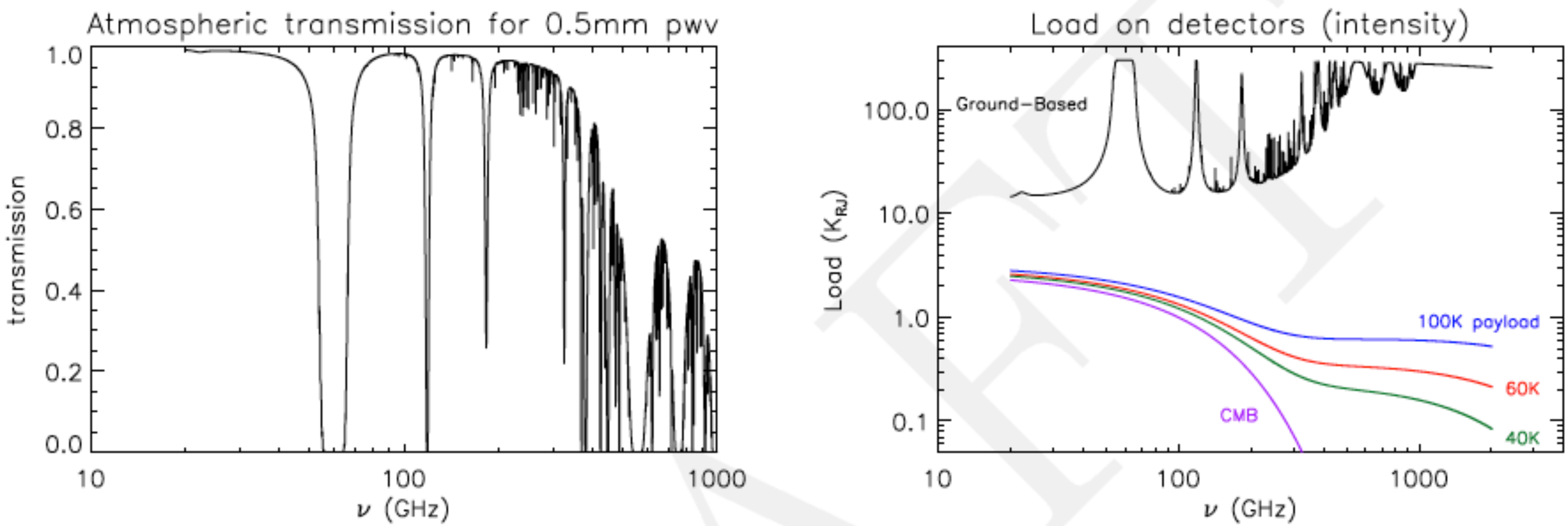

Figure 11. *Top left*: Typical atmospheric transmission from the Atacama plateau at 60° elevation, for an average of half a millimetre of integrated precipitable water vapour. *Top right*: Load on a detector for a ground-based instrument (black) and for a space-borne instrument with various payload temperatures.

A single space-borne detector can reach a sensitivity equivalent to 100-200 ground-based detectors (depending on frequency).

Ground- and space-based experiments

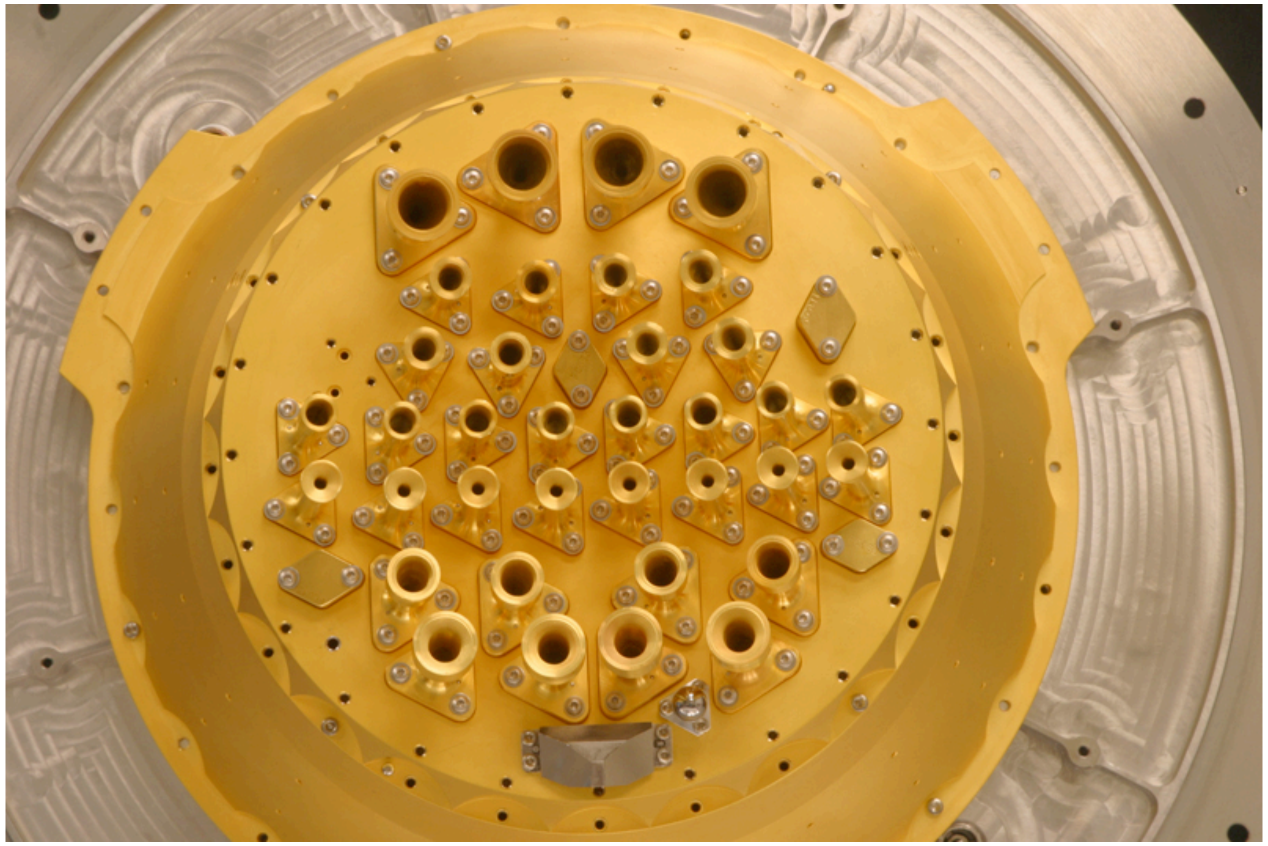

Planck HFI focal plane, showing the feed horns for 32 bolometer detectors

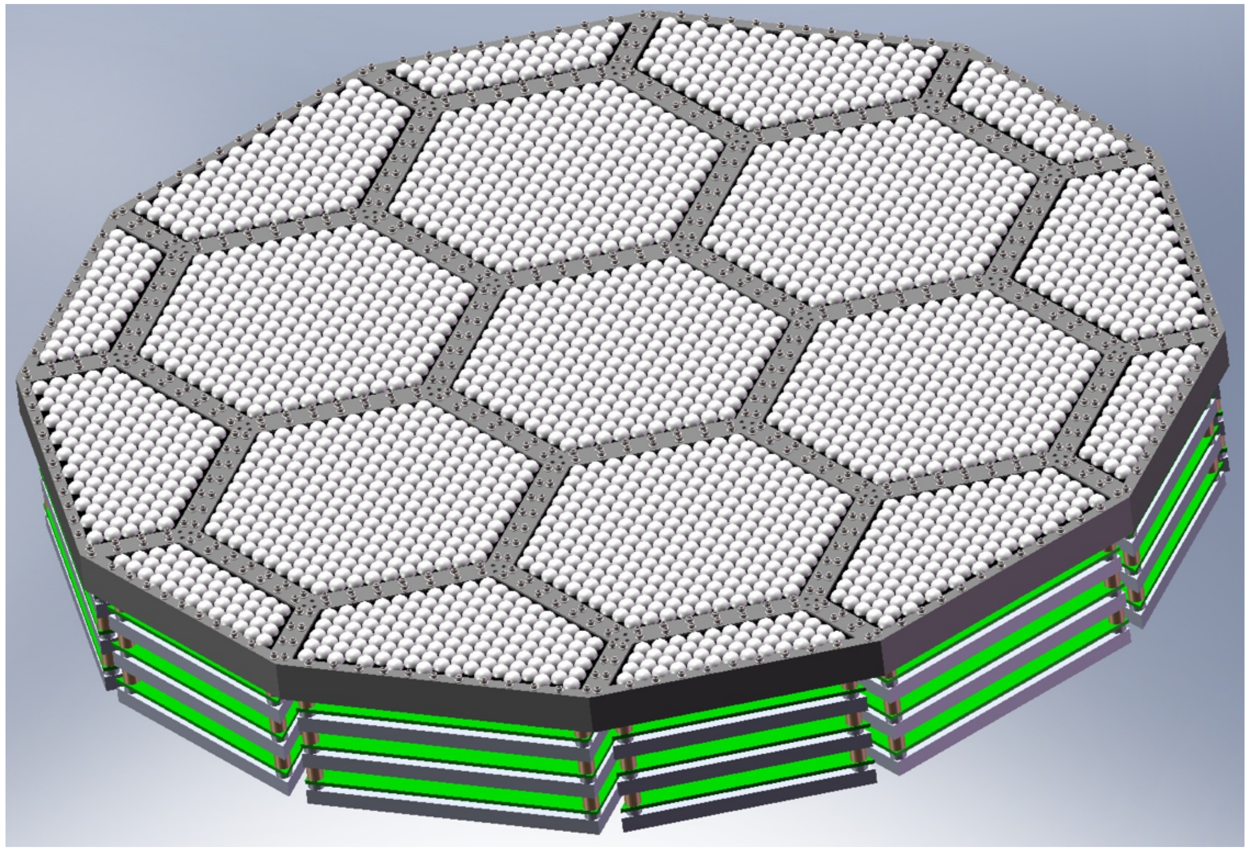

SPT-3G focal plane, with over 15 000 detectors (0.5 m diameter)

Detectors for the ground-based telescopes

(Credit: SPT collaboration)

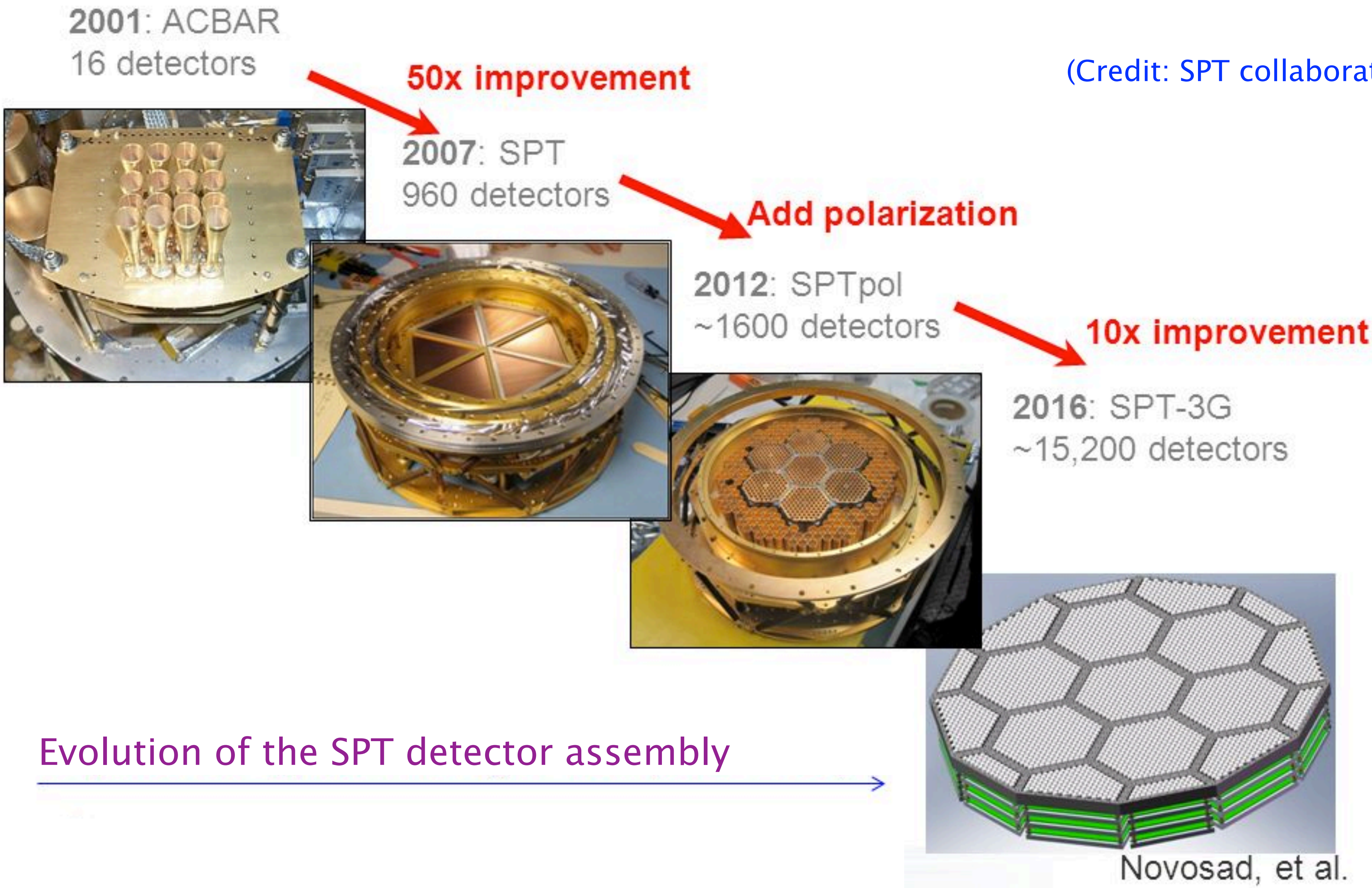

Evolution of the SPT detector assembly

Next generation ground-based telescopes

CCAT-prime

6 meter aperture extreme field-of-view sub-millimeter telescope on Cerro Chajnantor at 5600m, Chile

Partners: Cornell, **Bonn**-Cologne-Munich, Canadian universities

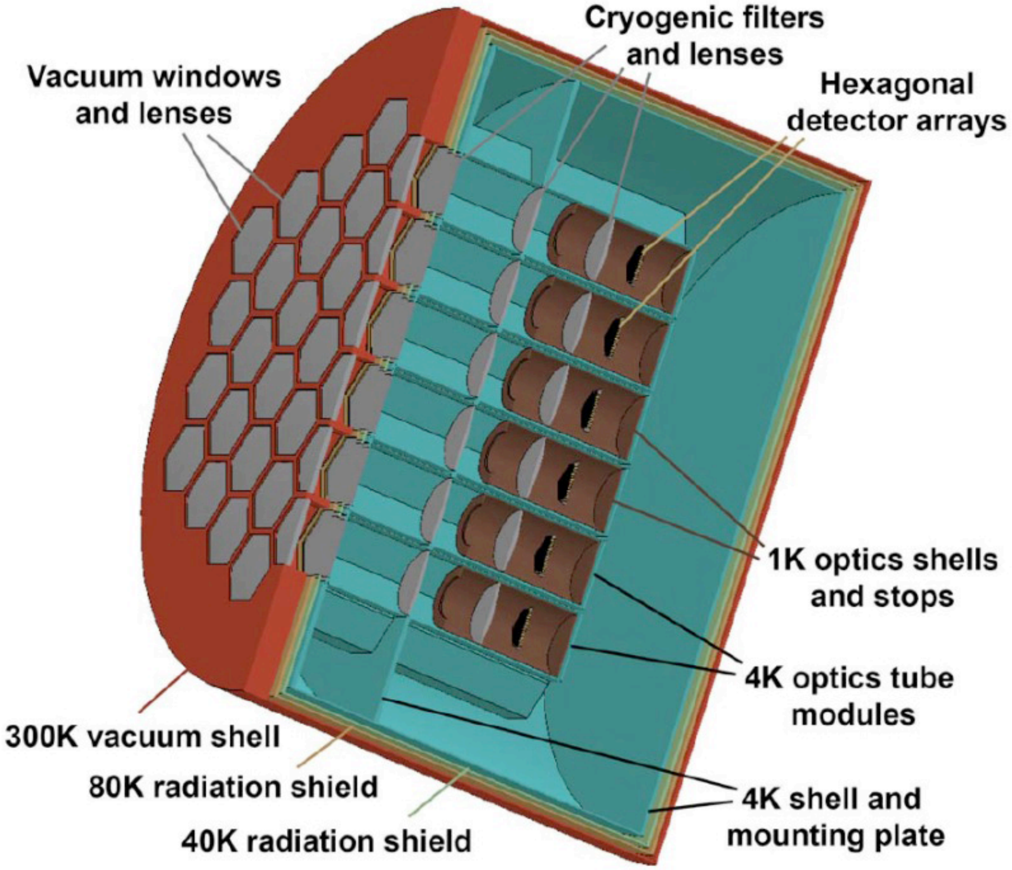

2.5 meter diameter receiver design

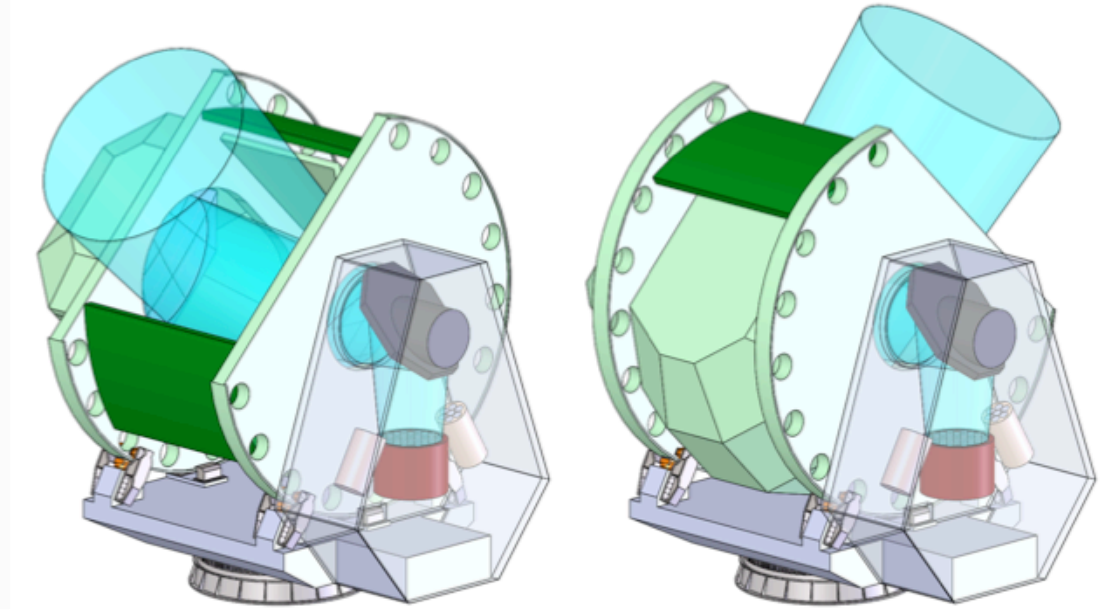

CMB Data Analysis

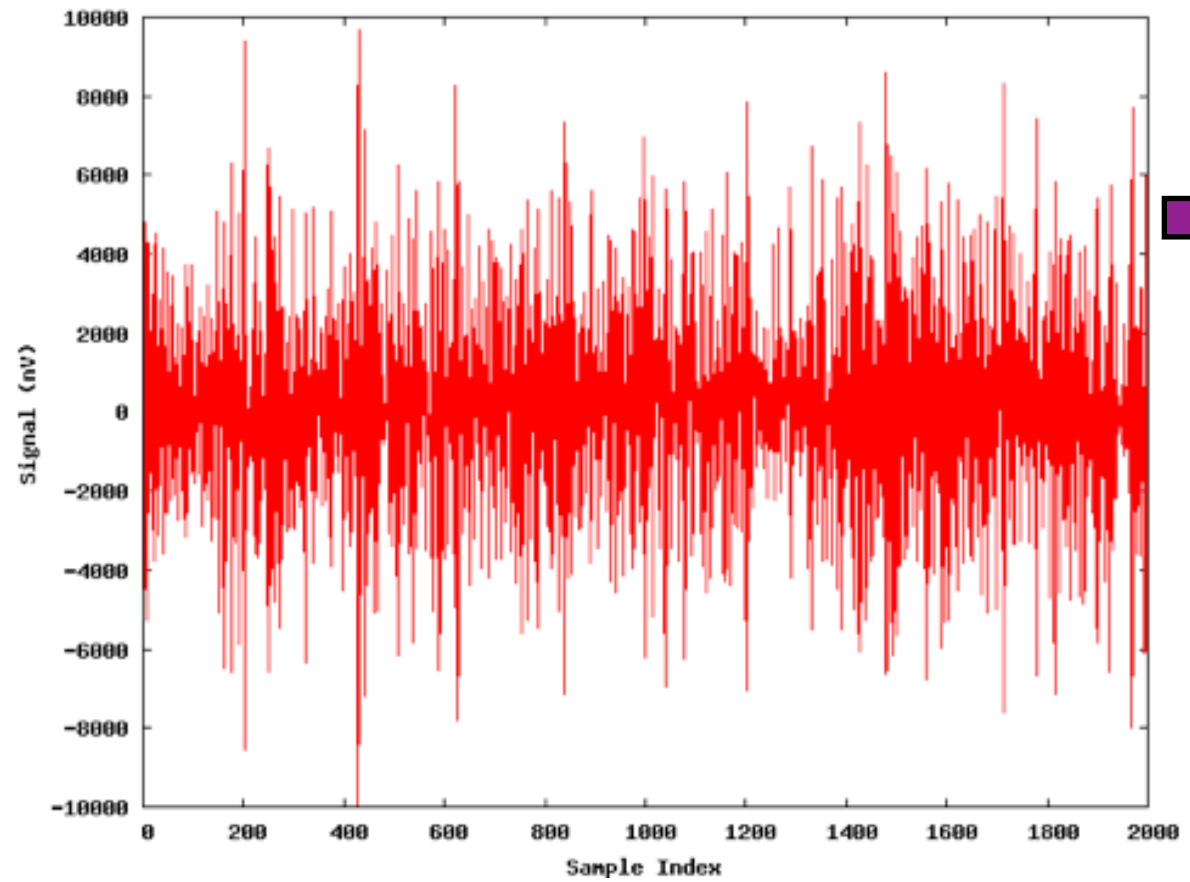

Data time-stream

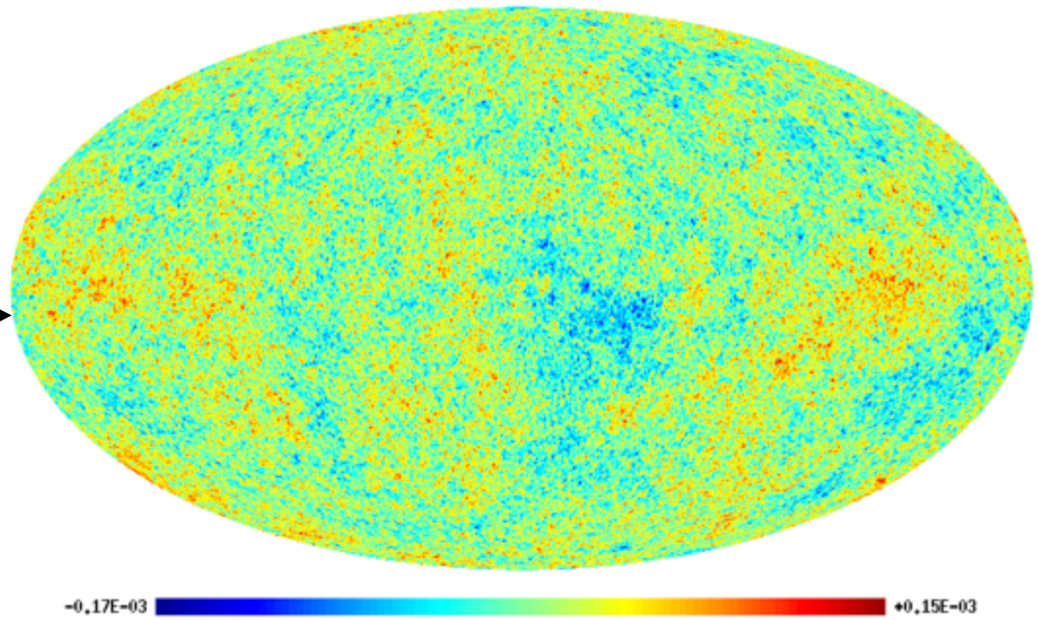

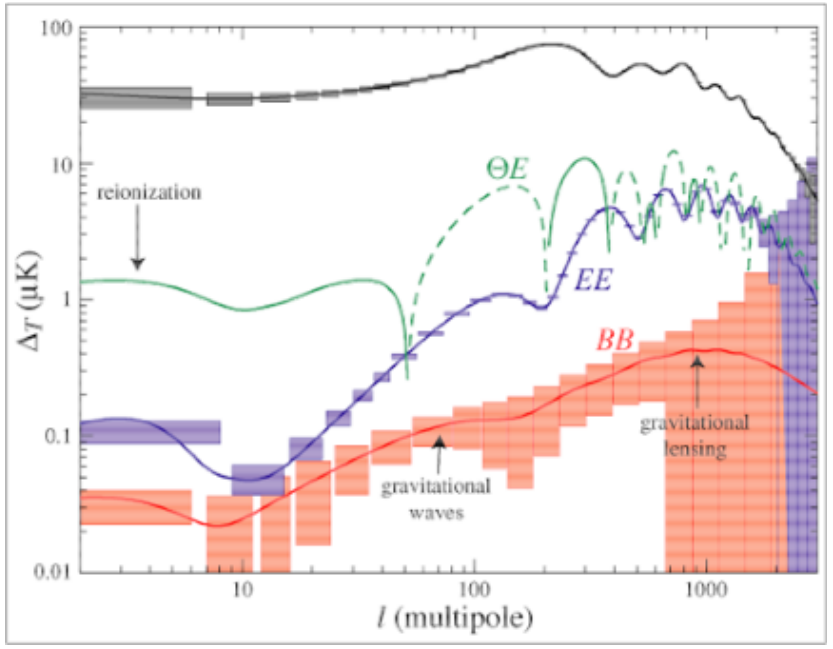

De-striping

Common to get stripes in the scan direction.

Removal easy in Fourier space.

Fourier transformation also helps to separate signal and noise better (different temporal signal).

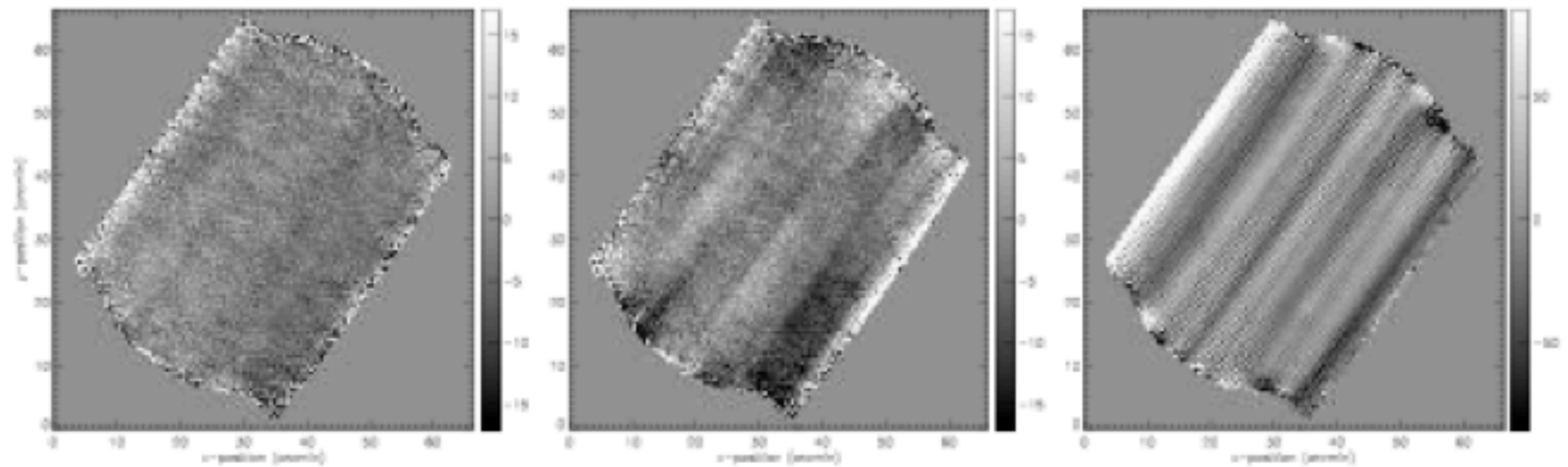

map space

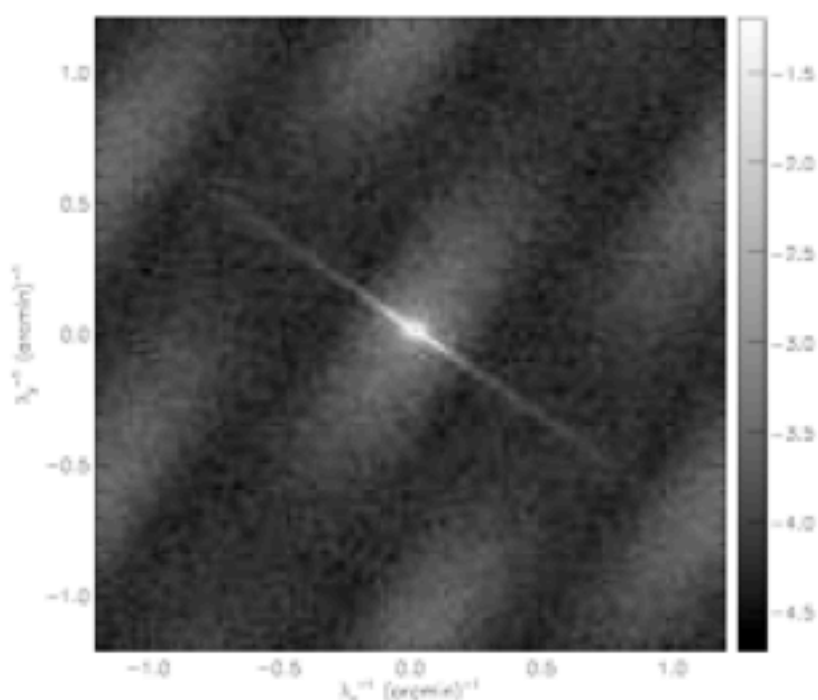

Fourier space

Patanchon et al ; BLAST data

De-glitching

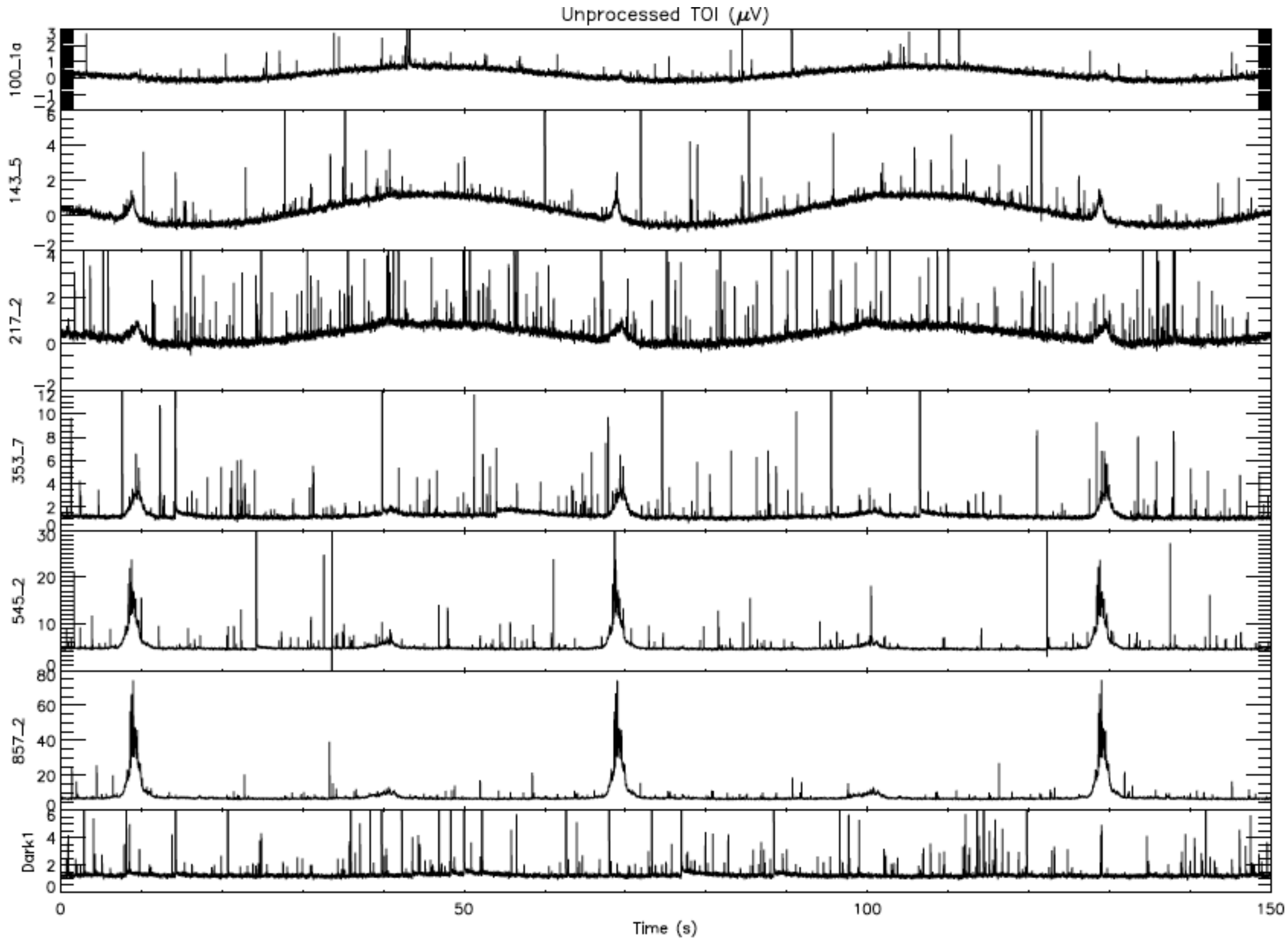

Figure 13. Examples of raw (unprocessed) TOI for one bolometer at each of six HFI frequencies and one dark bolometer. Slightly more than two scan circles are shown. The TOI is dominated by the CMB dipole, the Galactic dust emission, point sources, and glitches. The relative part of glitches is over represented on these plots due to the thickness of the lines that is larger than the real glitch duration.

Map making

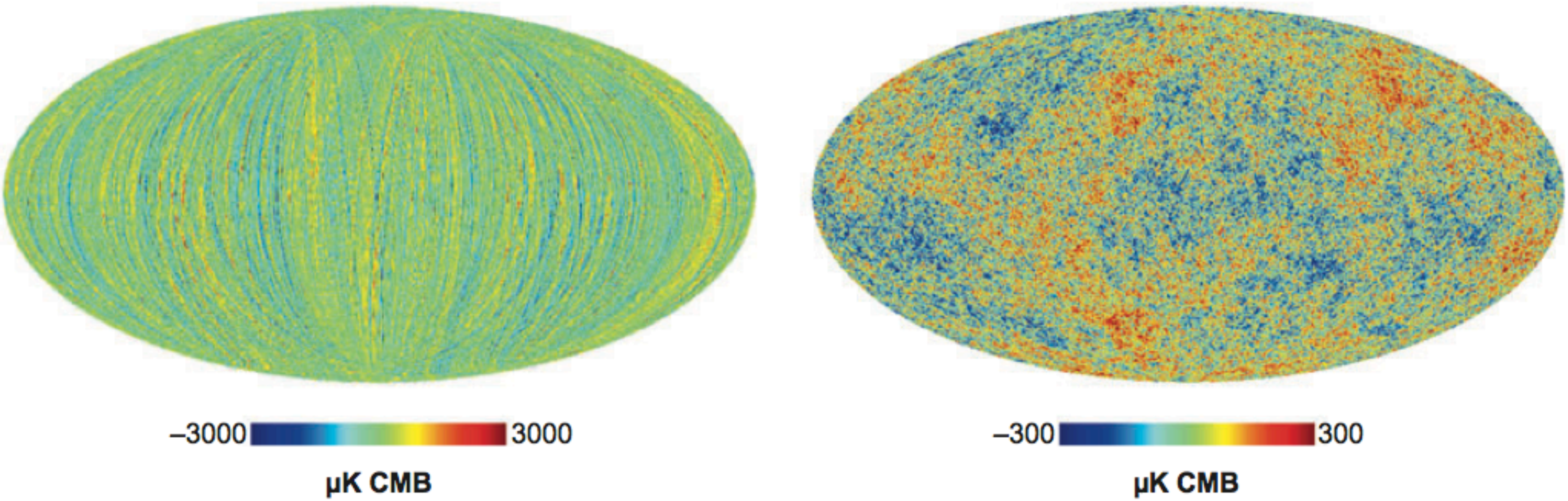

Figure 10

Effect of destriping on simulated sky maps. (*Left*) Map from a raw time stream. (*Right*) Map after applying a destriping algorithm (note the different scales). This simulation was done for the Planck High Frequency Instrument (38).

Figure taken from Samtleben et al. 2007.

Planck TOI data & differential noise

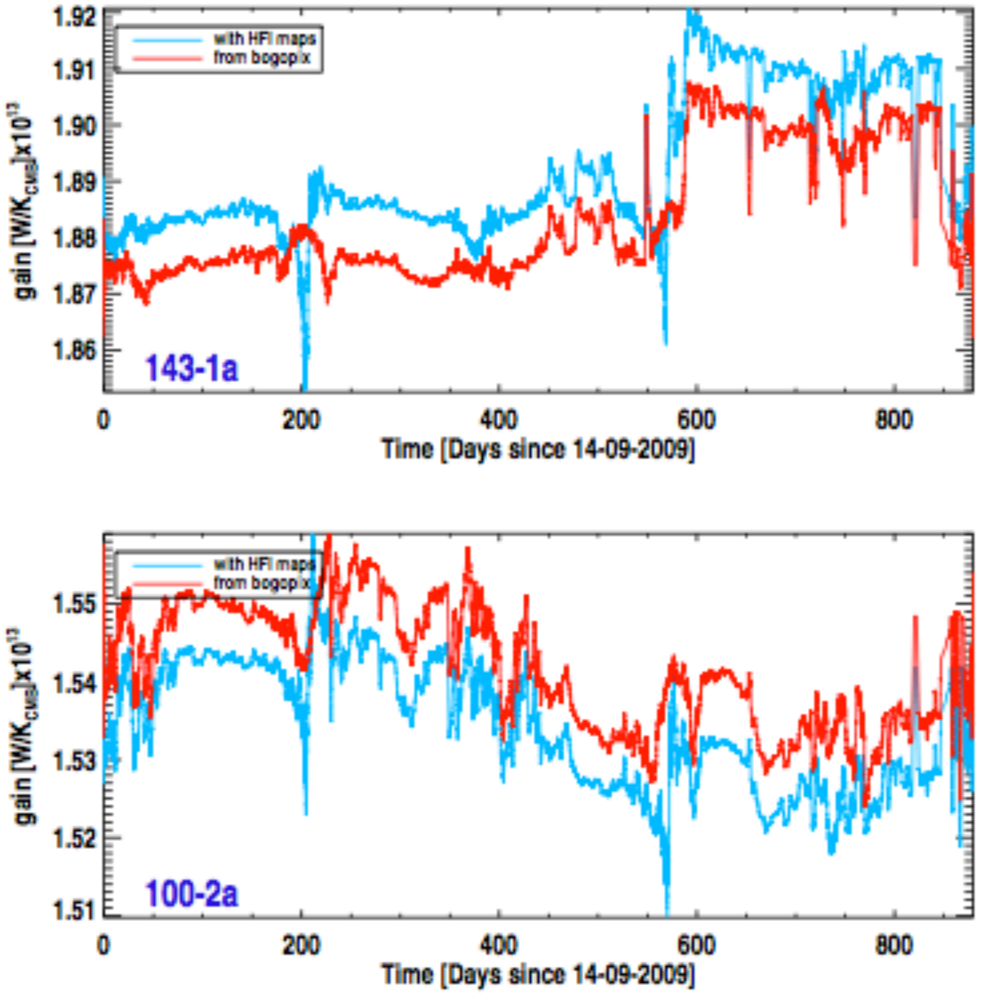

Figure 7. Example of results from `bogopix` obtained for two HFI detectors, compared with those of the Solar dipole calibration. Gain values for individual rings have been smoothed with a width of 50 rings (~ 2 days), to increase the signal-to-noise ratio of the plots. We observe a good agreement between `bogopix` results and those obtained with the HFI maps, for the relative gain variation, except for the time intervals where the Solar dipole's amplitude is low with respect to the Galactic emission. The averaged value of the gains are, however, offset by factors (different from one detector to the other) of the order of 0.5 to 1 %.

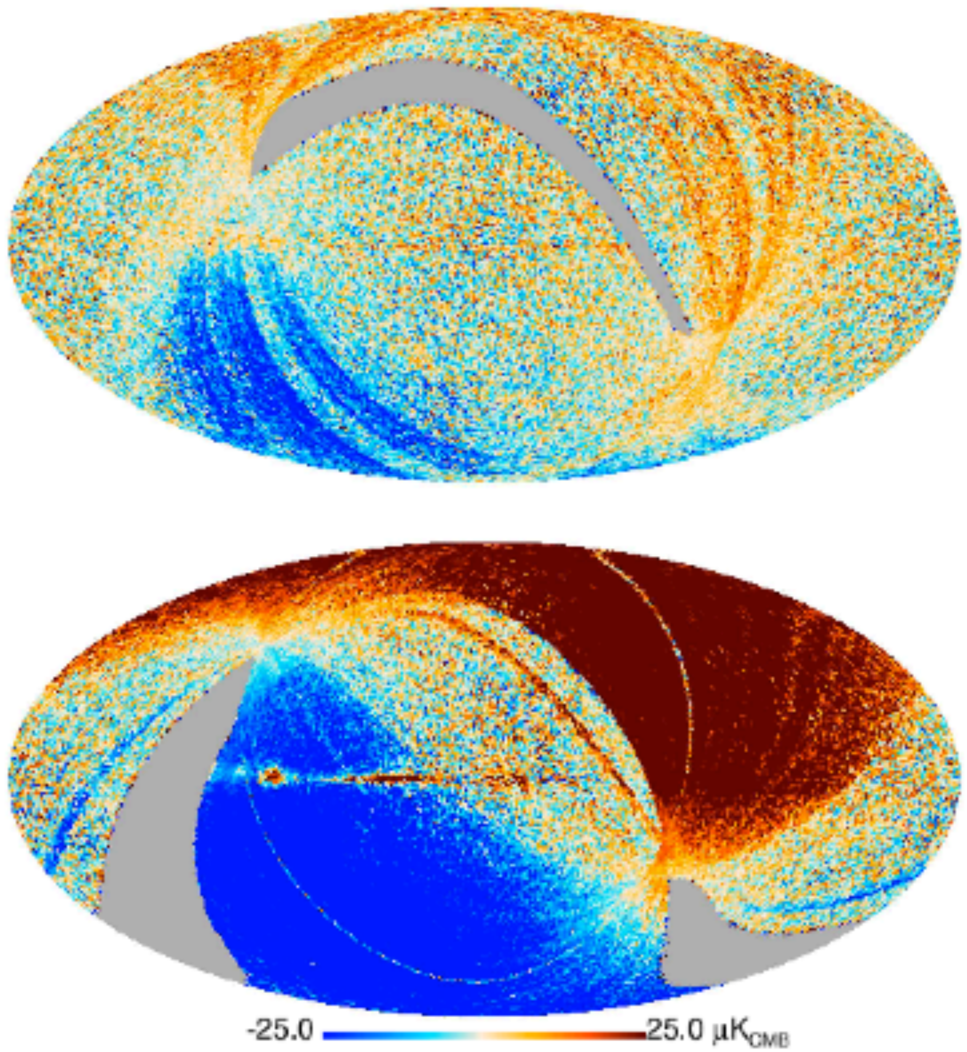

Figure 4. Differences between temperature maps built using data from detector 143-1a, for surveys 1 and 3 (top) and 2 and 4 (bottom). In both cases, large scale features appear. Their amplitude and disposition on the sky are compatible with residuals from the Solar dipole, due to time variations of the detector gain, of the order of 1 to 2 % These residuals should be compared to the amplitude of the Solar dipole, 3.353 mK_{CMB}.

Planck sky maps

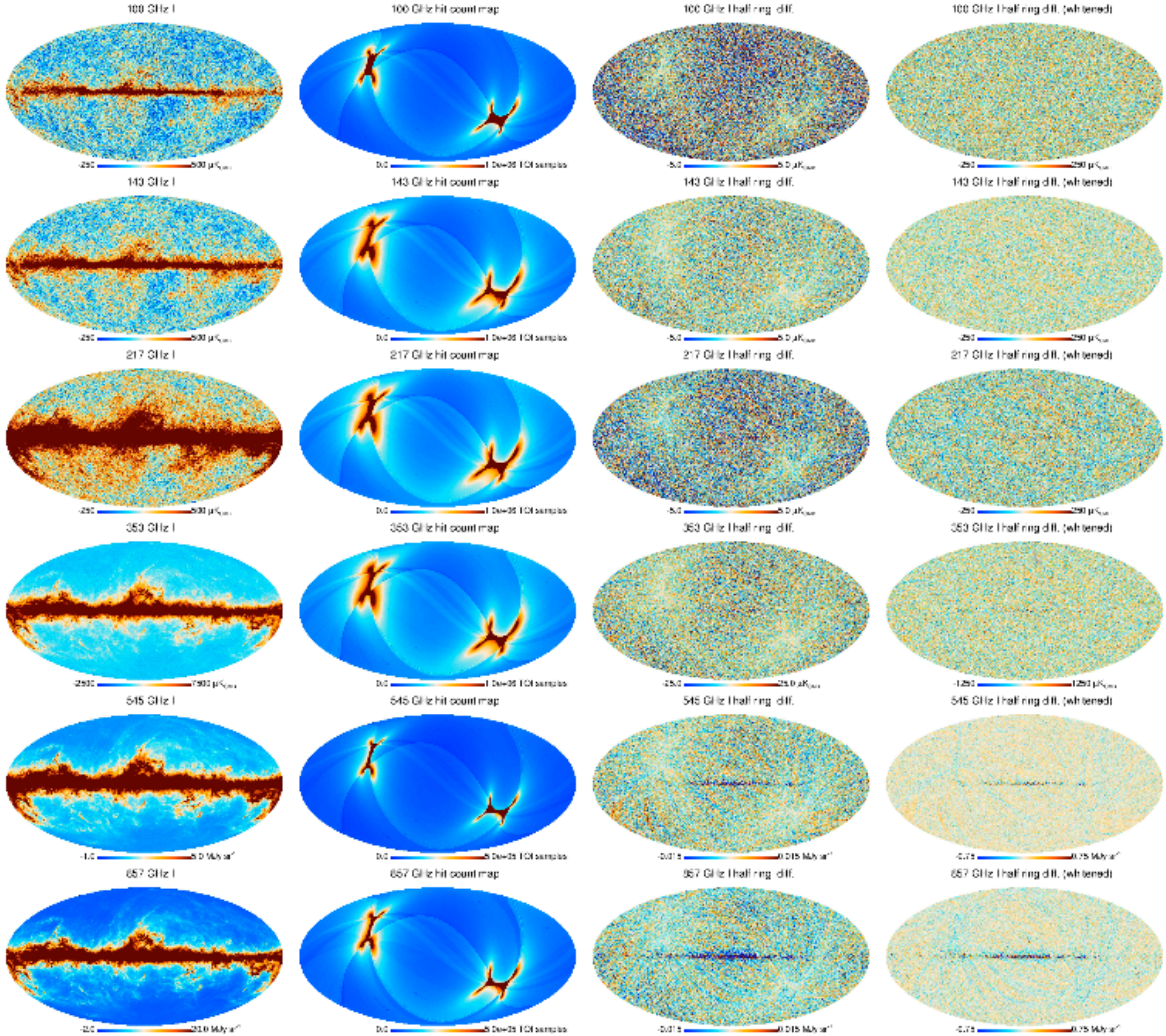

Planck collaboration (2013)

Removing the (Galactic) foregrounds

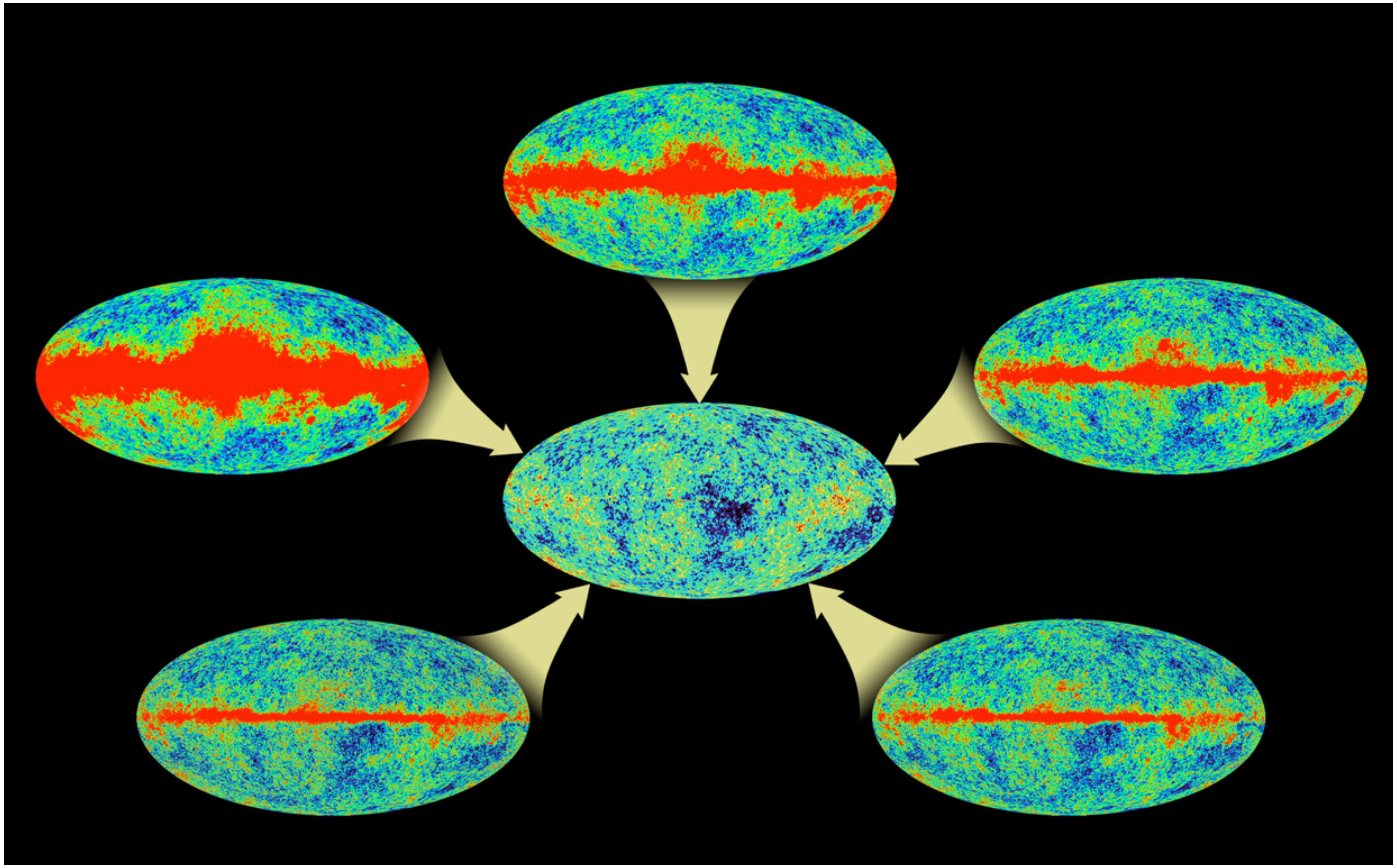

Galaxy vs. the CMB

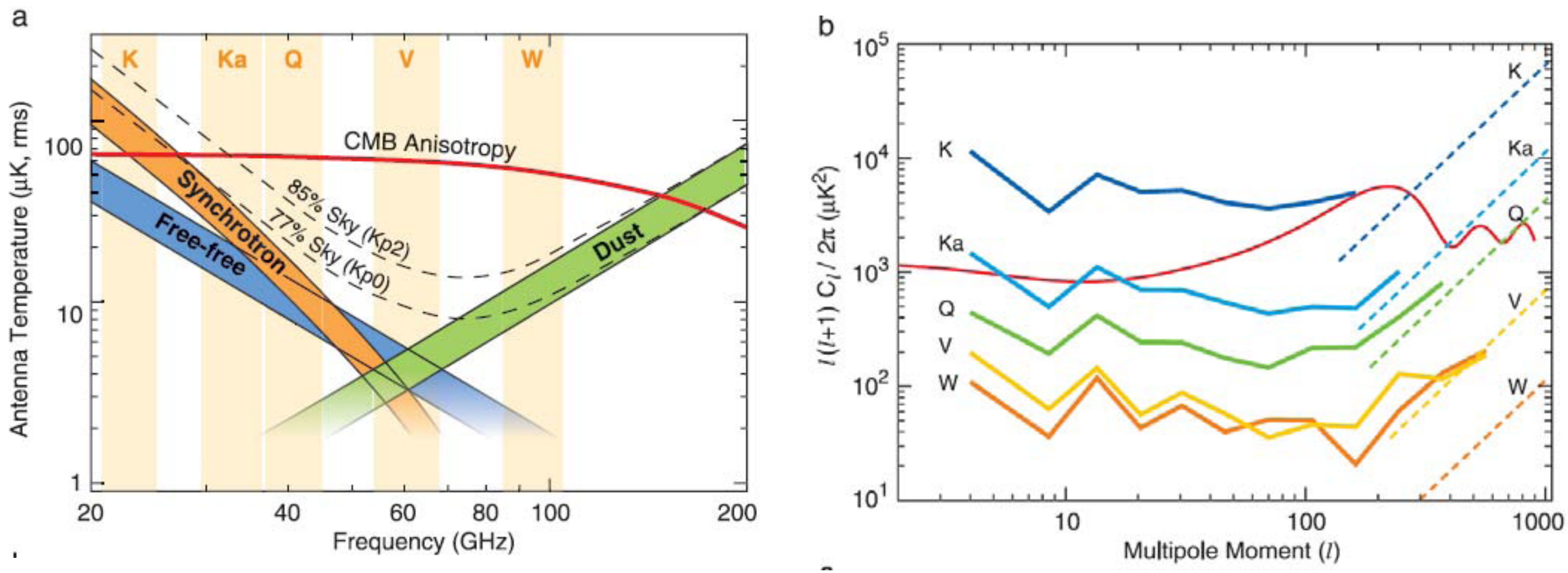

CMB vs. foreground anisotropies (Bennett et al. 2003, WMAP 1st year)

Left: Spectrum of the CMB and foreground emissions (models). WMAP frequencies were chosen such CMB mostly dominates.

Right: Foreground power spectra for each WMAP band. The dashed lines at the right are estimated point source contributions.

Polarized foregrounds

(CMB Task Force Report)

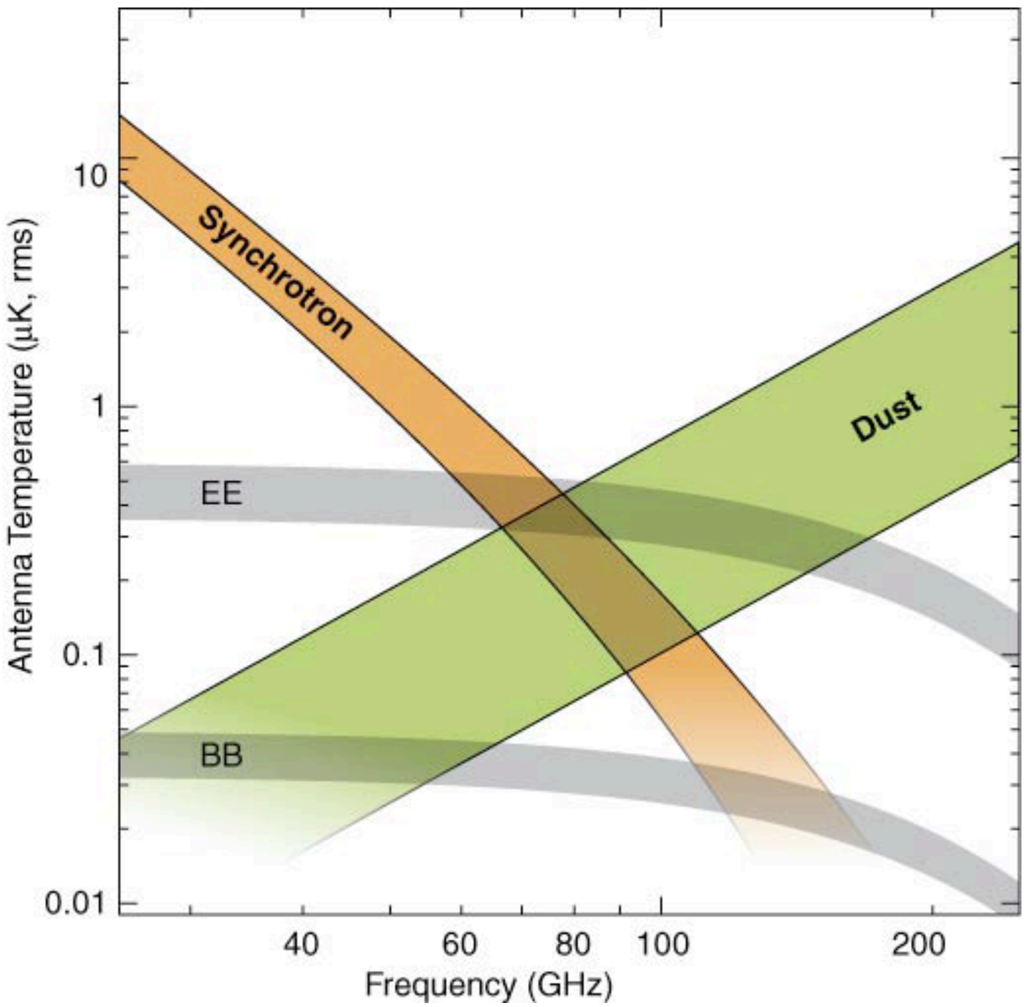

RMS fluctuations in the polarized CMB and foreground signals as function of frequency

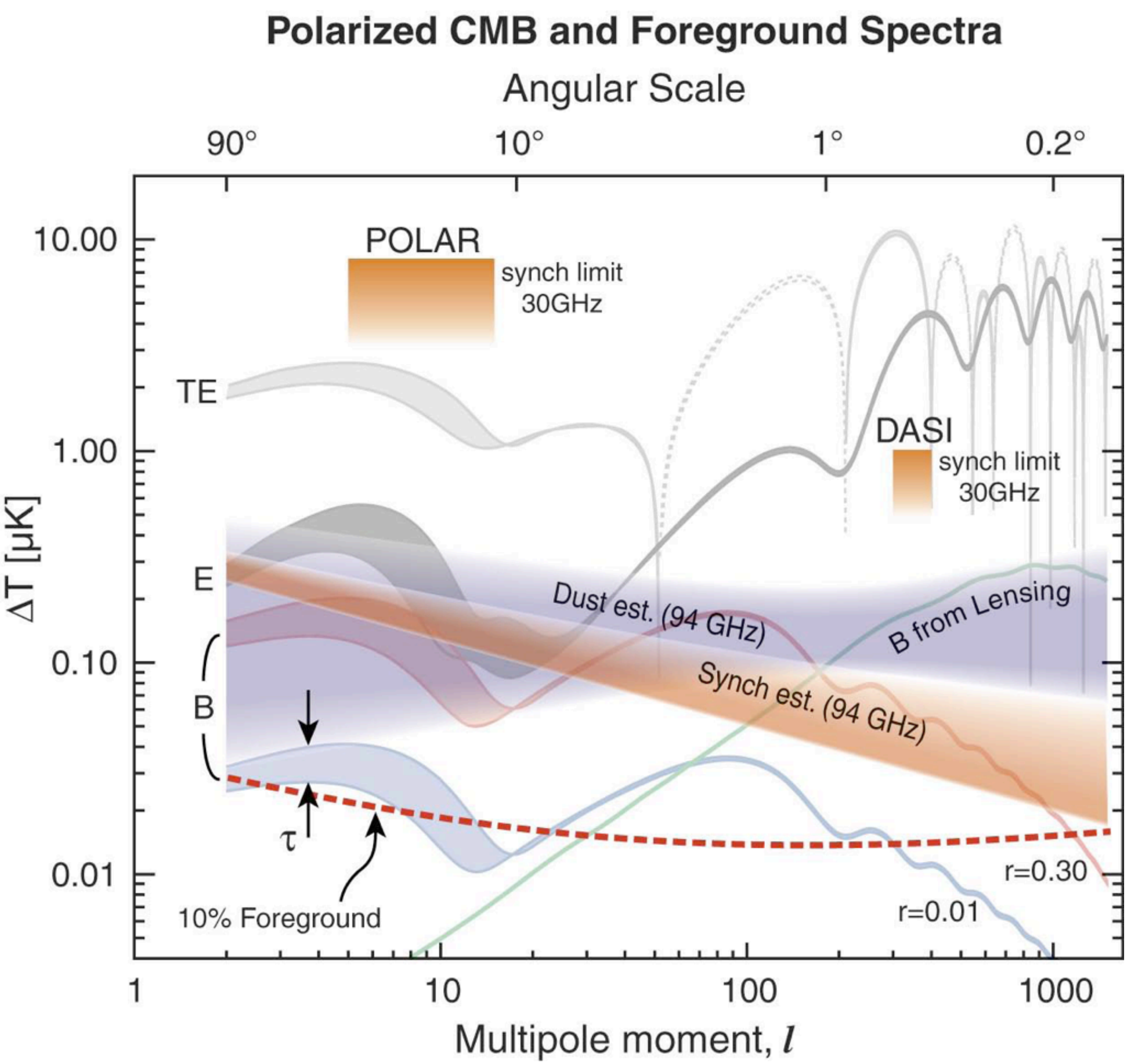

How to remove CMB foregrounds?

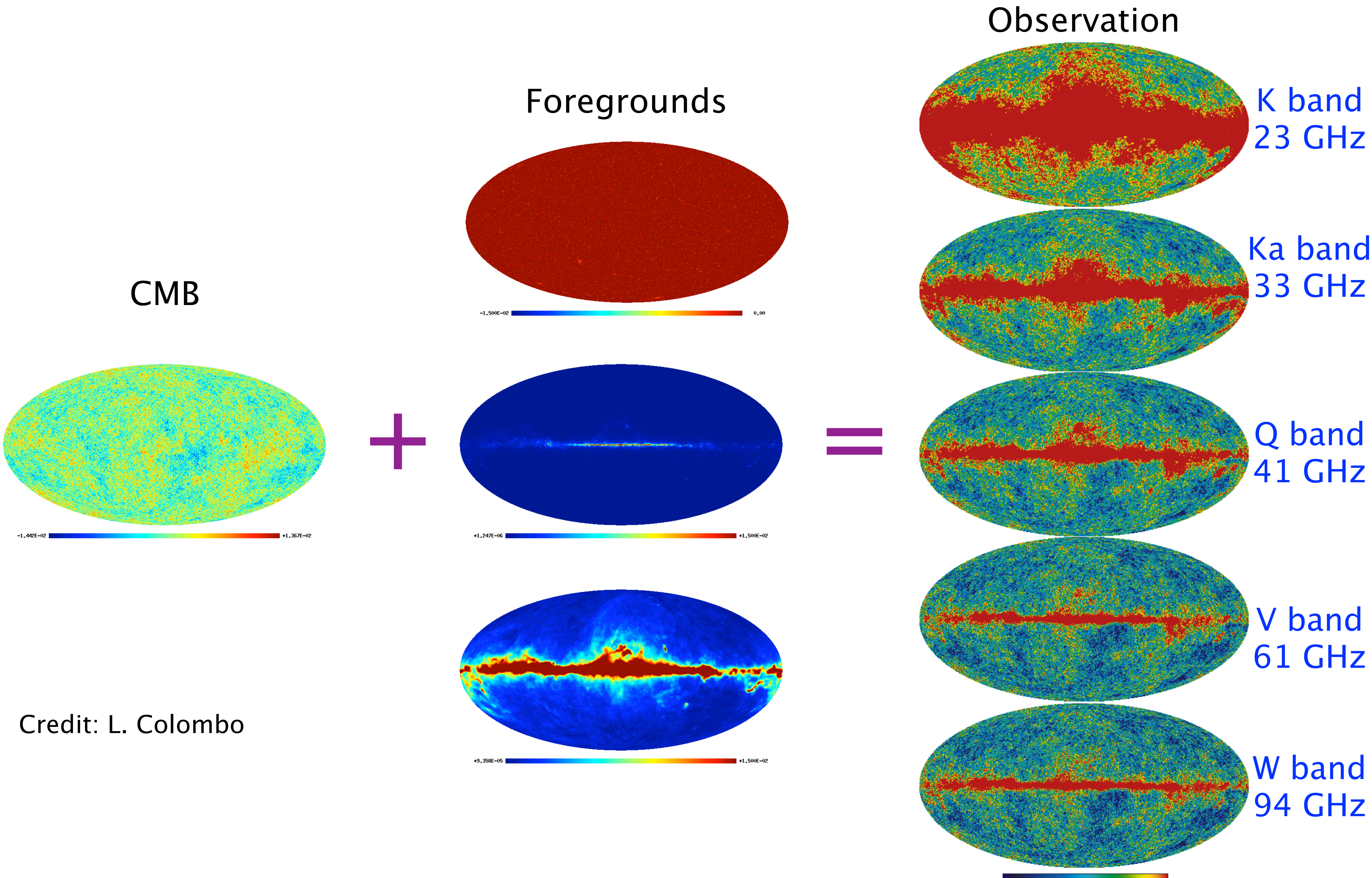

Credit: L. Colombo

Component Separation: general

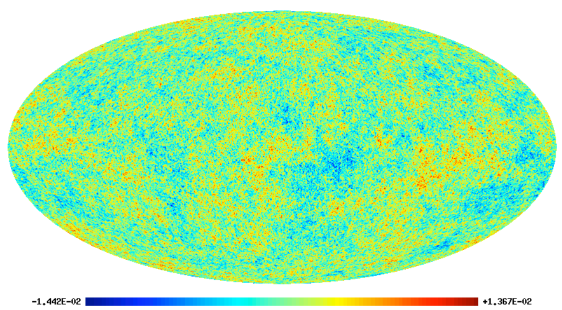

S_1

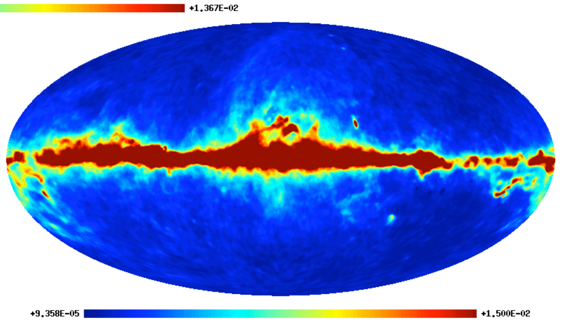

S_2

Two observing frequencies: ν_1, ν_2

$$x_1 = a_{11}\, s_1 + a_{12}\, s_2 + n_1$$
$$x_2 = a_{21}\, s_1 + a_{22}\, s_2 + n_2$$

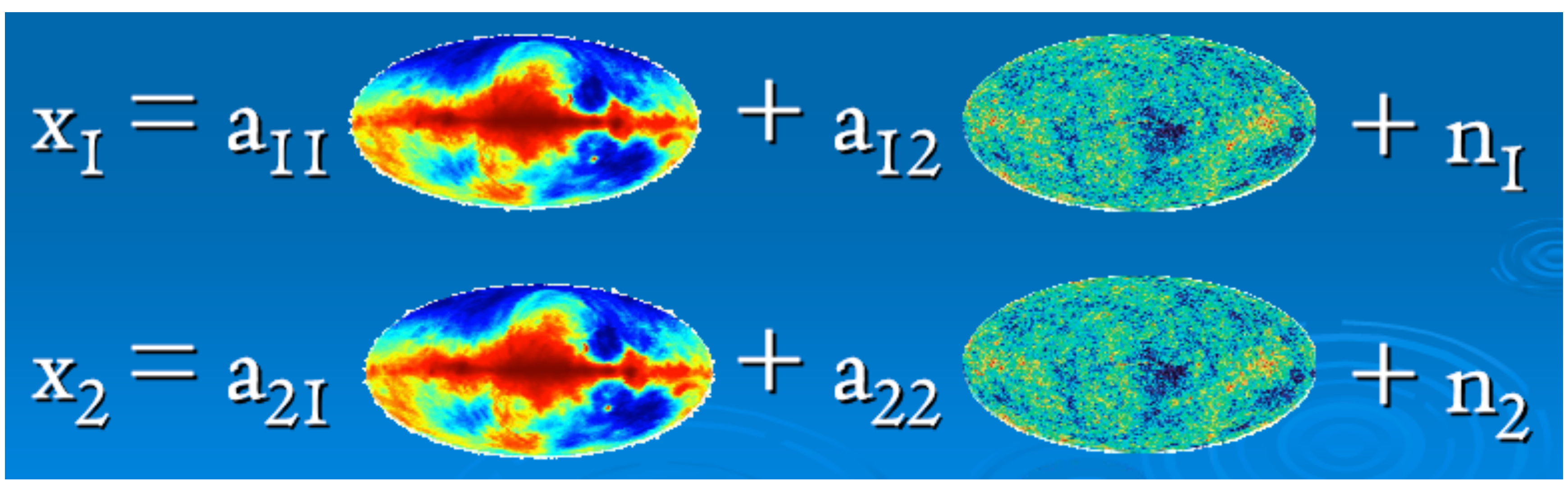

$\mathbf{x} = \mathbf{A}\mathbf{s} + \mathbf{n}$

Invert for $\mathbf{s}$

Component separation: ILC method

The Internal Linear Combination (ILC) method aims to combine different frequency maps with specific weights, such that contributions from all the contaminating signals (plus noise) are minimized.

This works especially well when we have poor knowledge of the foregrounds (but assumes foreground and the signal are independent).

But we must have a precise knowledge of the signal spectrum! Also ILC should be used separately on different spacial scales.

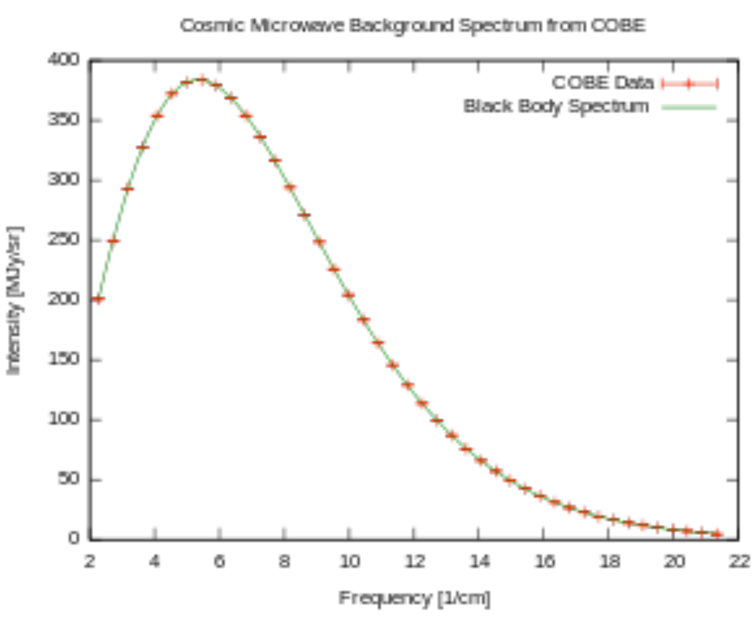

+

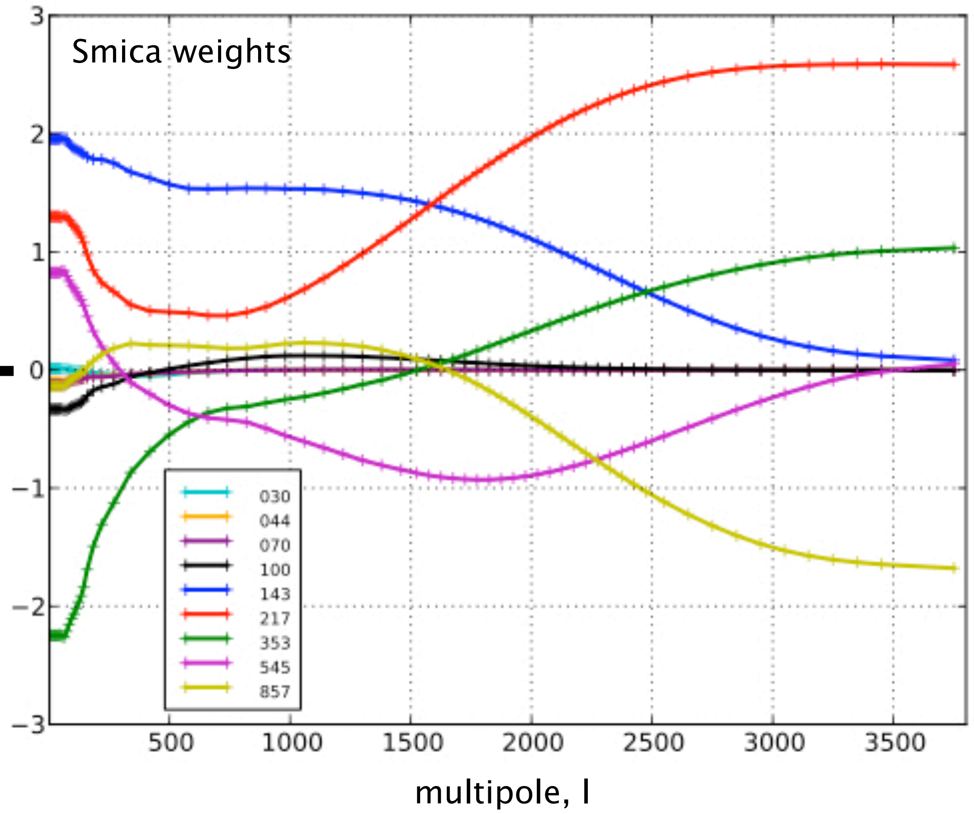

=

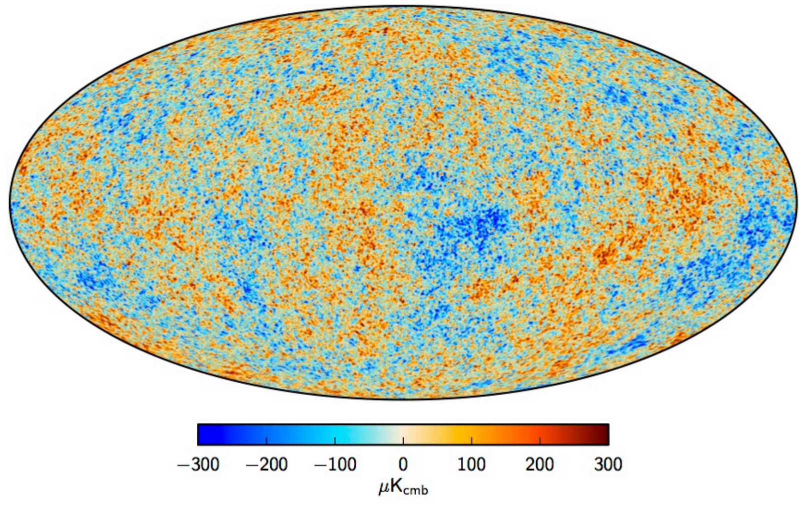

Component separation: ILC method

Example: Extraction of Compton-y (SZ effect) map

(Master's thesis work by Jens Erler)

Maps of the Comptonization parameter y can be recovered by forming linear combinations of the observed temperature maps.

$$y = \sum_i \omega_i \frac{T_i}{T_{\rm CMB}}$$

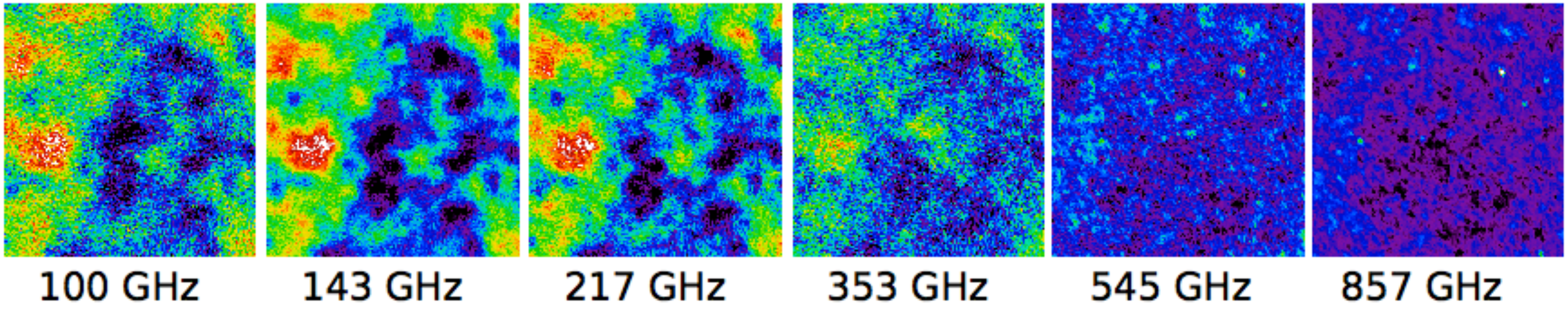

(4.3° x 4.3° cut-outs of the Coma-field)

Component separation: ILC method

Example: Extraction of Compton-y (SZ effect) map

(Master's thesis work by Jens Erler)

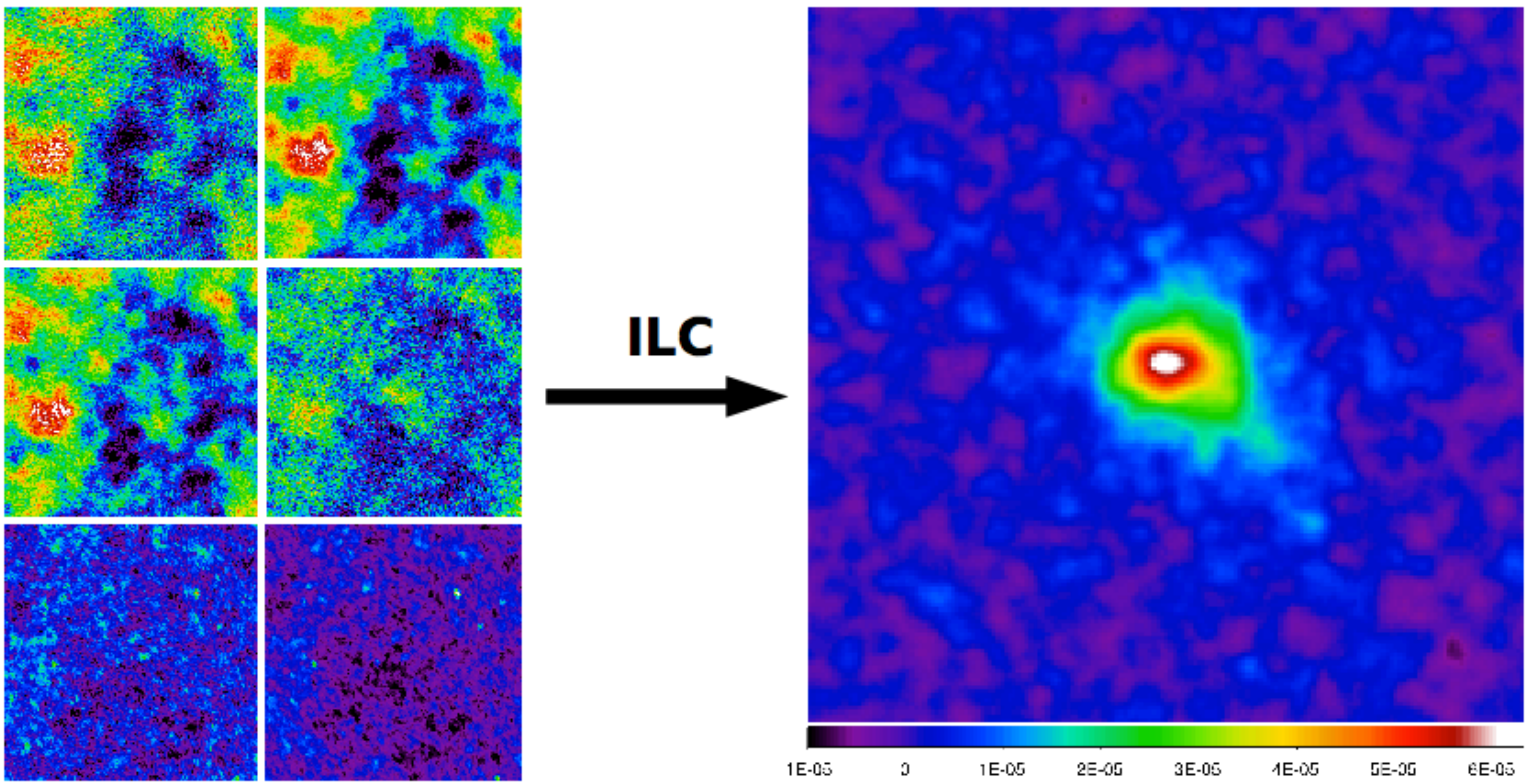

Component separation: ILC method

Planck all-sky y-map (Planck collaboration 2015)

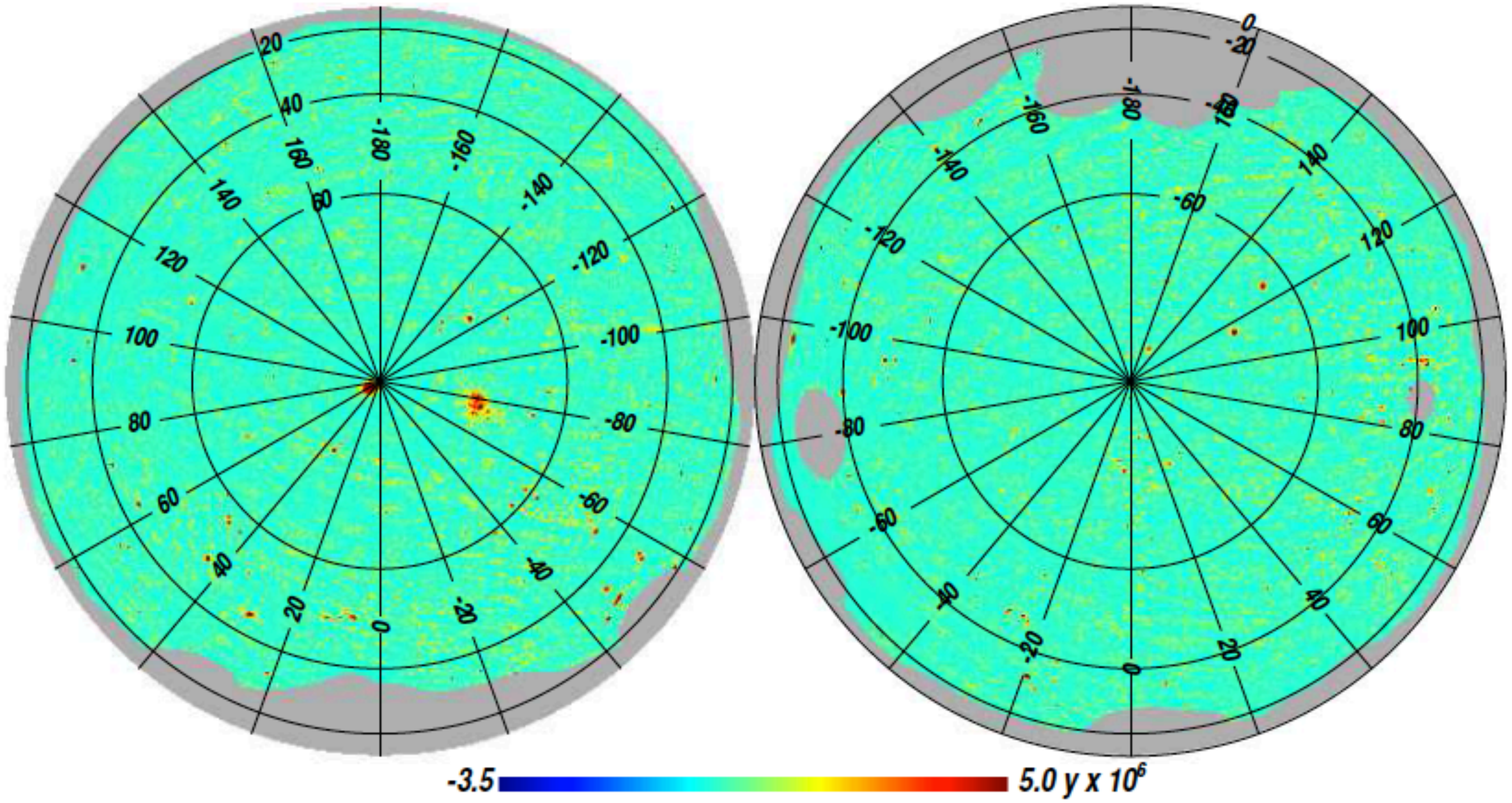

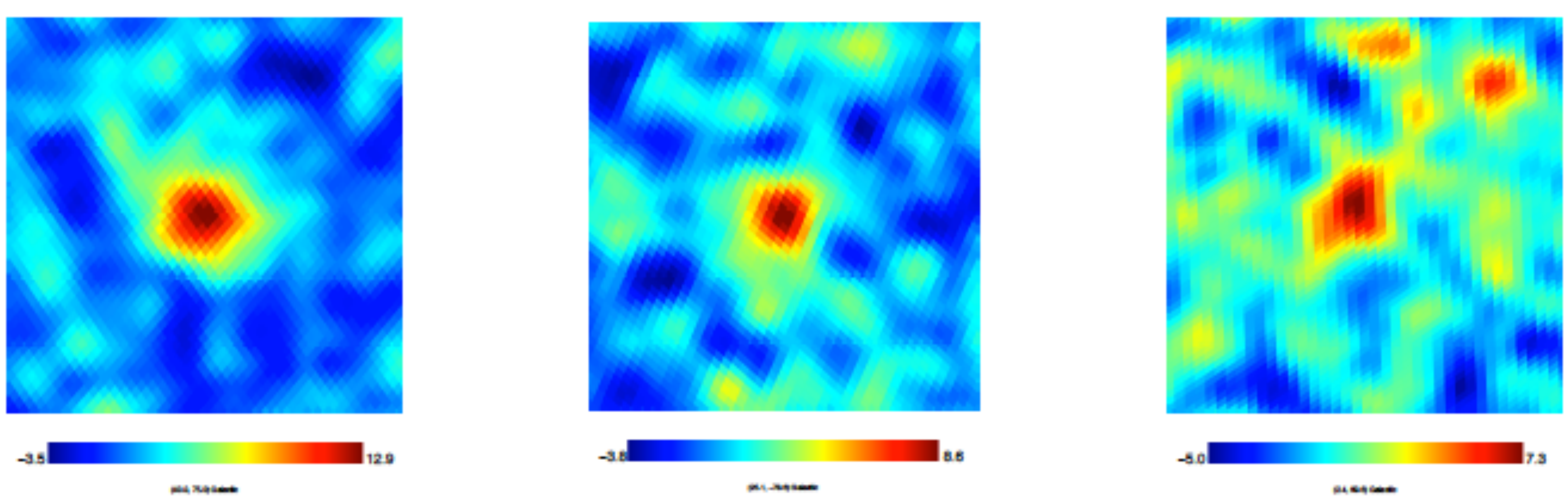

Questions?